

TO

MY PARENTS

Uddin and Sadiqa Zaka.

*PROPERTIES OF INTRINSIC AND
DOPED AMORPHOUS SILICON
PRODUCED BY R.F. SPUTTERING.*

BY

YASIN ZAKA B.Sc.

*A THESIS SUBMITTED TO THE
FACULTY OF SCIENCE AT THE
UNIVERSITY OF ASTON IN
BIRMINGHAM FOR THE DEGREE OF
DOCTOR OF PHILOSOPHY.*

FEBRUARY 1985.

PROPERTIES OF INTRINSIC AND DOPED AMORPHOUS SILICON PRODUCED BY

R.F. SPUTTERING

Submitted for the Degree of Doctor of Philosophy

FEBRUARY 1985

YASIN ZAKA

ABSTRACT

The effect of varying the preparation conditions on the electrical and optical properties of a-Si films prepared by r.f. sputtering in pure noble gases was investigated. In particular the effect of varying the sputtering gas and gas pressure was considered. Other parameters varied were the target substrate distance, d.c. self-bias voltage on the target, the application of an axial magnetic field and the variation of the substrate temperature. The films were characterized by measuring the d.c. dark conductivity as a function of temperature over a range of about 170 K, determining the thermal activation energy, room-temperature photoconductivity, the optical gap and the composition of the films.

The results suggest that the density of defect states can be reduced substantially by sputtering at high pressures, since the dark conductivity decreases and the photoconductivity, thermal activation energy and optical gap increase on increasing the sputtering pressure. For argon sputtered films the conductivity was decreased by more than four orders of magnitude to $10^{-7} (\Omega\text{cm})^{-1}$ by increasing the pressure from the conventionally used value of 5 mtorr to about 25-30 mtorr. Films sputtered at higher pressures exhibited even lower conductivities but were found to contain large quantities of oxygen (~ 20 at.%). Films sputtered in neon exhibited properties comparable to optimally prepared hydrogenated silicon. By increasing the sputtering pressure the room temperature conductivity was decreased by more than six orders of magnitude to $<10^{-9} (\Omega\text{cm})^{-1}$.

Neon sputtered films were doped n-type by incorporation of tantalum by co-sputtering and arsenic and antimony by sputtering predoped targets. The results showed that the room-temperature conductivity could be varied systematically over range of nine orders of magnitude by substitutional doping.

Increasing the target substrate spacing or decreasing the d.c. self-bias voltage on the target also resulted in a reduction in the density of defect states. Increasing the substrate temperature also slightly reduced the density of defect states.

KEY WORDS: R.F. sputtering, amorphous silicon, electrical conductivity, optical gap, substitutional doping.

ACKNOWLEDGEMENTS

I would like to express my deepest gratitude to the many members of the Physics Department who have contributed to this research effort. I am particularly indebted to Drs D C Crumpton and R W Fane for their guidance and encouragement given to me during the course of this work.

The expertise of the members of the Physics Department workshop are acknowledged. I would also like to thank Mr A Abbot for his assistance with the XPS and AES experiments and Mr J Phull for his companionship and assistance with the RBS experiments. Thanks are also due to Mr L Keen for his assistance with the electron microscope experiments. Special thanks are due to Mr R S Bassi for his technical assistance and companionship throughout the course of this work.

Miss Diane Stretton is thanked for the excellence of her typing and the craftsmanship of Mr A E Marriot-Reynolds in drawing the figures is highly appreciated.

Finally I would like to express my deepest gratitude to my family for their endless love, support and encouragement they have given to me throughout my life. Special thanks are given to my parents and grandfather Mr N D Malik for their encouragement and prayers for my success. Thanks are also due to my sisters for their love and support. Finally, I would like to thank my wife Asma for her love and understanding and also my daughter Saiher and my son Baber for being a source of pleasure to me.

CONTENTS

	<u>Page</u>
SUMMARY	iii
ACKNOWLEDGEMENTS	iv
LIST OF FIGURES	ix
LIST OF PHOTOGRAPHS	xviii
LIST OF TABLES	xix
CHAPTER 1: INTRODUCTION	1
CHAPTER 2: LITERATURE SURVEY	3
2.1 Introduction	3
2.2 Preparation Techniques	4
2.2.1 Preparation of hydrogenated amorphous silicon	4
2.2.1a Decomposition of Silane (SiH_4)	5
(i) Glow-discharge decomposition of silane	5
(ii) Chemical vapour deposition of silane	6
2.2.1b Reactive r.f. Sputtering	7
2.2.1c Diffusion of Hydrogen into a Material Deposited by other Techniques	9
2.2.2 Preparation of Unhydrogenated a-Si Films	10
2.3 Characterization of a-Si Films	13
2.3.1 Electrical and optical property measurements	13
2.3.1a Measurement of electrical dark conductivity	13
2.3.1b Measurement of photoconductivity	17
2.3.1c Optical absorption	20
2.3.2 Compositional Analysis	21
2.3.2a Determination of hydrogen content	21
2.3.2b Argon Content	21
2.3.2c Neon Content	22
2.3.2d Oxygen Content	22
2.4 Doping effects of Group III and V elements	23

	<u>Page</u>
CHAPTER 3: THEORETICAL CONSIDERATIONS	25
3.1 Theoretical models of amorphous semiconductors	25
3.1.1 The gap states in amorphous silicon	25
3.2 The interpretation of the transport measurements	29
3.2.1 Electrical conduction in amorphous semiconductors	29
3.2.1a Extended state conduction	30
3.2.1b Conduction in the band tail states	32
3.2.1c Conduction in the localised states at the Fermi level	32
3.2.2 Temperature dependence of electrical conductivity	35
3.3 Optical Absorption	38
3.4 Background Theories of the Techniques for Compositional Analysis	41
3.4.1 Rutherford backscattering spectroscopy	41
3.4.1a Introduction	41
3.4.1b Mass Analysis	43
3.4.1c Quantitative Analysis	45
3.4.1d Depth Analysis	46
3.4.2 Auger Electron Spectroscopy (AES) and X-ray Photoelectron Spectroscopy (XPS)	47
3.4.2a The basic principles of AES	47
3.4.2b The basic principles of XPS	50
3.5 The Basic Theory of r.f Sputtering	51
3.5.1 The mechanism of sputtering	51
3.5.2 R.f. sputtering	53
CHAPTER 4: EXPERIMENTAL DETAILS	56
4.1 Production of amorphous silicon	56
4.1.1 Design of the r.f. sputtering system	56
4.1.2 Experimental Procedure	70
4.1.2a Substrate Preparation	70
4.1.2b Deposition of Amorphous Silicon	72
4.1.2c Evaporation of aluminium	75

	<u>Page</u>	
4.2	Characterization of amorphous silicon films	75
4.2.1	Thickness measurement	75
4.2.2	Measurement of electrical conductivity	78
4.2.3	Measurement of photoconductivity	86
4.2.4	Optical absorption	88
4.3.5	X-ray diffraction	89
4.3.6	Electron diffraction and micrography	89
4.3	Compositional Analysis	90
4.3.1	Rutherford backscattering spectroscopy	93
4.3.1a	Substrate Preparation	93
4.3.1b	Instrumentation	93
4.3.1c	Procedure	100
4.3.2	X-ray Photoelectron Spectroscopy (XPS) and Auger Electron Spectroscopy (AES)	101
4.3.2a	Instrumentation	101
4.3.2b	Experimental Procedure	104
4.3.3	Infra-Red Spectroscopy	105
	CHAPTER 5: RESULTS	108
5.1	The effect of varying the argon pressure on the electrical and optical properties of amorphous silicon film	108
5.2	The effect of preparation conditions on the properties of neon sputtered amorphous silicon	122
5.2.1	Variation of the neon sputtering pressure	122
5.2.2	Variation of target-substrate spacing	134
5.2.3	Variation of d.c. self-bias voltage	136
5.2.4	Variation of the magnetic field	141
5.2.5	Variation of the substrate temperature	142
5.3	Substitutional doping by group V elements	145
5.3.1	Doping by co-sputtering with tantalum	149
5.3.2	Doping from pre-doped targets	159

	<u>Page</u>
CHAPTER 6: DISCUSSION OF EXPERIMENTAL RESULTS	163
6.1 The effect of increasing the argon pressure on the properties of amorphous silicon films	163
6.2 The significance of preparation conditions of neon sputtered films	167
6.3 The effect of varying the magnetic field	177
6.4 Influence of the substrate temperature	178
6.5 Doping effects of group V elements	180
6.6 The compositional analysis of the films	188
CHAPTER 7: CONCLUSIONS	196
REFERENCES	199
PUBLICATIONS	207
1. Highly doped sputtered amorphous silicon without hydrogen	208
2. Highly doped amorphous silicon withough hydrogen	215
3. Dependence of the Electronic and Optical properties of Unhydrogenated a-Si on preparation conditions	221
4. Dependence of photo-conductive properties of unhydrogenated Ne-sputtered a-Si on preparation conditions	227
5. Composition and properties of unhydrogenated amorphous silicon produced by sputtering in argon or neon gas	231
6. Doping effects of groups III and V elements in unhydrogenated Ne-sputtered a-Si	235
7. Control of electrical and optical properties of unhydrogenated Ne-sputtered a-Si by preparation conditions	253
8. Data Review, EMIS (INSPEC)	267

LIST OF FIGURES

2.1	Pre-exponential term (σ_0) versus the activation energy (ΔE) for a number of doped a-Si:H films	16
3.1	Various models for the density of states distribution in the mobility gap (a) CFO, (b) Davis and Mott and (c) Dundee model.	28
3.2	Model used by the Dundee group for the analysis of the Hall effect data.	33
3.3a	The variation of electrical conductivity with inverse temperature of g.d. produced films.	36
3.3b	Conductivity versus $10^3/T$ for a series of phosphorous doped samples.	37
3.4	The variation of the absorption coefficient with photon energy for amorphous semiconductors.	40
3.5	The variations of the absorption coefficient with photon energy for a number of amorphous-silicon samples prepared by different methods.	42
3.6	RBS spectrum from a hypothetical sample containing equal amounts of C, Al, Fe and Ag.	44

3.7	Schematic representation of (a) the Auger proces and (b) the XPS mechanism.	48
3.8	The essential features of a grounded diode sputtering system.	54
4.1	General layout of the sputtering system.	58
4.2a	The target assembly.	59
4.2b	The new target holder.	60
4.3a	The substrate heater.	63
4.3b	New substrate heater	64
4.4a	Axial magnetic field at the centre of the chamber as function of the current applied to the Helmholtz pair of coils.	66
4.4b	The shape of the combined magnetic field of Helmholtz pair of coils.	67
4.5	Circuit for measuring the d.c. self-bias voltage.	69
4.6	Substrate temperature as a function of heater voltage.	74

	<u>Page</u>
4.7a Mask for depositing aluminium over the amorphous silicon films for thickness and conductivity measurement.	76
4.7b Appearance of the fringes in the interference microscope.	77
4.8 Conductivity vs temperature; the effect of temperature cycling.	80
4.9 Schematic diagram of the apparatus for measuring the electrical conductivity.	82
4.10 Circuit for measuring the electrical conductivity.	84
4.11 Some of the typical electron diffraction pattern	91
4.12 Some of the typical electron micrographs.	92
4.13 Major components of the RBS system	95
4.14 Schematic diagram of the backscattering chamber	96
4.15 The geometric relationship between the target and the detector.	97
4.16 Spectrum obtained from a Ti target used as a standard.	98

	<u>Page</u>
4.17 Calibration curve of backscattered energy versus the channel number	99
4.18 Typical spectrum from IR experiments	106
5.1 The variation of electrical conductivity with inverse temperature for films sputtered at various argon pressures.	110
5.2 The variation of room-temperature, electrical conductivity (σ_{RT}) and photoconductivity (σ_{ph}) with sputtering pressure of argon	112
5.3 Variation of thermal activation energy (ΔE) and optical gap (E_0) with sputtering pressure	113
5.4 Some of the typical plots of $(\propto \hbar\omega)^{\frac{1}{2}}$ vs $\hbar\omega$ from which E_0 was deduced for argon sputtered films	115
5.5 Shift of the absorption edge with argon pressure	116
5.6 Typical RBS spectrum of an argon sputtered a-Si film deposited on Al_2O_3 substrate	117
5.7 The composition of argon sputtered films as a function of sputtering pressure	119

5.8	The variation of the sputtering rate with argon pressure.	120
5.9	Conductivity vs inverse temperature for films sputtered at various neon pressures.	125
5.10	The variation of room-temperature dark (σ_{RT}) and photo (σ_{ph}) conductivities with neon sputtering pressure.	126
5.11	Variation of thermal activation energy (ΔE) and the optical gap (E_0) with neon sputtering pressure.	127
5.12	Plots of $(\hbar\omega)^{\frac{1}{2}}$ vs $\hbar\omega$ of a selected number of samples sputtered at various neon pressures.	129
5.13	The absorption coefficient (α) vs photon energy ($\hbar\omega$) for films deposited at various pressures.	130
5.14	Variation of deposition rate with sputtering pressure.	131
5.15	Concentration of neon in the films as a function of neon sputtering pressures.	135

5.16	Variation of room-temperature electrical conductivity (σ_{RT}), photoconductivity (σ_{ph}), thermal activation energy (ΔE) and the optical gap (E_0) with target-substrate distance. (d).	137
5.17	The d.c. self bias voltage on the target as a function of the applied power density.	139
5.18	Variation of room-temperature electrical conductivity (σ_{RT}), photoconductivity (σ_{ph}), thermal activation energy (ΔE) and the optical gap (E_0), with the d.c self bias voltage.	140
5.19a	The effect of varying the magnetic field on room-temperature dark conductivity (σ_{RT}) and photoconductivity (σ_{ph})	143
5.19b	The effect of varying the magnetic field on the thermal activation energy (ΔE) and the optical gap (E_0).	143
5.20	Variation of sputtering rate and d.c self-bias voltage with magnetic field.	144

5.21	The variation of the room-temperature dark conductivity (σ_{RT}) , photoconductivity (σ_{ph}), thermal activation energy (ΔE) and the optical gap (E_0) with substrate temperature.	146
5.22	The effect of varying the substrate temperature on the concentrations of neon and oxygen in the films.	147
5.23	Dark conductivity vs $1000/T$ for various concentration of tantalum.	150
5.24	Room-temperature electrical conductivity of tantalum doped films against the concentration of tantalum.	152
5.25	Thermal activation energy (ΔE) and the optical gap (E_0) versus the concentration of tantalum in the films.	153
5.26	Plots of $(\alpha h\nu)^{\frac{1}{2}}$ vs $h\nu$ for various concentration of tantalum.	154
5.27	Variation of room-temperature electrical conductivity and thermal activation energy of films containing 0.2% tantalum with the sputtering pressure.	156

	<u>Page</u>
5.28 A typical RBS spectrum of a film deposited on an alumina (Al_2O_3) substrate.	157
5.29 Area ratio of tantalum and silicon vs the concentration of tantalum as determined by RBS.	158
5.30 The variation of room-temperature, dark conductivity (σ_{RT}) and photoconductivity (σ_{ph}) with sputtering pressure for films sputtered from targets pre-doped with arsenic for antimony.	161
5.31 The variation of thermal activation energy (ΔE) and the optical gap (E_0) with sputtering pressure for films sputtered from targets pre-doped with arsenic for antimony.	162
6.1 Variation of the various measured properties as a function of the argon sputtering pressure.	168
6.2 Variation of the various measured properties as a function of the neon sputtering pressure.	176
6.3 Room temperature conductivity (σ_{RT}) as a function of the density of impurity atoms. Curve A gas phase doping of a-Si:H by Phosphorus ; Curve B, Ion implantation of phosphorus in a-Si:H; Curve C, tantalum doping by neon sputtering.	184

	<u>Page</u>	
6.4	Conductivity activation energy as a function of the density of impurity atoms for films prepared by various methods.	185
6.5a	I.V characteristics for n-type a-Si/p-type crystalline junction.	187
6.5b	I.V characteristics for a typical p/n amorphous silicon junction.	187
6.6a	A model for the surface of the neon sputtered amorphous-silicon film.	194
6.6b	Concentration of neon ^{aS} / _k a function of the etching period.	195

LIST OF PHOTOGRAPHS

Plate No.

Plate (4.1)	The r.f sputtering unit in operation.	57
Plate (4.2)	The apparatus for measuring the electrical conductivity.	81
Plate (4.3)	The apparatus for measuring the photocurrent	87
Plate (4.5)	the Kratos (XSAM800) Auger and X-ray Photo- electron Spectrometer.	102

LIST OF TABLES

5.1	The variation of the electrical and optical properties and the composition of the films with argon sputtering pressure.	121
5.2	Summary of the results of the variation of electrical and optical properties of amorphous silicon with neon sputtering pressure.	133
6.1	Comparison of the properties of conventionally produced amorphous silicon with those of reactivity sputtered hydrogenated amorphous silicon.	164

1. INTRODUCTION

The last decade has seen an explosion of interest in the production, characterization and application of amorphous silicon films. Much of this interest has stemmed from realisation of its potential applicability as a low cost material for photovoltaic solar energy conversion. It possesses the attractive properties of appropriate band gap, high absorption coefficient, ease of preparation and the control over electronic properties over a wide range.

The systematic control of electronic properties of a-Si was first demonstrated in 1975 by Spear et al (1975) who successfully doped a-Si produced by the glow-discharge decomposition of silane n- and p-type by incorporating phosphorus and boron respectively in to a silicon matrix. It was then realised that inherent in all methods of producing a-Si films is the presence of a large number of unpaired dangling bonds and microvoids. These defects introduce localised states in the energy gap, thus hindering the control of electrical and optical properties by substitutional doping. The success of the glow-discharge method was due to the fact that the hydrogen present in the plasma acted as a dangling bond terminator thus reducing the number of defects in the mobility gap. Soon after, a-Si produced by rf sputtering in Ar/H₂ plasma was also doped successfully (Paul et al 1976). The success with doping a-Si:H alloy and the realisation of its potential device capabilities have however diverted a lot of attention away from the need to investigate the basic parameters affecting film properties and to optimise them to achieve 'pure' a-Si films with a low density of defect states. Instead experimentalists have saturated the silicon with dangling bond terminators such as hydrogen or halogens to achieve

the desired properties. Concentration of these intentionally incorporated impurities can be as large as 50 at.% (Brodsky et al 1977b). Dangling bond termination by hydrogen may remove the gap states, but interaction of nearby Si-H units can re-introduce the gap states near the conduction band (Moustakas et al 1977). The long-term stability of these films has also been questioned since hydrogen effuses at approximately 350°C (Tsai et al 1977). It is therefore important to optimise the preparation conditions to give pure a-Si films with a low density of defect states.

The work presented in this dissertation is an extension of preliminary experiments reported by Fane (1981). Fane showed that the density of defect states of pure a-Si produced by sputtering in high pressure neon rather than argon was low enough to enable efficient substitutional p-type doping by aluminium. The aim of the present work is to investigate the effect of varying the preparation conditions on the electrical and optical properties and the composition of the films. In particular the effect of varying the sputtering gas and gas pressure is to be considered. The doping capabilities are to be extended by incorporating n-type dopants.

The films have been characterised by measuring the electrical conductivity over a temperature range of 200°C and the magnitude of the room-temperature photoconductivity. The optical gap has been determined by transmission measurements in a UV-Vis spectrophotometer. Compositional analysis has been carried out by Rutherford backscattering spectroscopy (RBS), X-ray photoelectron spectroscopy (XPS) and Auger electron spectroscopy (AES).

2. LITERATURE SURVEY

2.1 Introduction

During the last decade interest in the production and control of electrical and optical properties of amorphous silicon has grown rapidly. This surge in interest has stemmed from the pioneering work of Professor Spear and Dr LeComber at Dundee University and Professor William Paul and his co-workers at Harvard University. In 1975 Spear and LeComber demonstrated that the electrical and optical properties of a-Si produced by the glow-discharge decomposition of silane (SiH_4) could be varied by n- or p- type doping, by the controlled addition of phosphine (PH_3) or diborane (B_2H_6) to silane. Soon after, Paul et al also produced amorphous silicon which could be doped by rf sputtering in a plasma of argon and hydrogen (Paul et al 1976). With the advent of these techniques for producing amorphous silicon which could be substitutionally doped, the potential device applications of the material were realised and research into the preparation, characterization and production of electronic devices grew.

Since 1975 numerous papers have been published on the effect of varying the preparation conditions on the electrical and optical properties of a-Si produced by glow-discharge decomposition of SiH_4 or sputtering in an Ar/ H_2 mixture. Many other techniques for producing amorphous silicon with low density of defect states capable of being doped have also been developed. The materials produced by the various techniques have been characterized extensively by structural, compositional and electrical and optical property measurements.

Several comprehensive reviews of the present understanding of amorphous silicon have been published recently. (Paul and Anderson 1981, Fritzsche1980, Knights and Lucorsky 1980, Moustakas 1978, Brodsky 1978). More detailed discussion on several aspects of amorphous silicon technology can be found in the recent monographs published on the subject (Mott and Davies 1979, Brodsky et al 1979, Yonezawa Ed., 1981). The development of the subject has been well documented and catalogued in the proceedings of the Bi-Annual Conferences on Amorphous and Liquid Semiconductors. (Proceedings of International Conference on amorphous and liquid semiconductors 1977, 1979, 1981, 1983).

In this chapter the development of the techniques for producing and characterizing amorphous silicon films will be reviewed briefly, with particular emphasis on the preparation by rf sputtering. Similarly the discussion on characterization will be concentrated on those techniques which are pertinent to the present study. However because of the lack of published work on the characterization of pure amorphous silicon films most of the references are of work on hydrogenated amorphous silicons.

2.2 PREPARATION TECHNIQUES

2.2.1 Preparation of Hydrogenated Amorphous Silicon

Since the realisation that hydrogen could terminate the dangling bonds and hence reduce the density of defect states in the mobility gap (Paul et al 1976) many techniques for producing hydrogenated amorphous silicon have been developed. The majority

of the techniques can be grouped into three main classes.

- (a) Decomposition or reaction of a hydrogen containing compound (e.g. SiH_4).
- (b) Addition of hydrogen during a physical deposition process.
- (c) Diffusion of hydrogen into a material deposited by some other process.

The techniques which fall in each of these categories are briefly discussed below. Two main techniques fall into the first category. They are (i) glow discharge decomposition of hydrides and (ii) the pyrolytic decomposition of hydrides.

2.2.1a Decomposition of Silane (SiH_4)

(i) The Glow Discharge Decomposition of Silane

The glow-discharge decomposition of silane (SiH_4) is probably the most widely used method at present, of producing a-Si:H. The technique was first applied by Sterling and his co-workers to obtain amorphous Si and Ge. (Sterling and Siram 1965, Chittick et al 1969) but only assumed significance after the seminal work of Spear and LeComber (Spear and LeComber 1972, 1975, 1976, 1977).

The method essentially consists of passing silane gas through a quartz reaction tube which contains the substrate holder. The flow rate of SiH_4 is adjusted to maintain pressures inside the tube of about 0.5 torr. The silane is decomposed by initiating

and maintaining a plasma induced by applying rf power to the gas. The rf power level is small, typically 1-50 W and frequencies in the range 1-100 MHz have been used. The rf power can be coupled to the gas either inductively (Chittick et al 1969) or capacitively (Knights 1976). Because of the difficulty of scaling up in the former system, capacitive arrangements have become more popular. Extensive work has been done on optimising the preparation conditions, the progress has been reviewed in recent articles (LeComber and Spear 1979, Carlson 1980, Fritzsche 1980). Several variations to the basic method have been suggested recently; these include, operating at microwave frequencies (Mejia et al 1983) and producing the film in a UHV deposition system to reduce the high contaminant impurity levels (Tsai et al 1983).

(ii) Chemical Vapour Deposition (CVD) of Silane

Hydrogenated amorphous silicon can also be obtained by the thermal decomposition of silane, usually at atmospheric pressure on a heated substrate (Janai et al 1979, Booth et al 1979). The systems used are essentially the same design as those used for the deposition of crystalline silicon by chemical vapour deposition (CVD). The electronic properties of CVD produced a-Si:H are relatively poor compared to g.d. material. This is because insufficient hydrogen is incorporated in the films due to high substrate temperatures employed ($T_s \approx 600^\circ\text{C}$). To overcome this problem laser induced chemical vapour deposition of silane (Meunier et al 1983) has recently been suggested.

2.2.1b Reactive rf Sputtering

The only technique that falls in the second category for which extensive work has been reported is reactive sputtering in a plasma of argon and hydrogen. Although some work on the evaporation of silicon in the presence of hydrogen has been reported (Malhotra and Neudick 1976, Shindo et al 1983), the discussion here will be limited to r.f. sputtering. The technique of reactive sputtering of silicon in an Ar-H₂ plasma was developed by the group at Harvard University (Lewis et al 1974, Paul et al 1976, Connell and Pawlik 1976). The sputtering pressure is typically 5 mtorr with a partial pressure of hydrogen of about 1 mtorr resulting in about 20% hydrogen in the films (Paul and Anderson 1981) although hydrogen concentrations of up to 50% have been reported (Brodsky et al 1977b). The effect of varying the sputtering pressure, the hydrogen partial pressure and the substrate temperature have been extensively investigated. It has been reported that increasing the sputtering pressure from 5 mtorr to 10 mtorr improves the electronic and optical properties of the material, but further increase in pressure to 30 mtorr results in porous films, susceptible to post-deposition oxidation (Anderson et al 1979). The effect of varying the hydrogen partial pressure and the substrate temperature on the structure and electronic and optical properties has been recently reviewed by Paul and Anderson (Paul and Anderson 1981). It has been found that for low partial pressures of hydrogen ($P_H \leq 1$ mtorr) the concentration of hydrogen in the film increases linearly with P_H to a value of about 20% at 1 mtorr (Oguz et al 1978, Freeman and Paul 1978). Increasing the concentration of hydrogen in this range has a dramatic effect on the electrical and optical properties. Films produced without any hydrogen exhibit relatively high conductivity ($\sigma_{RT} \sim 10^{-3} \Omega^{-1} \text{ cm}^{-1}$)

which is weakly temperature dependent. Increasing the hydrogen concentration to about 1 mtorr results in a decrease in the hopping conductivity, as is evident by the increase in the thermal activation energy (ΔE) to about 0.95 eV and a decrease in the room-temperature conductivity to about $10^{-9} (\Omega \text{ cm})^{-1}$. (Anderson and Paul 1977).

The photoconductivity (σ_{ph}), is about $10^{-11} (\Omega \text{ cm})^{-1}$ for films sputtered in pure argon; it increases sharply to a value of about $10^{-7} (\Omega \text{ cm})^{-1}$ as P_{H} is increased to 0.2 mtorr. However further increasing P_{H} to 1.0 mtorr results in a decrease in σ_{ph} , but it again increases to a value of $10^{-6} (\Omega \text{ cm})^{-1}$ as P_{H} is increased to 3.0 mtorr. (Moustakas et al 1977). The absorption edge is shifted to higher energies resulting in an increase in the optical gap from about 1.44 eV for unhydrogenated film to about 1.9 eV as P_{H} is increased 1 mtorr. (Freeman and Paul 1978, Paul and Anderson 1981). The spin density N_{S} associated with the concentration of uncompensated dangling bonds also decreases as P_{H} is increased. (Pawlik and Paul 1977). The variation of all these properties is consistent with the suggestion that hydrogen compensates the dangling bonds, hence reducing the density of defect states in the mobility gap.

Increasing P_{H} to about 5 mtorr results in little change in the concentration of hydrogen, except perhaps for a slight decrease at the highest pressures. However, the electrical and optical properties deteriorate ($\sigma_{\text{RT}} - 10^{-3} \Omega^{-1} \text{cm}^{-1}$, $\Delta E - 0.7 \text{ eV}$, $\sigma_{\text{ph}} - 10^{-8} \Omega^{-1} \text{cm}^{-1}$).

The effect of varying the substrate temperature on the electrical and optical properties is comparatively straight forward.

Increasing the substrate temperature to about 300°C improves the properties. This improvement is largely due to the increased efficiency of hydrogen compensation (Anderson et al 1977, Freeman and Paul 1979). Substrate temperatures higher than 300°C, however produce inferior films, because hydrogen begins to evolve at about 300°C (Fritzsche 1977).

In the literature no systematic investigation of studying the effect of varying the target-substrate spacing or the target voltage was found. The typical sputtering conditions of the Harvard group are; the forward rf power applied to a 12.5 cm.diameter target is about 200 W, giving a power density of 1.6 W/cm² and a dc self-bias voltage on the target of approximately 1.6 kV. The substrate target spacing is typically set at 7cm. (Anderson et al 1979).

2.2.1c Diffusion of Hydrogen into a Material Deposited by Other Techniques

Amorphous silicon produced by thermal evaporation contains a large concentration of defects. To reduce these defects and hence improve the electrical and optical properties, post-hydrogenation of vacuum deposited films has been attempted. LeComber et al exposed vacuum evaporated films to a hydrogen glow discharge at room temperature (LeComber et al 1974) and although the dangling bond concentration was reduced no appreciable effect on the electrical and optical properties was observed. However Kaplan et al have repeated this experiment using UHV deposited films and obtained considerable variation in the transport properties (Kaplan et al 1978). The properties of their post-hydrogenated material were claimed to be similar to glow-discharge produced material.

2.2.2 Preparation of Unhydrogenated Amorphous Silicon Films

Pure amorphous silicon films have been produced either by thermal evaporation or rf sputtering in pure argon (Brodsky et al 1970). However, the films produced by these techniques are plagued by a large density of dangling bonds which inhibit the control of electrical and optical properties by substitutional doping (Davis 1979).

Typically amorphous silicon films produced by rf sputtering in pure argon are deposited at a pressure of 5 mtorr. The films have relatively high conductivity ($\sigma_{RT} \sim 10^{-3} \Omega^{-1} \text{cm}^{-1}$) which has a non-activated temperature dependence. The conductivity has been reduced by an order of magnitude by raising the substrate temperature from 250 to 540°C (Anderson et al 1977).

Due to the success of reducing the density of defects by hydrogenation little work has been carried out on optimising the preparation conditions for producing pure amorphous silicon films with a low density of defect states. Notable exceptions are; Pawlewicz who studied the influence of varying the argon pressure (P) and the target-substrate distance (d) (Pawlewicz 1978). The Japanese groups have extended Pawlewicz work by studying the effect of, varying the product of gas pressure(P) and substrate-target distance (d) (Shimizu et al 1979), applying a negative bias to the substrate (Suzuki et al 1981) and the doping effects of group III and V elements (Suzuki et al 1980). Most recent contributions to this field have been from the group at Aston University, who have studied the effect of sputtering in neon rather than the conventionally used argon (Zaka et al 1984a) and the variation of electrical and

optical properties with the sputtering pressure, target-substrate distance, the dc self-bias voltage, and the substrate temperature. (Zaka et al 1984 (a, b)), the doping effects of group III (Fane 1983, Fane and Abo-Namous 1983) and group V (Fane and Zaka 1983a, b) elements have also been investigated.

Pawlewicz sputter deposited amorphous silicon in an r.f. diode sputtering system with a fixed rf power density of 3 Wcm^{-2} and target-substrate spacing of 3.2 cm, deposition rates of 2.4 to 4.3 \AA S^{-1} were achieved. By increasing the argon gas pressure from 25 mtorr to 150 mtorr the resistivity of the films was increased from 100 to $3 \times 10^6 \text{ } \Omega \text{ cm}$, with a corresponding increase in the thermal activation energy from 0.2 to 0.3 eV. For some of the films, sputtered at 50 mtorr pressure the substrate-target spacing was increased from 2 to 12 cm, this resulted in an increase in resistivity from 1×10^4 to $5 \times 10^5 \text{ } \Omega \text{ cm}$. Pawlewicz found little dependence of properties on the substrate temperature, the resistivity increased from 100 to $1200 \text{ } \Omega \text{ cm}$ as the temperature was raised from 20 to 500°C . Pawlewicz suggested that increasing the sputtering pressure or distance reduced the kinetic energy of the various species bombarding the film, thus reducing the number of defects. Pawlewicz also determined the argon concentration in the films as a function of sputtering pressure. The argon concentration decreased sharply from about 7% at a sputtering pressure of 25 mtorr to about 1.0% at 60 mtorr, further increases in pressure produced little change in the argon concentration.

The Japanese groups, inspired by the work of Pawlewicz have studied in detail the effect of varying the product of pressure (P) and target substrate distance (d). The room-temperature electrical conductivity was decreased by more than five orders of magnitude

from 3×10^{-3} to 2×10^{-8} ($\Omega \text{ cm}$)⁻¹ by increasing the (Pd) product from 0.1 to 1.0 torr cm. A further decrease in σ_{RT} of two orders was achieved by annealing at 300°C for 2 hours (Shimizu et al 1979). Some of the later studies of this group suggested that the low conductivity of high pressure films could be due partly to post-deposition oxidation. In situ measurements on a film produced at 300 mtorr showed σ_{RT} to be about 10^{-7} ($\Omega \text{ cm}$)⁻¹ which decreased to less than 10^{-9} on exposure to atmosphere. It was suggested that high pressure films have a porous structure and hence absorb oxygen from the atmosphere (Shimizu et al 1980).

Fane was the first to demonstrate the possibility of producing dopable amorphous silicon by rf sputtering in high pressure neon rather than the conventionally used argon. Films of relatively low conductivity ($\sim 10^{-8}$ $\Omega \text{ cm}^{-1}$) were produced which were doped p-type by aluminium incorporation (Fane 1983). Later n-type doping was achieved by co-sputtering with tantalum (Fane and Zaka 1983 a, b). In these films the conductivity was varied over ten orders of magnitude, and the thermal activation energy by over 0.6 eV by incorporating upto 3.3% tantalum. The effect of varying the sputtering gas and pressure, the target-substrate spacing, dc self-bias voltage on the target and the substrate temperature on the electrical and optical properties and the composition of the film has been studied extensively. The detailed results of these experiments are presented in later sections of this thesis (Chapter 5) but some of the work has also been reported elsewhere (Zaka et al 1984 (a, b), Abonamous et al (1983).

Amorphous silicon films produced by glow-discharge decomposition of silane or reactive sputtering in an Ar-H₂ plasma have been studied extensively. Detailed investigations of structural and chemical characterization and electrical and optical property measurements have been reported. The characterization of glow-discharge deposited a-Si:H has been recently reviewed by Fritzsche and Carlson (Fritzsche 1980, Carlson 1980), while the properties of reactively sputtered a-Si:H have been reviewed by Moustakas and more recently by Paul and Anderson (Moustakas 1979, Paul and Anderson 1981). Little detailed work on the properties of pure amorphous silicon has been reported recently, although the earlier work on conventionally produced a-Si by evaporation or rf sputtering has been reviewed comprehensively (Adler 1972, Brodsky 1971).

2.3.1a Measurement of Electrical Dark Conductivity

The measurement of the electrical conductivity as a function of temperature is an important property for characterizing a-Si films. It has been shown that the magnitude of the electrical conductivity and its variation with temperature depend critically on the density of defect states in the mobility gap and hence the method of preparation (Mott and Davis 1979, Anderson et al 1977, Anderson and Paul 1981).

Films deposited by conventional evaporation or sputtering generally exhibit relatively high conductivity which has a weak temperature dependence. Mott and Davis have explained this behaviour as due to conduction by charge carriers hopping between the high

density of localised states around the Fermi level, and generally in the gap (Mott and Davis 1979). The observation of $T^{-1/4}$ dependence of conductivity especially at low temperatures and small values of the thermopower are normally cited as evidence of variable range hopping at the Fermi level, in a material containing a high density of defect states. (Beyer and Stuke 1974, Beyer et al 1975).

In films containing a low density of defect states, hopping conductivity around the Fermi level is negligible and hence the magnitude of the conductivity is reduced. In these films the predominant mode of transport is via thermally activated conduction in the extended states. Room temperature conductivities of about $10^{-9} (\Omega \text{ cm})^{-1}$ for glow-discharge and reactively sputtered films deposited at the optimum conditions have been reported. Plots of conductivity (σ) against temperature ($10^3/T$) indicate that the conduction is singly activated. From the slope of the plot the thermal activation energy (ΔE) can be obtained, and is found to be in the range 0.7 to 1.0 eV (Anderson et al 1977, Spear and LeComber 1976). The conductivity and the thermal activation energy are related by the equation (2.1) (Mott and Davies 1979).

$$\sigma = \sigma_0 \exp(-\Delta E/k_b T) \quad (2.1)$$

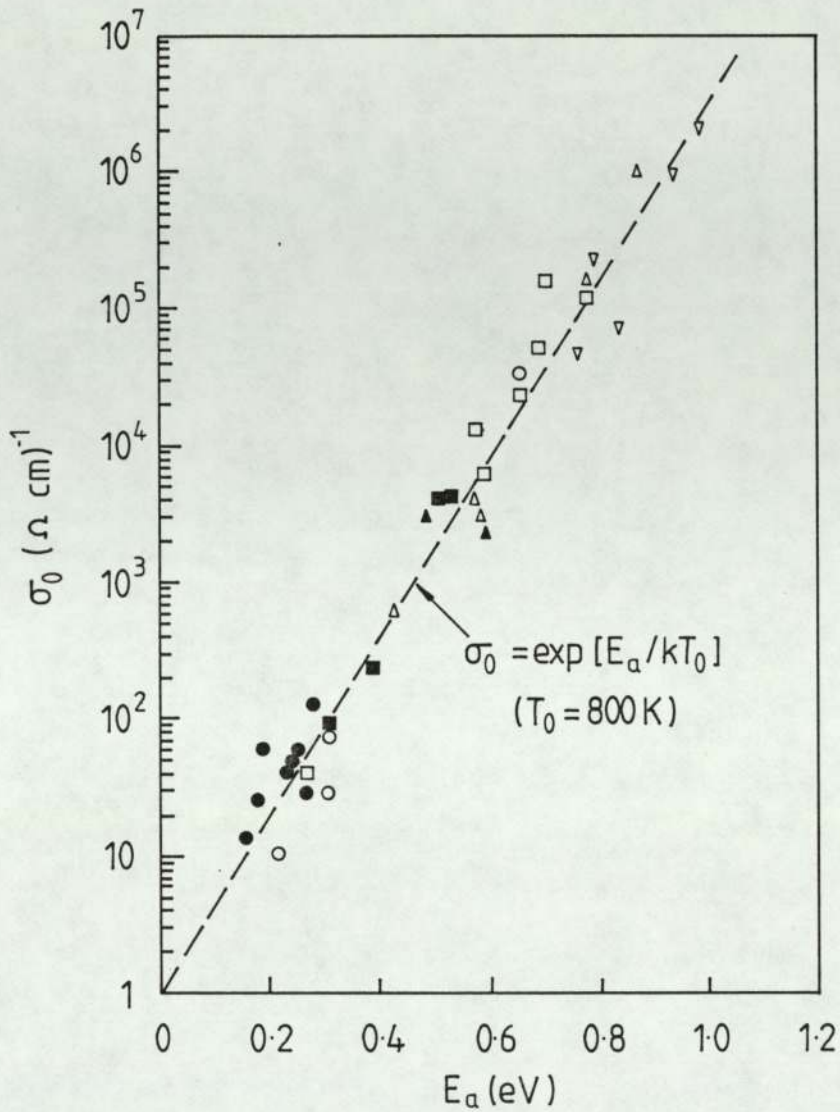
where σ_0 is the conductivity pre-factor and k_b the Boltzmann constant. The decrease in conductivity (σ) observed with hydrogenation is thought to arise from an increase in ΔE rather than a decrease in σ_0 , which has values in the range $10^3-10^5 (\Omega \text{ cm})^{-1}$ for intrinsic films (Mott and Davis 1970, Spear et al 1980, Anderson and Paul 1981).

Several authors have observed a correlation between σ_0 and ΔE , the prefactor (σ_0) is given by:

$$\sigma_0 = \sigma_{00} \exp(\Delta E/k_b T_0) \quad (2.2)$$

where σ_{00} and $k_b T_0$ are constants. Figure (2.1) shows the results of σ_0 versus ΔE_0 for n-type and p-type doped a-Si:H samples obtained by Carlson and Wronski (Carlson and Wronski 1979). Although several suggestions have been put forward to explain this behaviour (Spear et al 1980, Paul and Anderson 1981) no satisfactory model has emerged (Fritzche 1980).

Finally, some of the experimental difficulties encountered in measuring the conductivity will be briefly discussed. The conductivity is normally measured by evaporating top surface electrodes, usually aluminium or nichrome which give ohmic contacts. Both four probe and the two-probe techniques have been employed, and give essentially the same results (Lewis 1976). However using top surface electrodes the conductivity measurements are affected by surface contamination, some authors have reported changes of several orders of magnitude in the conductivity of g.d. produced a-Si:H films due to surface adsorbates such as water vapour (Tanielian et al 1980). Paul and Anderson have observed a similar effect, although not as strong in some of their sputtered films. They suggest that to obtain unambiguous results the samples should be heated in vacuum to about 200°C before taking conductivity measurements. This is because any water vapour present on the surface would be desorbed at about 100-150°C (Paul and Anderson 1981).



KEY

	1.0%	0.1%
PH ₃	●	○
AsH ₃	■	□
Sb(CH ₃) ₃	▲	△
Bi(CH ₃) ₃		▽

Figure 2.1 Pre-exponential term (σ_0) versus the activation energy (ΔE) for a number of doped α -Si-H films. (Carlson and Wronski 1979)

One could alternatively measure the conductivity using sandwich-type rather than coplanar electrode arrangements. However, it is difficult to obtain reliable ohmic contacts with the electrodes in the sandwich configuration.

Several authors have suggested that the transport properties are thickness dependent (Solomon et al 1978, Ast and Brodsky 1980). Although the transport properties were measured over a wide range of thicknesses (0.2 - 20 μm) no systematic dependence was observed.

Staebler and Wronski have discovered that g.d. produced films are effected dramatically when exposed to high-intensity light (Staebler and Wronski 1977, 1980). On exposure to light the conductivity is found to decrease by several orders of magnitude. The low conductivity state is stable at room-temperature for many days, however the samples revert to their original state if annealed at temperature between 160-200°C. The effect has also been observed in rf sputtered films but is much smaller. Although Staebler and Wronski put forward suggestions to explain the effect, its origins are still not clear.

2.3.1b Measurement of Photoconductivity

By investigating the photoconductivity of amorphous silicon films important information about the density of states in the gap, transport mechanism and trapping and recombination processes can be obtained. Extensive work has been done on photoconductive properties of g.d. produced a-Si:H (Loveland et al 1973/1974, Spear et al 1974, Spear and LeComber 1976b, Ray et al 1983). The photoconductive properties of reactively sputtered a-Si:H and their dependence on

the preparation conditions have been reviewed in detail by Moustakas and recently by Paul and Anderson (Moustakas 1978, Paul and Anderson 1981).

Moustakas et al (1977) have investigated in detail the effect of varying the preparation conditions on the properties of amorphous silicon. By correlating the magnitude of photoconductivity with the substrate temperature (T_s) and the hydrogen partial pressure (P_H) they were able to optimise these parameters to obtain low defect density material. The optimum substrate temperature was found to be between 200 to 250°C. The variation of photoconductivity with P_H showed two maxima, one at around 0.4 mtorr and the second at about 3.0 mtorr. The decrease in photoconductivity between the first and second maxima was thought to arise from the introduction of Si-H antibonding states at the bottom of the conduction band. Thus suggesting that increasing the hydrogen concentration above a certain level has a detrimental effect on the film properties.

Anderson et al (1979) have investigated the effect of varying the argon pressure (P_{Ar}) on the properties of amorphous silicon films, particularly the dependence of the magnitude of photoconductivity on P_{Ar} . They found that photoconductivity increased by as much as three orders of magnitude as the sputtering pressure was increased from 5 to 30 mtorr. However further increase in pressure resulted in a decrease in photoconductivity. However they observed post-deposition contamination for films deposited at pressures greater than 10 mtorr. They suggested that the increase in photoconductivity with argon pressure was due to the decrease in the kinetic energy of the silicon atoms bombarding the film during its growth. They estimated that for their system at pressures of

about 10 mtorr all the silicon would be thermalised, thus removing the bombardment. This they suggested caused the films produced at P_{Ar} greater than 10 mtorr to be porous and susceptible to post-deposition oxidation. However in their analysis Anderson et al did not consider the effect of hydrogen or argon bombardment which could also significantly affect the properties of the film.

Paesler et al (1978) have considered the affect of incorporating oxygen with the a-Si:H films. They found that incorporating about 1.0 at.% oxygen could increase the photoconductivity by as much as three orders of magnitude.

Due to the negligible photocurrent, the work on the photoconductive properties of conventionally produced pure amorphous silicon has been limited. However amorphous silicon produced by high pressure neon sputtering exhibits similar properties to a:Si:H and detailed work on its photoconductive properties has been reported by the group at Aston University (Abo-Namous and Fane 1984, Abo-Namous et al 1983).

As in the case of dark conductivity, the measurements of photoconductivity can be obscured by surface effects and σ_{ph} has also been found to be thickness dependent. (Brodsky et al 1980, Fritzsche 1980). The photoconductivity can also be affected by light induced changes in the bulk, (Staebler and Wronski 1977, 1980) but this effect is not as common in sputtered films as it is in g.d. produced films.

2.3.1c Optical Absorption

Several extensive reviews on the optical properties of a-Si and amorphous semiconductors in general are available (Mott and Davis 1979, Tauc 1970, 1972, 1974). However in this section the discussion will be limited to rf sputtered a-Si.

The Harvard group have studied in detail the effect of varying the sputtering conditions on the optical absorption in reactively sputtered a-Si:H. (Freeman and Paul 1979, Paul and Anderson 1981). By comparing the absorption edge spectra of unhydrogenated a-Si with those of sputtered samples, where the concentration of hydrogen has been increased systematically, they have observed that the absorption edge sharpens and shifts to higher energies with increasing hydrogen content, and hence, a decreasing density of defect states (Freeman and Paul 1979). The edge sharpness is described by the edge parameter B, which is defined by the equation:

$$(\alpha \hbar\omega)^{\frac{1}{2}} = B(\hbar\omega - E_0) \quad (2.3)$$

where B the edge parameter is a constant, α is the absorption coefficient, $\hbar\omega$ the photon energy and E_0 is the optical gap. This formula was developed by Tauc and is used to define the optical gap of amorphous semiconductors (Tauc 1970).

2.3.2 Compositional Analysis

2.3.2a Determination of the Hydrogen Content

The concentration of hydrogen in a-Si:H films varies from 5 to 50% depending on the preparation conditions. The concentration of hydrogen has been determined by various methods; these include, ^{15}N or ^{19}F nuclear reactions (Brodsky et al 1977 B), secondary ion mass spectrometry (SIMS) (Magee and Carlson 1980), infrared vibrational absorption (Connell and Pawlik 1976, Brodsky et al 1977) and hydrogen evolution (Tsai and Fritzsche 1979). Although the study of the amount of hydrogen incorporated in the films and the mode in which it bonds to the silicon atoms is a very important parameter for optimising the preparation conditions of a-Si:H films, it is not pertinent to the present investigation and will not be discussed further.

Amorphous silicon films termed 'pure' or 'intrinsic' nearly always contain large amounts of the sputtering gas (Ar or Ne) and trace amounts of oxygen. The concentration of these intrinsic impurities depends on the preparation conditions and can significantly influence the optical and electronic properties of the films.

2.3.2b Argon Content

Depending on the preparation conditions the argon content of argon sputtered films can be as high as 8.0 at.%. Ross and Mesier have measured the argon concentration as a function of the sputtering pressure, with various hydrogen partial pressures (Ross and Messier 1981). They have found that the argon concentration decreases from

7 at.% at ^a/sputtering pressure of 5 mtorr to about 0.4 at % at 70 mtorr. They suggest that the self-bias of the substrate platform with respect to the plasma might depend on the sputtering pressure. Thus at low pressures ($P_{Ar} \leq 5$ mtorr) the substrate is more negatively biased, resulting in the bombardment of the film by Ar⁺ ions, however at high pressure ($P_{Ar} > 10$ mtorr) the substrate assumes a self-bias positive with respect to the ground. They also comment that films deposited at low pressures, exhibit little micro-structure or porosity and hence are not effected by post-deposition contamination, whereas films deposited at high pressures suffer from these ill effects. Similar concentrations of argon have been reported by other workers (Tanaka et al 1980, Imura et al 1980, Zaka et al 1984 a).

2.3.2c Neon Content

Usami et al have determined the neon content of a-Si:H film deposited, by rf sputtering, with X-ray photoelectron spectroscopy (XPS). The neon content of a-Si:H films prepared in a plasma of 93% Ne and 7% H₂ gas molecules was found to decrease monotonically from 7 at.% until it becomes undetectable, as the total pressure is increased from 0.2 to 30 Pa(1.5 to 225 mtorr). Films produced under the same neon partial pressure but without any H₂ were found to contain approximately 1.7 times as many neon atoms as those prepared with H₂ (Usami et al 1980).

2.3.2d Oxygen Content

Oxygen incorporated into the film during sputtering or adsorped from the atmosphere after the film has been deposited can greatly

influence the properties. Due to the presence of water vapour in the base vacuum and in the walls of the chamber it is very difficult to reduce the concentration of O_2 to less than about 0.1 at.% (Paul and Anderson 1981). For oxygen concentration greater than 1.0 at.% IR absorption spectroscopy is most commonly used. Qualitative (Paesler et al 1979) and quantitative (Ross and Messier 1981) determination of oxygen content can be obtained by IR absorption studies. Si-O vibrational bands centred at 950 cm^{-1} are due to oxygen incorporated during sputtering, while bands at 1050 cm^{-1} are assigned to post-deposition adsorbed oxygen.

Several workers have reported the effect of varying the preparation conditions on the concentration of oxygen in the films. No post-deposition contamination has been reported for films prepared at argon pressure of less than about 20 mtorr but for films sputtered at higher pressures upto 20 at.% adsorbed oxygen has been reported (Anderson et al 1979, Ross and Messier 1981, Imura et al 1980, Zaka et al 1984 a).

2.4 Doping Effects of Group III and V Elements

Spear and LeComber were the first to successfully dope amorphous silicon films produced by the glow-discharge decomposition of silane (Spear and LeComber 1975). Soon afterwards the substitutional doping of reactively sputtered amorphous silicon was reported by the Harvard group (Paul et al 1976). Recently other techniques of producing a-Si have also been optimised to produce a material with a density of defect states low enough to enable efficient substitutional doping. These techniques include; sputtering at high argon pressures, and high neon pressures. The Japanese groups have done extensive

work on reducing the density of defect states in pure amorphous silicon films by sputtering at high argon pressures. They have successfully doped their films by group III and V elements (Suzuki et al 1980). By co-sputtering boron with silicon they could vary the conductivity of the films over five orders of magnitude. This change in conductivity was accompanied by a corresponding change in the thermal activation energy of over 0.5 eV. Thus indicating that the increase in conductivity with boron incorporation is due to the shift of the Fermi level towards the valance band.

Similar variations in the conductivity and thermal activation energy were obtained with phosphorus, also incorporated into the films by co-sputtering. Doping effects of antimony, aluminium and nitrogen are also reported but the variation in the conductivity is not as significant when these elements are incorporated in the films.

Doping effects comparable with those observed in a-Si:H films have been reported for films prepared by sputtering in pure neon. The conductivity of intrinsic films has been increased by nearly eight orders of magnitude and the thermal activation energy varied over 0.6 eV by co-sputtering with aluminium (Fane and Abonamous 1983). Similar results have also been reported for n-type doping by tantalum (Fane and Zaka 1983 a, b). A more detailed discussion on the effect of n-type doping in neon sputtered amorphous silicon is presented in section (5.3) of this thesis.

3. THEORETICAL CONSIDERATIONS

3.1 Theoretical Models of Amorphous Semiconductors

In this section the electronic and structural models of a-Si, which have been proposed to interpret the experimental results, are briefly discussed. The discussion of the theory is limited to those areas where it is pertinent to the present study. Comprehensive reviews on the theoretical considerations in the study of amorphous materials can be found elsewhere (Mott and Davis 1979, Brodsky 1979). Also included in this chapter is a brief review of the background theories of the techniques employed in the present study for compositional analysis (e.g. RBS, AES, XPS). Finally in this chapter a section is included on the basic theory of rf sputtering, a topic which is of paramount importance in a study concerned with optimising the preparation condition to achieve 'good quality' amorphous silicon films.

3.1.1 The Gap States in Amorphous Silicon

Amorphous semiconductors are defined as semiconducting materials which lack long range ordering of their constituent atoms, but retain some short range order, in that the nearest neighbour bond length and to some extent the bond angle are preserved (Brodsky 1979). Crystalline semiconductors which possess both long and short range order, have a density of electronic states characterized by sharp band edges at the top of the valence band and at the bottom of the conduction band, giving rise to a well defined energy gap between the valence and the conduction bands. Since the short range order of most materials in the amorphous state is similar to

that in the crystalline state, there is a general similarity of the overall distribution of the density of states in the valence and conduction bands (Davis 1979). The effect of the destruction of the long range order in amorphous semiconductors is to introduce electronic states in the energy gap. One of the first suggestions to explain the effect of disorder on the electronic states in the energy gap of amorphous semiconductors was made by Sir Neville Mott. He suggested that the conduction and valence band edges tailed into the gap, and that these tail states were localised in space (Mott 1967). The states are localised in the sense that an electron placed in these states will not diffuse at zero temperature to other states. The destruction of long range order will also create many structural defects such as dangling bonds and microvoids in the material. These defects have the effect of introducing acceptor and donor like states in the gap. These defect states, like the tail states are also localised. In the valence and conduction bands the states are extended which means that the electron wave functions occupy the entire volume. It has further been suggested that at $T = 0$ the mobility is zero in the localised states but finite in the extended. Thus sharp mobility edges occur at the top of the valence band (E_V) and the bottom of the conduction band (E_C).

Several models have been proposed for the band structure of an amorphous semiconductor. Most of the models are similar in the sense that they all incorporate the ideas discussed above, but differ in the description of the structure of the density of states in the mobility gap.

Figure (3.1 a) shows the model proposed by Cohen, Fritzsche and Ovshinsky, known as the CFO model (Cohen et al 1969). The model was proposed to explain the electrical and optical properties of amorphous covalent alloys, of group IV, V, and VI elements. The authors suggested that due to the compositional and structural disorder, a high density of localised states tailing in from the valence and conduction bands would occur in the gap. They further proposed that the valence and conduction band tails extend across the gap in a structureless distribution, overlapping in the middle of the gap. This means that there are states in the valence band, which are normally filled, that have higher energies than states in conduction band which are normally unfilled. Therefore a redistribution of the electrons must take place. The electrons from the top of the valence band tail fall into the spatially distinct states in the lower conduction band tail. This self-compensation ensures that the Fermi level is pinned near the middle of the gap, as required to explain the electrical properties of these materials.

Figure (3.1 b) illustrates the model developed by Davis and Mott (Davis and Mott 1970, Mott et al 1975). Mott and Davis envisage the tail states extending only a few tenths of an electron volt into the gap. They suggest that these states arise from the absence of long-range order in the material they further propose that due to the dangling bonds and microvoids present in the material bands of donor and acceptor like states are introduced into the middle of the gap. As with the CFO model sharp mobility edges at E_C and E_V are postulated.

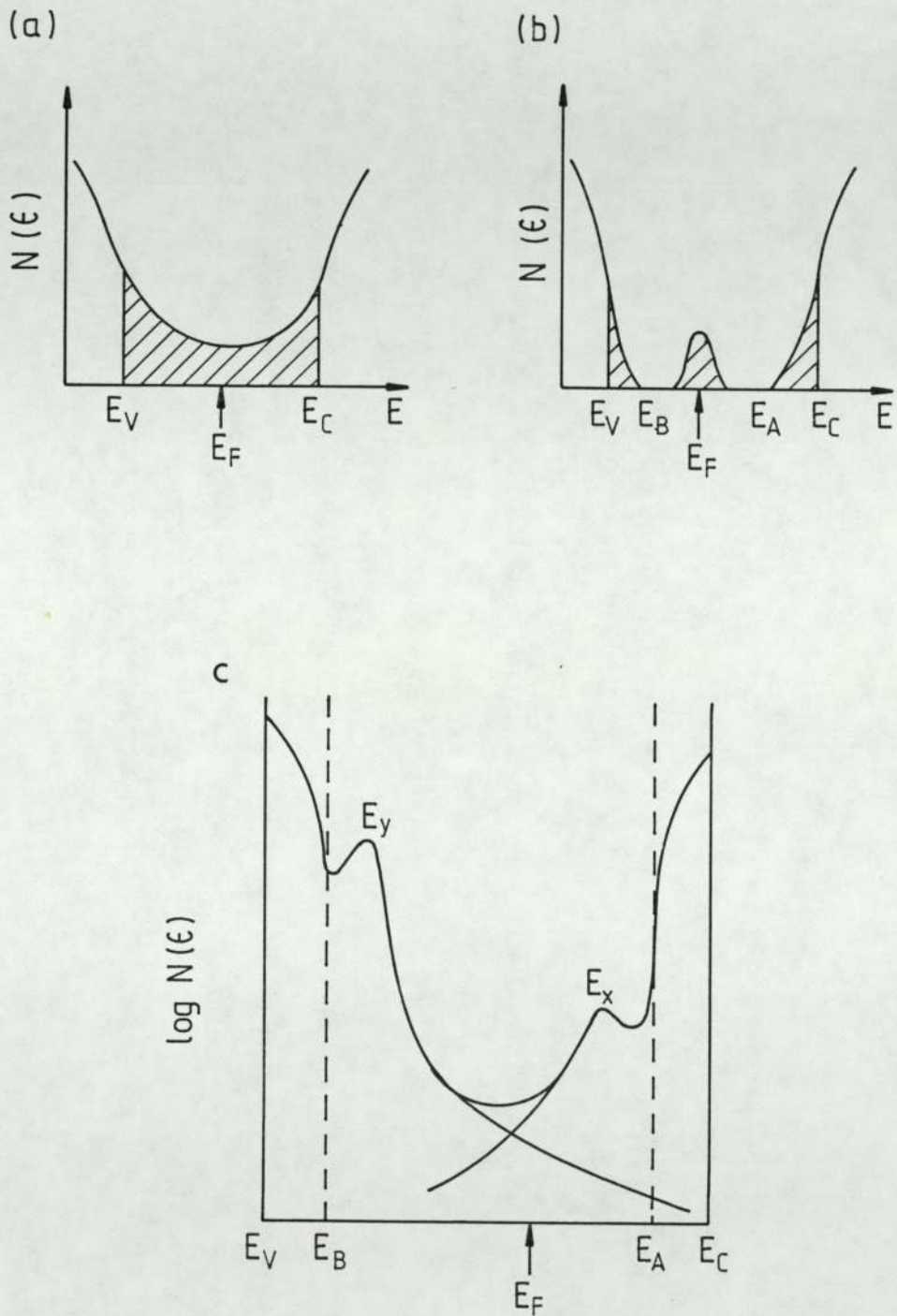


Figure 3.1 Various models for the density of states distribution in the mobility gap. (a) CFO, (b) Davis and Mott and (c) Dundee model.

Finally, figure (3.1c) shows the model for the density of states in the 'mobility' gap developed by the Dundee Group (Spear et al 1974, Madan et al 1976). This model has perhaps gained the most significance in describing the electrical and optical properties of amorphous silicon. The model was developed after extensive studies of the density of states of glow-discharge produced amorphous silicon by the field effect technique. This model is in many respects a combination of the CFO and the Davis and Mott models. As suggested by the CFO model the density of states extends across the gap, but states in the middle of the gap are not thought to be the tail states but originate from defect states centred at E_x and E_y . The tail states from the conduction and valance bands are thought to end at E_a and E_b .

3.2 THE INTERPRETATION OF TRANSPORT MEASUREMENTS

3.2.1 Electrical Conduction in Amorphous Semiconductors

The interpretation of the electrical transport data depends on the model for the energy distribution of the density of defect states. The present data can be interpreted consistently by employing the model proposed by the Dundee Group (figure 3.1 c). To re-cap, the main features of this model are mobility edges at E_c and E_v separating the extended states in the bands from the localised states in the gap. There is a continuous distribution of localised states in the gap, with the tail states ending at E_a and E_b and bands of defect states centred at E_x and E_y and overlapping in the centre of the gap. On the basis of this model there can be three processes leading to conduction in amorphous semiconductors. However their relative contribution to the total conductivity will

predominate at different temperature regions. At very low temperatures the conduction is predominantly by electrons hopping from one localised site to another at the Fermi level (E_f). At higher temperatures the charge carriers are excited into the localised states of the band tails and they contribute to conductivity by hopping at energies close to E_a and E_b . At still higher temperatures the charge carriers are excited across the mobility gap into the extended states, where the mobility is much higher than that in the localised states. Therefore by measuring the electrical conductivity over a wide temperature range the density of states in the 'mobility gap' can be probed. The formulae of electrical conductivity dealing with these processes will be discussed in the next sections. The discussion will be limited to electrons as the charge carriers although analagous formulae can be derived for hole conduction.

3.2.1a Extended State Conduction

The conductivity (σ) due to electrons excited beyond the mobility edge at E_c into the extended states is given by (Mott and Davis 1979).

$$\sigma = \sigma_0 \exp \left[\frac{-(E_c - E_f)}{\kappa_b T} \right] \quad (3.1)$$

where E_f is the Fermi level and σ_0 the pre-exponent parameter.

Optical absorption measurements on amorphous semiconductors (Freeman and Paul 1979) have shown that the optical gap decreases with increasing temperature. Therefore the energy distance $E_c - E_f$

will show a similar behaviour, assuming a linear temperature dependence.

$$E_c - E_f = (E_c - E_f)_0 - \delta T \quad (3.2)$$

where $(E_c - E_f)_0$ is the energy difference between the Fermi level and the mobility edge at E_c at $T = 0$ K, and δ is the temperature coefficient. Estimates of δ can be obtained by measuring the temperature coefficient (γ) of the optical gap and assuming $\gamma = \delta/2$.

When this type of conduction is predominant a plot of $\ln \sigma$ versus $1/T$ will yield a straight line. The thermal activation energy ($\Delta E = E_c - E_f$) can be obtained from the slope of the plot and the pre-exponent factor from the intercept on the σ axis.

The pre-exponent parameter σ_0 is given by the expression.

$$\sigma_0 = e N(E_c) \kappa_b T \mu_c \exp(\delta / \kappa_b) \quad (3.3)$$

where $N(E_c) \kappa_b T$ is the effective density of states, μ_c is the electron mobility at E_c . Mott (1970) has estimated that for extended state conduction the pre-exponential (σ_0) should lie in the range between 10 and $10^3 (\Omega \text{cm})^{-1}$ in most semiconductors. For amorphous silicon prepared over a wide range of preparation conditions σ_0 is found to be consistently between 10^3 and $10^4 \Omega^{-1} \text{cm}^{-1}$.

3.2.1b Conduction in the Band Tails

At lower temperatures the electrons are only excited as far as the localised states at the band edges. There they contribute to conductivity by thermally activated hopping at energies close to E_a and E_b (Fig 3.1c). For this process the conductivity is given by (Mott and Davis 1979).

$$\sigma = \sigma_1 \exp \left[\frac{E_a - E_f + W_1}{\kappa_b T} \right] \quad (3.4)$$

where W_1 is the activation energy for hopping and σ_1 is the pre-exponent factor. When this type of conductivity is predominant, $\ln \sigma$ versus $1/T$ will again yield a straight line, but with a reduced slope. The value of σ_1 is expected to be much smaller than σ_0 . This is because of a lower effective density of states at E_a compared to E_c and also because the mobility will be lower. For doped samples it is expected that the predominant current path will shift from the band tail states at E_A to donor states at an energy E_d . Le Comber et al (1977) have estimated from Hall effect measurements the approximate energies at which E_a and E_d are likely to occur. Figure 3.2 illustrates the model used by them to explain their results. It shows the density of state distribution, $g(E)$ near E_c and on the right the three current paths: in the extended states above E_c , the donor band at E_d and the tail states at E_a .

3.2.1c Conduction in Localised States at the Fermi Energy

In all the models discussed, there is a finite density of states at the Fermi level (E_f). At very low temperatures the pre-

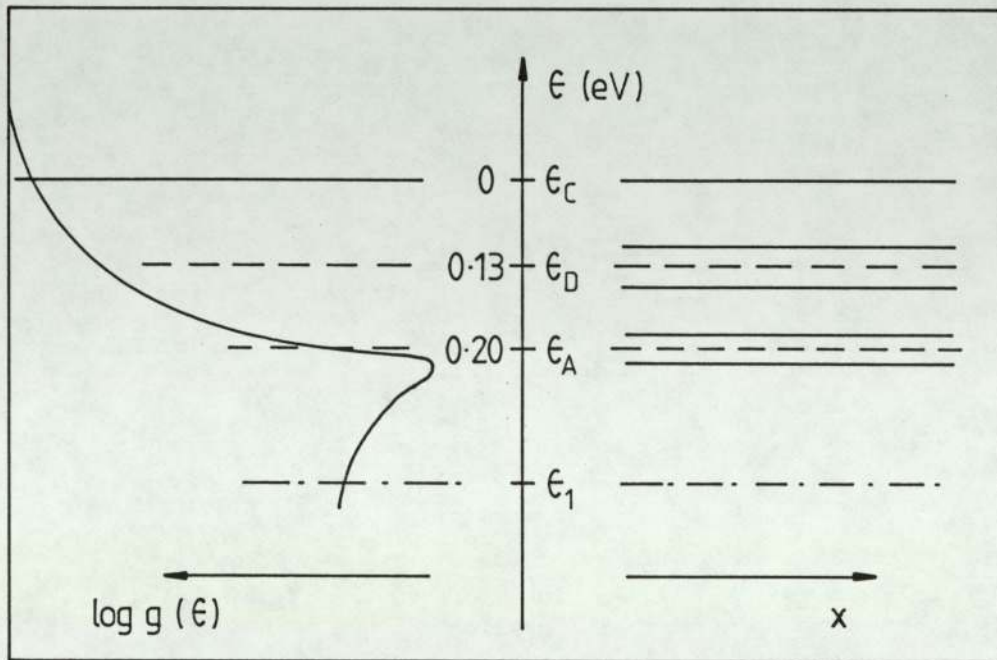


Figure 3-2 Model used by Dundee group for the analysis of the Hall effect data. LeComber et al (1977)

dominate mode of transport is thought to be by charge carriers hopping between the states around the Fermi level by phonon-assisted tunnelling. This type of process is thought to be analogous to conduction in heavily doped crystalline semiconductor. The conductivity for this type of transport is given by (Mott and Davis 1979).

$$\sigma = \sigma_2 \exp(-W_2/k_b T) \quad (3.5)$$

where W_2 is the hopping energy and σ_2 the pre-exponent factor. However Mott (1969) has suggested that at very low temperatures, rather than hop to the nearest neighbour site, for which the electron needs to gain an energy W_2 from the lattice, it is more likely that it will hop a longer distance if this requires a smaller energy jump. This process is called variable range hopping. When it occurs via localised states around the Fermi-level it leads to an expression for the conductivity of the form (Mott 1969, 1979).

$$\sigma = \sigma_2 \exp(-B/T)^{\frac{1}{4}} \quad (3.6)$$

where σ_2 is the pre-exponent factor and B is the parameter containing the density of states at the Fermi level $N(E_f)$ and given by the expression:

$$B = \frac{16 a^3}{k_b N(E_f)} \quad (3.7)$$

where a^{-1} represents the rate of fall-off of the wave function at a site. By plotting $\ln \sigma$ against $T^{-\frac{1}{4}}$ an estimate of $N(E_f)$ can be made from equation (3.6) and (3.7), if a reasonable guess is made for a^{-1} .

3.2.2 Temperature Dependence of Electrical Conductivity

Although there is general consensus on the various modes of transport discussed above, there is still considerable controversy regarding which process dominates at a particular temperature range. To illustrate the point the interpretation put forward by the Dundee and Harvard groups will be discussed. Detailed discussion with reference to other equally plausible models can be found elsewhere (Mott and Davis 1979, Anderson and Paul 1981, 1982, Döhler 1979, Overhof and Beyer 1980).

A typical plot of $\ln \sigma$ versus $1/T$ obtained by the Dundee group is shown in figure (3.3a) (LeComber and Spear 1970). LeComber et al suggest that the transport in region (1) is due to carriers excited into the extended states just above E_c where they estimate the mobility to be between 1 and $10 \text{ cm}^2\text{V}^{-1}\text{S}^{-1}$. From the slope of the plot in this temperature range (Room temperature to $T_1 \approx 250\text{K}$) they estimated the thermal activation energy ($\Delta E = E_c - E_f$) to be about 0.62 eV. They suggested that in the second temperature range (250 - 200 K) the major conduction path has switched to hopping at the tail states close to E_a . In this region they calculated the thermal activation energy to be approximately 0.52 eV. For the third region (200 - 100 K) they suggest that as the temperature is lowered the major electron hopping path shifts closer and closer to the Fermi energy.

The Harvard group have measured the temperature variation of conductivity of their intrinsic and doped films to much higher temperatures ($\approx 500\text{K}$). Figure (3.3b) shows plots of $\ln \sigma$ versus $1/T$ for a series of phosphorous doped samples (Anderson and Paul 1982).

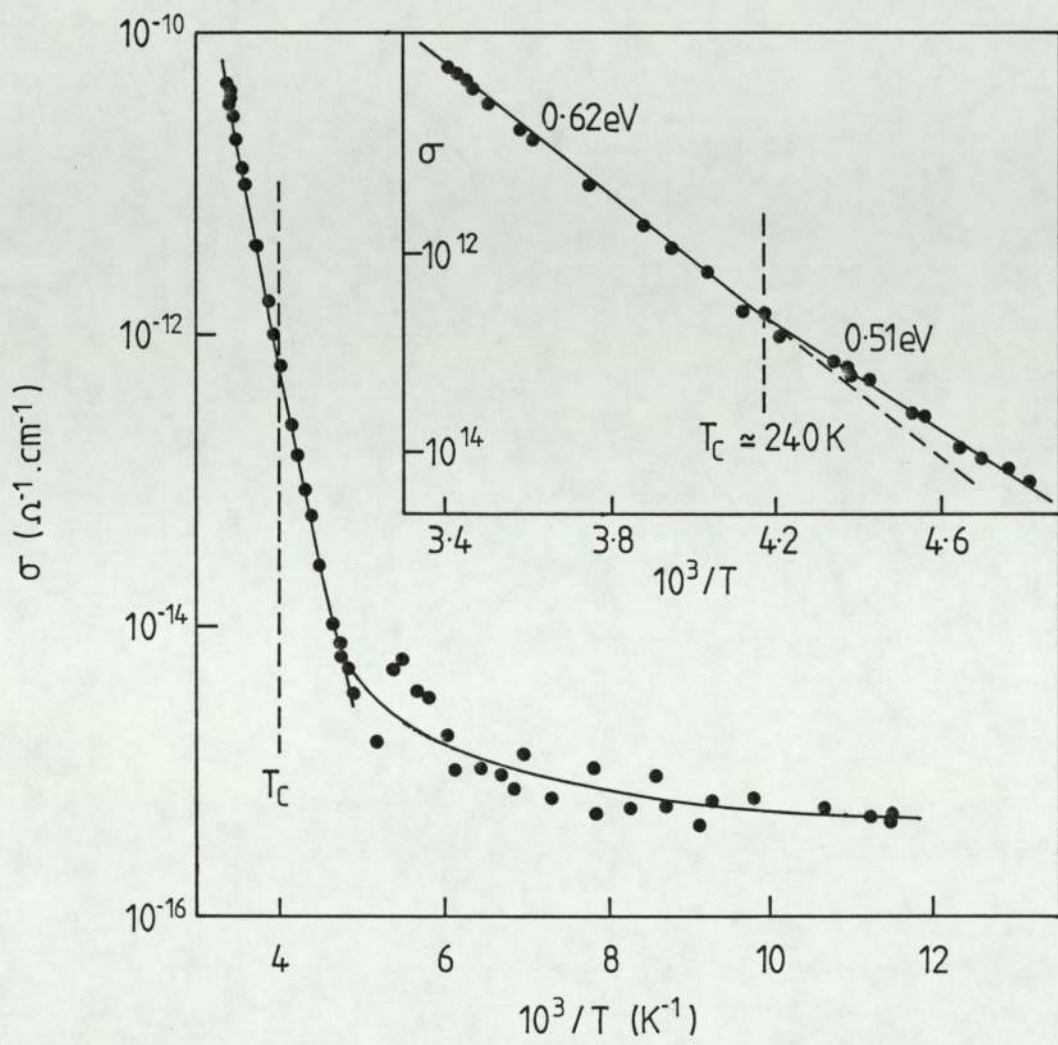


Figure 3.3a The variation of electrical conductivity with inverse temperature of g.d. produced films. (LeComber and Spear 1970)

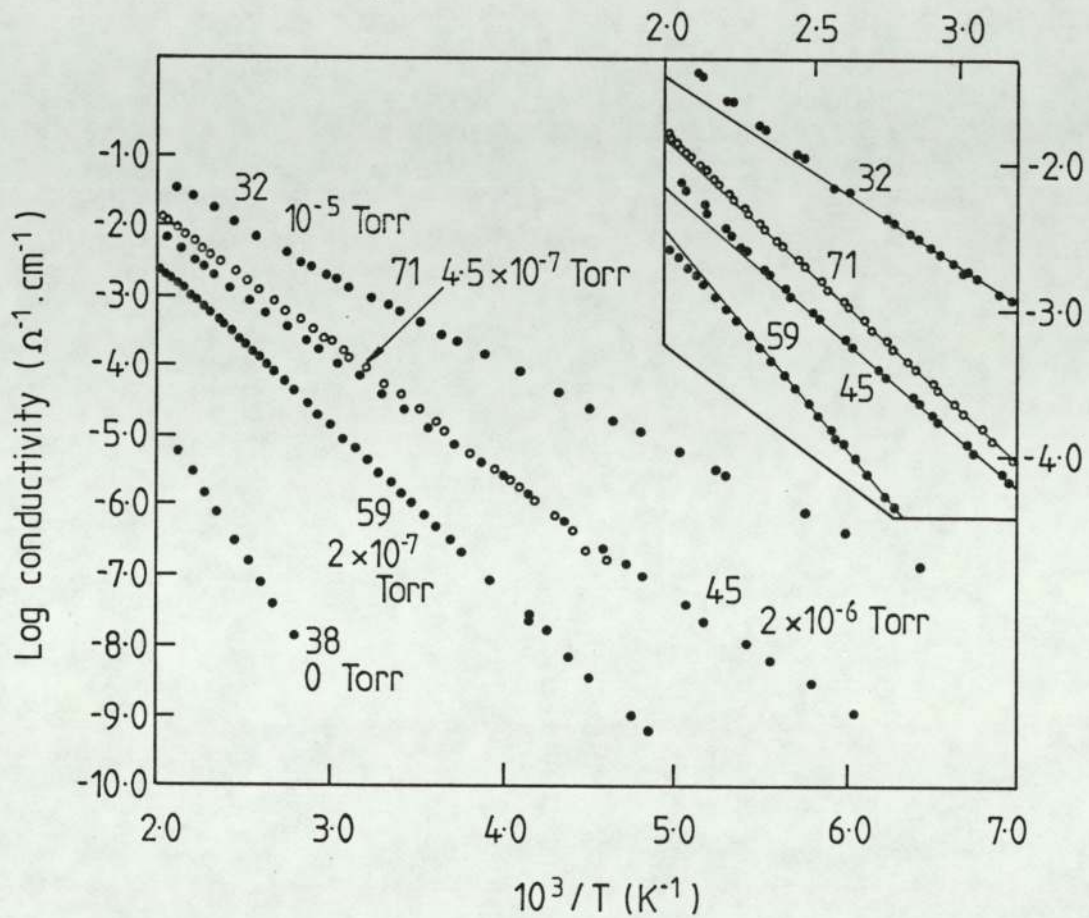


Figure 3.3b Conductivity versus $10^3/T$ for a series of phosphorus doped sample. (Anderson and Paul 1982)

Again three temperature regions have been defined but in this case the high temperature region is for temperatures above 400K, the intermediate region extends from 200 to 400 K. To explain their results the Harvard group suggest that the transport takes place in two parallel energy levels. Extended state transport is thought to be only dominant at temperatures in excess of 400 K. As evidence for this hypothesis the kinks observed in the plots of $\ln \sigma$ versus $1/T$ at high temperatures are cited.

None of the models for the electrical transport in amorphous semiconductors advocated in the literature can explain the totallity of the experimental results. In the present investigation the high temperature kinks in plots of $\ln \sigma$ versus $1/T$ were observed in many of the doped samples. However to facilitate comparison of the present results with other published data the broad temperature region from room temperature to about 400 K is identified with extended state conduction.

3.3 Optical Absorption

The optical properties have been studied extensively to investigate the electronic structure of amorphous silicon. The discussion in this section will be limited to the determination of absorption coefficient and the optical gap from transmission measurements in the UV-VIS region.

The optical gap in crystalline materials is generally obtained by fitting the data to some model of how the absorption coefficient (α) depends on the photon energy ($E = \hbar \omega$). In general, for amorphous semiconducts the spectral dependence of α can be divided into three

regions (Connell 1979, Tame 1974). Figure (3.4) illustrates schematically the variation of α with $\hbar \omega$ (Connell 1979). The optical absorption edge in region C ($\alpha > 10^5 \text{ cm}^{-1}$) represents transitions between extended states. At intermediate energies, region B ($10^3 \text{ cm}^{-1} < \alpha < 10^5 \text{ cm}^{-1}$) an exponential variation of with $\hbar \omega$ is observed. This is generally attributed to transitions involving the valance and conduction band tail states. The absorption edge at the lowest energies (region A) is related to the defect states in the mobility gap.

However only region C can be probed by direct absorption measurements, due to the weak absorption signal below the optical gap (E_0). To determine the absorption edge at intermediate and low energies, other indirect techniques for obtaining the absorption coefficient are employed (Abeles et al 1980).

The absorption coefficient (α) can be deduced from the transmittance, Tr , with a reasonable accuracy for $\alpha > 10^3 \text{ cm}^{-1}$, using the relation.

$$Tr = (1 - R) \exp (-\alpha t) \quad (3.8)$$

where t is the thickness of the film and $(1 - R)$ is the value at which the interference averaged transmittance levels off at higher wavelengths. By plotting the absorption coefficient thus obtained, as a function of the photon energy the shape of the absorption edge can be obtained. Extensive studies have been carried out on the correlation of the shape of the absorption edge with the preparation conditions (Loveland et al 1973, 1974). The general conclusion is that as the preparation conditions are optimised, and hence the density

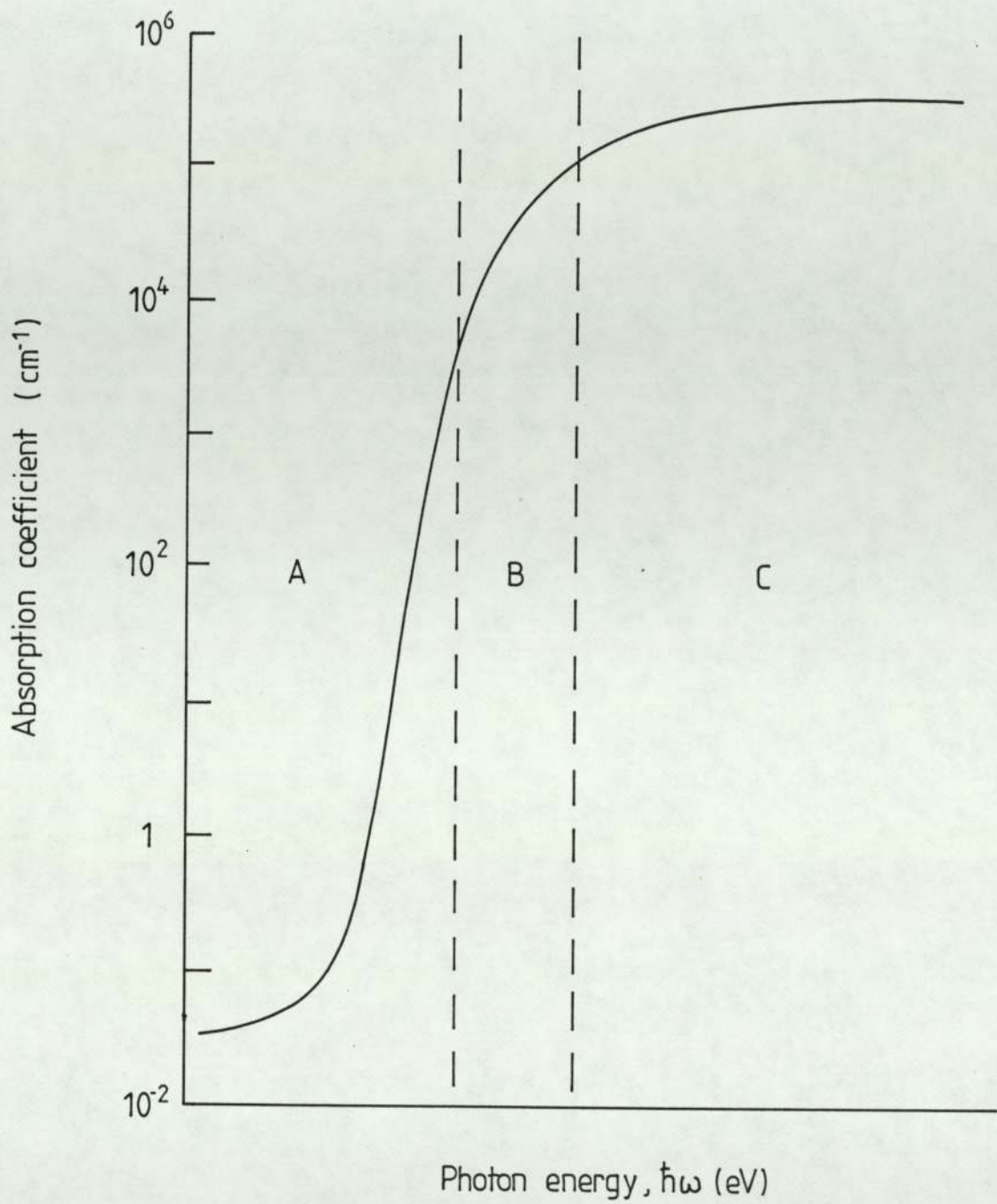


Figure 3.4 The variation of the absorption coefficient with photon energy for amorphous semiconductors. (Connell 1979)

of states in the mobility gap reduced, the absorption edge sharpens and shifts to higher energies. Figure (3.5) shows the absorption edges in amorphous silicon prepared by different methods (Loveland et al 1973, 1974).

To determine the optical gap, expression (3.9), developed by Tauc to describe the high absorption region, is normally employed (Tauc 1974)

$$(\alpha \hbar \omega)^{\frac{1}{2}} = B (\hbar \omega - E_0) \quad (3.9)$$

where B is a constant containing the average matrix element and the joint density of states for the conduction and valence bands. In deriving this formula it has been assumed that the transitions are between two parabolic densities of states region and that all energetically allowed transitions are equally possible. Thus the optical gap can be obtained by plotting $(\alpha \hbar \omega)^{\frac{1}{2}}$ versus $\hbar \omega$ and extrapolating to zero.

3.4 BACKGROUND THEORY OF THE TECHNIQUES FOR COMPOSITIONAL ANALYSIS

3.4.1 Rutherford Backscattering Spectroscopy (RBS)

3.4.1a Introduction

The basic concepts of RBS are quite simple. A beam of monoenergetic alpha particles (${}^4\text{He}^{+}$) is directed towards the sample. Most of the beam penetrates deep into the sample but a few of the ions undergo large angle collision with the target nuclei and come back out of the sample. The energy of backscattered ions is then determined by a detector (normally, surface barrier detectors are

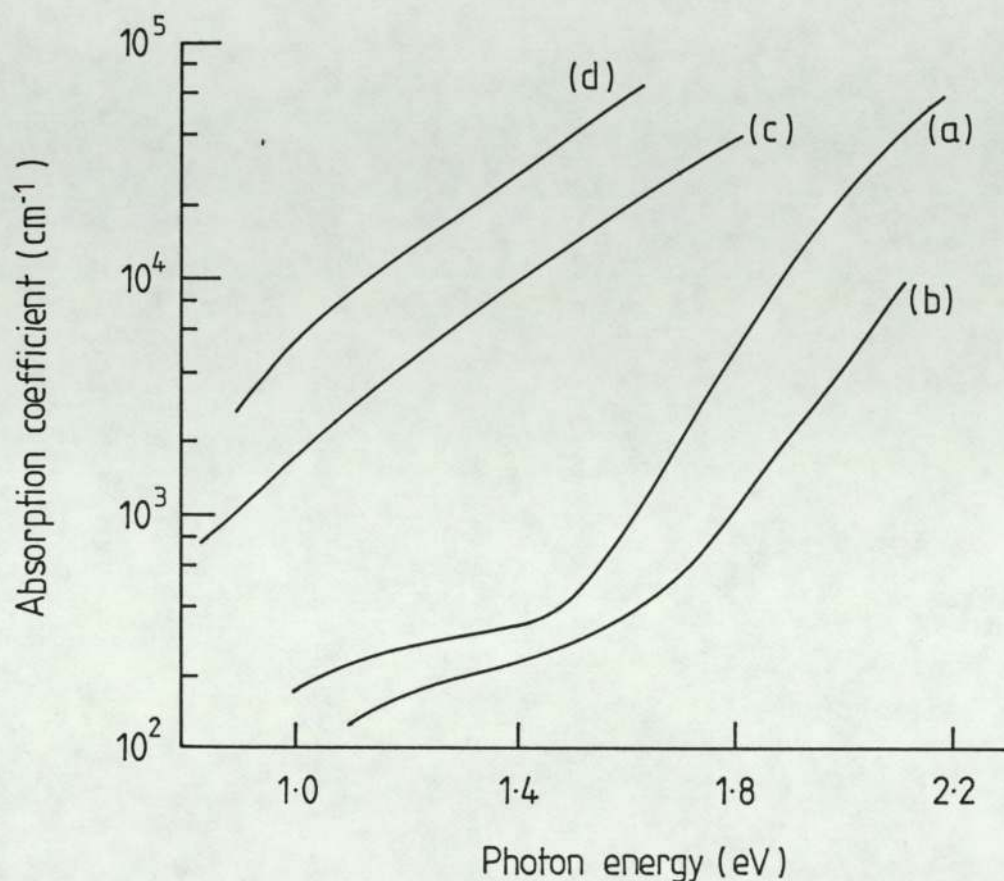


Figure 3.5 The variation of the absorption coefficient with photon energy for a number of amorphous - silicon sample prepared by different methods. (a) glow discharge specimens, T_d from 500 to 600K, (b) glow discharge specimens, $T_d \approx 300K$, (c) specimen produced by r.f. sputtering, (d) specimen produced by evaporation (Loveland et 1973/74)

employed). The energy of the backscattered ion can be related to the mass of the target nuclei via the rule of the conservation of momentum. Thus the energy of the backscattered ion is proportional to the difference between the mass of the helium ion and the target nuclei. How many ions are scattered depends on the scattering cross-section. The scattering cross-section is proportional to $(Z \text{ target})^2$, thus more scattering occurs from high atomic number atoms and less from lower ones. The strength of RBS lies in its ability to depth profile a sample, this is due to the fact that as the ion beam penetrates the sample; it loses small amounts of energy due to interactions with electrons in the solid. The ions scattered from deeper in the film will appear with slightly less energy. These concepts are summarised schematically in figure (3.6), which shows the position of the peaks for various elemental samples. The detailed derivation of the equations describing the processes outlined above can be found elsewhere (Ziegler et al, Chu et al 1978). Here the discussion will be limited to citing the equations and briefly discussing their significance.

3.4.1b Mass Analysis

The energy of the backscattered particles are governed by the conservation laws. The ratio of backscattered energy (E_b) to the initial energy (E_i) is given by the expression.

$$K = \frac{E_b}{E_i} = \left[\frac{m \cos \theta + \sqrt{M^2 - m^2 \sin^2 \theta}}{m + M} \right]^{1/2} \quad (3.10)$$

where K is the kinematic factor, m the mass of the projectile, M the mass of the target atom and θ is the scattering angle in the lab system.

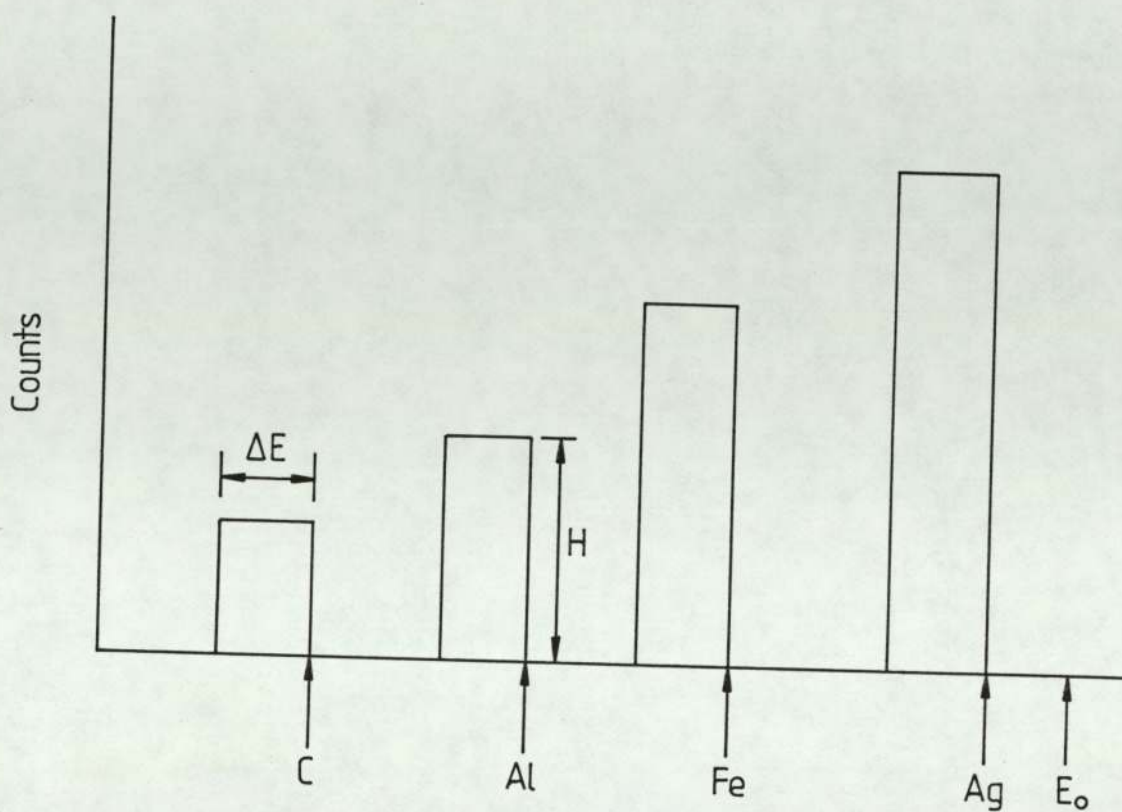


Figure 3.6 RBS spectrum from a hypothetical sample containing equal amounts of C, Al, Fe and Ag. E_0 is the energy of the bombarding ions.

Since E_i , θ and m are known, by measuring E_b the equation (3.10) can be solved for M .

3.4.1c Quantitative Analysis

Quantitative compositional analysis can be obtained by measuring the peak heights (H) of the various elements present in the film. If H_m and H_i are the peak heights of the host material and the impurity element respectively at the surface of the sample. Then H_m and H_i are given by the expression.

$$H_m = Q \Omega \sigma_m N_m \delta E_1 / [S]_m^m \quad (3.11 a)$$

$$H_i = Q \Omega \sigma_i N_i \delta E_1 / [S]_i^m \quad (3.11 b)$$

where Q = incident charge

Ω = solid angle of the detector

σ_m and σ_i = average differential scattering cross section evaluated at the incident energy (E_0)

N_m and N_i = intrinsic densities

$[S]_m^m$ and $[S]_i^m$ = are backscattering energy loss factor

δE_1 = the energy width of a channel

The impurity concentration can be obtained by eliminating Q , Ω and δE , from equation 3.11 a and 3.11 b, ie.

$$\frac{H_m}{H_i} = \frac{N_m}{N_i} \cdot \frac{\sigma_m}{\sigma_i} \cdot \frac{[S]_i^m}{[S]_m^m} \quad (3.12 a)$$

$$\text{or } N_i = \frac{H_i}{H_m} \cdot \frac{\sigma_m}{\sigma_i} \cdot \frac{[S]_i^m}{[S]_m^m} \cdot N_m \quad (3.12 \text{ b})$$

since the values of σ 's are tabulated and the energy loss factors can be estimated (Chu et al 1978) the impurity concentration can be calculated from the measurement of the spectrum height ratio H_i/H_m .

3.4.1d Depth Analysis

As the beam of ions penetrates the sample it will lose some energy due to the interaction of the ions with the electrons in the solid. Similarly after the ions have been scattered at a depth t they will lose energy is emerging from the sample. Thus the energy loss of the $^4\text{He}^+$ can be directly related to the thickness of the films. If dE is the difference in energy of ions scattered from the front face and from the back face of the sample then.

$$dE = N[E]t \quad (3.13)$$

where N is the atomic density, t the thickness of film and $[E]$ the stopping cross-section. The stopping cross-section is given by

$$[E] = \frac{K}{\cos \theta_1} E_{in} + \frac{1}{\cos \theta_2} E_{out} \quad (3.14)$$

where E_{in} is the stopping cross-section of the ions during their inward path and E_{out} is the stopping cross-section during the outward path, θ_1 is the angle between the target normal and the incident beam direction and θ_2 is the angle between the target normal and the exit path. Various approximations for the determination of E_{in}

and E_{out} may be used since their value depends on the energy of the ions as they traverses the material. These approximations are discussed in the literature and will not be given here (Chu et al 1978, Foti et al).

Thus if the atomic density ($N = \text{atoms/cm}^3$) is known the energy width of a peak (dE) can be directly related to the thickness. Alternatively since, $N = N_0 \rho / A$, where N_0 is the Avagadro's number, ρ the density of the film and A the atomic weight, the density (ρ), can be determined from equation 3.13 if the thickness of the films is measured independently.

3.4.2 Auger Electron Spectroscopy (AES) and X-ray Photoelectron Spectroscopy (XPS)

3.4.2a The Basic Principles of AES

In Auger electron spectroscopy a focused beam of electrons in the energy range of 1-10eV irradiates the sample. The electrons can penetrate as much as 1-2 μm into the sample. Some of the atoms of the sample will become ionised in the core level (X). One of the processes by which the atom can return to the ground state is by an electron falling from a higher level (Y) to occupy the vacancy at the X level, to balance the energy an electron from an outer level (Z) is then emitted. This electron is called the Auger electron and was first discovered by Pierre Auger (1925). The process is illustrated schematically in figure (3.7a).

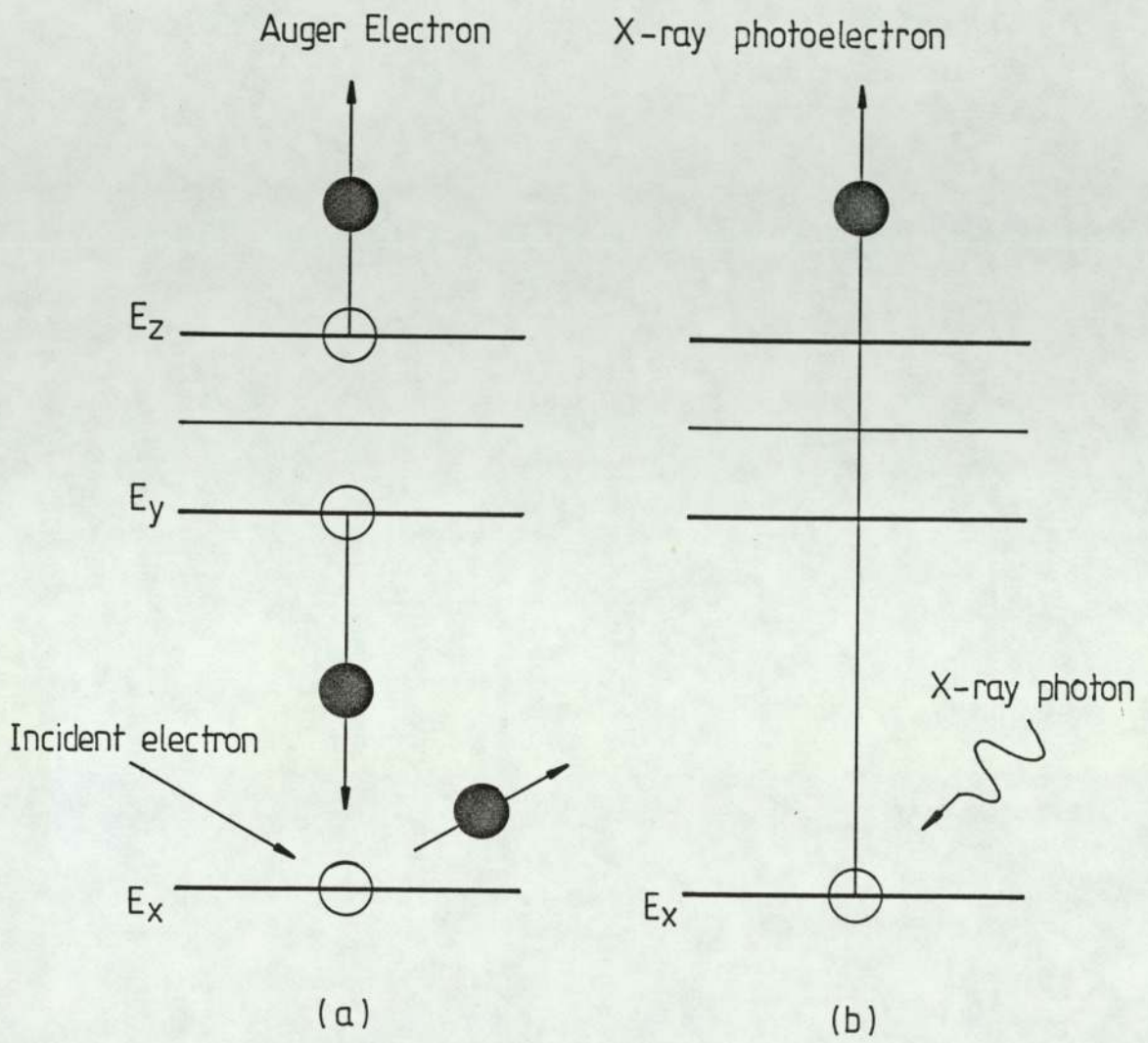


Figure 3-7 Schematic representation of (a) the Auger process and (b) the XPS mechanism.

The Auger electron is emitted with an energy E_A , defined algebraically by:

$$E_A = E_Z - E_Y - E_X - \Delta A \quad (3.15)$$

where E_X , E_Y and E_Z are the ground state core level energies of the pure element. ΔA is a term to allow for the local chemistry and possible final state effects and is generally less than 20 eV (Briggs and Rivierre 1983). Since the energy of the Auger electron (E_A) as expressed in equation (3.15) depends only on atomic energy levels, analysis of the Auger energy immediately leads to elemental identification.

Although the atoms of the sample are ionised to depths of upto 1-2 μm by the electron bombardment only Auger electrons of the atoms in the top few layers escape without suffering inelastic scattering. It is this which makes the process so surface sensitive. The characteristic information length is given by the inelastic mean free path, λ , which depends on the Auger electron energy, E_A , and the matrix element.

Besides the Auger electrons there are a large number of secondary and inelastically scattered primary electrons. The emitted spectrum thus shows Auger electron peaks on a large smoothly varying background. To make the Auger peaks prominent it is customary to differentiate the spectrum.

To quantify the spectrum it is best to determine a set of empirical sensitivity factors, S_i , for each element, i , in the pure state for the spectrometer used in the analysis. Alternatively

relative sensitivity factors reported in the literature can be used (Davis et al 1978). However to use the tabulated sensitivity factors the analyser must be of the same model and be operated at the resolution and modulation as that used for deriving the reference data (Sheah 1983). Once the relative sensitivity factors have been determined the concentration of any impurity can be found by employing the equation:

$$C_A = \frac{I_A/S_A}{\sum I_i S_i} \quad (3.16)$$

where I_A is the intensity of the signal from element A which is present in the solid with a concentration of C_A . Equation (3.16) has been derived by Chang (1974) from basic principles on the assumption that backscattering contributions to the Auger electron intensity and the inelastic mean free path are matrix insensitive.

3.4.2 Basic Principles of XPS

In X-ray Photoelectron Spectroscopy (XPS) the atoms are ionised by irradiating the sample with a mono-energetic beam of x-rays. Usually Al or Mg K α X-rays of energies 1486.6 eV and 1253.6 eV respectively are used. The X-rays of energy, $\hbar\omega$ eject photoelectrons directly from the core level E_X as shown in figure (3.7b). The kinetic energy (E_K) of the emitted electron is given by the equation:

$$E_K = \hbar\omega - E_B - \phi \quad (3.17)$$

where E_B is the binding energy of the electron in the solid and ϕ is the difference between the work functions of the solid and the spectrometer.

Therefore the kinetic energy of the photoelectron can be directly related to the binding energy of the material and hence provide chemical identification.

Equation (3.16) is also used for quantitative analysis in XPS. The intensity of the photoelectron peak can be measured either by measuring the peak height or the peak area. Various methods of subtracting the background have been suggested (Shirley 1972). The relative sensitivity factors for XPS have been determined by Wagner et al (1979). In determining the relative sensitivity factors Wagner et al (1979) used the values of the photoionisation cross-section calculated by Scofield (1976) and the values of the elastic mean-free path calculated by Penn (1976).

3.5 BASIC THEORY OF RF SPUTTERING

3.5.1 The Mechanism of Sputtering

Sputtering is defined as the ejection of surface particles by positive ion bombardment. Observations of this phenomena was first recorded over a century ago by Grove (1852) who noticed the disintegration of cathodes in glow discharge tubes. Although several mechanisms have been proposed to explain the phenomena of sputtering, many have been discarded, it is now thought that the ejection of particles occurs as a result of the direct transfer of momentum from the bombarding ion to the atoms of the target (Stark 1909). The collision between the bombarding ion and the target atom can be considered as a binary collision. The energy transferred is characterised by the energy transfer function.

$$\frac{4 M_i M_t}{(M_i + M_t)^2} \quad (3.18)$$

where M_i and M_t are the masses of the incident and the target atoms respectively. However since the sputtered atoms can only come from the surface layers the sputtering yield (S) will also depend on how much energy is deposited in a given distance; this is given by the nuclear stopping power $S(E)$. For low bombarding energies an expression for $S(E)$ has been developed by Sigmund (1969).

$$S(E) = \frac{M_i M_t}{(M_i + M_t)^2} E \times \text{constant} \quad (3.19)$$

where E is the energy of the incident ion, equation (3.19) has been employed to predict the sputtering yield S .

$$S = 3 \alpha \frac{4 M_i M_t}{(M_i + M_t)^2} \frac{E}{U_0} \quad (3.20)$$

where U_0 is the surface binding energy of the material being sputtered and α is a monotonic increasing function of M_t/M_i ranging from 0.17 for $M_t/M_i = 0.1$ to 1.4 for $M_t/M_i = 10$. Equation (3.19) predicts that the sputtering yield will increase linearly with energy (E) but we should not expect to find a maximum yield when $M_i = M_t$ as suggested by the energy transfer function alone. This is borne out by experimental observation, that although neon and argon ions would transfer equal amounts of energy when colliding with a silicon atom as given by equation (3.18) the sputtering yield is higher for the argon atoms because of their higher stopping cross-section.

3.5.2 R.f. Sputtering

DC sputtering cannot be used to sputter insulating targets. This is because positive charge would accumulate on the surface of the target and hence repel any further bombardment by positive ions. Wehner (1955) suggested that these problems could be overcome if a high frequency potential was applied to a metal electrode placed underneath the insulator. His ideas were put into practice by Anderson et al (1962) who were the first to develop an r.f. sputtering system. However their apparatus had many disadvantages. Many of the problems were overcome by the modifications made by Davidse and Maissel (1965). The present system is based on their design and is known as the grounded diode arrangement. Figure (3.8) shows the essential features of such an arrangement. Usually the substrate electrode is grounded and the target electrode is capacitively coupled to the r.f. generator. The target is also capacitively coupled to the target electrode and hence an rf voltage is induced on the front surface of the target. In the negative half of the r.f. cycle, the ions are attracted towards the target and in the positive half cycle, the electrons are attracted towards the target. This results in the dielectric surface acquiring a negative bias for most of the r.f. cycle. The surface potential is positive for only a short period of time in which enough electrons are attracted to the surface to neutralise the positive ion charge accumulated during the rest of the cycle. The process is described in detail by Butler and Kino (1963) who have also developed a quantitative theory to explain the effect.

The accumulation of positive charge around the target is referred to as the plasma sheath, and most of the voltage drop is

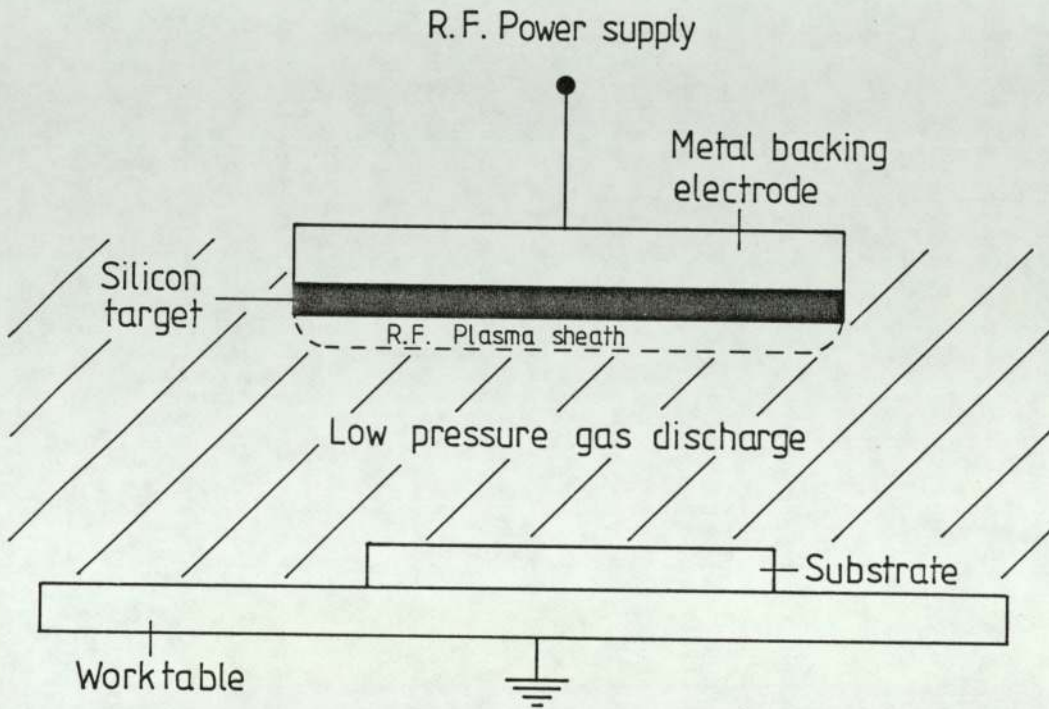


Figure 3·8 The essential features of a grounded diode sputtering system

across this sheath. The plasma sheath has a much lower luminosity than the glow region and is commonly known as the 'dark space'. This is because the discharge glows as a result of the relaxation of atoms excited by electron impact, but since the density of electrons in the sheath is very low, it does not glow as much. The self bias potential is close to half the value of the peak to peak rf voltage appearing on the target surface. The ions are accelerated essentially by the bias potential (V_{sb}) rather than the r.f. potential and bombard the target with an energy of the order of V_{sb} electron volts.

The plasma which contains approximately equal densities of positive and negative charge is essentially field free. This is because of the high mobility of the electrons in the plasma. Also as a consequence of the high electron mobility the plasma is the most positive part of the system.

In an r.f. system with two electrodes of equal areas one would expect both the electrodes (target and the substrate holder) to assume equal self-bias voltages. If however the electrodes are of unequal areas than the voltage developed will be greater on the smaller electrode. In the present system the 'large' electrode consists of the ground shield around the target, the ground substrate holder, the base plate and all other ground parts in the system. Thus the self bias voltage developed on the target electrode is much greater. The detailed discussion of the significance of the relative size of the target electrode and the non-target area in contact with an r.f. discharge can be found elsewhere (Butler and Kino 1963, Koenig and Maissel 1970, Horwitz 1982).

4. EXPERIMENTAL DETAILS

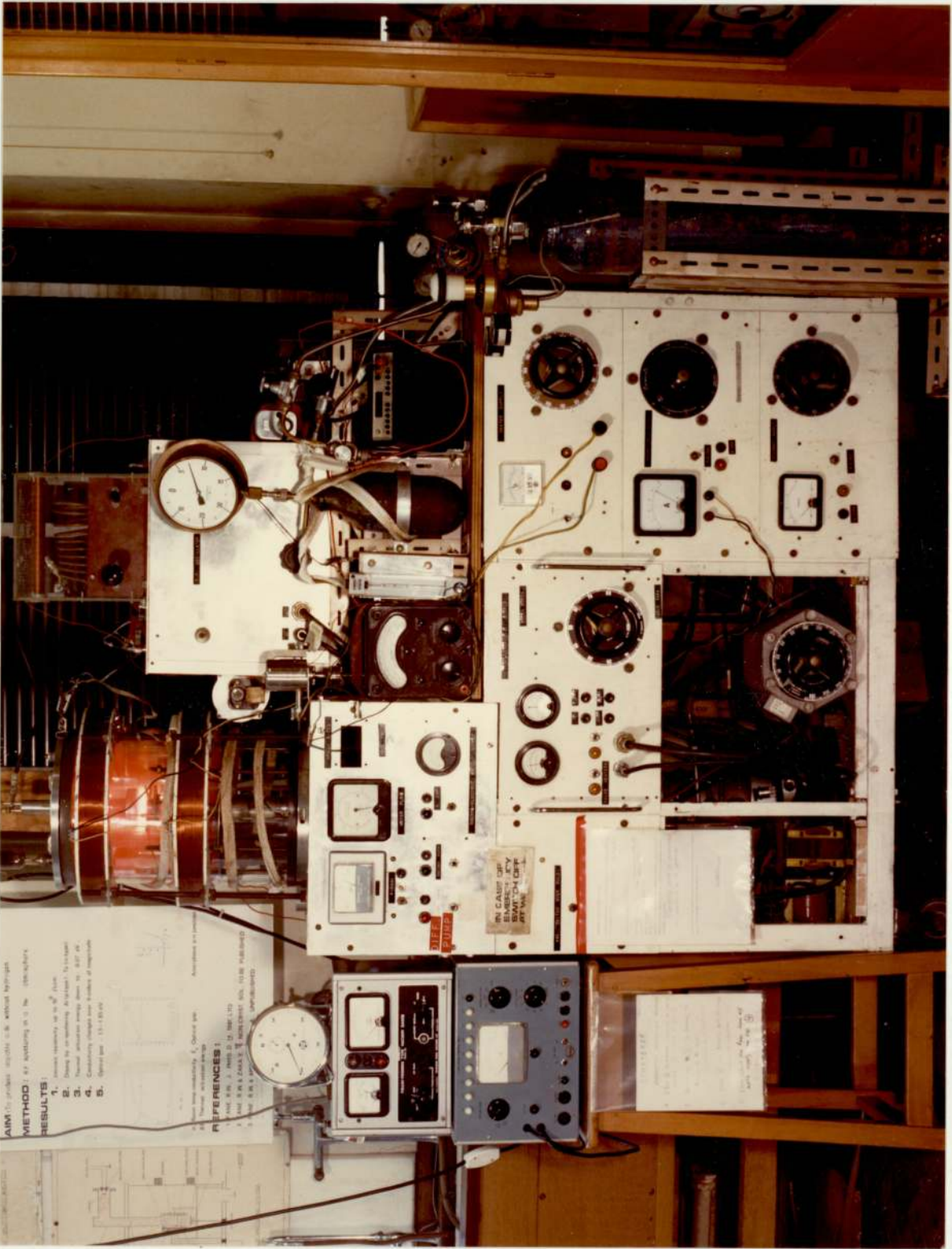
4.1 PRODUCTION OF AMORPHOUS SILICON FILMS

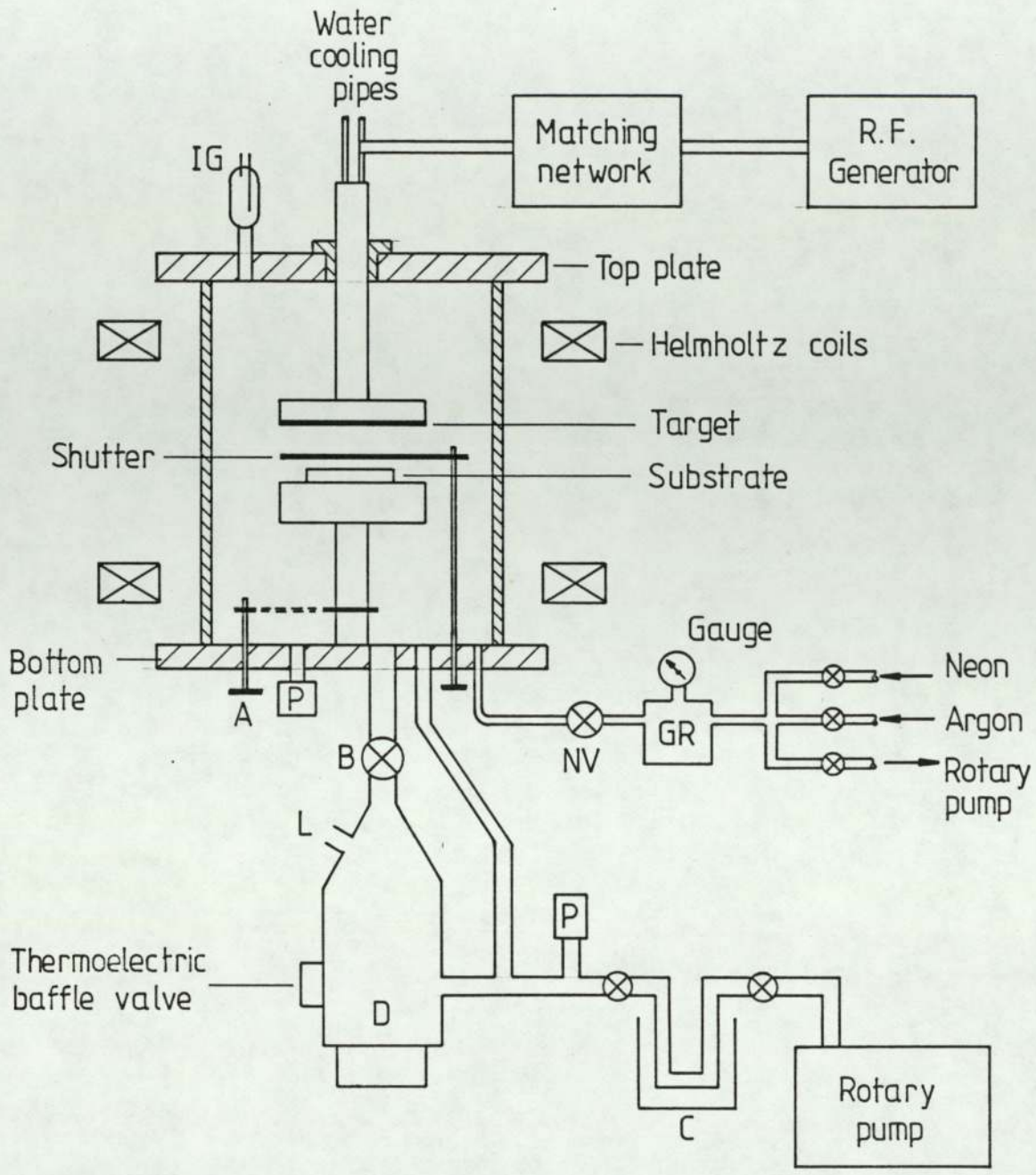
4.1.1 DESIGN OF THE RF SPUTTERING SYSTEM

The films employed in this study were deposited in an rf diode sputtering system constructed in the laboratory. The design of the basic arrangement is described in detail by Newman (1972). In this section a general description of the system is given and the modifications made during the course of the present work are described. The design of the apparatus follows a conventional rf powered diode sputtering arrangement (Jackson 1970). The general layout of the equipment is illustrated schematically in figure (4.1) and the whole assembly is pictured, in operation in plate (4.1).

The sputtering chamber was constructed from a 12" diameter $\frac{1}{4}$ " thick borosilicate glass cylinder 18" long with flat ground ends. These were sealed by viton L gaskets to the top and base plates, both of which had ports let in them to allow the introduction of various components into the chamber. The top plate carried the ionization gauge and the target assembly. The target assembly is shown schematically in figure (4.2 a). Tubes for water cooling the target also served as leads for the rf supply. The water cooling tubes and the target electrode were made from stainless steel. To prevent the electrode from being sputtered it was surrounded by an earth^{ed} shield. The cooling water lead through tubes were earthed by a tube bolted to the top plate. The target holder was shielded by a copper shroud which was held in position by bolting it to the earth tube shielding the water lead through. To prevent

Plate 4·1 The r.f. sputtering unit in operation.





- | | | | |
|---|---|----|----------------------|
| A | Arrangement to lift and lower substrate | IG | Ionization gauge |
| B | Baffle valve | NV | Needle valve |
| C | Cold trap | GR | Gas reservoir |
| D | Diffusion pump | P | Piranni gauge |
| | | L | Liquid nitrogen trap |

Figure 4-1 General layout of the sputtering system.

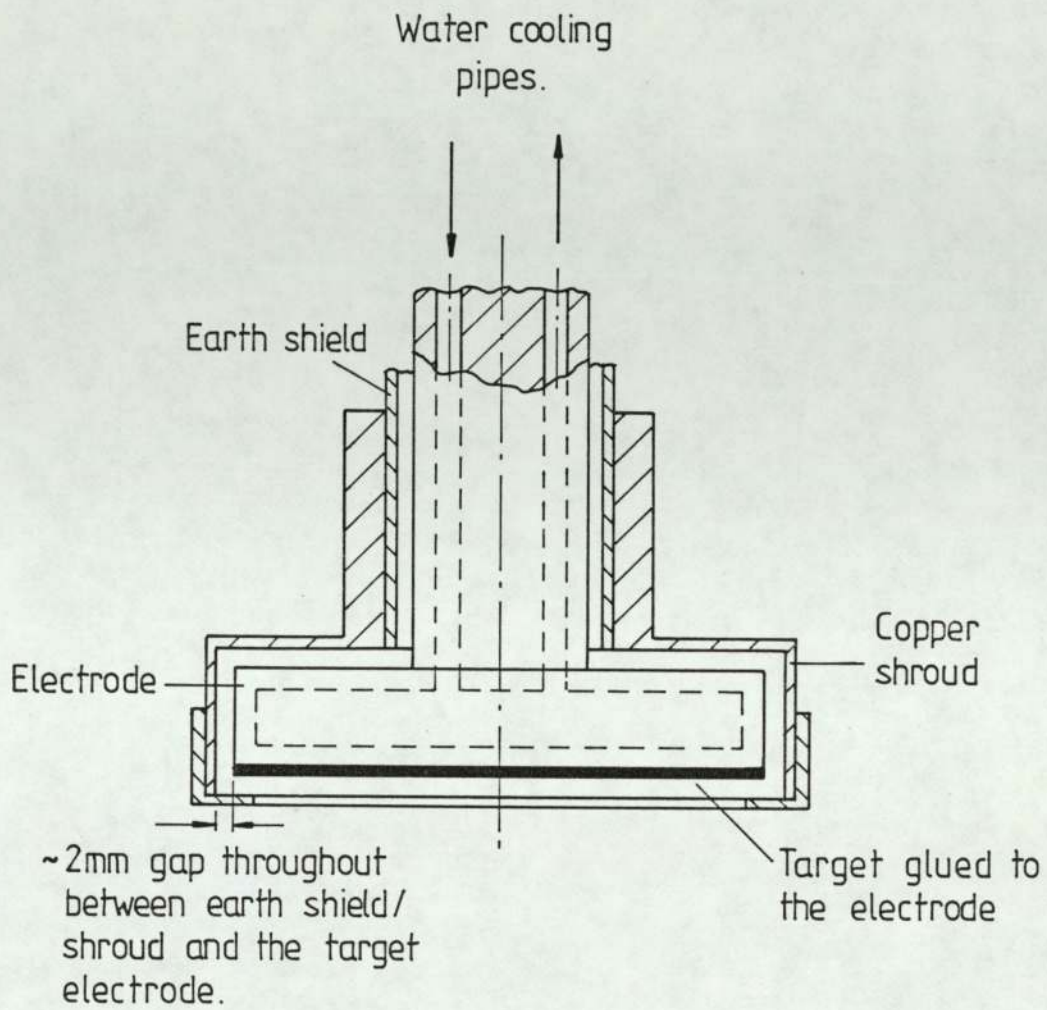


Figure 4.2a The target electrode.

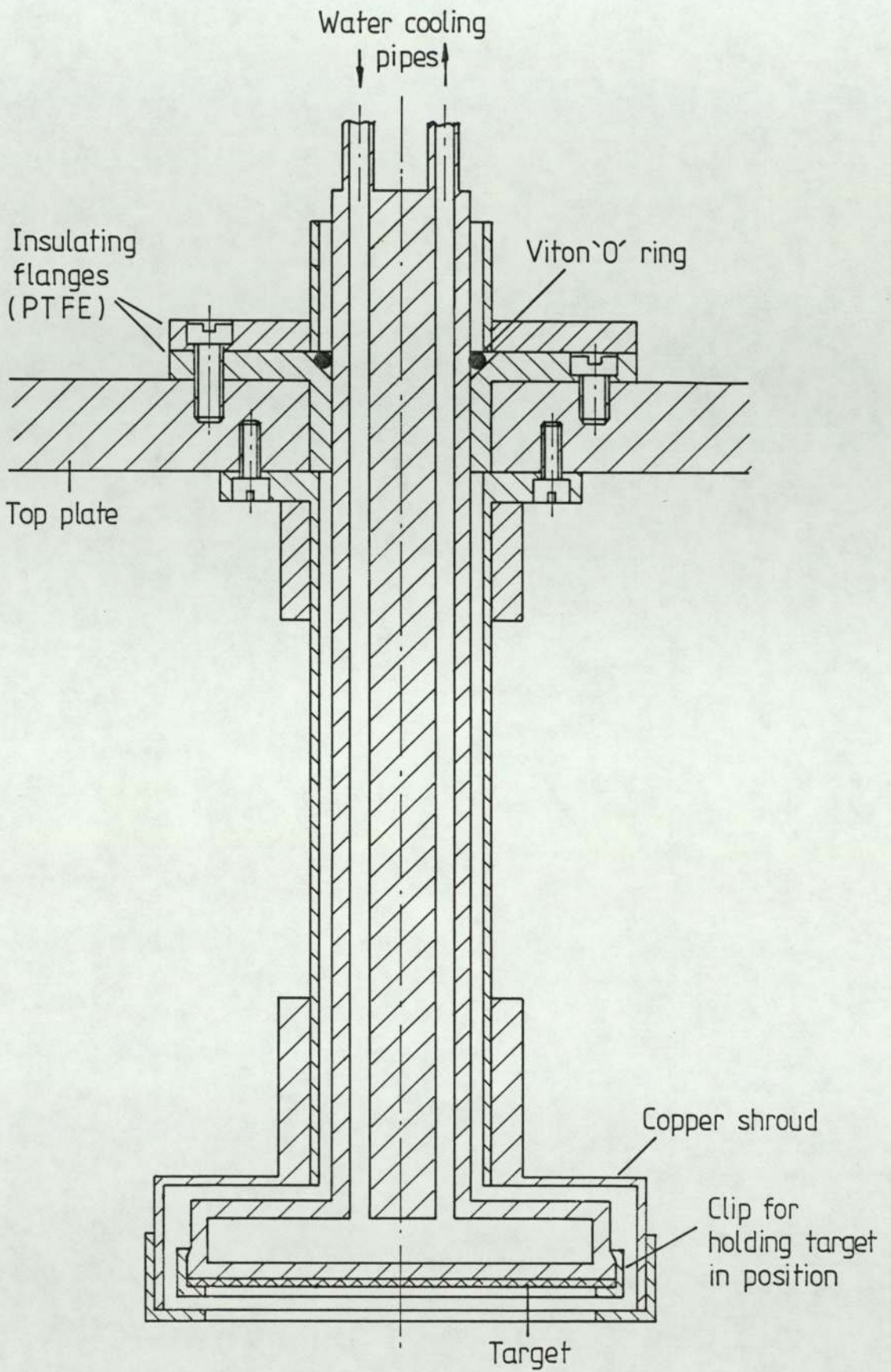


Figure 4·2b The target assembly ,with the 'new' target holder.

the sides of the electrodes from being sputtered the copper shroud slightly overlapped the target. The spacing between the target electrode and the earth shielding was kept at 2mm, which is just less than the length of the dark space at the highest pressures used during the course of this work. To operate at higher pressures one would have to reduce this spacing so that it was always less than the dark space, but in doing so capacitive losses to earth would be increased (Rock and Smith 1975). By setting the spacing between the target and the earth shield at 2mm an upper limit to the sputtering pressure was about 120 mtorr in argon and 300 mtorr in neon.

Electronic grade, single crystal silicon in the form of thin wafers (7.0 cm dia., 0.4 mm thickness) were used as targets. The wafers had a room-temperature resistivity of about $12 \Omega\text{cm}$ and were kindly supplied by Mullard Southampton. The silicon target was stuck onto the electrode by glueing it with a thermally conductive adhesive (732-Dow Corning). However, with this arrangement the target was always destroyed when attempts were made to change it. To overcome this problem a new electrode was designed so that the silicon target could be clipped onto the electrode, thus avoiding the use of an adhesive. A thin layer of "RS Heat Sink Compound" ensured good thermal contact between silicon and the electrode. Figure (4.2 b) is a schematic diagram of the new electrode; it also indicates the modifications made to the copper shroud to satisfy the changes in the electrode.

The substrates were placed on the grounded electrode, positioned directly beneath the target electrode. The substrate heater could be heated up to 450°C by a nichrome strip with a

resistance of $3.6 \Omega\text{m}^{-1}$ wound on a cut mica former. The heating element was sandwiched between two mica sheets, which insulated the nichrome strip from stainless steel and copper plates bolted on either side of the heating element. The stainless steel plate was bolted onto the substrate holder as shown in figure (4.3a). The temperature of the substrate holder was measured by a chromel-alumel thermocouple which was attached to the surface. Although with this arrangement temperatures up to 350°C could readily be obtained, operations at higher temperatures resulted in the mica flaking and contaminating the chamber, which can lead to the increase in the number of pin holes in the sputtered film. It was also noticed that there was a slight curvature in the top plate, due to it being bolted on to the substrate holder. This probably led to non-uniform heating of the substrate. To overcome these problems a new substrate heater was designed. Four 100Ω , 17W , wire wound resistors were connected in parallel and encased in a copper holder as shown in figure (4.3b). The temperature was measured at two points by chromel-alumel thermocouples. For all the experiments the reading between the two thermocouples was the same within the experimental errors. For some of the experiments one of the thermocouples was placed on top of a Corning 7059 glass slide. During the baking period and just prior to sputtering the temperature of the glass slide was about $15\text{--}20^\circ\text{C}$ below that of the copper plate, but after sputtering it was nearly always slightly greater than the temperature of the copper plate. Since it is very difficult to determine the real surface temperature of a growing film (Anderson and Paul 1981) all the temperature measurements reported here, are the average temperature of the substrate holder during sputtering. The average temperature of the substrate holder was determined by measuring the temperature of the copper plate just before and after

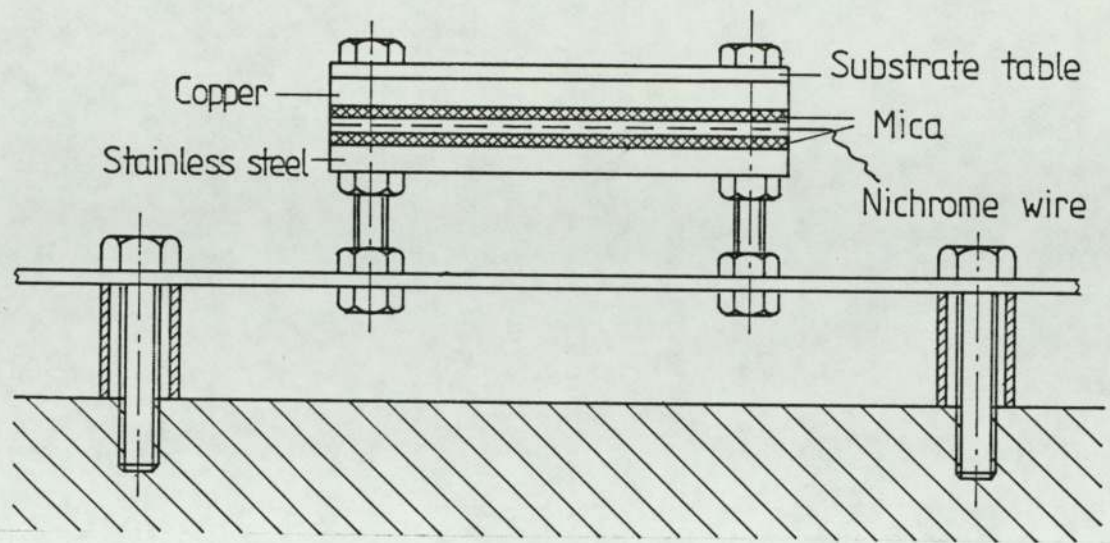


Figure 4-3a. The substrate holder assembly.

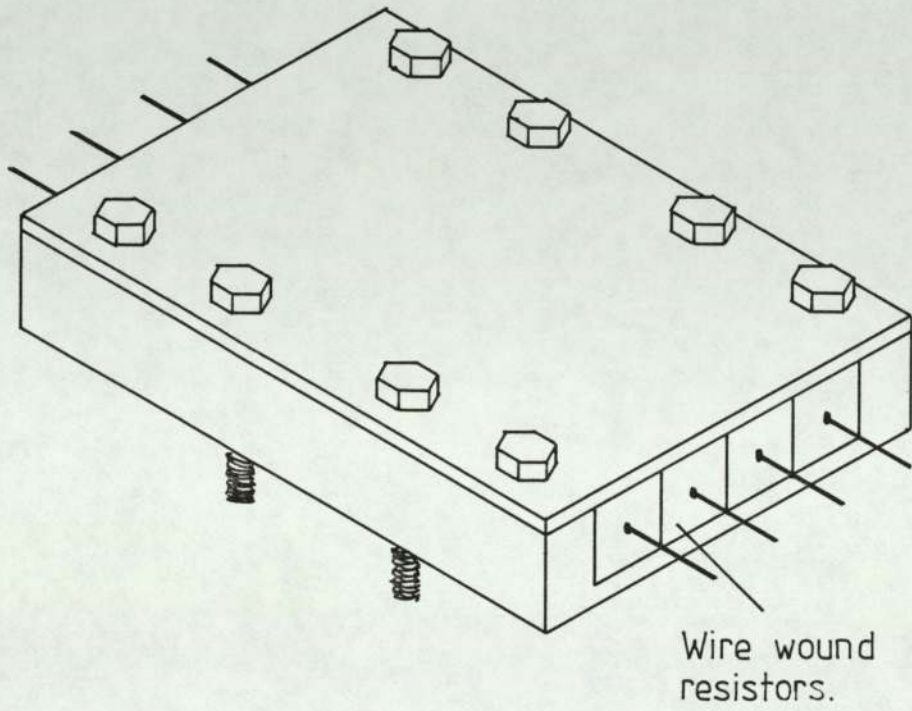


Figure 4.3b The 'new' substrate holder.

sputtering. During sputtering the temperature of the substrate holder increased due to bombardment by the plasma species. To offset this increase in temperature the current to the heater was reduced during sputtering and the temperature could be kept to within $\pm 20^{\circ}\text{C}$ of the desired value. The second junction of the chromel-alumel thermocouple was at room temperature and the overall accuracy of the temperature measurement about $\pm 5^{\circ}\text{C}$.

The substrate electrode could be moved vertically and the distance between the target and substrate electrodes varied from 2 to 6 cm. The position of the substrate holder was varied from outside the chamber by a rotating lead through.

A Helmholtz pair of coils placed outside the chamber gave a magnetic field perpendicular to the plane of the target and substrate holder. This has the effect of concentrating the discharge in the centre of the chamber thus reducing the plasma interaction with the walls. A maximum current of about 5.0 A to the coils gave a field of about 0.015T at the centre of the discharge. Figure (4.4a) is a plot of the axial magnetic field at the centre of the chamber versus the current supplied to the Helmholtz pair of coils. The magnetic field was measured using a Hall effect magnetometer. The shape of the combined magnetic field from the coils has been determined by Newman and is illustrated in figure (4.4b).

Pure (99.999%) noble gases were stored in a bottle fitted with a 'Budenberg' gauge which measured pressure up to 15 lb/in² and vacuum level down to 30 in.Hg. Gases were always kept at a pressure greater than 5 lb/in² so that contamination of the chamber could be avoided even if a small leak developed in the system. The gas

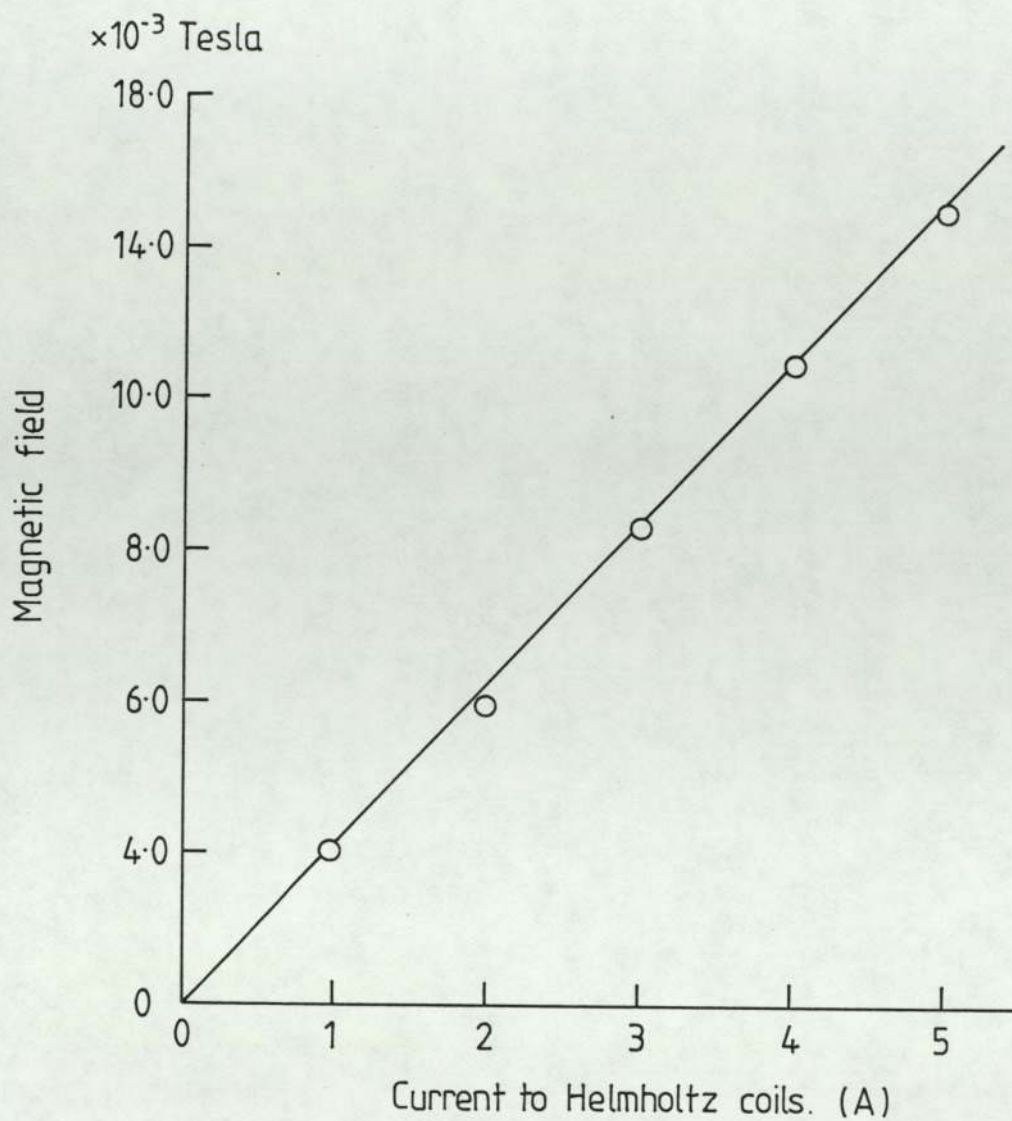


Figure 4.4a. Axial magnetic field at the centre of the chamber as a function of the current applied to the Helmholtz pair of coils.

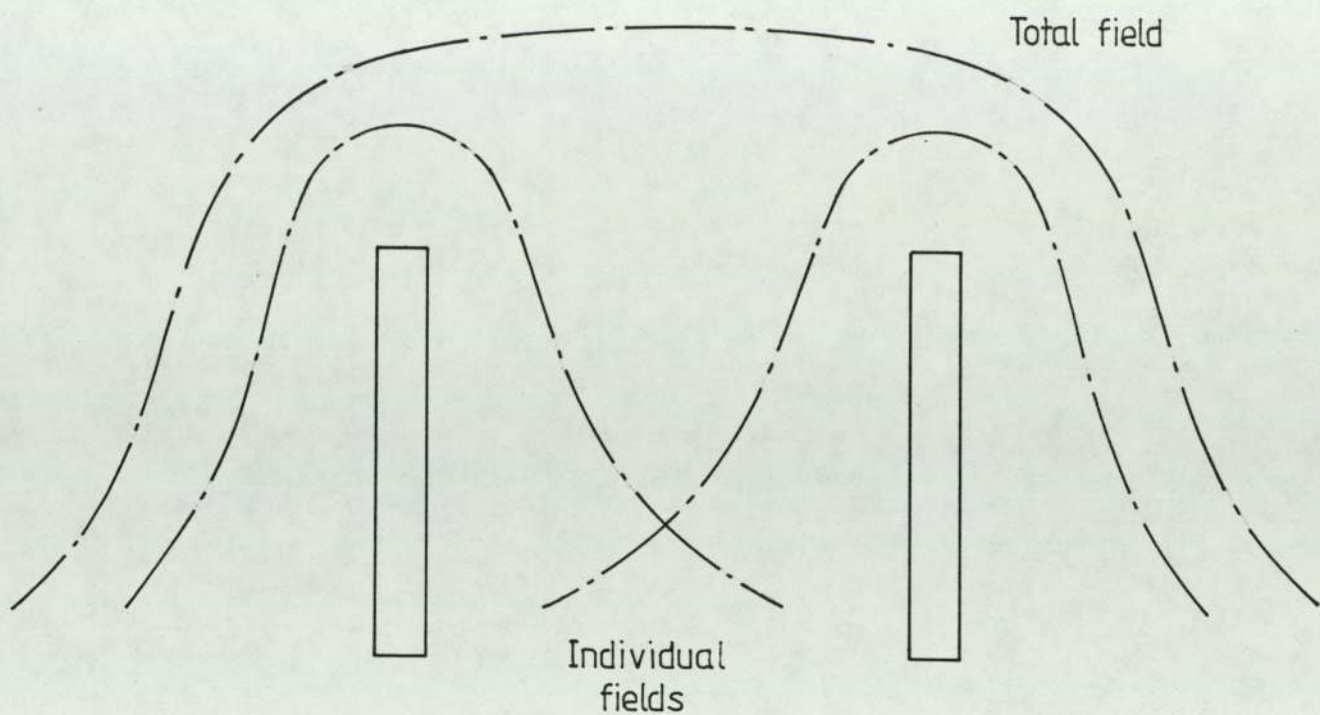


Figure 4.4b Shape of the combined magnetic field from the pair of Helmholtz coils (Newman 1972)



reservoir was connected to the chamber via a needle valve and by controlling the flow rate the desired sputtering pressure in the chamber could be attained. The bottle for storing the gases was supplied with gases from cylinders of five nines pure neon or argon gases available from BOC. Flexible stainless steel tubing was used to connect the cylinders to the bottle via valves which could be used to select the gas to be let into the chamber.

The power from the rf generator fed to the target via the matching network was estimated by measuring the voltage with an electrostatic 3.5 kV voltmeter and the current with a 500 mA ammeter. However this value cannot be related to the power in the r.f. discharge with any reliability. This is because of uncertain power losses in the matching network and the sputtering chamber. To overcome this problem one can measure the rf peak to peak voltage (Horwitz 1982) or the dc self-bias voltage on the target electrode (Lamont and Turner, 1973). In this system the dc self-bias voltage was measured by a circuit similar to that described by Rock and Smith (1975) and is shown in figure (4.5).

The chamber was evacuated by a standard vacuum arrangement consisting of a diffusion pump backed by a rotary pump. Liquid nitrogen traps in the roughing line and on top of the diffusion pump ensured base pressures below 5×10^{-7} torr with overnight baking of the chamber. An Edwards 6" diffusion pump with a speed of about 600-650 $l \text{ sec}^{-1}$ was employed. The flow rate of water for cooling the diffusion pump and the thermoelectric baffle valve was monitored by an "Edwards FSM1" flowtrol unit. The minimum recommended flow rate of water is 1.9 l / min , the flowtrol contained a pressure differential switch which operated below this rate to disconnect

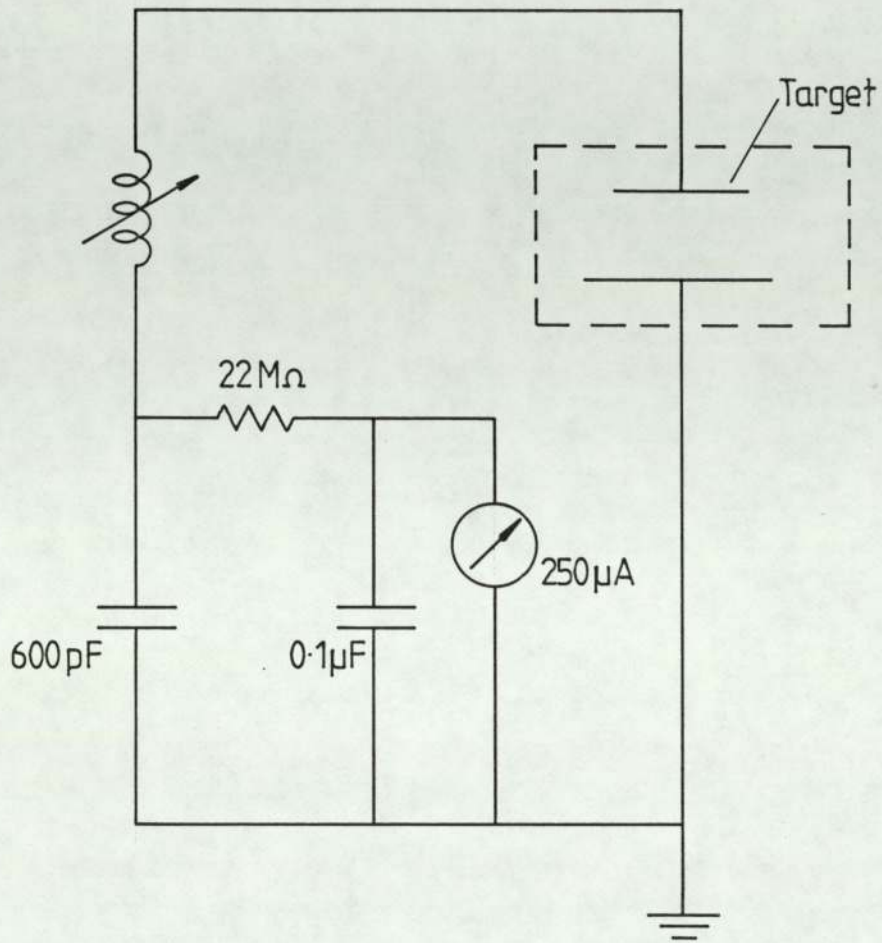


Figure 4.5 Circuit for measuring the D.C. self-bias voltage.

the power to the diffusion pump heater and the thermoelectric baffle valve. Therefore any damage to the diffusion pump or the thermoelectric baffle valve due to over heating could be avoided. The cold trap between the top of the diffusion pump and the chamber was filled with liquid nitrogen a few hours' prior to sputtering. This not only reduces the back streaming from the diffusion pump but also facilitates the removal of water vapour from the chamber. To reduce the back streaming from the rotary pump a liquid nitrogen cold trap was fitted in the fore-line. A 'Speedivac E 5.250' rotary pump was used in this system.

Pirani' gauges fitted in the fore-line and at the bottom of the chamber were used to measure the pressure during the roughing cycle. These gauges cover the pressure range $760-10^{-3}$ torr. Pressures below 10^{-3} torr were monitored by a hot filament ionization gauge which covers the pressure range 10^{-2} to 10^{-10} torr. Pressure measurements during sputtering were made with the pirrani gauge fitted at the bottom of the chamber. This gauge can be operated between the pressure range indicated above, thus covering the range of sputtering pressures used in this work (0.3 to 5×10^{-3} torr).

4.1.2 EXPERIMENTAL PROCEDURE

4.1.2a Substrate Preparation

A number of different substrates were used during the course of the present work. This is because different techniques require different substrate material which conform with their special requirements. For example, Corning 7059 glass slides are suitable for

measurement of electrical conductivity because of their high resistivity but for the same reason they are unsuitable for compositional analysis by Auger Spectrometry, because the sample would become charged, here a metallic substrate would be more useful.

The electrical and optical properties reported here were measured on films deposited on Corning 7059 glass slides. To measure the thickness of the film the slides were partly covered by a glass cover slip so that a sharp edge could be produced. For X-ray photo-electron spectroscopy (XPS) and Auger electron spectroscopy (AES), five pure aluminium substrates were used. For Rutherford back scattering analysis a variety of substrates were employed, these included, carbon, aluminium oxide, magnesium oxide, silicon, quartz and carbon coated with a thin layer of gold. The reasons for using the various substrates are discussed in section (6.6)

To ensure that all traces of grease and dirt were removed from the surface of the substrates, they were cleaned thoroughly before being placed in the chamber. The cleaning procedure employed was as follows:

- (1) Slides were placed in a beaker containing 5% solution of 'Tot' detergent, and boiled. The beaker was then placed in an ultrasonic cleaner for about 15 minutes.
- (2) The slides were then rinsed in de-ionised water several times, and cleaned ultrasonically in water for about 15 minutes.

- (3) Finally the slides were boiled in isopropyl alcohol and then immediately placed in the chamber.

An alternative detergent available in the laboratory was 'Deacon 90' but this was found to attack aluminium substrates and react with glass slides if boiled. Although neutral 'Deacon 90' detergent has recently become available 'tot' was used throughout the present work.

4.1.2b Deposition of Amorphous Silicon Films

In each run, three or four substrates were placed on the substrate holder, so that various properties could be measured for films produced under the same conditions. Corning 7059 glass slides were always included, so that the electrical and photo - conductivities, thermal activation energy, optical gap and the film thickness could be routinely determined. For nearly all the runs aluminium substrates were included for analysis of the composition by XPS and AES.

The chamber was evacuated following standard procedures (Glang et al 1983). With overnight baking of the chamber and the substrate holder, base pressures of less than 5×10^{-7} torr were regularly achieved. The current to the substrate heater was adjusted so that the temperature of the substrate holder was about 100°C higher than that required during sputtering. The maximum temperature obtainable was about 450°C which meant an upper limit in the sputtering temperature of about 380°C, but since the substrate holder invariably heated up during sputtering due to bombardment by the energetic plasma species the lowest temperature achieved was about 100°C. By decreasing the current to the heater during

sputtering, this increase could be offset and the temperature maintained to within $\pm 20^{\circ}\text{C}$ of the desired temperature. Figure (4.6) shows a calibration curve of the temperature of the substrate holder as a function of the heater voltage.

When base pressure was less than 5×10^{-7} torr, the diffusion pump was baffled and either neon or argon let into the chamber via the needle valve. By adjusting the flowrate the desired sputtering pressure could be achieved. Current was then applied to the Helmholtz pair of coils; for most of the runs the current was set at 4.0A giving an axial magnetic field in the centre of the chamber of about 0.01T. Power to the heaters of the valves of the rf oscillator and the HT supply were then switched on. A couple of minutes are normally required for the mercury diodes to warm up before the power to the HV transformer could be switched on. The power was then increased slowly until the required dc self-bias voltage was developed on the target. For the initial 15-20 minutes the substrates were shielded from the plasma by a rotatable shutter. After the pre-sputtering period the shutter was removed and the films deposited on the substrates. The duration of the sputtering was monitored by a clock, at the end of the sputtering period the shutter was again placed over the substrates before the power to the HV transformer was switched off.

Some of the experiments to characterize the films, such as Rutherford backscattering spectrometry were performed several weeks after depositing the films. During this period the films were stored in a vacuum desiccator.

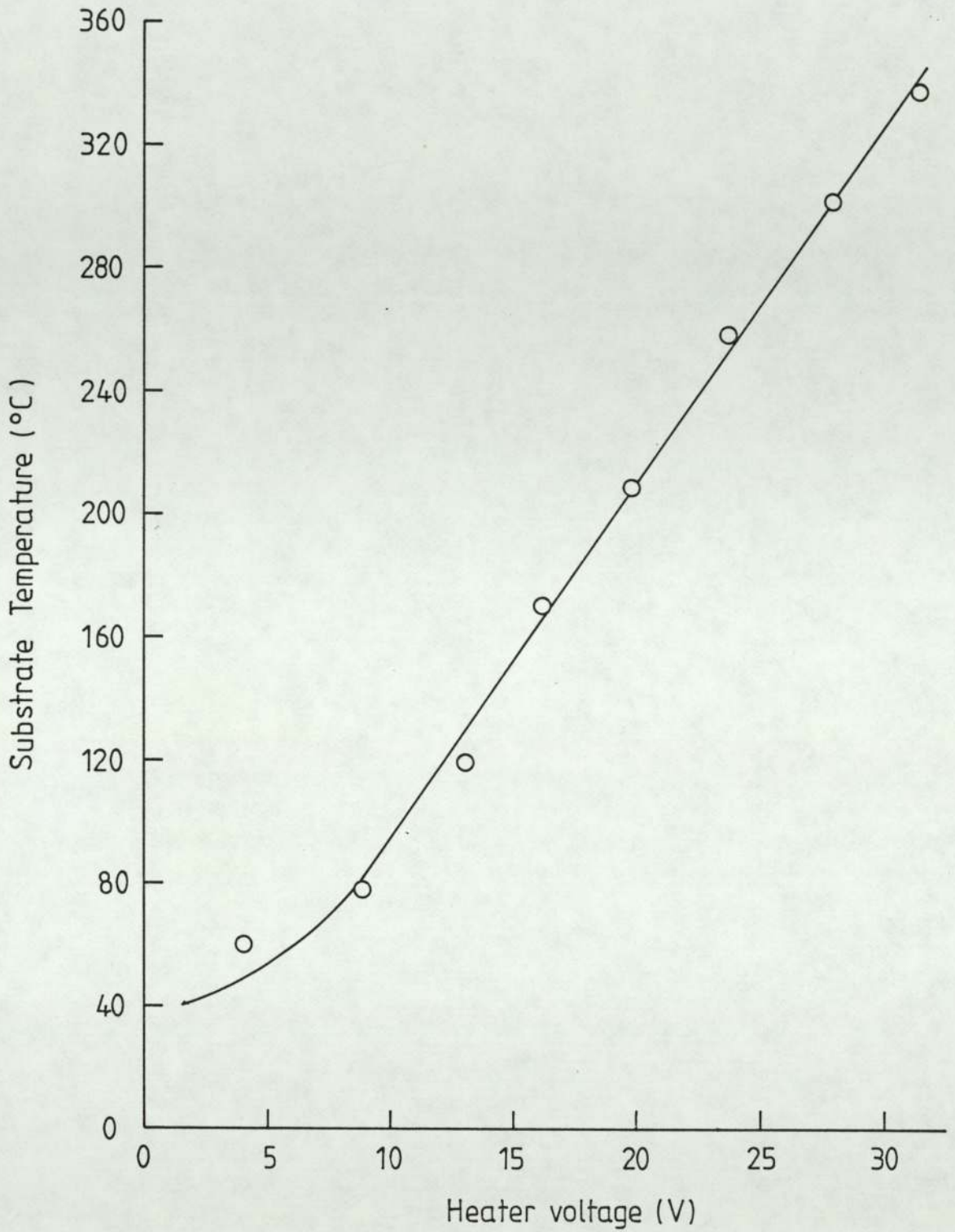


Figure 4.6 Substrate temperature as a function of heater voltage.

4.1.2c Evaporation of Aluminium

For the measurement of electrical conductivity and photo-conductivity aluminium electrodes were evaporated over the films in the gap cell configuration. Also, an aluminium layer needed to be deposited over the edge of the film to enable thickness determination by multiple beam interferometry. This was achieved by evaporating aluminium onto the films through a stainless steel mask. By using these masks, shown in figure (4.7a) both of these objectives could be achieved in one evaporation. The aluminium, wound on a tungsten filament, was evaporated at a base pressure of about 2×10^{-5} torr.

4.2 CHARACTERIZATION OF AMORPHOUS SILICON FILMS

4.2.1 Thickness Measurement

The thickness of the films produced varied from 0.1 to $5.0 \mu\text{m}$ and was measured by multiple beam interferometry and telesurf. For the majority of the films, which were about 0.5-1.0 μm thick multiple beam interferometry was used, and only for a few films, with thickness much greater than 1.0 μm telesurf was employed.

The technique of multiple beam interferometry was developed by Tolansky and his co-workers (Tolansky, 1960). To measure the film thickness using this technique a sharp step needs to be produced in the films. This was achieved by placing a thin glass cover slip over part of the slide. A highly reflective layer, such as silver or aluminium then needs to be deposited over the step. A small half-silvered flat is then placed over the edge, when it is illuminated by white light interference fringes are formed. Figure (4.7b) shows

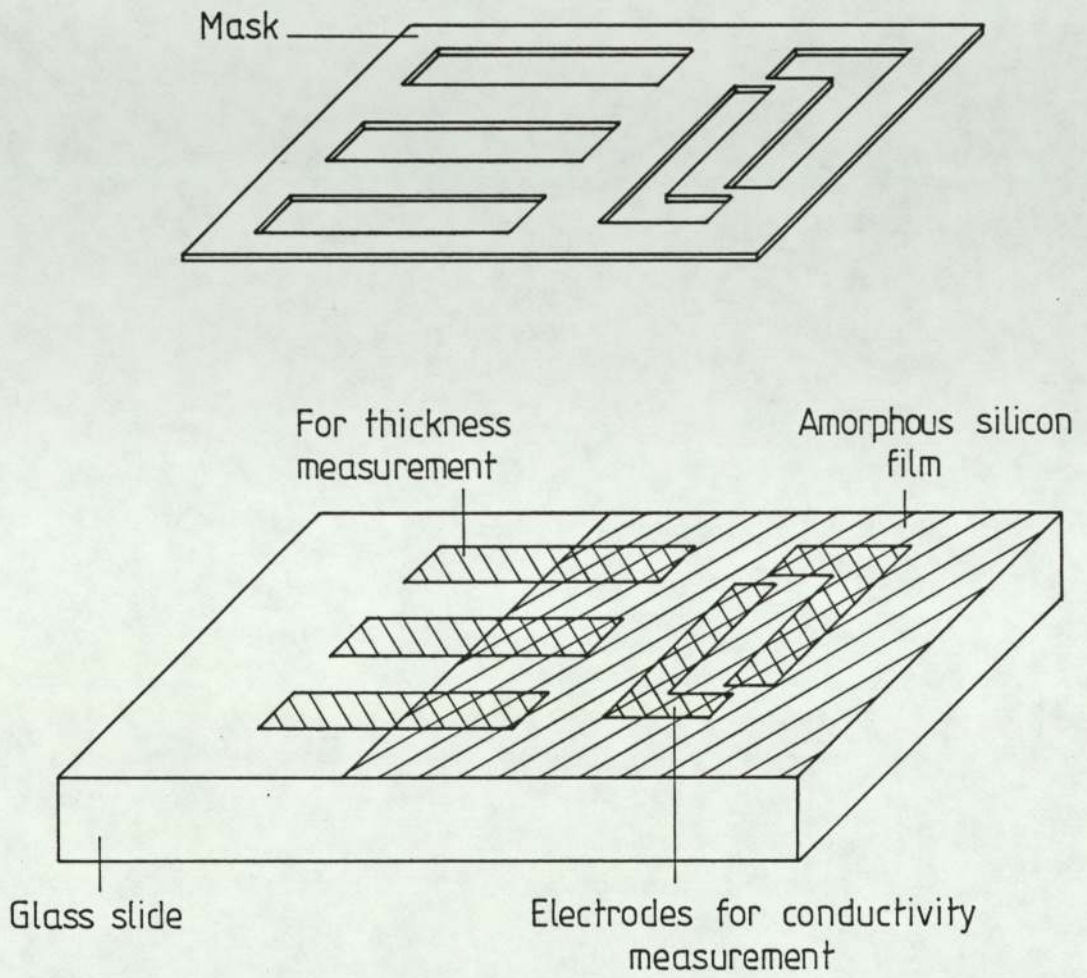


Figure 4.7a The mask for depositing aluminium over the amorphous silicon film for thickness and conductivity measurements.

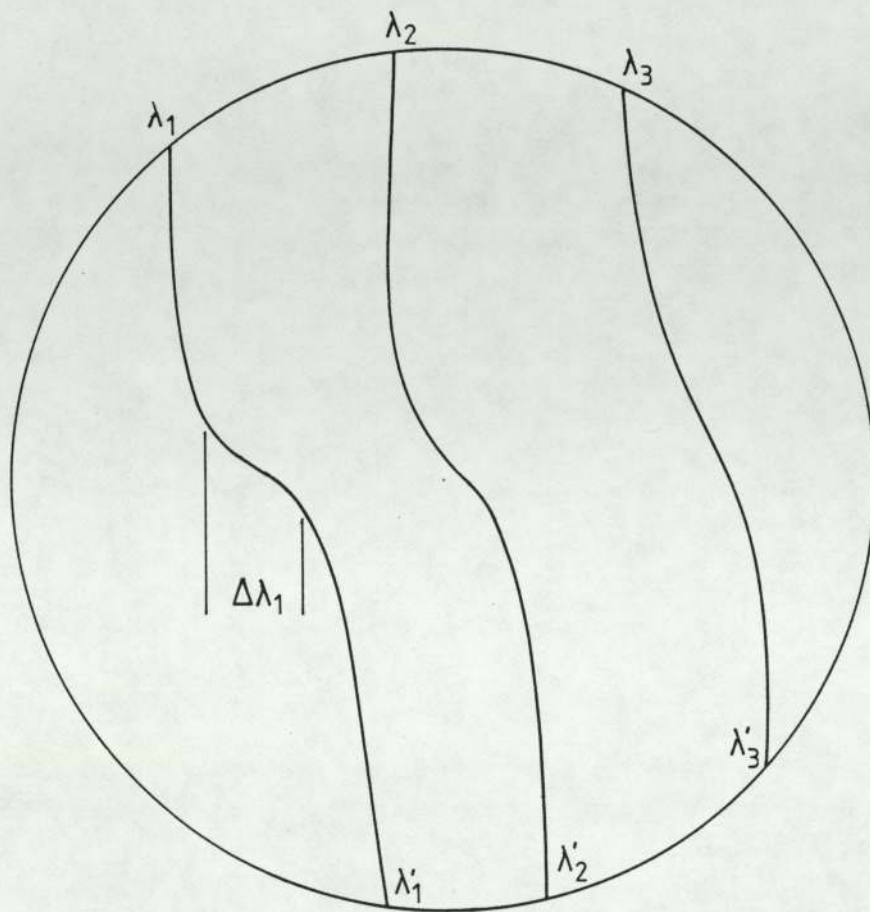


Figure 4-7b The appearance of fringes in the interference microscope.

the appearance of the fringes as observed through the Hilger and Watts N130 interference microscope. The thickness can then be determined by measuring the wavelengths of the fringe positions by using the equation:

$$t = \frac{n_1 \Delta \lambda}{2} \quad (4.1)$$

where n_1 the fringe order is an integer given by the equation:

$$n_1 = \frac{\lambda_2}{\lambda_1 - \lambda_2} \quad (4.2)$$

Using this technique the thickness of all the films reported in this work was measured to a precision better than $\pm 10\%$.

4.2.2 Measurement of Electrical Conductivity

The electrical conductivity of the films was measured after depositing aluminium electrodes over the film in the gap cell configuration. An alternative method is the 'sandwich' configuration where the electrodes are deposited on either side of the film but with this technique one generally encounters difficulty in obtaining ohmic contacts (Solomon 1981). In the present study aluminium was found to make good ohmic contacts for the electric field used, generally 10^2 Vcm^{-1} . Paul and Anderson (1981) have pointed out that when conductivity is measured by electrodes in the gap cell configuration surface adsorbates such as water vapour can greatly influence the conductivity and to get unambiguous results conductivity should be measured after the sample has been heated in vacuum to 200°C .

They observed that with samples containing large numbers of voids, the conductivity is high and remains high till a temperature of about 100-150°C is reached at which point the water vapour is desorbed from the surface, and the conductivity decreases, by as much as an order of magnitude. Although none of our films seemed to be influenced by surface adsorbates to such an extent, as a rule, conductivity was measured as the sample was heated upto temperatures greater than 150°C and when it was cooled again. Figure (4.8) shows a typical plot obtained. All the values of room temperature electrical conductivity and thermal activation energy were obtained from measurements of conductivity as the temperature was reduced.

The apparatus for measuring the electrical conductivity of amorphous silicon films was designed and constructed during the course of the present work. Plate (4.2) shows a picture of the apparatus. The notable features are:

- (1) Conductivity could be measured in a vacuum of about 10^{-5} torr.
- (2) The temperature of the substrate holder could be varied from about -150°C to 200°C.
- (3) All the electrical cables were screened from stray electromagnetic radiation, so that currents as low as 10^{-13} A could be read with a Keithley 610C electrometer.

Figure 4.9 shows a schematic diagram of the apparatus. The stainless steel substrate holder (S) was welded onto a stainless

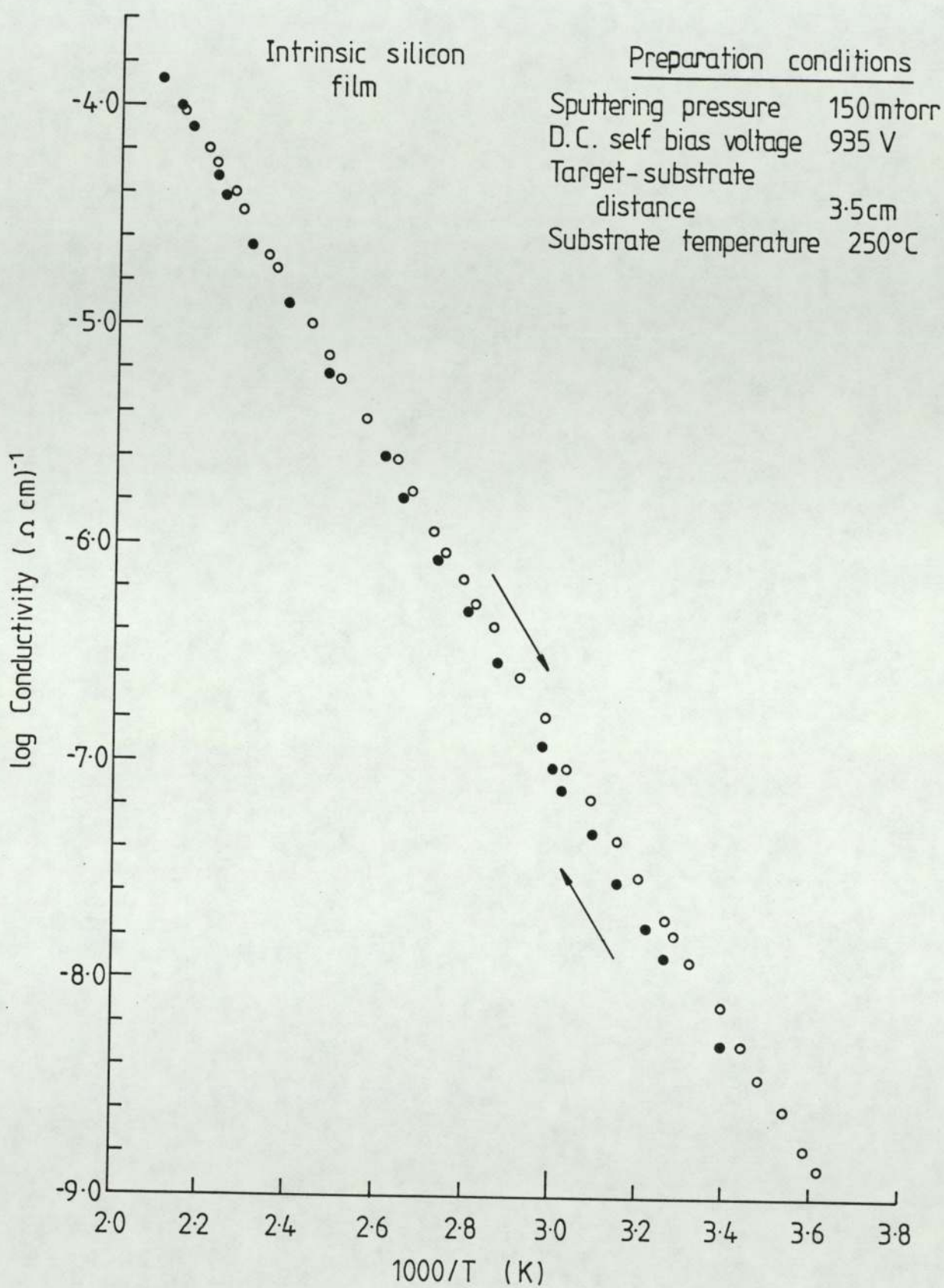


Figure 4.8 Conductivity vs temperature ; the effect of temperature cycling.

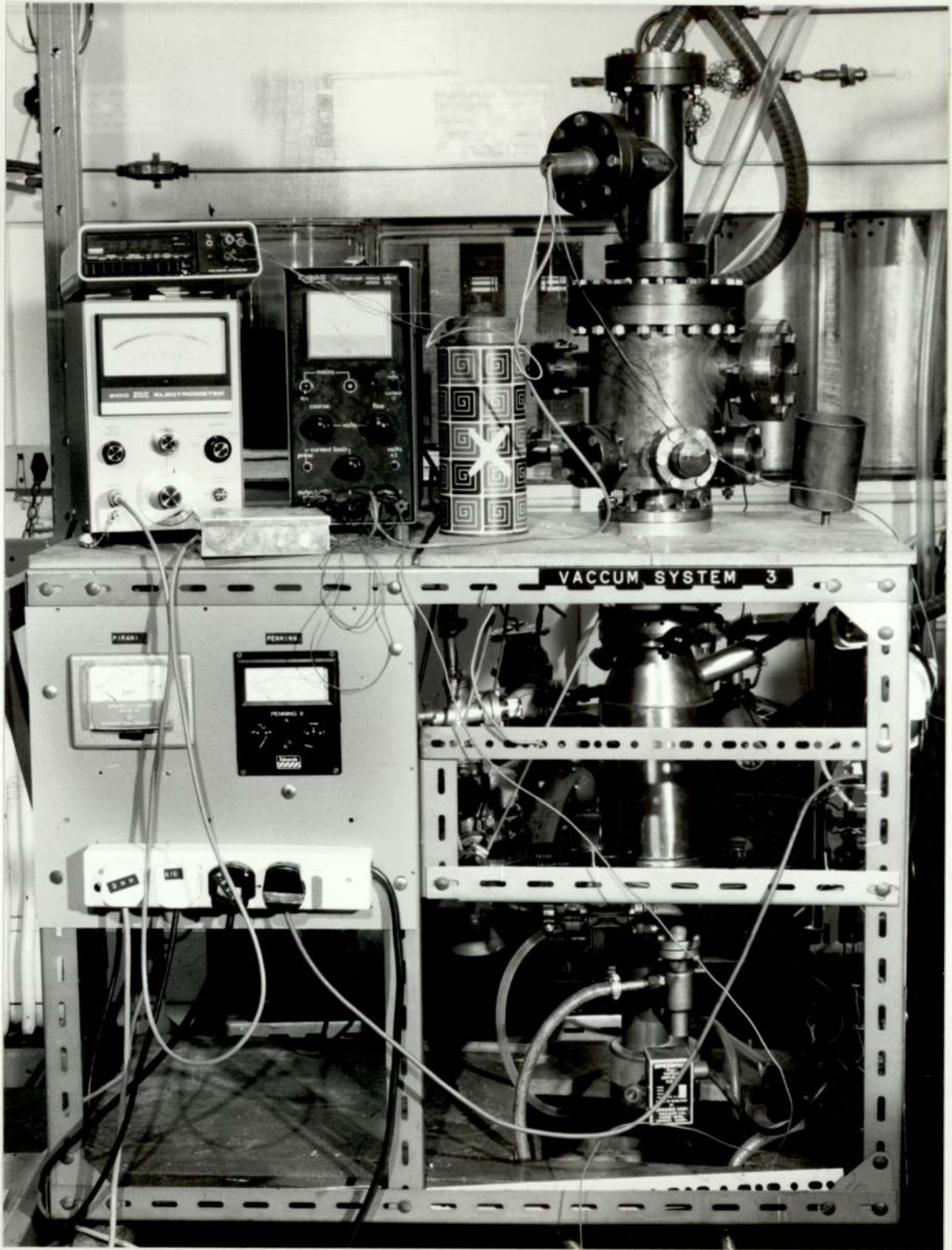
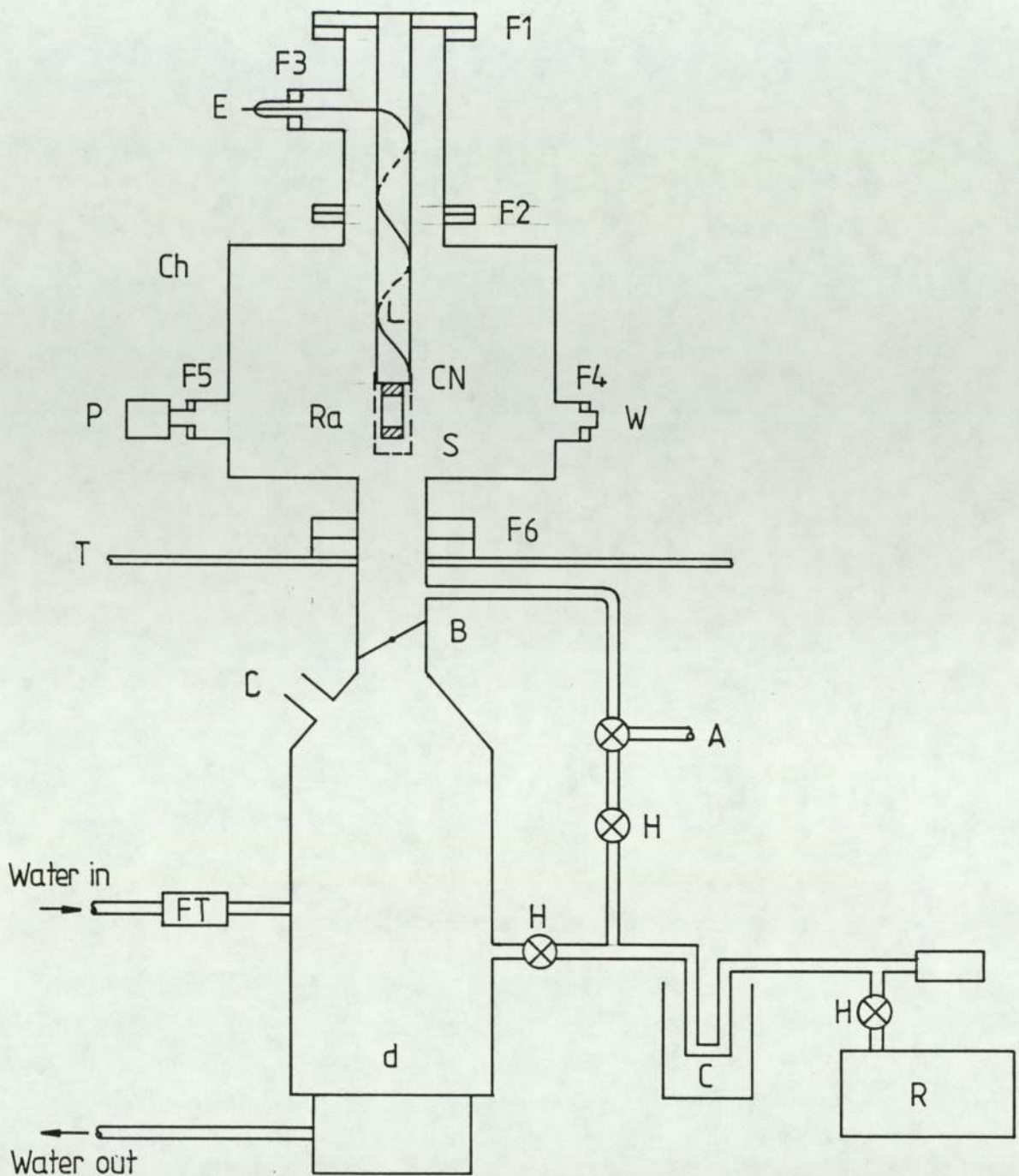


Plate 4.2 The apparatus for measuring the electrical conductivity.



- | | | | |
|------|------------------------|----|------------------------|
| d | Diffusion pump | FT | Flowtrol |
| R | Rotary pump | Ra | Radiation screen |
| C | Cold trap | P | Penning gauge |
| H | Hand valves | W | Window |
| A | Air inlet | CN | Ceramic block |
| B | Butterfly valve | E | Electrical feedthrough |
| F1-5 | Flanges (Cu gaskets) | T | Table |
| S | Substrate holder | Ch | Chamber |
| L | Liquid nitrogen holder | | |

Figure 4-9 Schematic diagram of the apparatus for measuring the electrical conductivity.

steel column (L) which was bolted onto the chamber via ^aflange marked (F2). A 17W, 100 Ω wire wound resistor, clipped to the back of the substrate holder was used as a heater. The substrate holder could be cooled by pouring liquid nitrogen into the column (L). The temperature of the substrate holder could thus be varied from about -150 to +200°C. A copper-constantan thermocouple bonded onto the substrate surface with silver paste was used to determine the temperature. The thermocouple and the electrical connections to the specimen and the heater were made via an eight way ultra-high vacuum lead out soldered into the flange marked (F3). The final connections to the specimen were made via connectors (CN) screwed onto the ends of the substrate holder. Final connections to the sample were made with gold wires (0.04" dia.,) bonded onto the aluminium electrodes by silver paste (Dupont Silver Suspension).

The substrate holder was surrounded by a copper radiation shield (RA) which could be clipped onto the main column. This reduced the heat loss from the surface by radiation, especially at the highest temperatures.

The chamber and the diffusion pump were connected via the flange marked (F6). This flange was also bolted onto the work table, thus holding the whole system in position. An Edwards 2" diffusion pump (D) backed by a rotary pump (R) were employed in this system. Cold traps (C) situated at the top of the diffusion pump and in the roughing line ensured pressures below 5×10^{-5} torr.

The circuit for measuring the electrical conductivity is shown in figure (4.10). A Kingshill stabilised power supply unit was used to apply a fixed voltage, normally 10V, across the

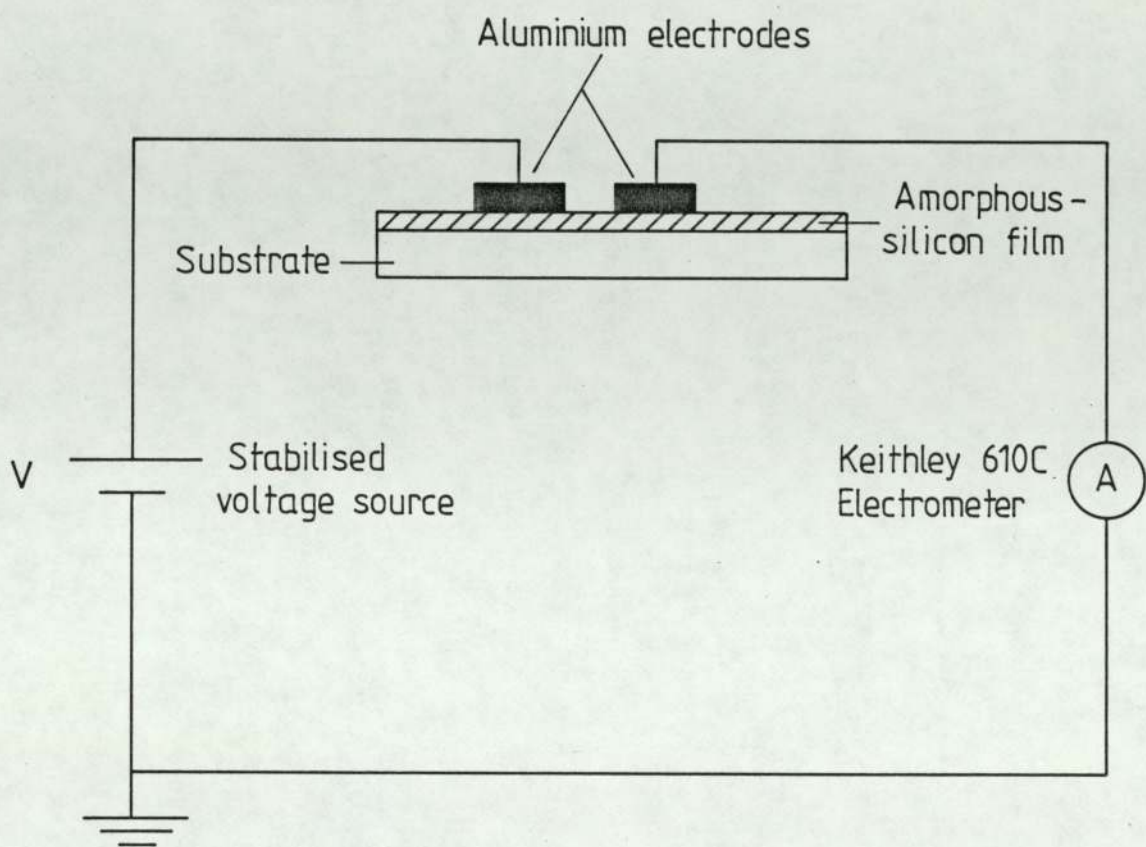


Figure 4-10 Circuit for measuring the electrical conductivity

electrodes. The current through the specimen was measured by a "Keithley 610C" electrometer. Thus by recording the variation of the current with temperature the variation of the conductivity with inverse temperature could be deduced from the equation:

$$\sigma = \frac{I \times l \cdot L}{V \cdot A} \quad (4.3)$$

where, σ = electrical conductivity

I = current

V = voltage

L = length of sample

A = cross-sectional area

L is the distance between the aluminium electrodes (0.1 cm) and A is the product of the length of the electrode (1.1 cm) and the thickness of the film. The voltage across the specimen was fixed at 10V giving a field of 10^2 V/cm. Thus the conductivity could be directly related to the current measured.

By plotting curves of log conductivity versus inverse temperature the thermal activation energy of electrical conductivity was determined from the equations:

$$\sigma = \sigma_0 \exp(-\Delta E / k_b T) \quad (4.4a)$$

$$\ln \sigma = \frac{-\Delta E}{k_b \cdot T} + \ln \sigma_0 \quad (4.4b)$$

$$\log \sigma = \frac{-\Delta E}{2.3 \cdot 10^3 \cdot k_b \cdot T} + \frac{\log \sigma_0}{2.3} \quad (4.4c)$$

where σ_0 is defined as the minimum metallic conductivity (Mott and Davies 1979), ΔE the thermal activation energy, T the temperature and k_b the Boltzman's constant. Thus the thermal activation energy was deduced by measuring the slope of the curve of log conductivity versus inverse temperature by employing the relation:

$$E = -\text{slope} \times 2.3 \times 10^3 \times k_b \quad (4.5)$$

4.2.3 Measurement of Photoconductivity

The photoconductivity experiments were carried out using the same gap-cell configuration as for the dark conductivity measurements. The steady state photocurrent was measured for an applied electric field of 10^2 Vcm^{-1} by illuminating the sample with a He/Ne gas laser (Sci^{en}tifica Cook Limited, Model No: SLH/5) of wavelength 6328 \AA and intensity of approximately $5 \times 10^{16} \text{ photon cm}^{-2} \text{ s}^{-1}$.

The electrical connections to the electrodes were made by pressure contacts. The circuit used for measuring the photoconductivity was similar to that shown in figure (4.10) except in this case a Kiethley 614 electrometer was employed.

The photocurrent was deduced from the relationship given in equation:

$$I_{ph} = I_{ill} - I_0 \quad (4.6)$$

where I_{ph} is the photocurrent, I_{ill} the current under illumination and I_0 the dark current. The photoconductivity was deduced from equation (4.3), but in this case the cross-sectional area (A) is the

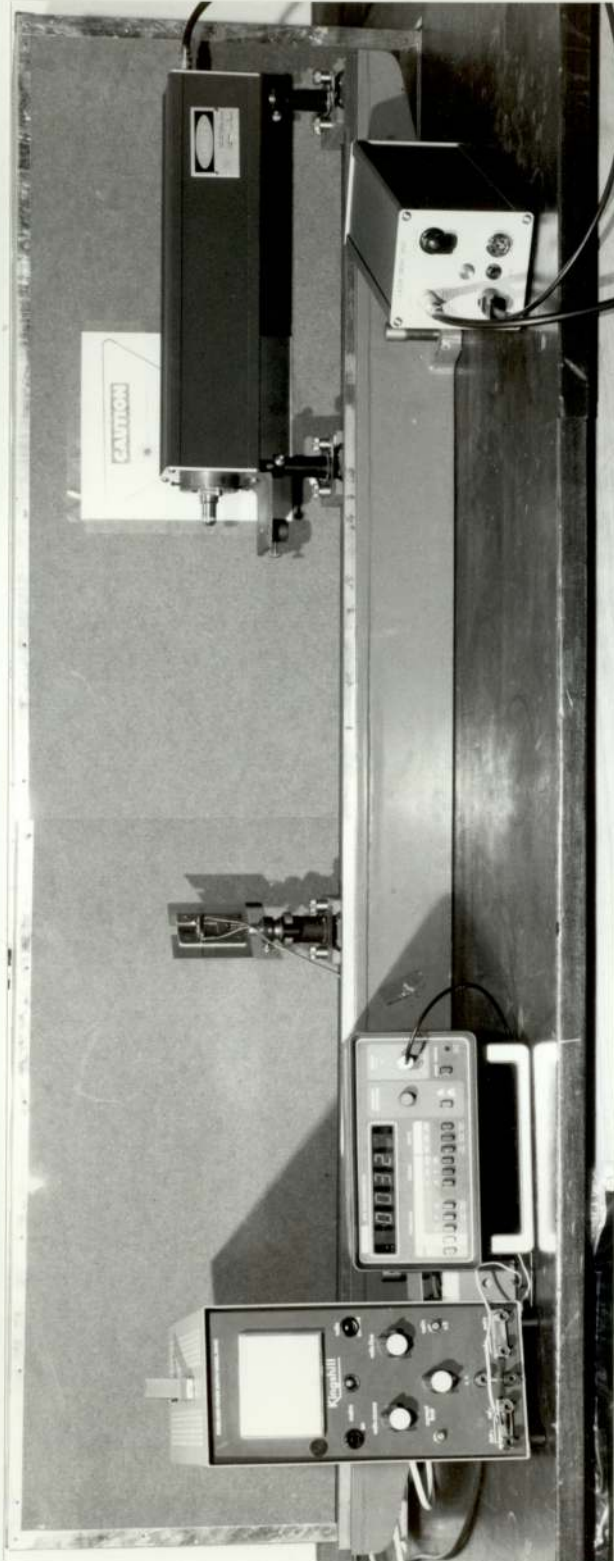


Plate 4-3 The apparatus for measuring the photoconductivity.

product of the laser beam diameter (2.5 mm) and the film thickness. Plate (4.3) illustrates the arrangement for measuring the photoconductivity. All the photoconductivity experiments were carried out at room temperature.

In the present work the photoconductivity experiments were limited to determining the measurement of the room temperature photoconductivity as a function of the preparation conditions. This is because as the density of defects is reduced the photoconductivity increases, thus the magnitude of the photoconductivity and its ratio to the dark conductivity can be used to determine the relative density of defects for the films produced under various preparation conditions (Loveland et al 1973, Moustakas and Paul 1977).

For hydrogenated a-Si it has been shown that in some cases measurement of the photoconductivity may be obscured by light induced changes in the material (Staebler and Wronski 1980). This phenomenon has not been investigated in this study but as a precaution the photoconductivity was measured immediately after the aluminium electrodes had been deposited and after the film had been annealed at temperatures in excess of 180°C.

4.2.4 Optical Absorption

A Unicam ultraviolet spectrophotometer was used to determine the transmission of the films as a function of wavenumber, for values of wavenumber from 11500 to 2500 cm^{-1} . From these plots the absorption coefficient could be determined as a function of energy

by employing the equation:

$$\alpha = -\frac{1}{d} \ln \left[\frac{T}{1-R} \right] \quad (4.7)$$

where α is the absorption coefficient, d is the thickness of the film, T the transmission and $(1-R)$ is the value at which the interference averaged transmittance levels off at higher wavelengths. The optical gap can then be determined by plotting $(\alpha \hbar \omega)^{\frac{1}{2}}$ against $\hbar \omega$ as given by the relation (Tauc 1974)

$$(\alpha \hbar \omega)^{\frac{1}{2}} = B (\hbar \omega - E_0) \quad (4.8)$$

where B is a constant and E_0 is the optical gap. The uncertainty in the value of α , for $\alpha > 10^3 \text{ cm}^{-1}$ was about 10%.

4.2.5 X-ray Diffraction

A selected number of films deposited on quartz substrates were tested for amorphicity by X-ray diffraction. None of the plots obtained showed any structure indicating that the films were amorphous. The thickness of the films was between 2-5 μm .

4.2.6 Electron Diffraction and Micrography

To check that the films were amorphous and contained no structural inhomogeneity they were studied by transmission electron microscopy. Films of about 1000\AA thickness were deposited on carbon coated copper grids. The instruments used were an AEI EM6 microscope at Aston University and a microscope at Birmingham University (EM7).

The instruments were operated to obtain electron diffraction patterns as well as dark field electron micrographs. The EM6 microscope could be operated at a maximum voltage of 100 kV whereas the microscope at Birmingham University could be operated at voltages up to 1000 kV. For the films investigated several selected area diffraction patterns were obtained from different regions of the film and at various voltages. All of the diffraction patterns exhibited broad rings characteristic of amorphous materials. Figure (4.11) shows some of the typical diffraction patterns obtained; also included for comparison is a diffraction pattern from evaporated aluminium films. By operating the microscope in the dark field mode, micrographs of the film can be obtained, some of the typical micrographs are shown in figure (4.12). These micrographs were obtained at magnification of up to 160k, and as can be seen no structure is observable.

4.3 COMPOSITIONAL ANALYSIS

The composition of the films was determined by three main techniques available in the department. A Kratos XSAM 800 spectrometer was used to analyse the samples by employing the techniques of X-ray photoelectron spectroscopy and Auger electron spectroscopy. The films could also be analysed by Rutherford backscattering spectroscopy, carried out at Birmingham University where a '3 MeV Dynamatron' jointly developed by Birmingham and Aston Universities could be used to obtain alpha particles of energies up to 3 MeV.

A limited number of samples were studied by infrared absorption spectroscopy. For these experiments a Perkin-Elmer double beam infra-red spectrophotometer was employed.

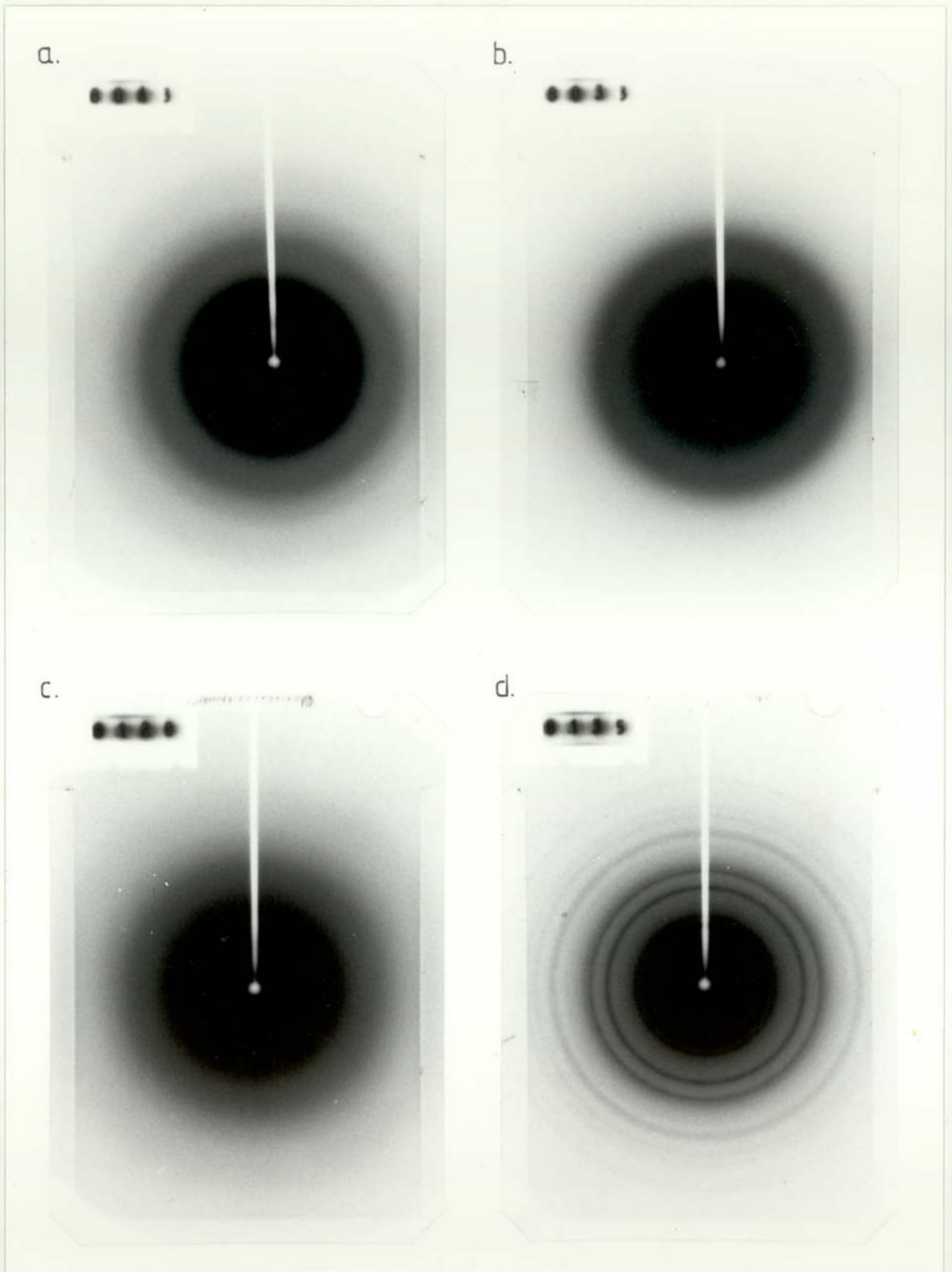


Figure 4.11 Typical electron diffraction patterns.

- (a) Intrinsic Silicon film sputtered in neon at a pressure of 11 mtorr.
- (b) Intrinsic Silicon film sputtered in neon at a pressure of 90 mtorr.
- (c) Silicon doped with 0.97% Ta. Sputtered in neon at pressure of 150 mtorr.
- (d) Aluminium standard.

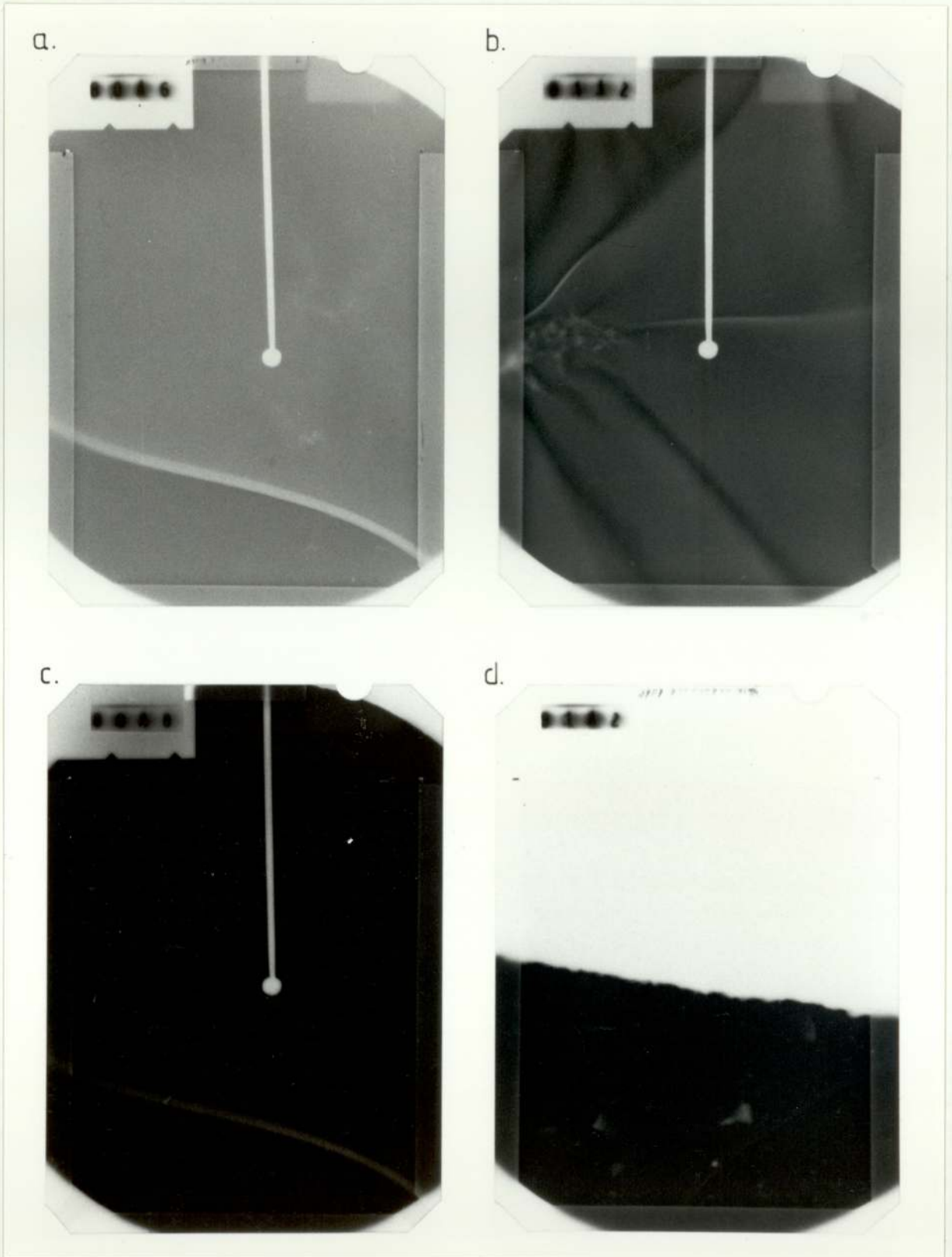


Figure 4-12 Typical electron micrographs.

- (a) Intrinsic Silicon film. Sputtering pressure 11mtorr. (Mag. $\times 160K$)
- (b) Silicon doped with 0.97% Ta. Sputtering pressure 150mtorr. (Mag. $\times 160K$)
- (c) Intrinsic Silicon film. Sputtering pressure 140mtorr. (Mag. $\times 160K$)
- (d) Intrinsic Silicon film. Sputtering pressure 90mtorr. (Mag. $\times 10K$)

The instrumentation and experimental procedure of these techniques is described briefly below.

4.3.1 Rutherford Backscattering Spectroscopy

4.3.1a Substrate Preparation

For RBS experiments films were deposited on a variety of substrates, which included, carbon, magnesia (MgO), alumina (Al_2O_3), quartz (SiO_2) and crystalline silicon. Carbon substrates were made by slicing and polishing discs of carbon 1 mm thick from a rod of pure carbon (99.999%). Magnesium oxide crystals were obtained from the Royal Military College, Shrivener^h_kam. Alumina substrates were obtained from MRC and quartz was obtained from Goosch and Housego Ltd. Silicon substrates were cut from 3" discs of electronic grade single crystal silicon obtained from Mullard Limited. All substrates were cleaned using the same procedure as that described earlier for Corning 7059 glass slides before being placed in the chamber.

The substrates were bonded by silver paste to specially designed substrate holders compatible with the carousel used for holding the samples in the RBS scattering chamber. The substrate holders had dimensions of 3 x 3 x 0.3 cm and were made from aluminium. A recess was let into the holders, so that when the substrate was placed on it their surface was level with the surface of the holder.

4.3.1b Instrumentation

In Rutherford backscattering spectroscopy the target is bombarded by high energy, monoenergetic ions, usually H^+ or He^+ .

As discussed earlier, in the present work, the samples were bombarded with helium ions of energy 2.8 MeV. Some of the particles incident on the target are backscattered, part of these backscattered ions are then energy analysed and counted. A spectrum can thus be obtained of number of counts versus backscattered energy of the ions, which can be stored on magnetic tape. Thus the experimental set up for RBS can be divided into three sections; (1) production of a collimated beam of monoenergetic ions, (2) scattering chamber and (3) electronics for backscattered ion energy analyses. Figure 4.13 illustrates schematically the major components of the system. The high energy alpha particles were obtained from a 3 MeV 'Dynamatron' accelerator. The beam of alpha particles is directed towards the chamber by magnets which bend the beam in the appropriate direction. Combination of a quadrupole pair of focussing magnets and collimators focus the beam, so that when incident on the target it covers an area of about 7.0 mm².

Figure (4.14) is a schematic diagram of the specially designed chamber, constructed at Aston University. Phull (1984) and Al-Armaghany (1985) have described in detail the design and construction of the chamber. The samples were mounted on a carousel capable of holding up to 80 samples. The carousel could be rotated, remotely and any particular sample slotted into the target holder. Thus up to 80 samples could be analysed without the need to break the vacuum. A silicon surface barrier detector was used in this system.

The signal from the detector is fed into the pre-amplifier (ORTEC 124) which is attached to the chamber, from there the signal is conveyed to the multichannel analyser via an amplifier (ORTEC 472A) situated in the control room. The mass and depth resolutions of

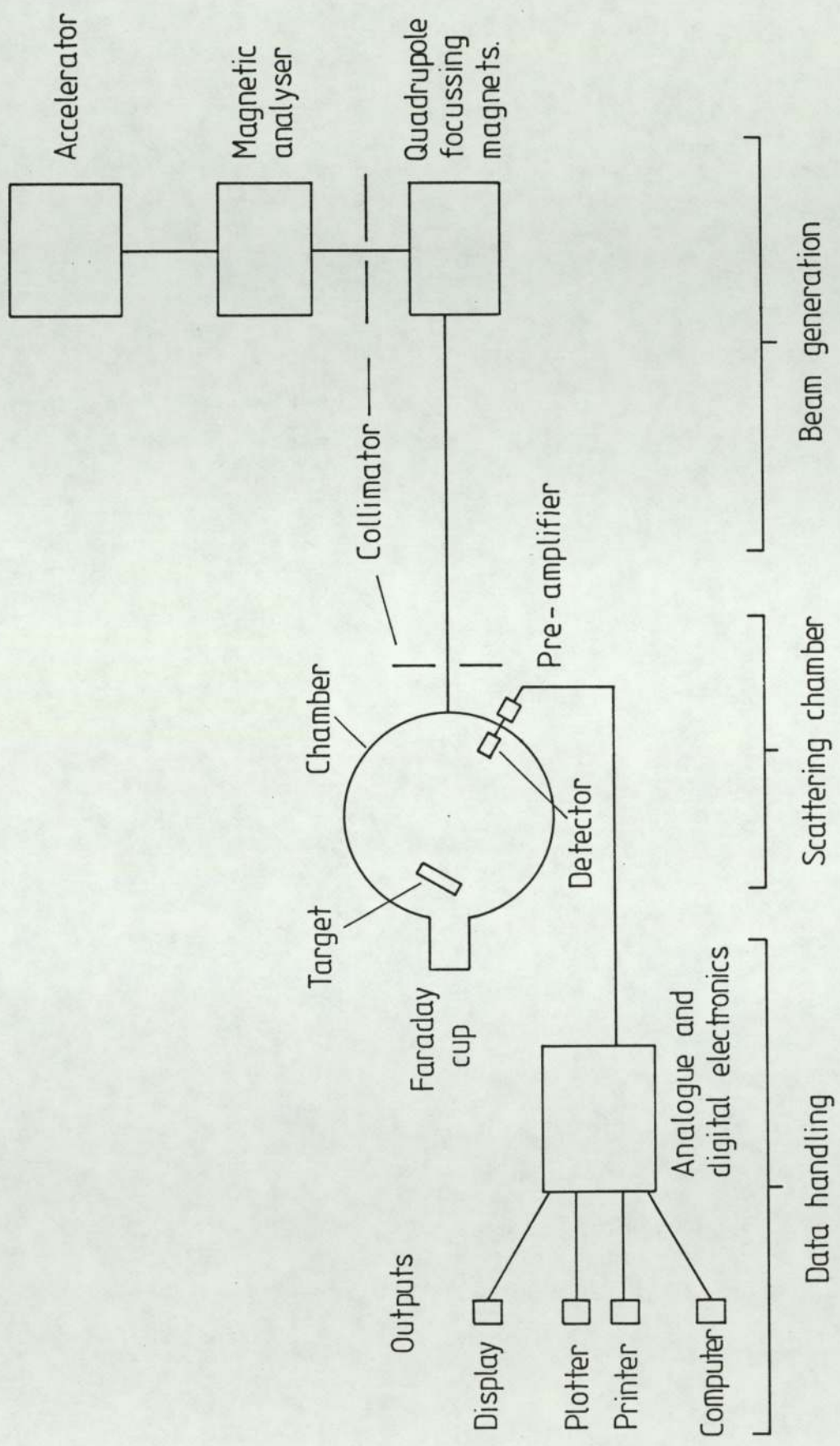


Figure 4.13 Major components of the RBS system.

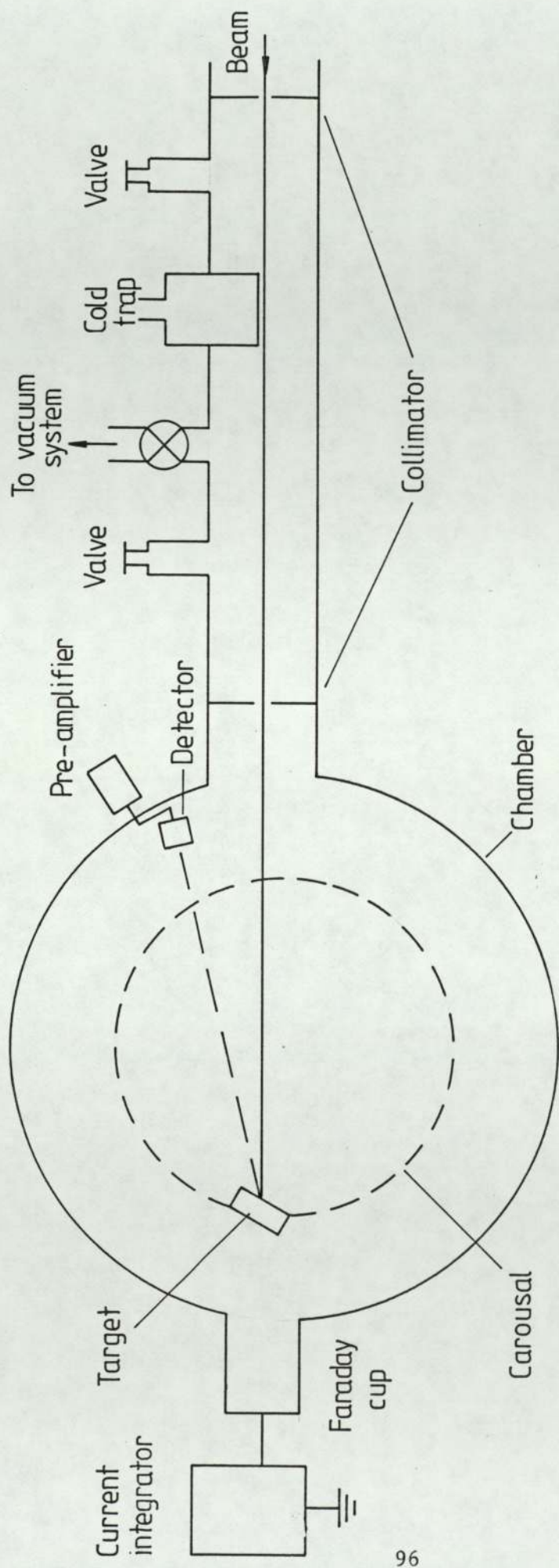


Figure 4.14 Schematic diagram of the backscattering chamber

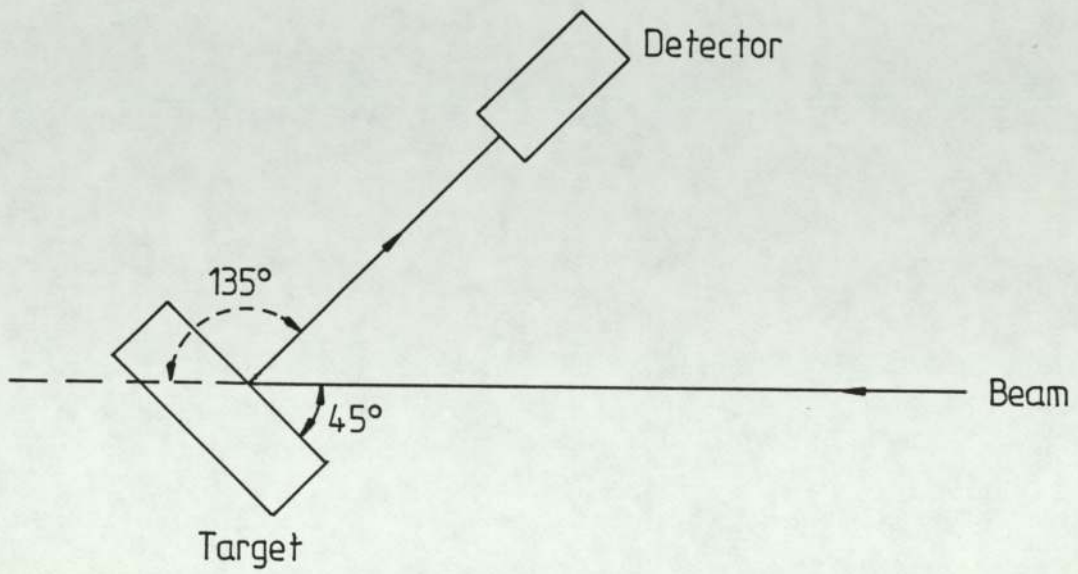


Figure 4-15 Geometric relationship between the target and detector.

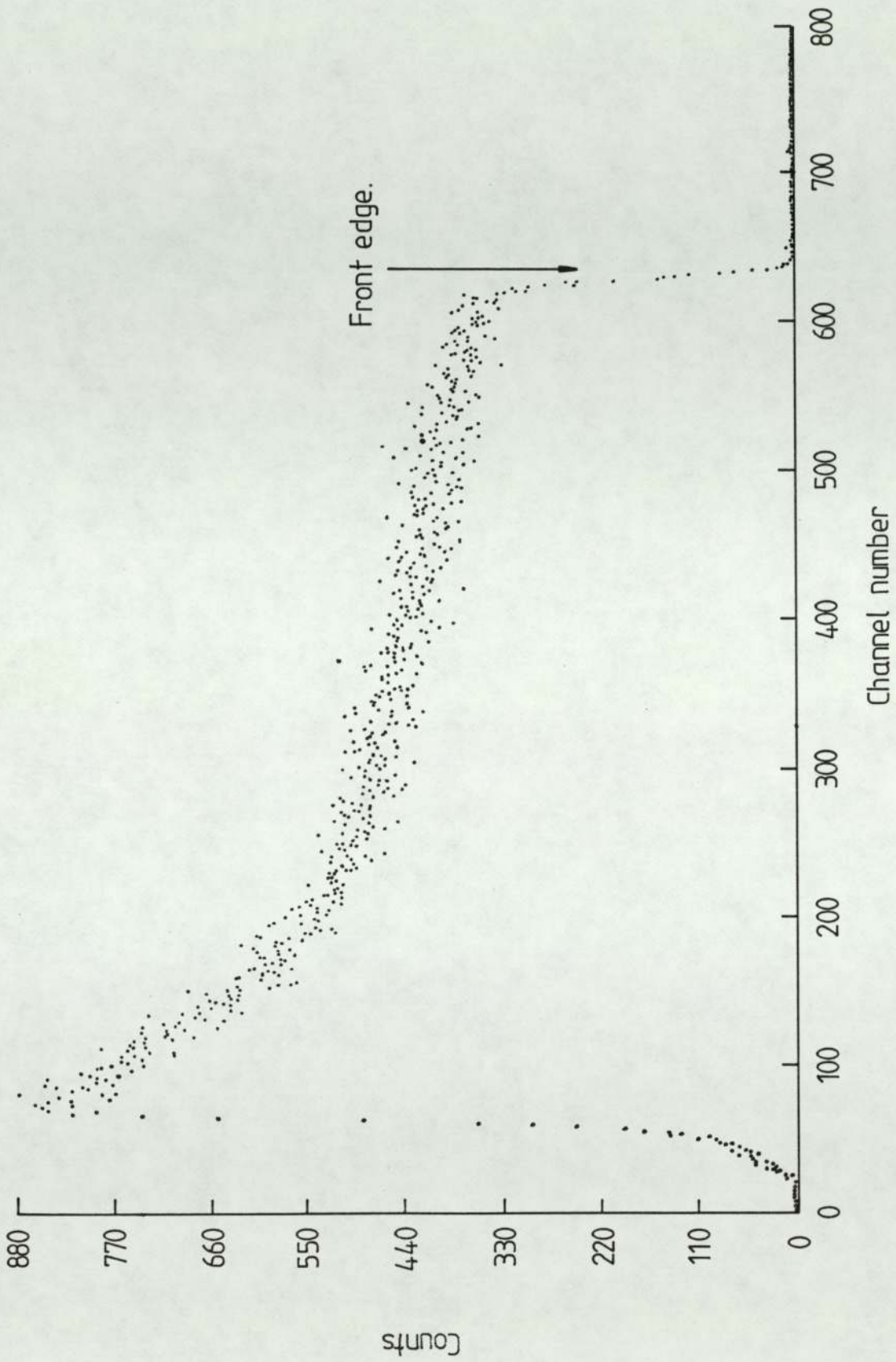


Figure 4.16 Spectrum obtained from a Ti target used as a standard.

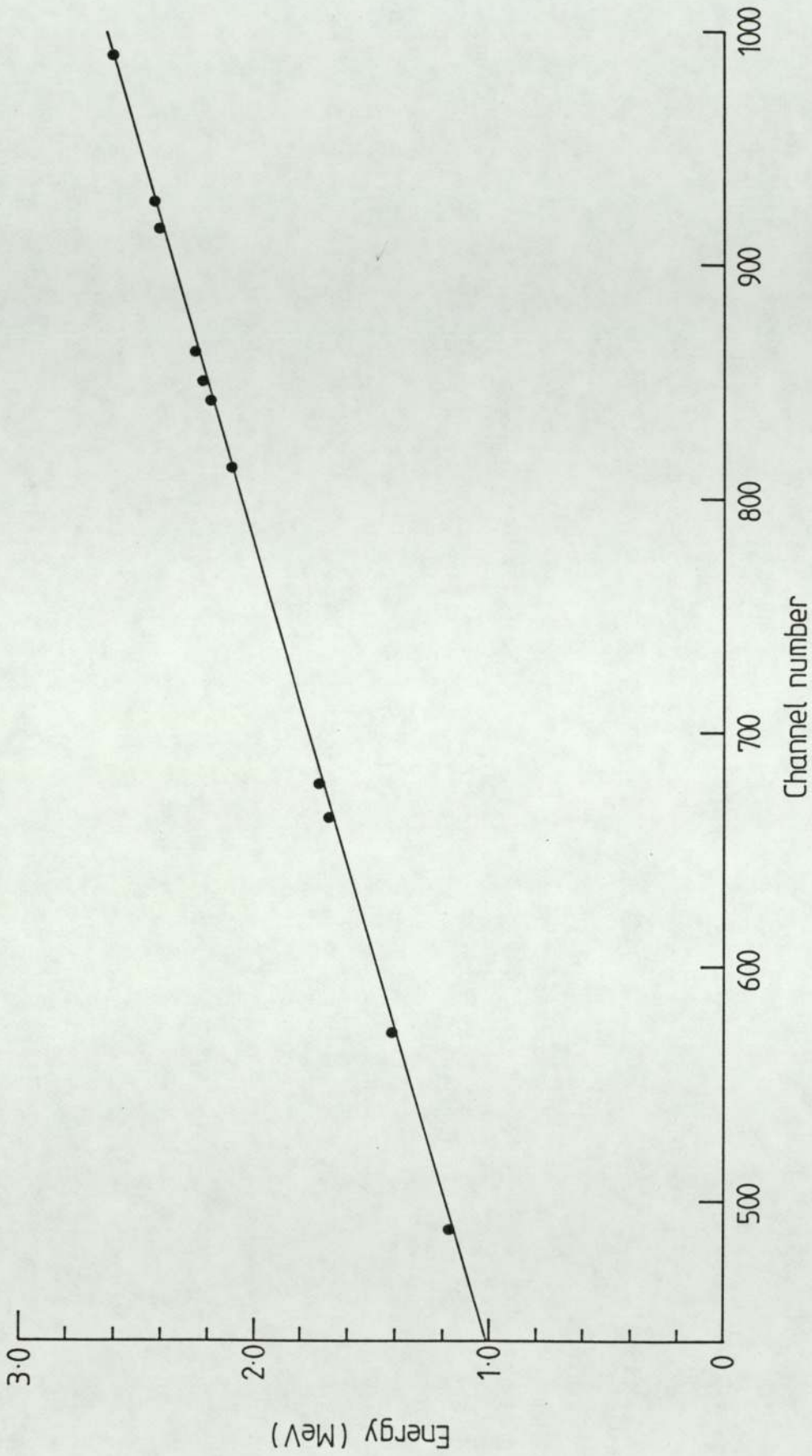


Figure 4.17 Calibration curve of backscattered energy vs channel number for 2.8 MeV $^4\text{He}_4^+$ ions

the system as well as depending on the performance of the detector and amplifiers depends on the geometry of the system. Figure (4.15) shows the geometric relationship between the target and the detector.

4.3.1c Procedure

For each run the system was calibrated and the energy resolution determined by using a set of pure elements as standards. As an example spectra obtained from a titanium target is shown in figure (4.16). From the spectra of these elements the channel number in which their front edge lies can be determined. This represents the particles backscattered from the front surface of the target. Since no energy loss is incurred by these particles in escaping from the target, their energy is simply given by:

$$E_b = K E_i \quad (4.9)$$

where E_i is the initial energy, E_b the energy of the backscattered particles and K the kinematic factor of the target element. The kinematic factors for the elements can be obtained from standard tables (Chu et al 1978), and since E_i is known E_b can be calculated. Then by plotting E_b versus the channel number at which the front edge occurs for different elements, a calibration curve relating energy to channel number can be obtained. Figure (4.17) shows a typical plot, where the resolution of the system is equal to the gradient of the line. Thus once the calibration curve is constructed any element can be identified by measuring the channel number at which its front edge lies.

4.3.2 X-ray Photoelectron Spectroscopy (XPS) and Auger Electron Spectroscopy (AES)

The techniques of X-ray photoelectron spectroscopy (XPS) and Auger Electron Spectroscopy (AES) have been employed in the present study to determine the concentrations of the impurities; argon, neon and oxygen in the intrinsic silicon films and the group V elements, arsenic, antimony and tantalum in the doped films. In this section the spectrometer and the experimental procedure, are briefly described. Detailed discussion on the instrumentation and the capabilities of these techniques can be found in a recent monograph (Briggs and Sheah 1983) and several review articles (for example Werner and Garten 1984, Sheah 1984).

4.3.2a Instrumentation

The instrument employed in the present study was a Kratos XSAM 800 spectrometer, pictured in plate (5). The spectrometer is composed of six basic components: (1) source, (2) sample compartment, (3) electron energy analyser (4) electron multiplier (5) sputter ion gun, (6) vacuum system.

(1) Source

In XPS the sample is irradiated by a monoenergetic beam of X-rays. In this system a dual anode X-ray gun was used with magnesium and aluminium as targets, the energies of the K_{α} X-rays of these materials are 1253.6 eV and 12486.6 eV respectively. For most of the experiments in the present study Al K_{α} radiation was employed. In AES experiments the atoms were ionised by electron bombardment.



Plate 4.4 The KRATOS (XSAM 800) Auger and x-ray photo-electron spectrometer.

Monoenergetic beams of electrons of energy up to 5 keV could be obtained from the electrostatic electron gun. The electron beam could be scanned across the sample, and its spot size could be varied from 0.5 to 120 μ m.

(2) Sample holder

For XPS and AES the films were deposited on aluminium substrates this was because in AES and XPS insulators can become charged due to the electron bombardment. The substrates were stuck to the holder by double sided adhesive tape, and introduced to the analysis region by means of an airlock arrangement, so that only a few minutes were required to achieve the UHV conditions.

(3) Electron Energy Analyser

The spectrometer was equipped with an electrostatic hemispherical sector analyser which was operated in the Fixed Analyser Transmission (FAT) mode for XPS and Fixed Retarding Ratio (FRR) mode for AES. In XPS analysis it is necessary to apply the same absolute resolution to all the photo-peaks. However this is difficult because the photoelectrons can have energies of up to 1253.6 eV if Al K α radiation is used. To overcome this problem the photoelectron energies are retarded to a fixed analyser energy, called the pass energy. In the FAT mode the system can be operated at low, medium and high magnifications which have pass energies of 100, 65 and 38 V respectively. In the FRR mode the electrons are decelerated by a constant ratio, from their initial kinetic energies, this process allows high sensitivity at high Auger energies and high absolute resolution at low Auger energies. Detailed

discussion into the merits of operating in either of the modes can be found elsewhere (Briggs and Sheah 1983).

(4) Sputter Ion Gun

The spectrometer was equipped with a Perkin-Elmer (PHI Model 04-161) sputter ion gun. Thus the sample could be etched by bombarding it with argon ions of energy upto 2 keV. Unfortunately the area etched by the gun, about 10 mm² was much less than the area analysed in XPS, thus depth profiling was limited with this technique. However in AES the area analysed is much smaller and the electron beam can be focussed at the centre of the crater made by the ion gun. Thus enabling the determination of the impurities at various depths.

(5) Vacuum System

The spectrometer was evacuated by a liquid nitrogen cooled 'Varian' diffusion pump with a speed of 300 l /s, backed by an 'Edwards' (E2M8) 2 stage rotary pump. Another rotary pump was used just as a roughing pump. The system was also equipped with a titanium sublimation pump, enabling base pressures in region of 10⁻¹⁰ torr. A small ion pump with a speed of 8 l /s was employed for evacuating the X-ray gun.

4.3.2b Experimental Procedure

XPS

At any particular depth the XPS spectra were usually obtained before the AES spectra. This is because of electron bombardment the

sample can become charged during an AES experiment. The procedure for both of the techniques was similar, in that, a wide scan was initially made and all major peaks identified using standard spectra. The standard spectra for XPS and AES can be found in the Handbook of X-ray photoelectron spectroscopy (Wagner et al 1978) and Handbook of Auger electron spectroscopy (Davis et al 1978) respectively. After identifying the major peaks, narrow scans of these peaks, were made for quantitative analysis. Concentration of the impurities was determined from the relation.

$$X_A = \frac{I_A/I_A^\infty}{\sum_i I_i/I_i^\infty} \quad (4.10)$$

$i = A, B$

where X_A is the concentration of the element and I_A the height of its peak in the spectrum. The sum is over all the constituents of the film and I_i represents the height of their peaks. I_A^∞ and I_i^∞ are the intensities from the pure elements, but they are not known, however the ratio I_A^∞/I_i^∞ , that is the relative sensitivity factors can be found. For XPS the relative sensitivity factors used were those given in the Handbook of X-ray photoelectron spectroscopy. For AES the relative sensitivity factors were determined in the laboratory (Abbot 1982).

4.3.3 Infra-red Spectroscopy

Infra-red spectroscopy is commonly used to reveal the presence of hydrogen (Brodsky et al 1977) and oxygen (Anderson et al 1979) in amorphous silicon films. In the present study infra-red transmission spectra were obtained for a selected number of samples using a Perkin-Elmer double beam infra-red spectrometer.

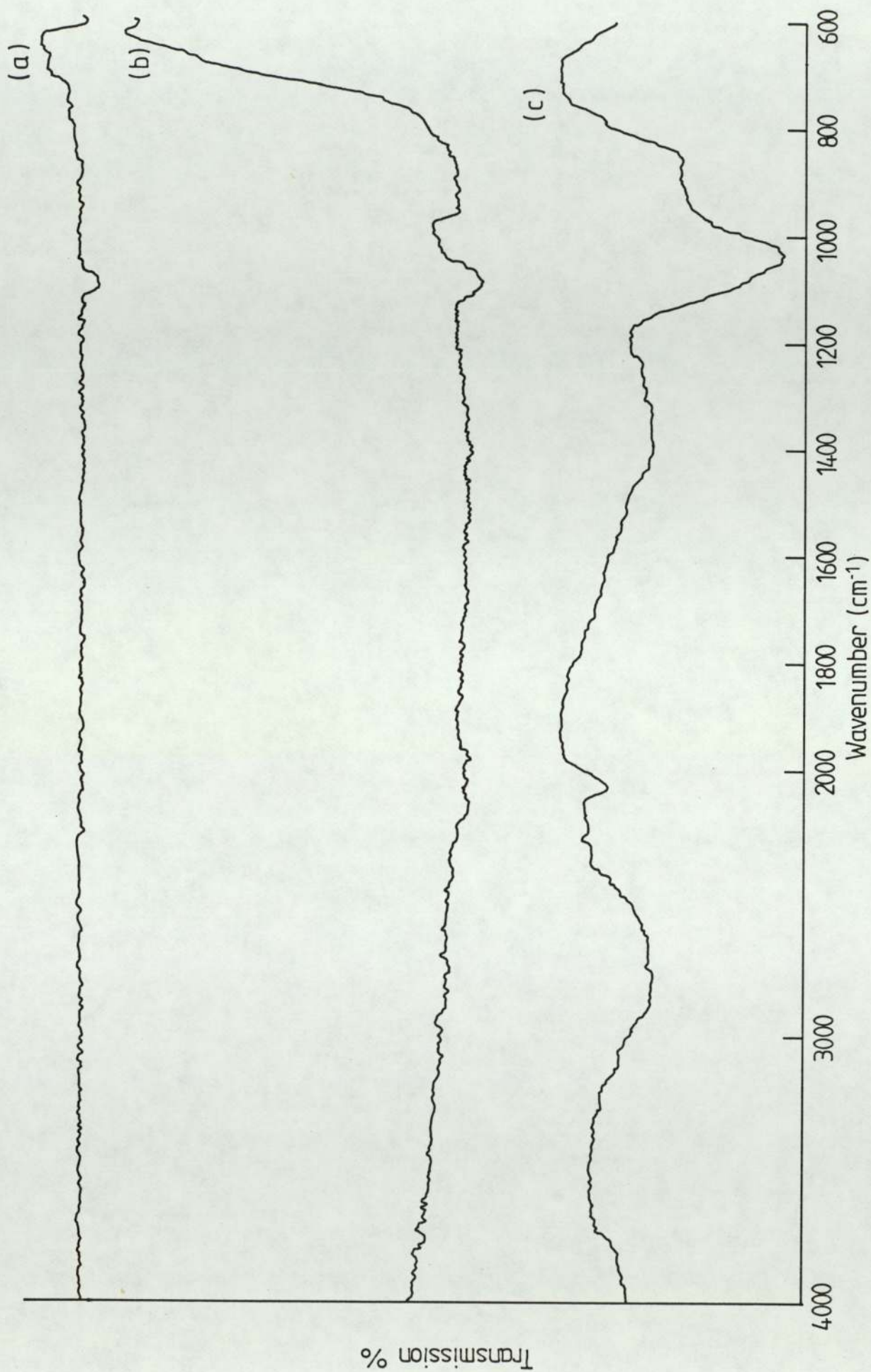


Figure 4-18 Typical I.R. spectrum; (a) crystalline silicon, (b) neon sputtered and (c) argon sputtered.

The samples were deposited on crystalline silicon, mirror polished on both sides. The thickness of the films was in the range 1.0-5.0 μ m. The spectrophoto-meter recorded the transmission of the films between the range of wave numbers 4000 to 600 cm^{-1} . In figure (4.18) three of the typical spectra are shown. Spectrum (a) is from crystalline silicon used as target. Spectrum (c) is of an argon sputtered film, the absorption peak at wavenumber of 1050 cm^{-1} has been attributed to oxygen. Spectrum (b) is typical of the neon sputtered films where oxygen peak is much reduced. None of the spectra showed any peaks which could arise from the silicon hydrogen bonds (Brodsky 1977), thus confirming the expectation that none of the films produced by the present techniques contain hydrogen.

5. RESULTS

5.1 THE EFFECT OF VARYING THE ARGON PRESSURE ON THE ELECTRICAL AND OPTICAL PROPERTIES OF AMORPHOUS SILICON FILMS

In this section the results of the effects of varying the argon sputtering pressure on the electrical and optical properties of amorphous silicon films are presented. Conventionally amorphous silicon is sputtered at a pressure of 5 mtorr (Anderson et al 1979). If the sputtering gas is pure argon the material contains a high density of dangling bonds ($\sim 10^{20} \text{ cm}^{-3}$) and hence a high density of defect states in the mobility gap (Brodsky and Title 1969). This results in a material with relatively high conductivity ($\sim 10^{-3} (\Omega \text{ cm})^{-1}$) which is only weakly temperature dependent, the thermal activation energy being of the order of 0.2 eV, photoconductivity is negligible and the optical gap is around 1.44 eV (Brodsky 1971). However, the density of dangling bonds can be reduced and the properties improved drastically by incorporating hydrogen into the silicon matrix (Paul et al 1976). Hydrogen incorporation is achieved by sputtering in a plasma of hydrogen and argon. Typically the partial pressure of hydrogen is about 1 mtorr resulting in approximately 20% atomic hydrogen in the films (Oguz, Paesler 1978). These films are characterized by relatively low conductivity ($\sigma_{\text{RT}} \sim 10^{-9} \Omega^{-1} \text{ cm}^{-1}$) which is thermally activated above room-temperature ($\Delta E \sim 0.9 \text{ eV}$) (Anderson et al 1977), further they exhibit photocurrents three to four orders of magnitude greater than the dark current (Moustakas and Paul 1977).

It has also been found that the optical gap increases and the absorption edge shifts to higher energies on the addition of hydrogen (Freeman and Paul 1978). Recent review articles on the effect of varying the preparation conditions on the properties

of rf sputtered amorphous silicon have been published by Moustakas (1979) and Paul and Anderson (1981).

Due to the success of controlling the properties of a-Si by hydrogenation, little work has been done on improving the properties of a-Si prepared by sputtering in pure argon, by optimising the preparation conditions. Notable exceptions are Pawlewicz (1978) who studied the effect of varying the argon pressure from 20 to 150 mtorr and target substrate spacing from 2 to 12.7 cm, and the Japanese groups who have studied extensively the effect of varying the product of pressure and target-substrate distance (Shimizu et al, 1979) and the effect of rf bias sputtering (Suzuki et al 1981).

Following Pawle^ewicz, we have studied the effect of varying the sputtering pressure from 5 to 110 mtorr, but the films have been characterized in considerably more detail by measurement of electrical conductivity (σ_{RT}), thermal activation energy (ΔE), photoconductivity (σ_{ph}), optical gap (E_0), and the composition, as a function of sputtering pressure. The significance and comparison, of these and other results with those obtained in the present study will be made in the next chapter.

The argon sputtering pressure was varied from 5 mtorr to 110 mtorr. Over ten films were deposited at various pressures on Corning 7059 glass slides and the variation of their electrical conductivity with temperature investigated. Figure (5.1) shows the variation of electrical conductivity (σ_{RT}) with inverse temperature for a selected number of samples. We see that for films deposited at 5 mtorr sputtering pressure (curve A), the dark conductivity is high and non-activated, but by increasing the sputtering pressure to 15 mtorr

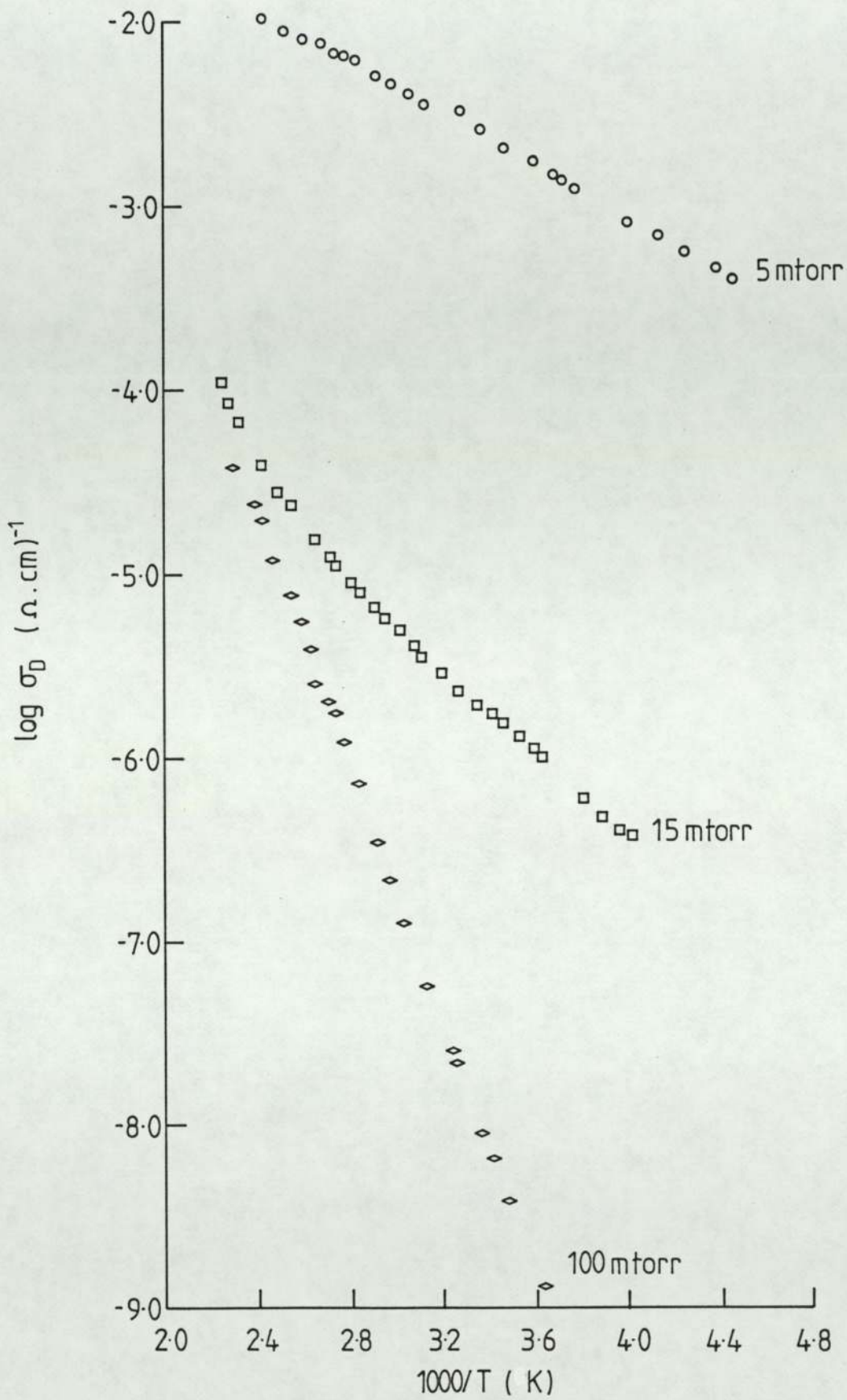


Figure 5.1 The variation of electrical conductivity with inverse temperature for films sputtered at various argon pressures.

(curve B) the conductivity has been decreased by more than three orders of magnitude and is activated above 100°C.

For all the films deposited at sputtering pressures above 40 mtorr a singly activated thermal activation energy could be defined above room temperature. The third plot (curve C) represents a typical sample in this range, sputtered at a pressure of 100 mtorr, the room temperature dark conductivity is about $8.0 \times 10^{-9} (\Omega\text{cm})^{-1}$ and is singly activated with an energy of about 0.66 eV.

The results of varying the sputtering pressure from 5 to 110 mtorr on the room-temperature dark and photoconductivities are summarised in figure (5.2). We see that for films sputtered at low pressures, room temperature dark conductivity (σ_{RT}) is about $3 \times 10^{-3} (\Omega\text{cm})^{-1}$ and the photoconductivity is negligible. By increasing the pressure to about 40 mtorr, σ_{RT} is decreased by more than five orders of magnitude but any further increase in pressure has little effect on σ_{RT} , however the photoconductivity (σ_{ph}) increases monotonically with pressure to a value of about $10^{-7} (\Omega\text{cm})^{-1}$ at the highest pressures. The highest pressure at which the system can be operated with argon is limited by the geometry of the target and is about 110 mtorr beyond which the mean free path of the argon ions becomes comparable to the spacing between the target and the earth shield surrounding it.

A similar behaviour to σ_{RT} is observed in the variation of thermal activation energy, ΔE , and the optical gap, E_0 , with pressure as illustrated in figure (5.3). ΔE increases from 0.14 eV to about 0.6 eV as the pressure is increased from 5 to 65 mtorr, any further increase in pressure having little effect. The optical gap, E_0 ,

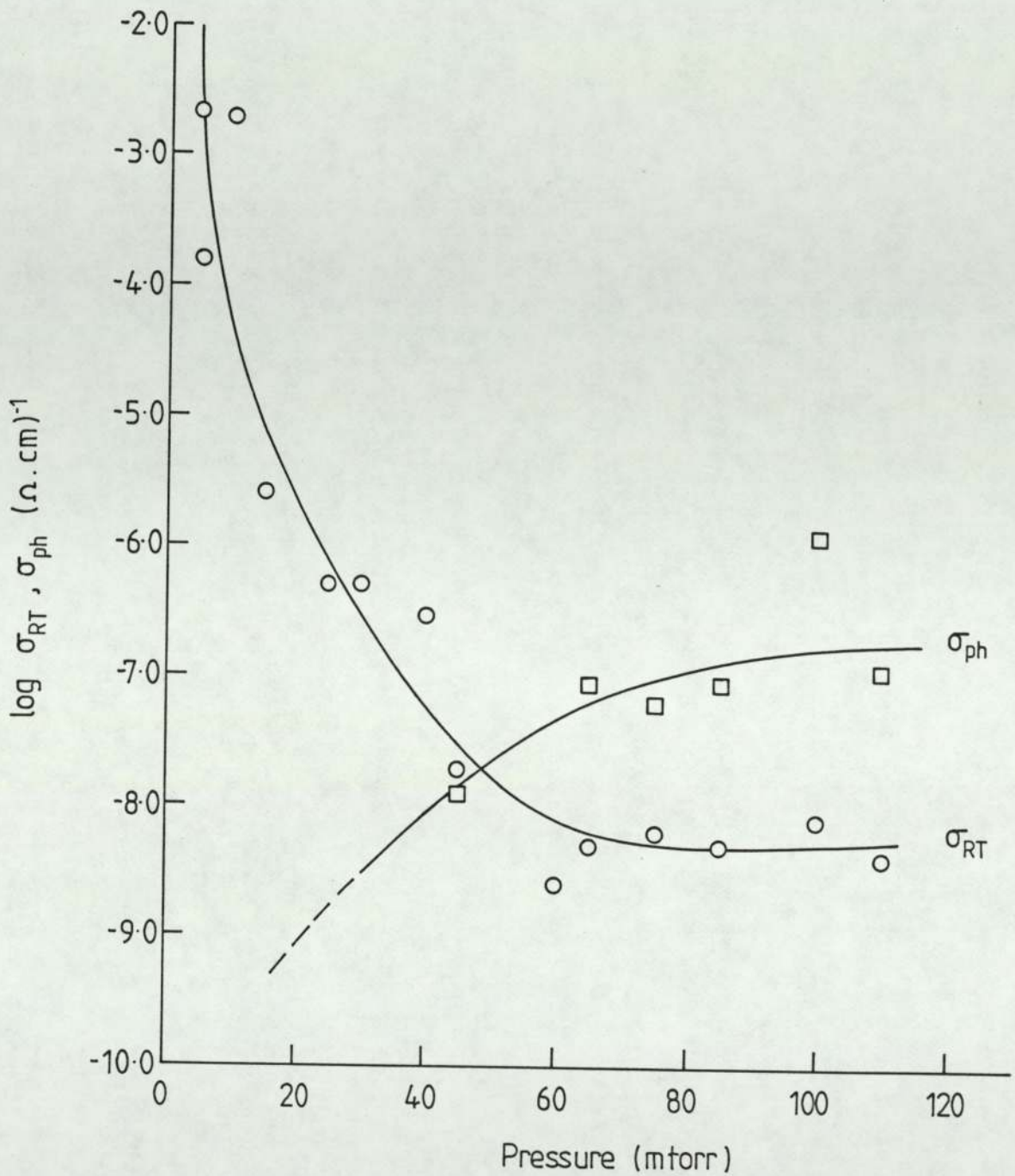


Figure 5.2 Variation of room-temperature dark conductivity (σ_{RT}) and photo conductivity (σ_{ph}) with sputtering pressure of argon.

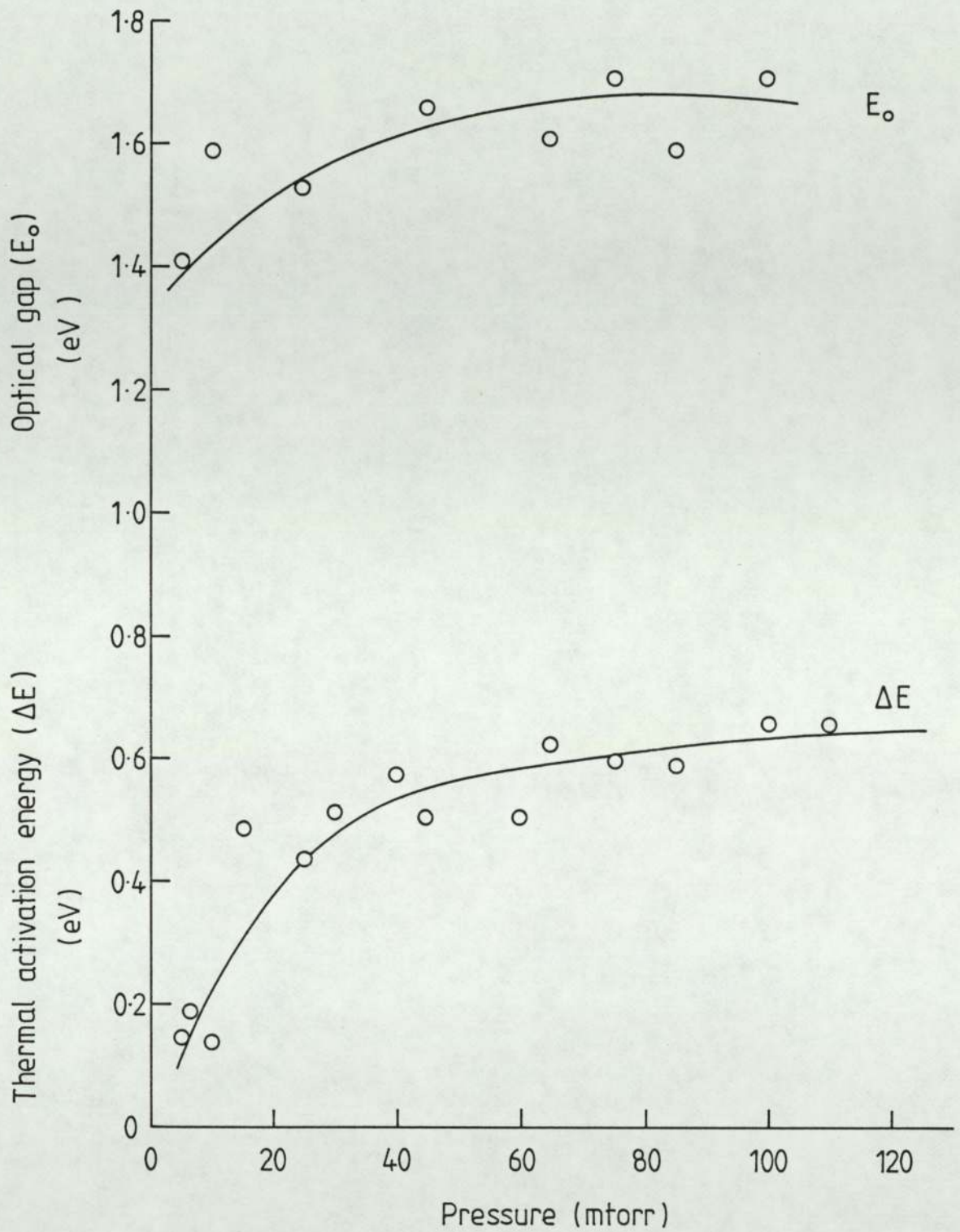


Figure 5.3 Variation of thermal activation energy (ΔE) and the optical gap (E_o) with sputtering pressure.

also increases sharply from about 1.4 eV at low pressure to about 1.7 eV around 65 mtorr but further increase in pressure produced little change. The optical gap was deduced from plots of $(\alpha \hbar \omega)^{\frac{1}{2}}$ vs $\hbar \omega$ as discussed earlier (section 4.2.4). Figure (5.4) shows some of the representative plots. The absorption edge has been shown to depend critically on the method of preparation (Freeman and Paul 1979). It is found that as the concentration of hydrogen is increased the optical gap increases and the absorption edge shifts to higher energies. It is thought that the absorption edge shifts to higher energies and sharpens because the density of states is reduced on incorporating hydrogen. Figure (5.5) shows the variation of the absorption coefficient with energy for a selected number of films. The absorption edge first shifts to higher energies as the sputtering pressure is increased to about 40 mtorr but then reverses on further increase in pressure.

The composition of the films was investigated by Rutherford backscattering spectroscopy (RBS), X-ray photoelectron spectroscopy (XPS) and Auger electron spectroscopy (AES). RBS was particularly useful because the depth distribution of the elements was also revealed. A typical RBS spectrum of an argon sputtered film deposited on Al_2O_3 substrate is shown in figure (5.6). By comparing the width of the argon and silicon peaks, it is evident that the argon is distributed uniformly in the a-Si film. The composition was determined by measuring the heights of the elemental peaks and using the equation (Chu et al 1978).

$$\frac{N_{\text{imp}}}{N_{\text{Si}}} = \frac{H_{\text{imp}}}{H_{\text{Si}}} \times \frac{\sigma_{\text{Si}}}{\sigma_{\text{imp}}} \quad (5.1)$$

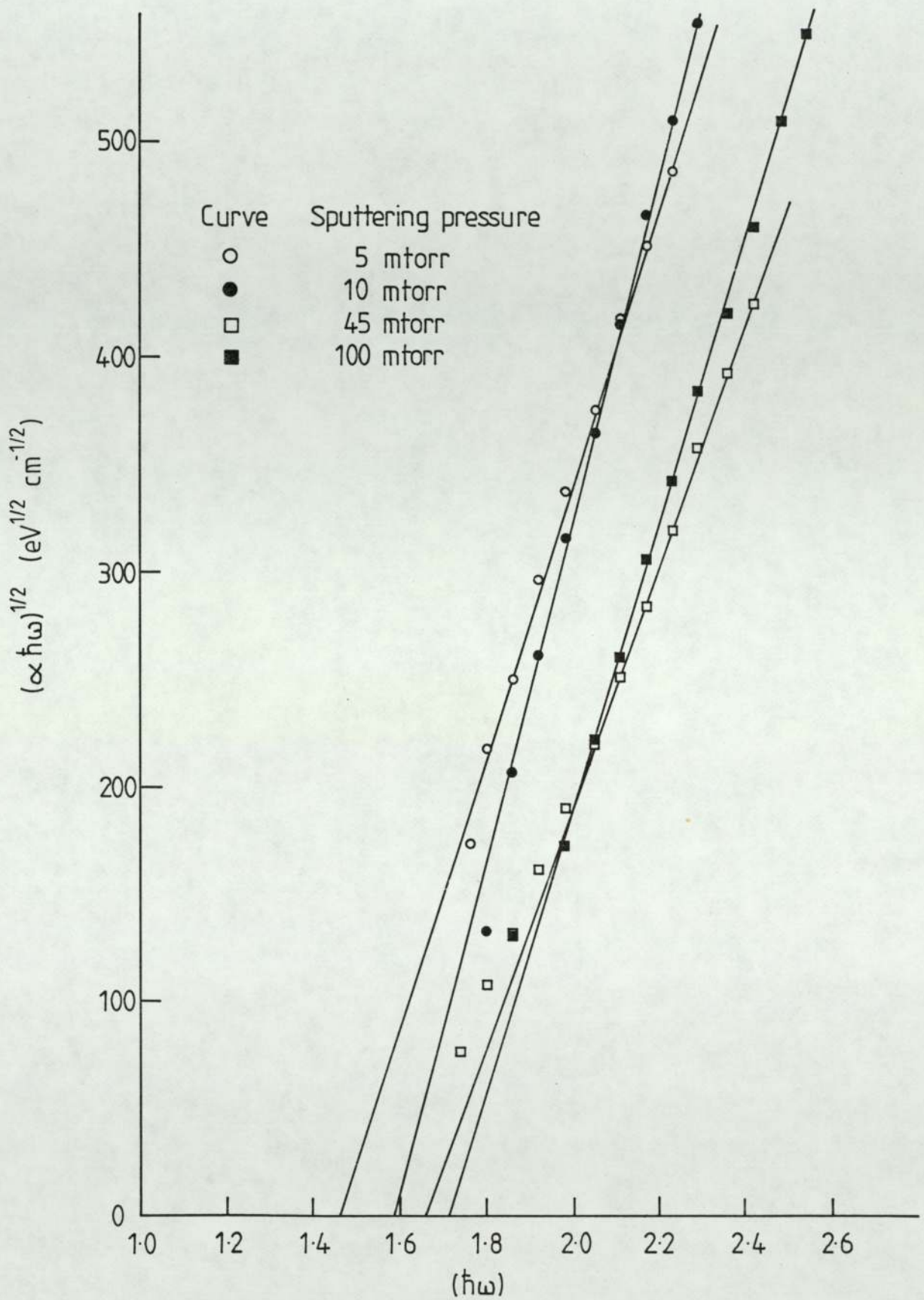


Figure 5-4 Some of the typical plots of $(\propto \hbar\omega)^{1/2}$ vs $\hbar\omega$ from which E_0 was deduced for argon sputtered films.

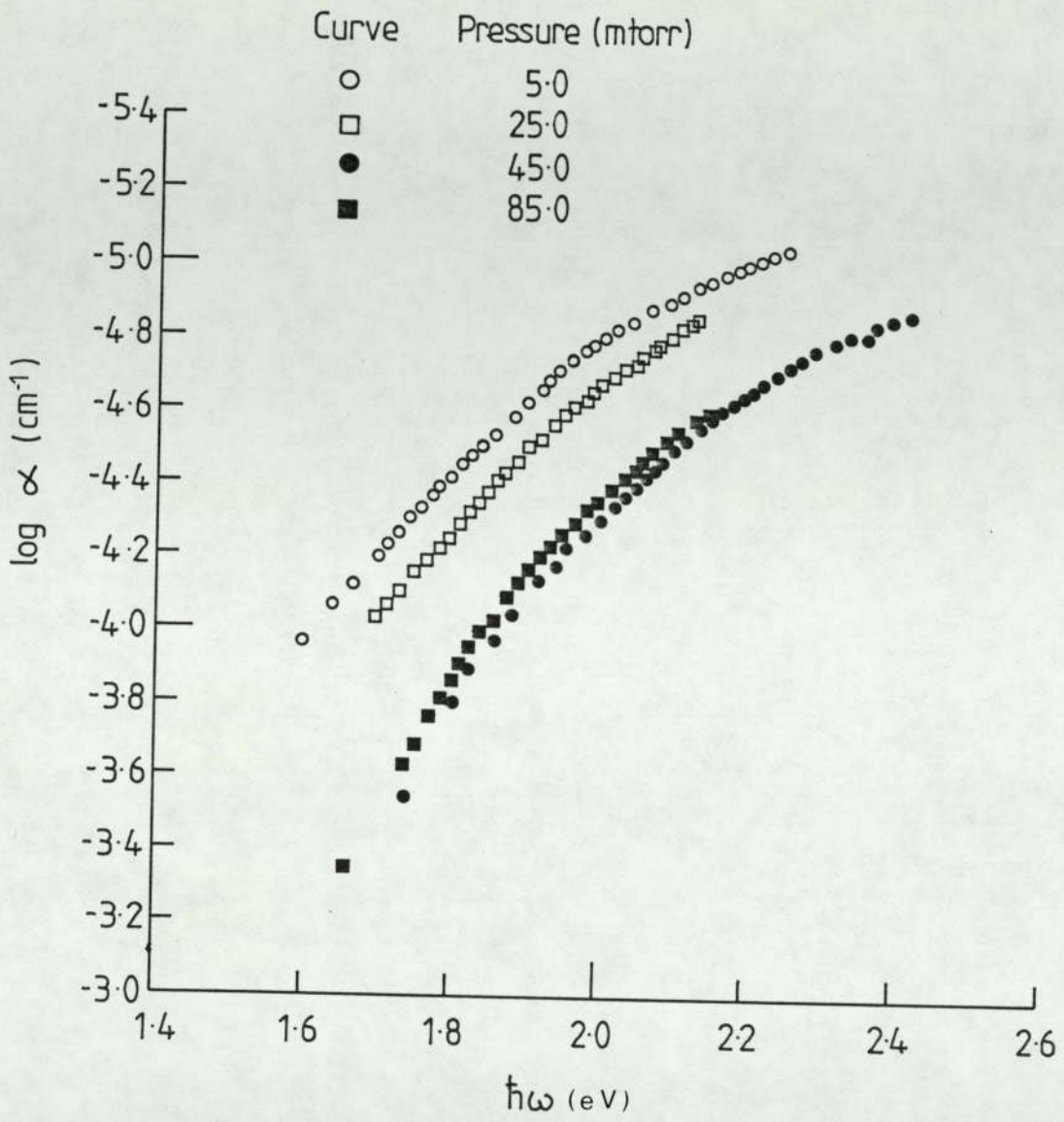


Figure 5.5 Shift of the absorption edge with argon pressure.

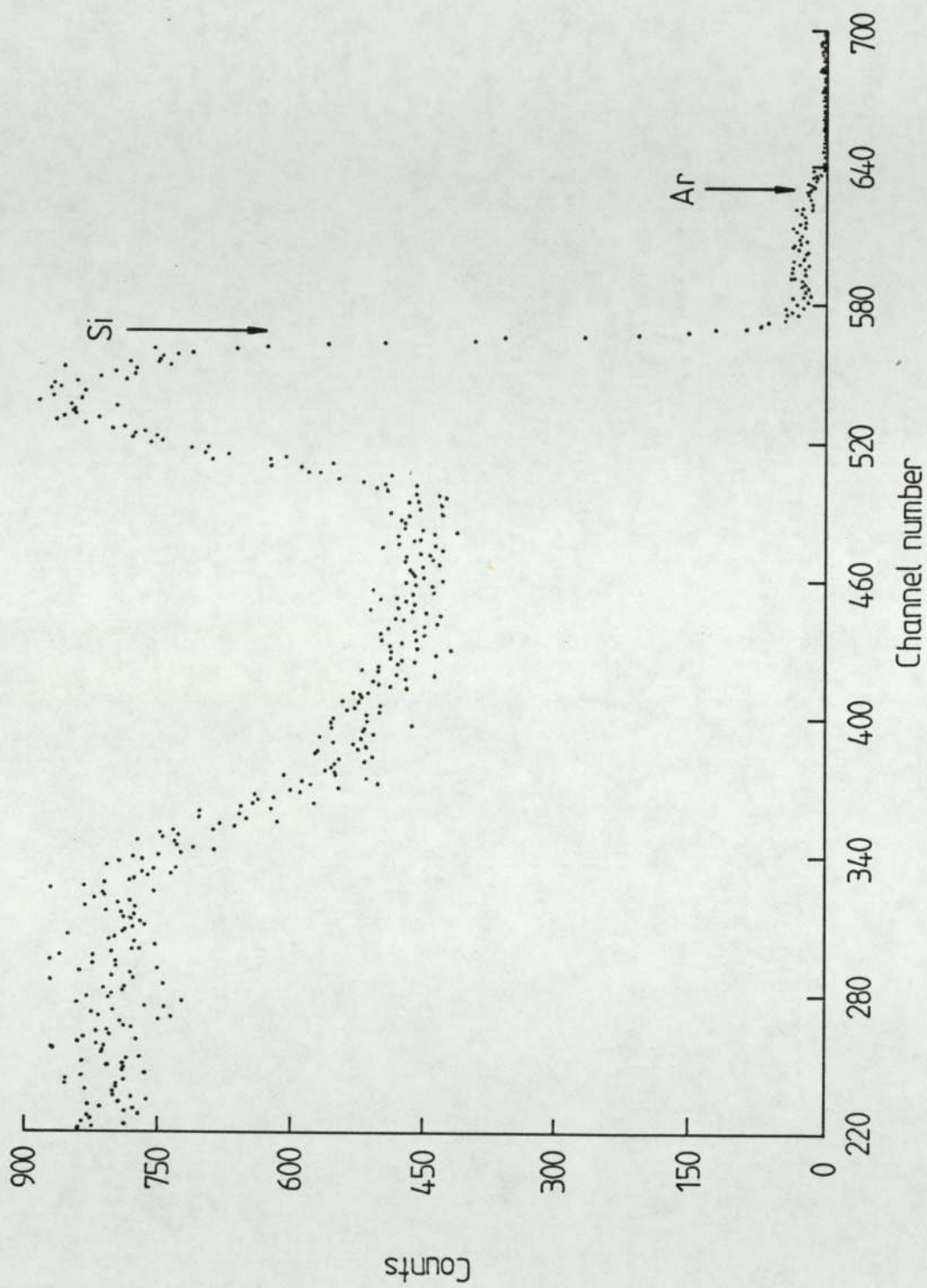


Figure 5.6 Typical RBS spectrum of an argon sputtered amorphous-silicon film deposited on Al_2O_3 substrate.

where $N_{\text{imp}}/N_{\text{Si}}$ is the ratio of the impurity atoms (O_2 or Ar) to silicon atoms, H_{imp} and H_{Si} are the heights of the impurity and silicon peaks and σ_{imp} and σ_{Si} are the Rutherford backscattering cross-sections of the impurity and silicon atoms respectively. The Rutherford backscattering cross-sections are available from standard tables (Chu et al 1978).

Figure (5.7) shows the composition of argon sputtered films as a function of sputtering pressure. The films were deposited at various sputtering pressures between 5 and 110 mtorr. The argon concentration which is about 8.0% at sputtering pressure of 5.0 mtorr, decreases sharply to about 2.0% as the pressure is increased to 30 mtorr. On further increasing the pressure to 110 mtorr the argon concentration decreases to about 0.5 mtorr. For films deposited at pressures upto 25-30 mtorr no oxygen was detected but for films deposited at higher pressures about 20% oxygen was observed. The error involved in determining the oxygen content is quite large, this is due to the low sensitivity this technique has for impurity elements lighter than the host element or the substrate material.

Finally, the effect of increasing the pressure on the deposition rate is shown in Figure (5.8). The deposition rate decreased monotonically from about 4.0 \AA S^{-1} at low pressure to about 2.0 \AA S^{-1} at the highest pressures. Although one would expect the sputtering rate to increase with increasing pressure due to the greater number of ions bombarding the target, the results are consistent with the fact that as the pressure is increased the fraction of sputtered silicon atoms backscattered into the target or scattered out of the target-substrate plane is also increased resulting in a net decrease in the deposition rate (Chapman, p188, 1980).

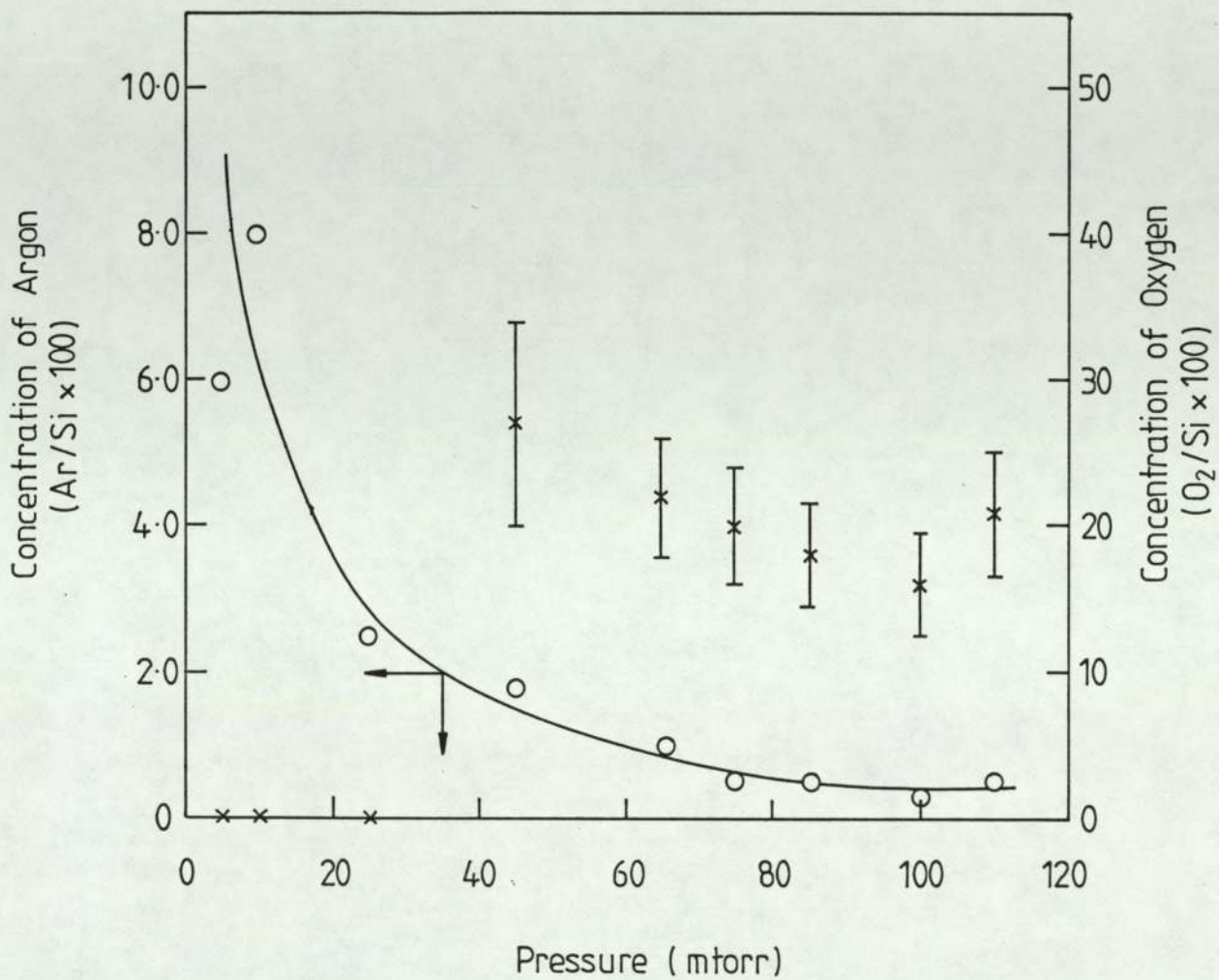


Figure 5.7 The composition of argon sputtered films as a function of sputtering pressure.

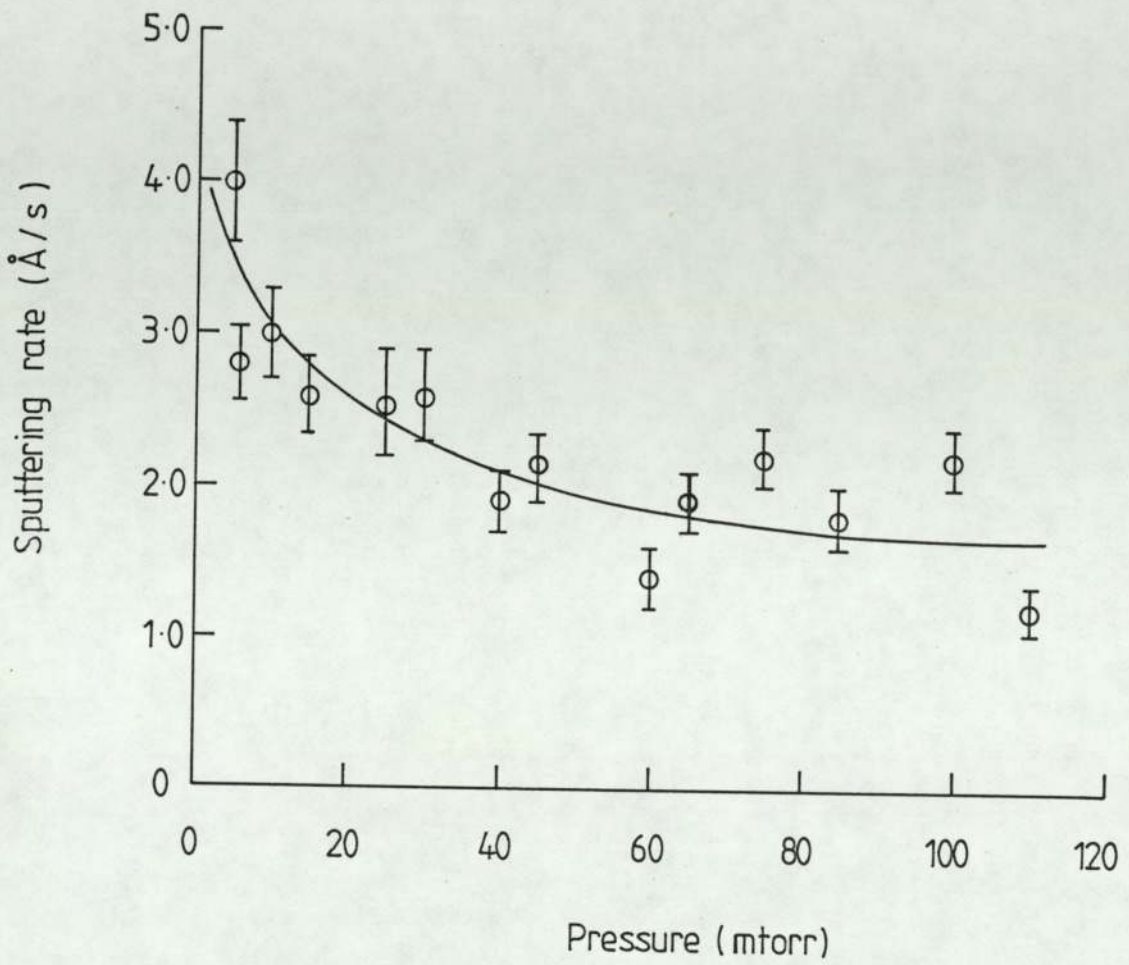


Figure 5·8 The variation of the sputtering rate with argon pressure.

Sample N°	Sputtering pressure (mtorr)	$\log \sigma_D$	$\log \sigma_{ph}$	ΔE (eV)	E_o (eV)	Conc. of Ar. (%)	Conc. of O ₂ (%)	Dep. rate (Å/s)
1	5	-2.63		0.15	1.41	6.0	0	4.0
2	6	-3.8		0.19				2.8
3	10	-2.7		0.14	1.59	8.0	0	3.0
4	15	-5.6		0.49				2.6
5	25	-6.3		0.44	1.53	2.5	0	2.53
6	30	-6.26		0.52				2.6
7	40	-6.52		0.58				1.9
8	45	-7.7	-7.91	0.51	1.66	1.8	27.0	2.3
9	60	-8.66		0.51				1.4
10	65	-8.3	-7.05	0.63	1.61	1.0	22.0	1.9
11	75	-8.2	-7.21	0.6	1.71	0.5	20.0	2.2
12	85	-8.3	-7.05	0.59	1.59	0.5	18.0	1.8
13	100	-8.1	-5.9	0.66	1.71	0.3	16.0	2.2
14	110	-8.4	-6.95	0.66		0.5	21.0	1.2

Table 5.1 The variation of the electrical and optical properties and the composition of the films with argon sputtering pressure.

The effect of varying the argon sputtering pressure on the electrical and optical properties and the composition of the films is summarised in table 5.1.

5.2 EFFECT OF PREPARATION CONDITIONS ON THE PROPERTIES OF NEON SPUTTERED AMORPHOUS SILICON

As discussed in the previous sections, investigations into the improvement in the properties of pure a-Si produced by rf sputtering have been limited. Mainly directed towards reducing the bombardment of the film by the plasma species, by increasing the sputtering pressure and/or the target-substrate spacing. To our knowledge the effect of varying the sputtering gas was not considered till Fane (1981) showed the possibility of producing a material with a low density of defect states, capable of being doped, by sputtering in high pressure neon. Results presented by Fane were preliminary, and detailed investigation into the effect of varying the sputtering conditions on the properties of a-Si was required. In the present work an extensive investigation into the effect of varying the sputtering pressure, target-substrate spacing, dc self-bias voltage on the target and the substrate temperature on the electrical and optical properties and the composition of the material has been carried out. It has also been shown that material produced at the optimum conditions can be doped efficiently.

5.2.1 Variation of the Neon Sputtering Pressure

Neon sputtering pressure was varied from 5 mtorr to 250 mtorr and its effects on the electrical and optical properties of amorphous silicon investigated. As in the case of argon sputtering the films

were characterized by measuring the electrical conductivity over a temperature range of 150°C, room-temperature photoconductivity, UV-Vis spectrophotometry and the determination of the composition as a function of the sputtering pressure. However for neon, the range of sputtering pressures was extended to about 250 mtorr; this is due to neon having a smaller mass and larger m.f.p. than argon.

Nearly thirty films were produced over a period of three years and although sputtering parameters other than pressure were kept constant, as discussed earlier (Chapter 4.1.1) the variation in the geometry of the system due to improved target and substrate holders and other minor alterations to the system probably affected the films, although no systematic dependence was found. Slight variations in the base pressure from one run to another also affected the properties, this point will be discussed in more detail in the next chapter. Films in the thickness range 0.5 - 1.0 μm were chosen for electrical and optical measurements. Films produced under the same conditions but ^{of} thicknesses beyond this range to enable the compositional and structural studies to be carried out usually showed variation in the electrical and optical properties. No systematic investigation into the thickness dependence of these properties was carried out, so attempts were made to produce films of nearly the same thickness (0.5 - 1.0 μm) and hence delineate this effect.

For this set of experiments, other sputtering parameters were fixed at the following values; target-substrate spacing was set at 3.5 cm, dc self-bias voltage was in the range 880-890 volts and the substrate temperature was maintained between 280-320°C. The target was pre-sputtered for about 20 minutes but the actual

sputtering period was varied to obtain films 0.1-3 μm thick for RBS experiments, 0.5-1.0 μm thick for electrical and optical measurements and 2.0-5.0 μm thick for IR and X-ray diffraction measurements.

For all the films the dc conductivity was measured over a temperature range of about 150°C. Figure (5.9) shows some of the representative plots of log conductivity versus inverse temperature; all these plots were for measurement of conductivity after the sample had been heated in vacuum to about 175-200°C. For films sputtered at low pressures the conductivity is high and unactivated. As the pressure is increased to about 90 mtorr the conductivity decreases sharply and a single activation energy can be defined over the whole temperature range. The results of the conductivity measurements are summarised in figures (5.10) and (5.11). In figure (5.10) the variation in room-temperature (295°K) conductivity (σ_{RT}) as the sputtering pressure is increased from 5 to 245 mtorr is plotted. A sharp decrease in σ_{RT} is observed as the sputtering pressure is increased. The value of σ_{RT} decreases by nearly six orders of magnitude from about $10^{-3} (\Omega \text{ cm})^{-1}$ at 5 mtorr to less than $10^{-9} (\Omega \text{ cm})^{-1}$ at a sputtering pressure of 90 mtorr. Increasing the pressure to 150 mtorr results in a slight decrease in conductivity but on further increasing the pressure the trend is reversed and the conductivity increases slightly.

The variation of thermal activation energy of electrical conductivity with sputtering pressure is plotted in Figure (5.11), again a similar type of behaviour is observed, ΔE increases sharply from about 0.19 eV at 5 mtorr to about 0.8 eV at 90 mtorr, and then a gradual increase to about 0.85 eV as the pressure is increased

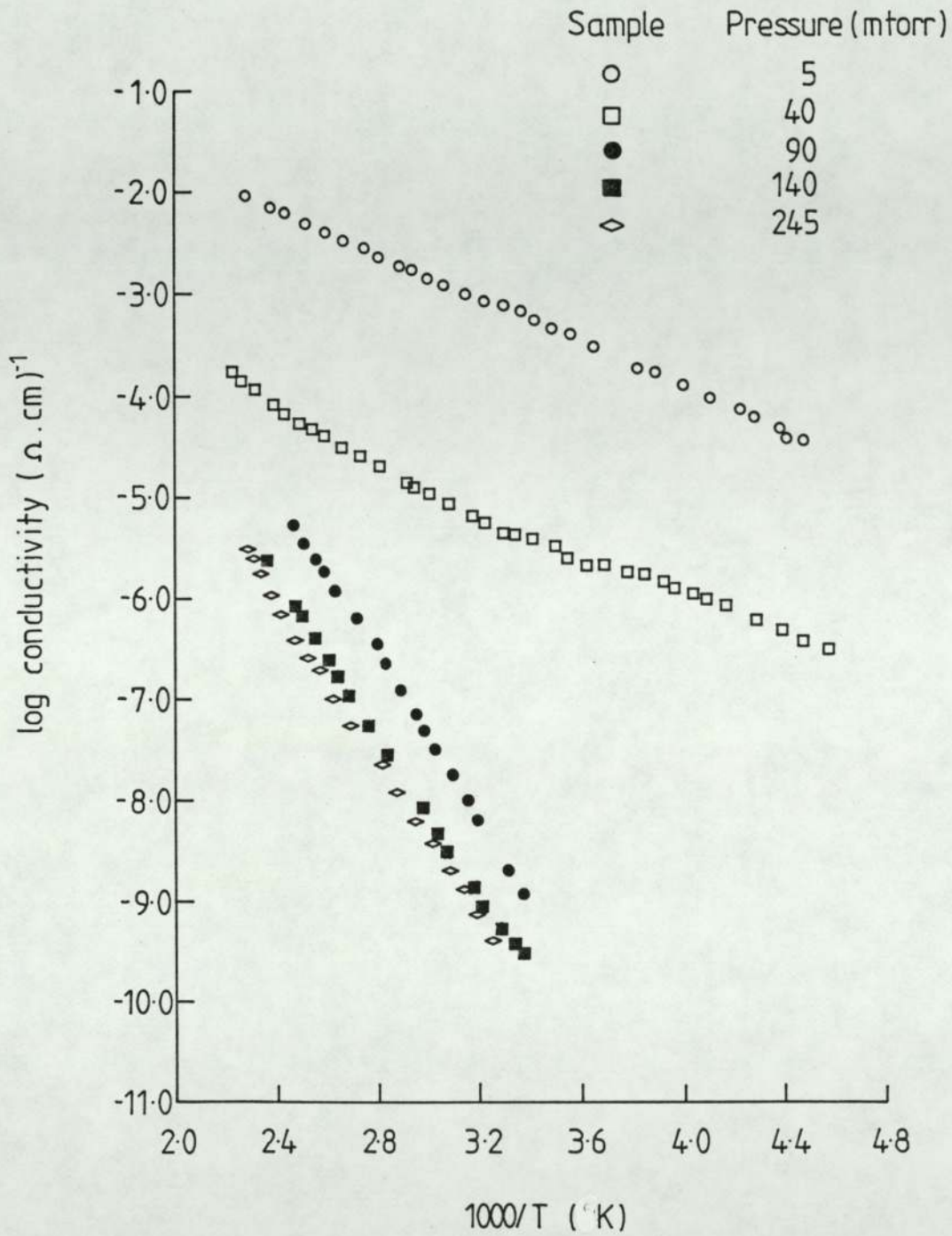


Figure 5-9 Conductivity versus inverse temperature for films sputtered at various neon pressures.

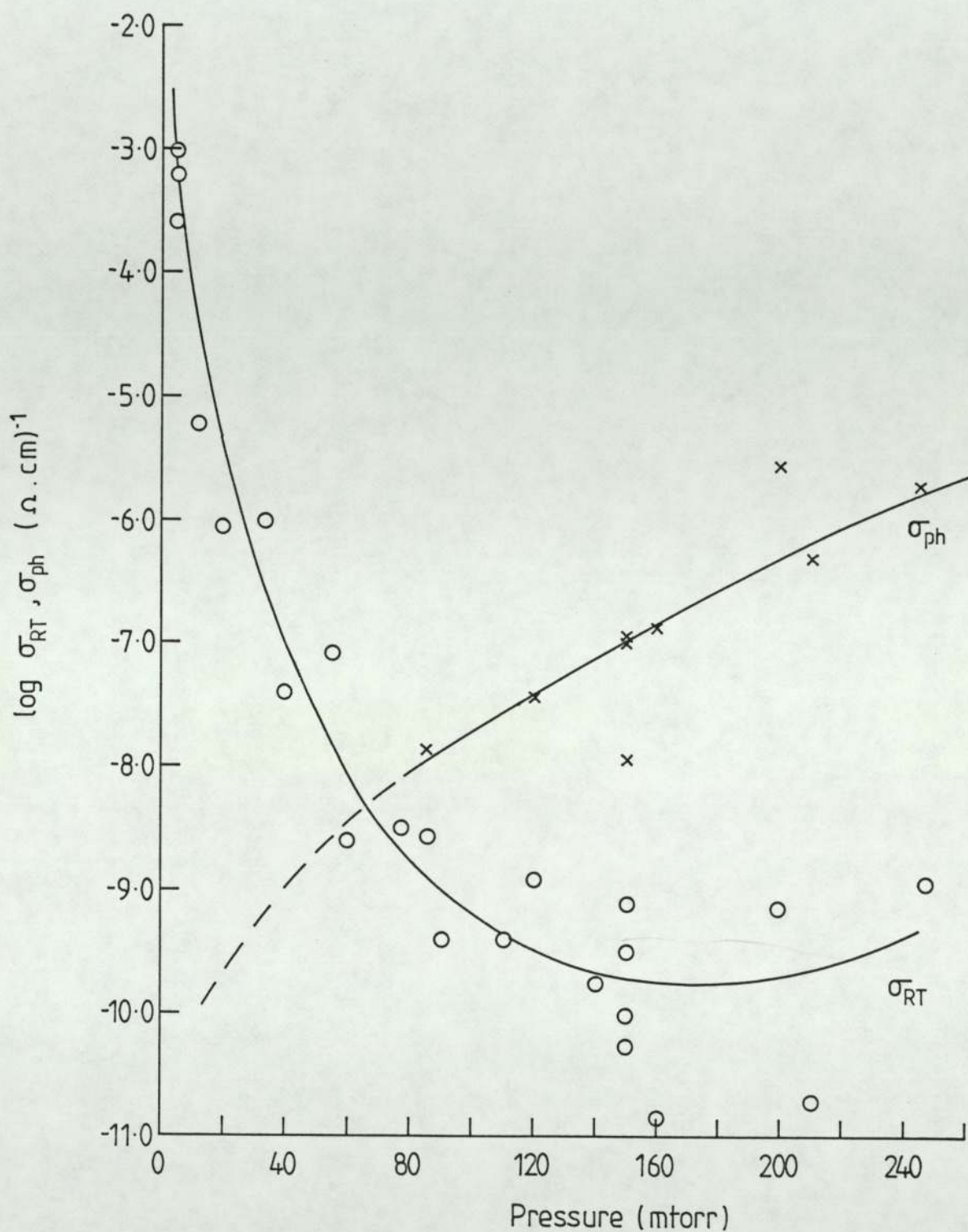


Figure 5.10 The variation of room-temperature dark (σ_{RT}) and photo (σ_{ph}) conductivities with neon sputtering pressure.

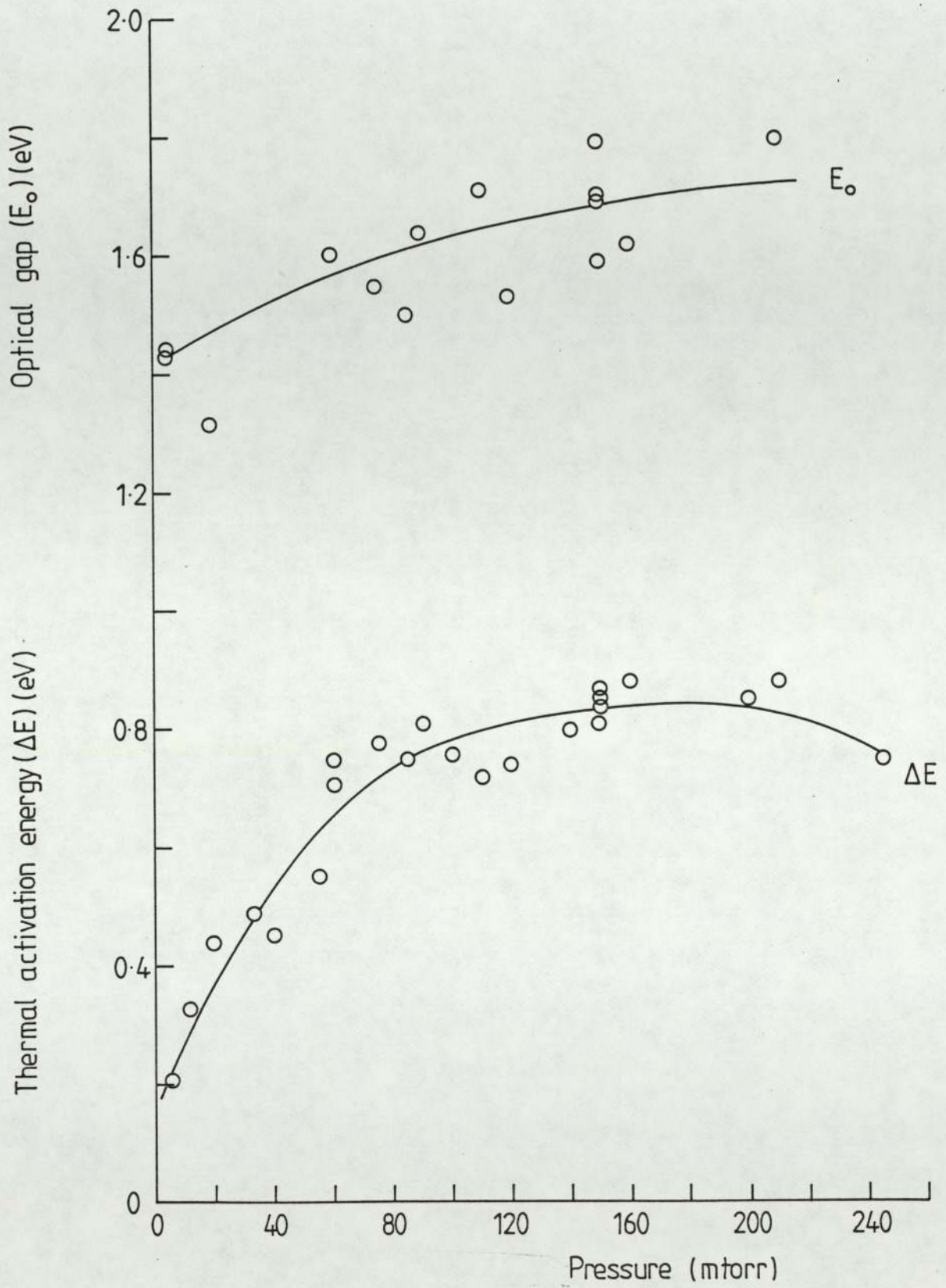


Figure 5-11 Variation of thermal activation energy (ΔE) and the optical gap (E_o) with neon sputtering pressure.

to 150 mtorr and again at the highest pressure a reversal in trend is observed with ΔE decreasing slightly.

The variation of photoconductivity with sputtering pressure is also shown in figure (5.10). The photoconductivity increases with pressure monotonically to a value of about $10^{-6} (\Omega \text{ cm})^{-1}$ at the highest pressures. The photoconductivity was not measurable for films deposited at pressure below about 40 mtorr, because the dark current was much larger than the photocurrent.

The variation of the optical gap with sputtering pressure is shown in figure (5.11). The optical gap increases from about 1.44 eV at 5 mtorr to about 1.7 eV at pressures around 150 mtorr. Some of the representative plots of $(\alpha \hbar \omega)^{\frac{1}{2}}$ vs $\hbar \omega$ from which E_0 was deduced are shown in figure (5.12). Results from the optical experiments were also plotted in the form of absorption coefficient versus energy and are shown in figure (5.13). The absorption edge sharpens and shifts to higher energies as the pressure is increased from 5 to 90 mtorr but on further increasing the pressure a reversal in the trend is observed.

The variation of these properties as the pressure is increased is similar to the variation observed on the addition of hydrogen to argon sputtered material (Paul et al 1976, Moustakas 1978) indicating that as in the case of hydrogenation, the density of defect states is reduced, by sputtering at higher pressures. The significance of the present results will be discussed in detail in the next chapter.

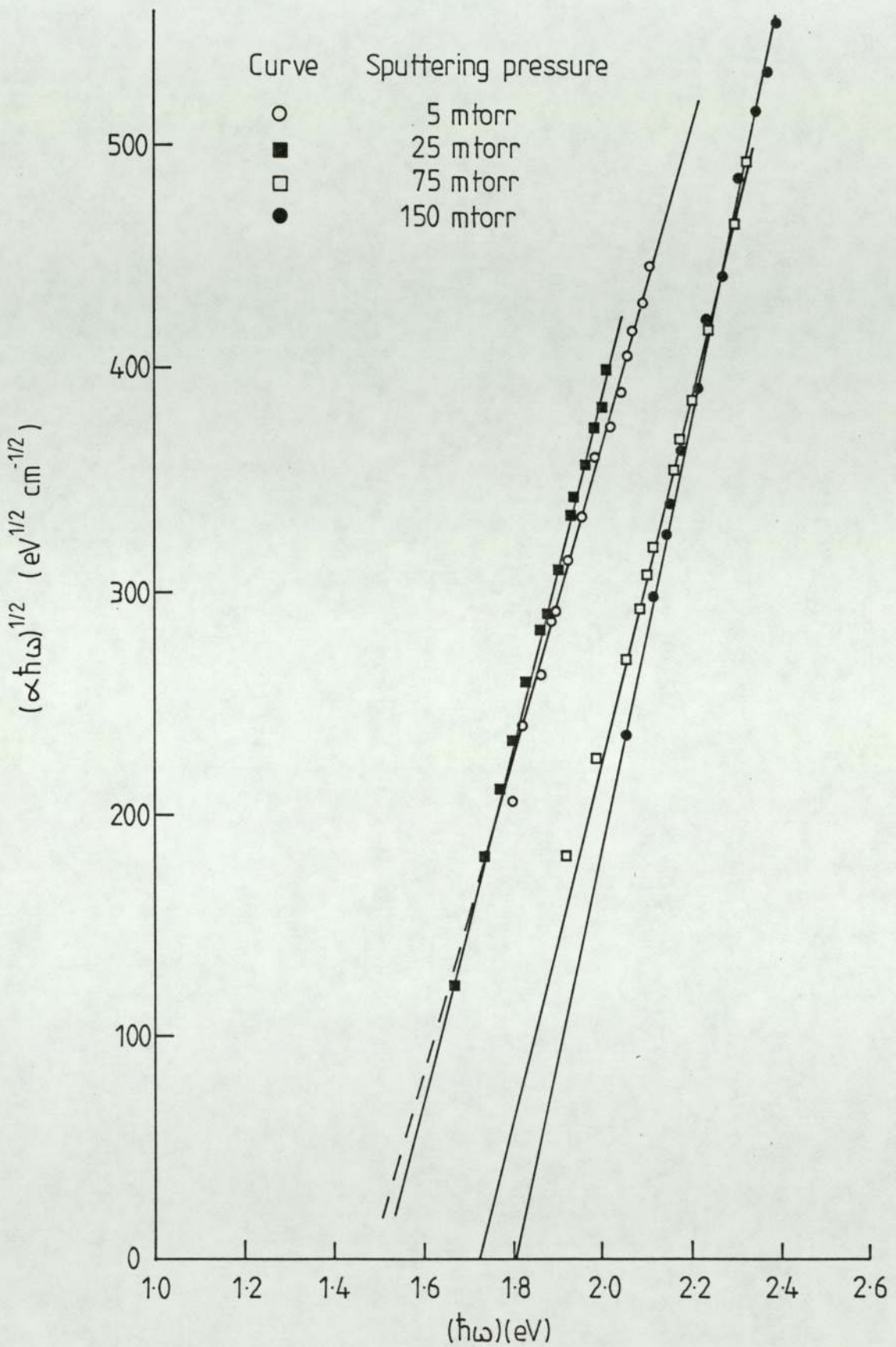


Figure 5.12 Plots of $(\propto \hbar\omega)^{1/2}$ vs $(\hbar\omega)$ for a selected number of samples sputtered at various neon pressures.

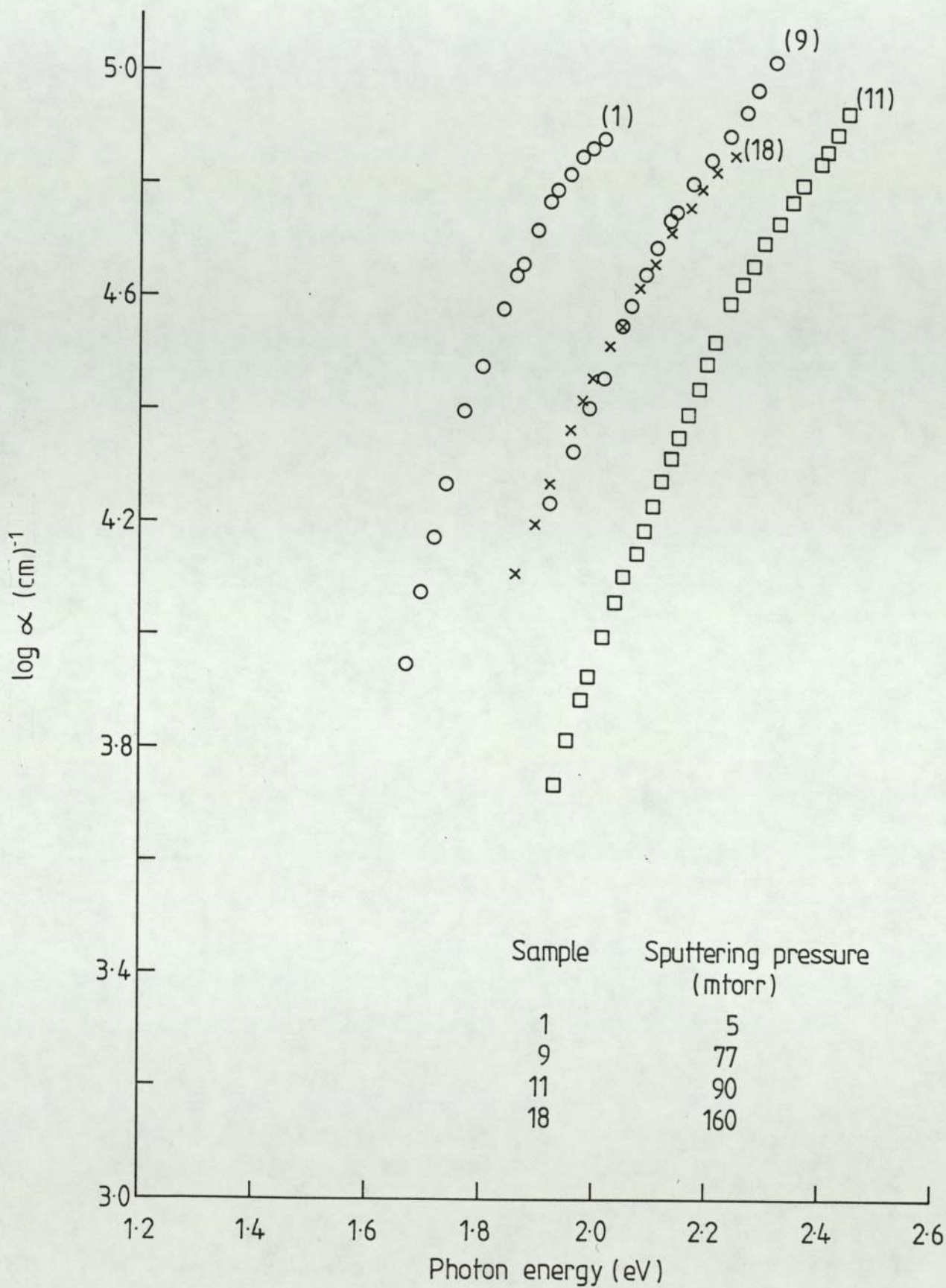


Figure 5.13 The absorption coefficient (α) vs. photon energy ($\hbar\omega$) for films deposited at various pressures

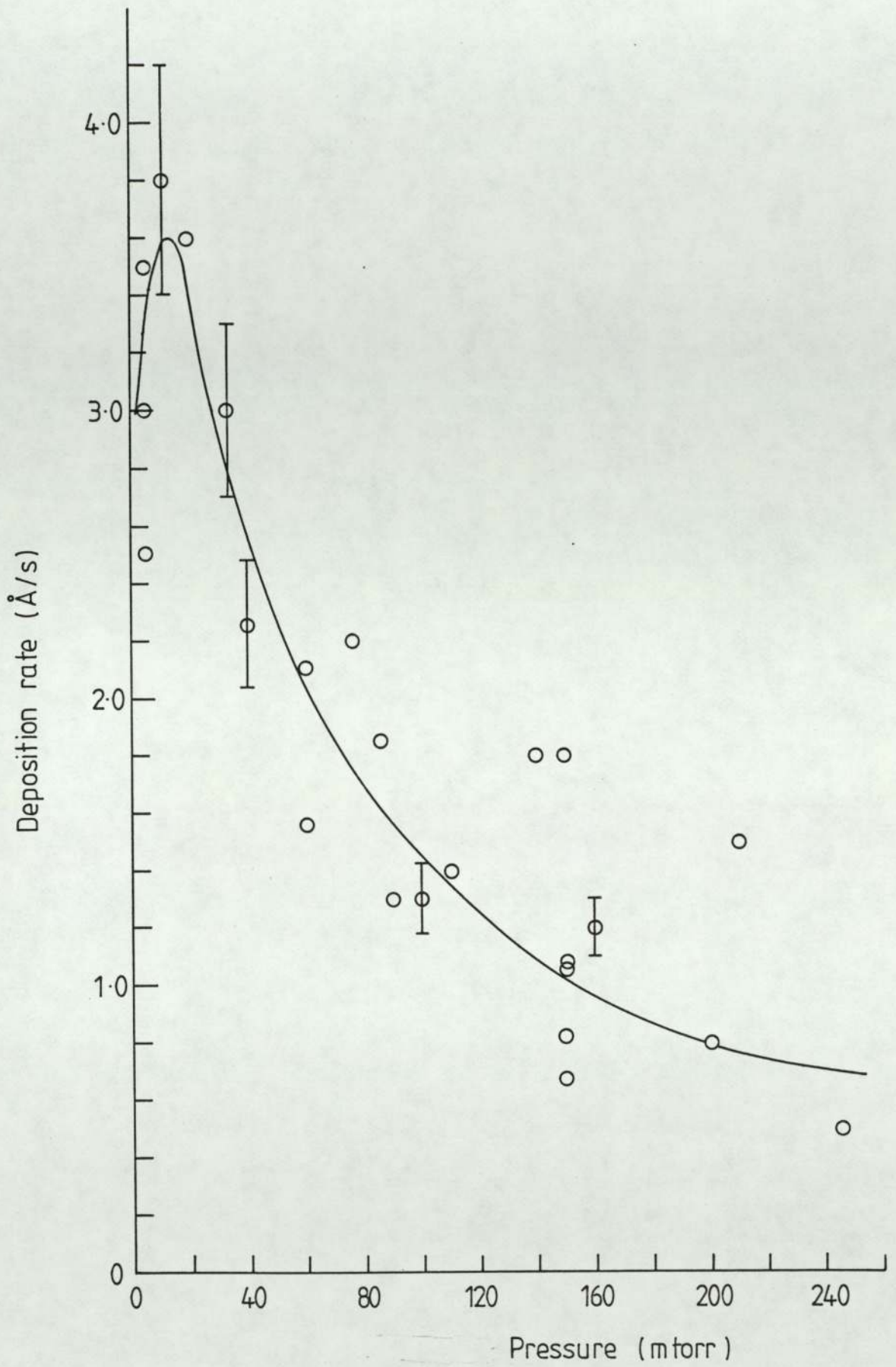


Figure 5-14 Variation of deposition rate with sputtering pressure.

The effect of varying the pressure on the deposition rate is shown in figure (5.14). The deposition rate increases from about 3.0 to 3.5 $\text{\AA}\text{S}^{-1}$ as the pressure is increased from 5.0 to about 15.0 mtorr but then decreases as the pressure is further increased. The deposition rate falls sharply from about 3.5 $\text{\AA}\text{S}^{-1}$ at 15 mtorr to about 1.5 $\text{\AA}\text{S}^{-1}$ as the pressure is increased to about 90-100 mtorr, on further increasing the pressure the deposition rate decreases gradually to a value of about 0.8 $\text{\AA}\text{S}^{-1}$ at the highest pressure. The results presented here on the variation of electrical and optical properties with sputtering pressure are summarised in Table (5.2).

The variation in the composition of the films as a function of the preparation conditions was also studied. This is because in the amorphous silicon terminology the words 'intrinsic' or 'pure' silicon have slightly different meaning to their more wider use in crystalline silicon technology. By 'intrinsic' amorphous silicon we mean that it contains no substitutional dopants (group III or V elements) but it may contain large amounts of impurities such as hydrogen and fluorine which are used as dangling bond terminators, argon or neon being the sputtering gases are nearly always incorporated, and other impurities such as oxygen could also be present in small amounts.

Films produced without the incorporation of any dangling bond terminators are described as 'pure' amorphous silicon films but again they always contain the sputtering gas and other trace impurities.

Sample N°	Sputtering pressure (mtorr)	$\log \sigma_{RT}$	$\log \sigma_{Dh}$	ΔE (eV)	E_o (eV)	Deposition rate (Å/s)
1	5	-3.0		0.21	1.43	2.5
2	5	-3.22		0.21		3.0
3	5	-3.58		0.21	1.44	3.5
4	11	-5.21		0.33		3.8
5	20	-6.04		0.44	1.32	3.6
6	33	-6.0		0.49		3.0
7	55	-7.8		0.55		
8	60	-8.6	-4.86	0.75		1.56
9	77	-8.5	-5.65	0.78	1.55	2.2
10	85	-8.54	-7.83	0.75	1.50	1.85
11	90	-9.4		0.81	1.64	1.3
12	110	-9.38	5.12	0.72	1.72	1.4
13	140	-9.78		0.8		1.8
14	150	-10.0	7.94	0.85	1.69	1.08
15	150	9.5	6.99	0.84	1.79	0.67
16	150	-9.1	-6.94	0.86	1.59	1.07
17	150	-10.28	-4.96	0.81		1.8
18	160	-10.86	6.81	0.88	1.62	1.2
19	200	-9.12	-5.55	0.85		0.8
20	210	-10.7	-6.3	0.88	1.80	1.5
21	245	-8.92	-5.7	0.75		0.5
22	120	8.82	-7.46	0.74	1.53	
23	150	9.5		0.84	1.70	0.83
24	60	-8.6		0.71	1.60	2.1
25	100	-8.8		0.76		1.5
26	40	-7.42		0.45		2.26

Table 5.2 Summary of the results of the variation of electrical and optical properties of amorphous silicon with neon sputtering pressure.

Therefore it is very important to determine the composition of 'pure' a-Si produced by neon sputtering as a function of pressure, and to determine the significance of these impurities on the properties of the films.

Although RBS proved to be a very useful technique in determining the concentration of argon in argon sputtered films it was less fruitful in analysing the composition of neon sputtered films. This is because RBS has a low sensitivity for lighter elements (Chu et al, p 127, 1978). However XPS and AES have relatively high sensitivity for these elements. Due to a design fault in the machine the concentration of oxygen could not be determined using these techniques but all other elements except hydrogen and helium could be analysed. The main impurity detected which varied systematically with the preparation conditions was neon. The concentration of neon in the film as a function of the sputtering pressure is shown in Figure (5.15). The results reported here for neon concentration are largely from AES experiments although some results from XPS and RBS are also included. Oxygen concentration however could not be determined by XPS or AES due to design faults in the machine. These will be discussed in a later section (section 6.6).

5.2.2 Variation of Target-Substrate Spacing

The distance between the target and the substrate holder could be varied from 2.0 to 6.0 cm by moving the substrate holder by a chain and cog mechanism described earlier section (4.1.1). To study the effect of varying the target-substrate spacing (d) on the properties of amorphous silicon films other sputtering parameters were kept constant, the sputtering pressure was fixed at 85 mtorr,

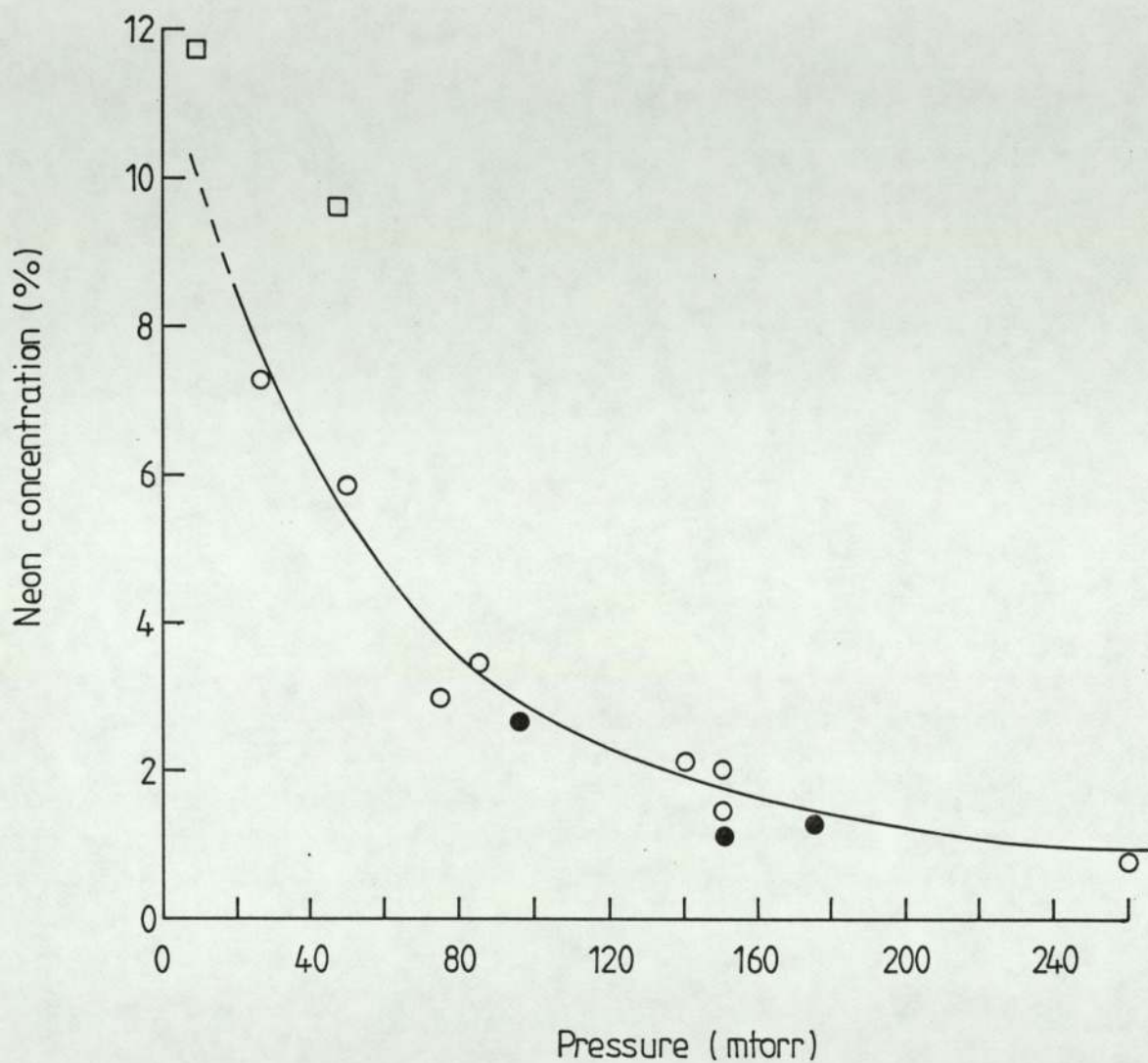


Figure 5-15 The concentration of neon in the films as a function of neon sputtering pressure.
 (○ - AES, ● - XPS, □ - RBS)

the input power was adjusted to give a dc self-bias voltage on the target of 880 volts and the substrate temperature was between 280-300°C.

Figure (5.16) shows the effect of increasing the target substrate spacing from 2.0 to 5.0 cm on the room temperature, electrical conductivity (σ_{RT}), photoconductivity (σ_{ph}), thermal activation energy (ΔE) and the optical gap (E_0). Increasing the distance induced a decrease in σ_{RT} of nearly four orders of magnitude with a corresponding increase in the thermal activation energy from about 0.4 to 0.8 eV. Photoconductivity, negligible for the film produced at a spacing of 2.0 cm increased to $\sim 10^{-7}$ (Ωcm)⁻¹ for the film produced at a spacing of 5.0 cm. The optical gap also increased slightly as the distance was increased. The sputtering rate decreased from 3.2 ÅS⁻¹ to about 0.7 ÅS⁻¹ on increasing the spacing from 2.0 to 5.0 cm.

5.4.3 The variation of the dc self-bias voltage on the target

In a dc sputtering system the target is attached to the cathode where it is bombarded by positive ions. Due to this bombardment the target material is sputtered and deposited on the opposite electrode (anode) or the chamber walls (Chapman p77, 1980). However with this technique it is difficult to sputter insulators. This is because the surface of the insulator would charge up to a floating potential, so that the number of ions and electrons at the surface become equal, regardless of the potential applied to the backing electrode. These problems can be overcome by operating at radio-frequencies (Wehner, 1955, Anderson et al 1962). When a radio-frequency (rf) voltage is applied to the

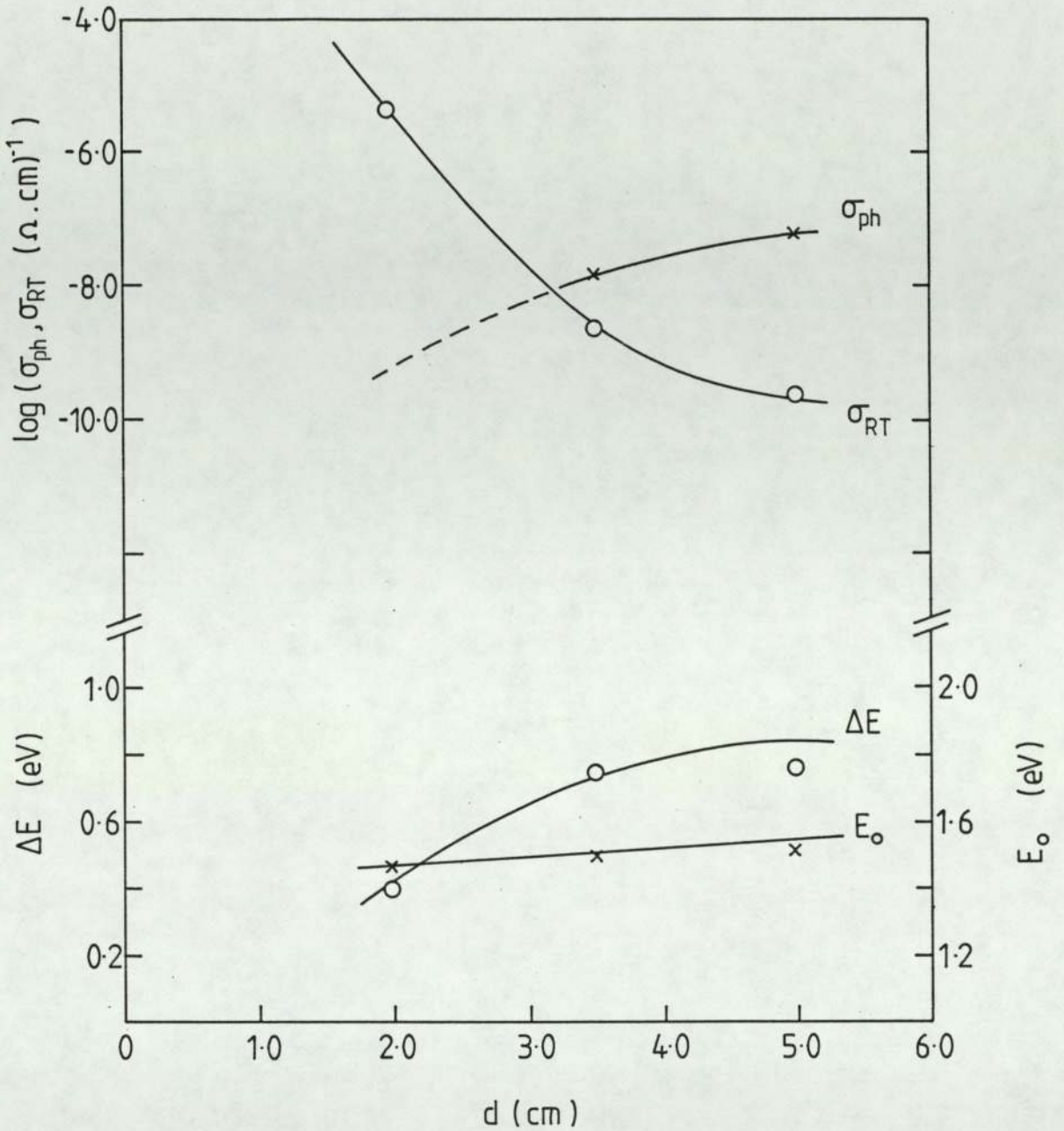


Figure 5-16 The variation of room temperature dark conductivity (σ_{RT}), photoconductivity (σ_{ph}), thermal activation (ΔE) and the optical gap (E_o) with the target-substrate distance (d).

backing electrode an rf voltage is induced on the front surface of the target. Since electrons are more mobile than positive ions, more electrons are attracted to the front surface of the target during the positive half cycle than positive ions in the negative half cycle. Therefore to maintain charge neutrality the surface of the insulator acquires a negative bias voltage for most of the rf cycle, thus repelling the electrons from the surface, and creating a positive ion sheath. Due to the negative self-bias, the ions in the plasma accelerate across the sheath and bombard the target. Hence the self-bias voltage is an important parameter since it determines the maximum energy with which the target is bombarded. However no systematic investigation into the effect of varying the dc self-bias voltage (V_{sb}) on the properties of a-Si films was found in the published literature.

The dc self-bias voltage (V_{sb}) developed on the target was varied from 550 to 1056 V by adjusting the input power to the rf oscillator. In figure (5.17) V_{sb} is plotted as a function of the applied power density (input power/target area). As before the electrical conductivity of all the films was measured over a temperature range of about 150°C, and from plots of conductivity against inverse temperature, the room-temperature electrical conductivity and thermal activation energy deduced. The variation of room-temperature, electrical conductivity (σ_{RT}) photoconductivity (σ_{ph}), thermal activation energy (ΔE) and the optical gap (E_0) with V_{sb} are plotted in figure (5.18).

For this set of experiments, other sputtering parameters were maintained at the following values; sputtering pressure 85 mtorr, target substrate spacing 3.5 cm, substrate temperature 280-300°C

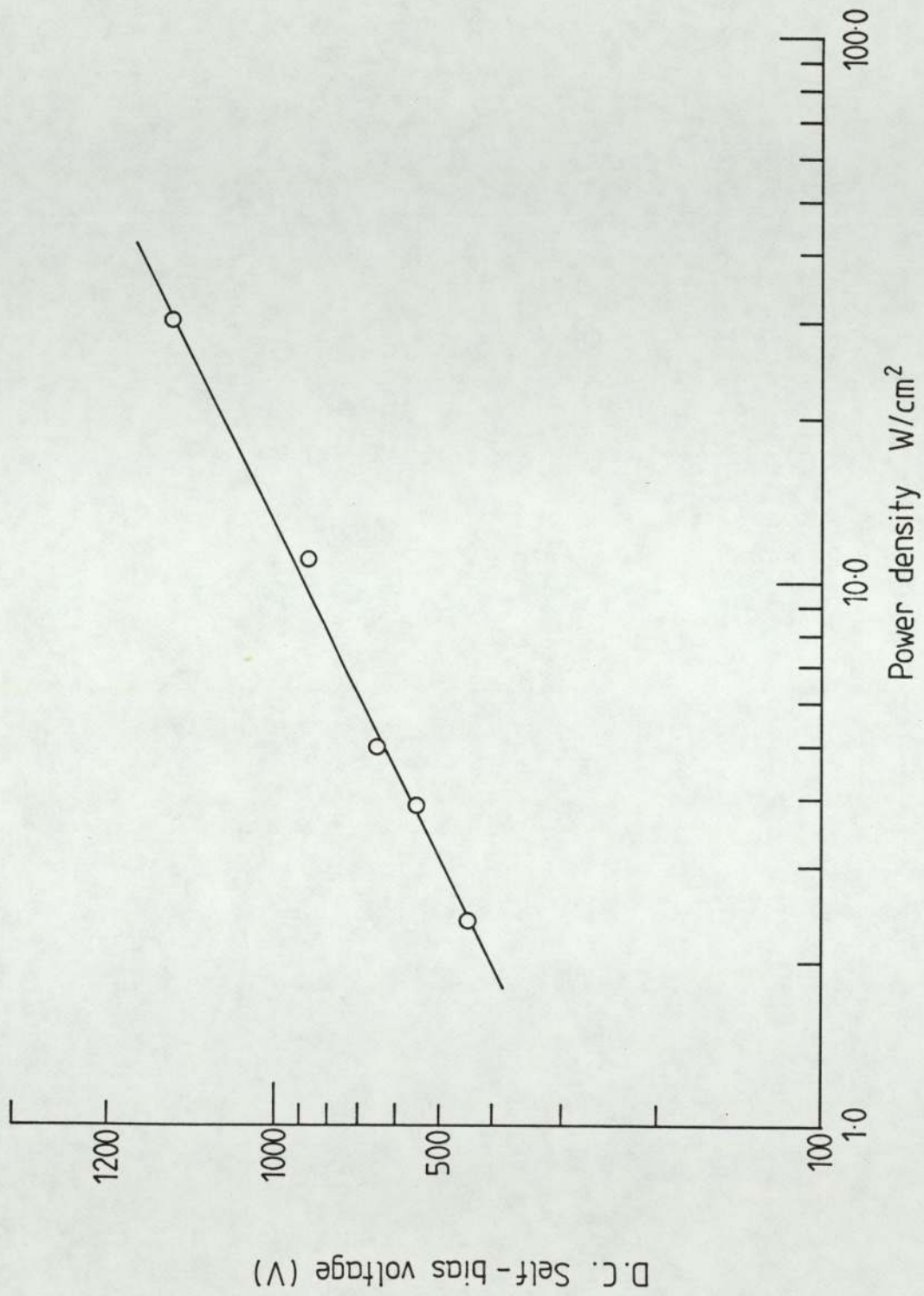


Figure 5.17 The D.C. self-bias voltage on the target as a function of the applied power density.

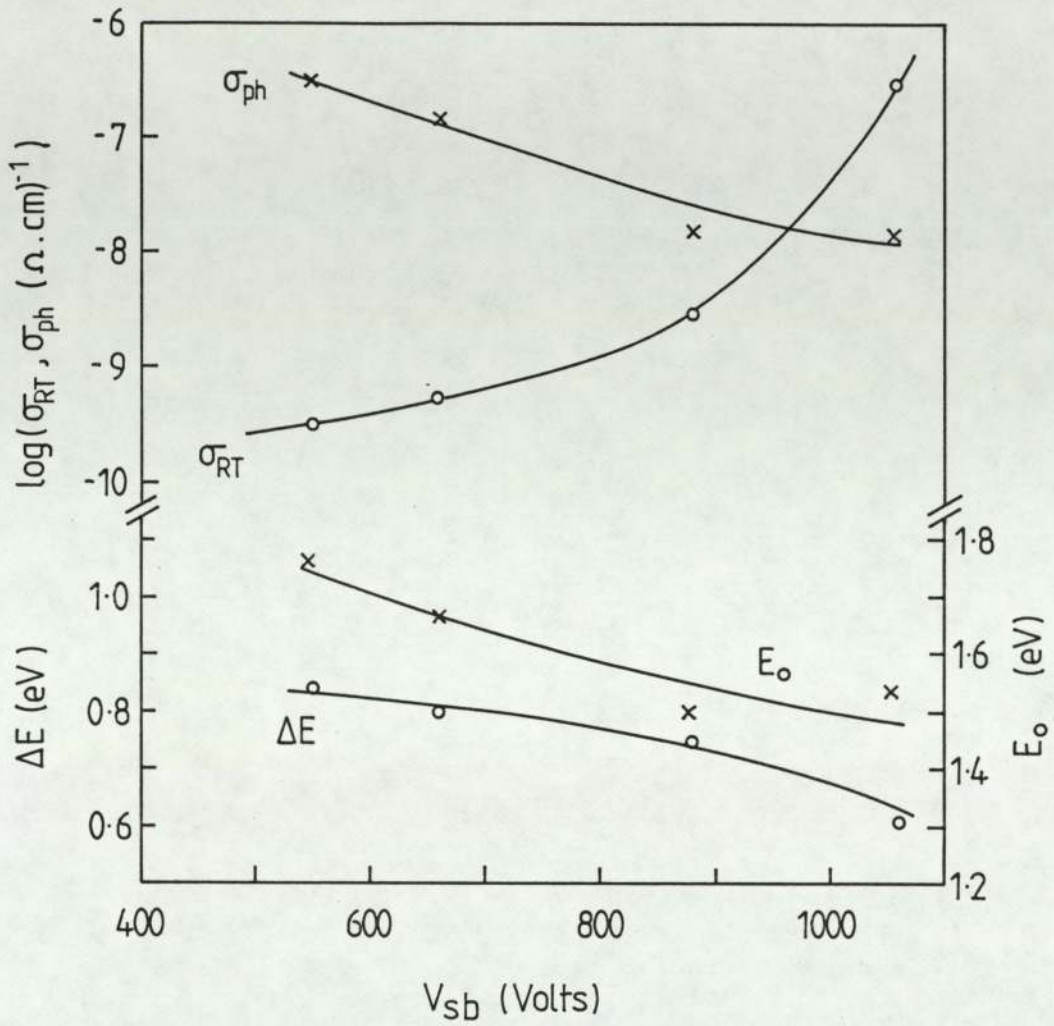


Figure 5-18 The variation of room-temperature electrical conductivity (σ_{RT}), photoconductivity (σ_{ph}), thermal activation energy (ΔE) and the optical gap (E_o) with the d.c. self-bias voltage.

and an axial magnetic field of 0.01T. The room temperature conductivity (σ_{RT}) was decreased by nearly three orders of magnitude by decreasing V_{sb} from 1056 to 550 V. The decrease in σ_{RT} was accompanied by an increase in the thermal activation energy (ΔE) from 0.52 to 0.84 eV. The photoconductivity and the optical gap also increased with decreasing power. The photoconductivity increased by more than one order of magnitude from $1.4 \times 10^{-8} (\Omega \text{ cm})^{-1}$ to $2.6 \times 10^{-7} (\Omega \text{ cm})^{-1}$ while the optical gap went up from 1.54 to 1.86 eV.

5.2.4 Variation of the Magnetic Field

Historically, magnetic fields were applied to sputtering systems to increase the current density so that sputtering could be carried out at lower pressures (Penning and Moubis 1940). An additional advantage of an axial magnetic field is that the plasma is concentrated in the centre of the discharge chamber. By reducing the plasma interaction with the chamber walls a possible source of contamination is removed. Although the application of axial magnetic fields is quite common no systematic investigation into the effect of varying the magnetic field on the properties of a-Si has been reported.

The axial magnetic field can be varied by adjusting the current to the Helmholtz pair of coils. The dependence of the axial magnetic field on the current applied to the Helmholtz pair of coils was shown in figure (4.4a). The maximum current that could be applied to the coils was 5.0 A, resulting in an axial magnetic field of about 0.015T. To examine the effect of varying the magnetic field on the properties of the material, films were deposited at various magnetic fields with the other sputtering

parameters maintained at the following values; sputtering pressure 150 mtorr, target substrate spacing 3.5 cm, self-bias voltage 880 V, and the substrate temperature 280-300°C. Figure (5.19a) shows the variation of the room-temperature dark (σ_{RT}) and photo (σ_{ph}) conductivities. Neither σ_{RT} nor σ_{ph} show any apparent dependence on the strength of the magnetic field. However, as shown in figure (5.19b) the thermal activation energy decreases from a value of about 0.83 eV at zero magnetic field to 0.78 eV at 0.015T. The variation of the optical gap, also shown in figure (5.19b) is similar; the optical gap decreases from about 1.7 eV at zero field to 1.58 eV at a field of about 0.015T.

Increasing the magnetic field concentrates the plasma into the centre of the discharge, increases the current density and hence the sputtering rate. Figure (5.20) shows the variation of sputtering rate with magnetic field, the sputtering rate increases from 0.7 ÅS⁻¹ at zero field to about 1.3 ÅS⁻¹ at a field of 0.015T. However, the variation of the self-bias voltage with magnetic field is ambiguous, because instead of increasing with the magnetic field, as one would expect, it decreases. The variation of V_{sb} with magnetic field is also shown in figure (5.20). For the same input power the self-bias voltage decreases from about 920 V at zero magnetic field to 835 V at fields exceeding 0.01T.

5.6 The Variation of Substrate Temperature

Although the temperature of the substrate heater could be raised to 450°C, the highest temperature during sputtering was about 360°C. As explained earlier this was because the substrate holder was baked at a temperature approximately 100°C above the

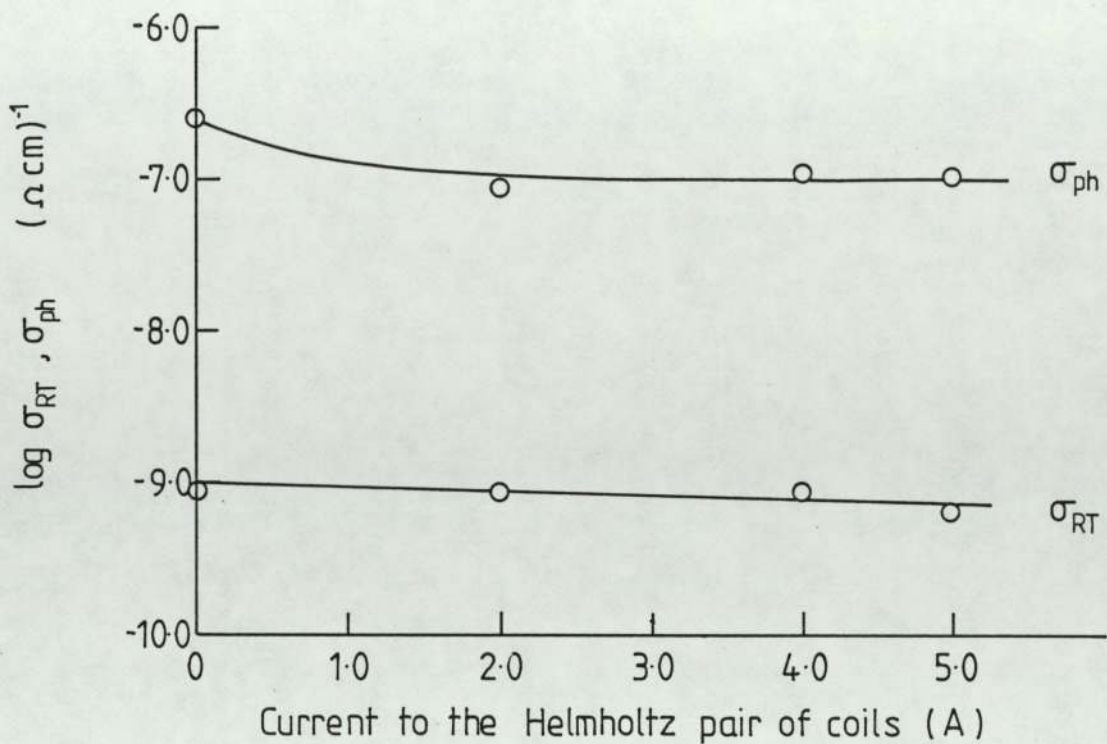


Figure 5-19a The effect of varying the magnetic field on room-temperature dark conductivity (σ_{RT}) and photoconductivity (σ_{ph})

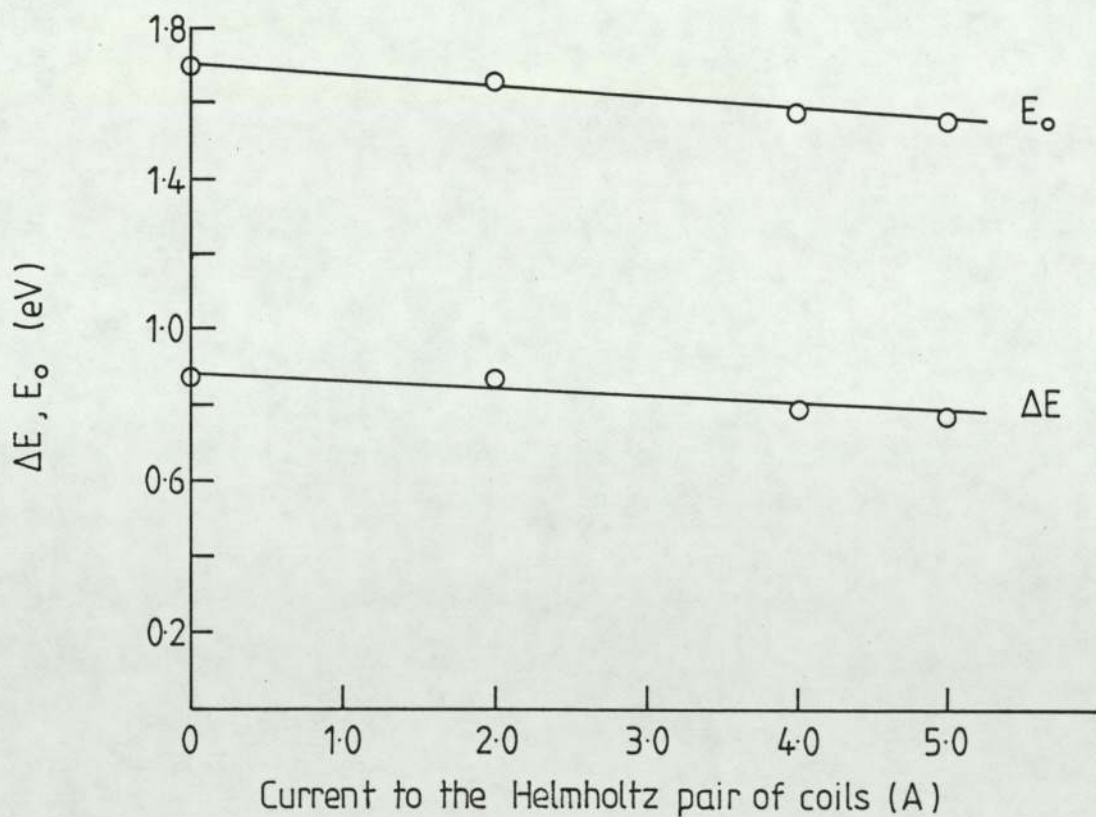


Figure 5-19b The effect of varying the magnetic field on the thermal activation energy (ΔE) and the optical gap (E_o)

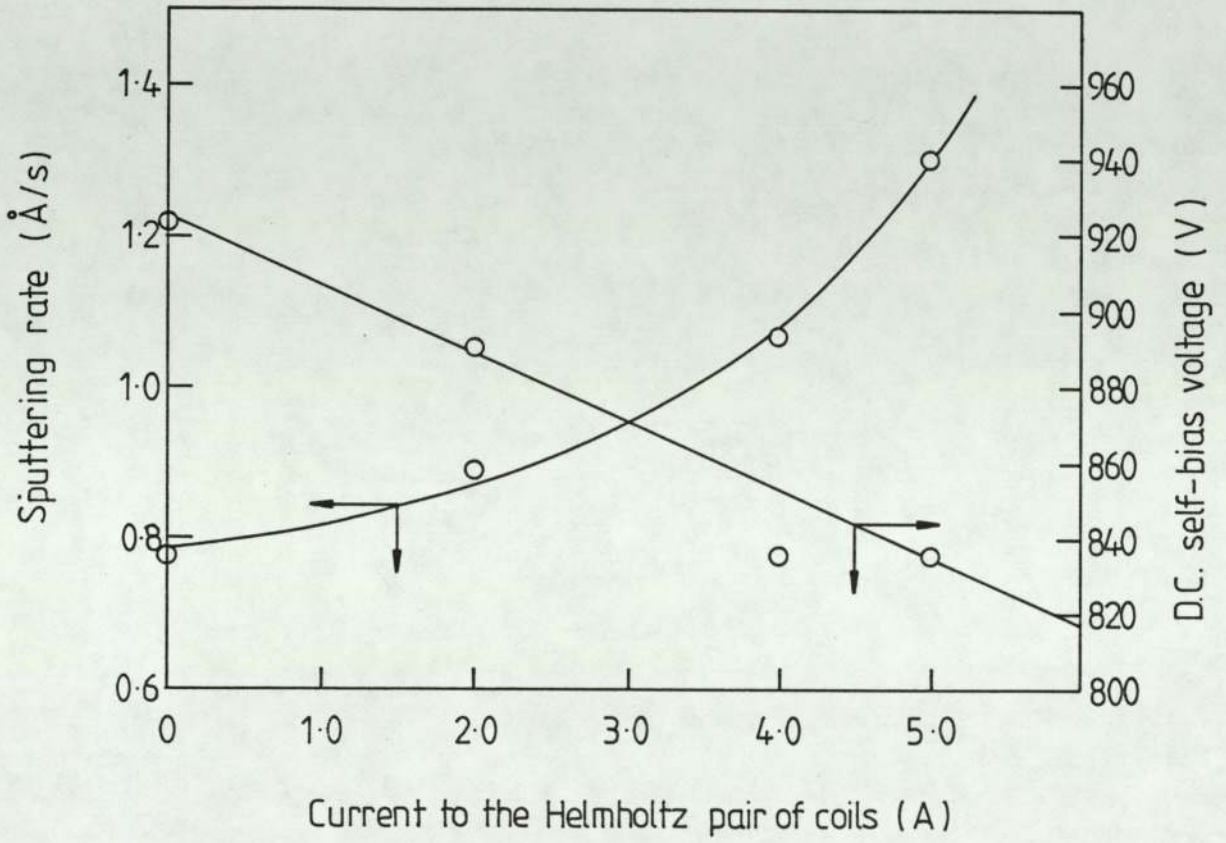


Figure 5.20 Variation of sputtering rate and D.C. self-bias voltage with magnetic field.

temperature during sputtering, to reduce the outgassing from the substrate holder during sputtering. For this set of runs the sputtering pressure was fixed at 150 mtorr, the target substrate spacing at 3.5 cm, self-bias voltage was 880 V and the magnetic field was about 0.01T.

Figure (5.21) shows the variation of the room-temperature dark (σ_{RT}) and photo-conductivities (σ_{ph}), thermal activation energy (ΔE) and the optical gap (E_0) with the substrate temperature. As can be seen varying the temperature over a range of nearly 200°C had very little effect on the electrical and optical properties of the films. The decrease in σ_{RT} and an increase in σ_{ph} , ΔE and E_0 on increasing the substrate temperature indicates a slight decrease in the defect density, probably due to enhanced structural reorganisation on increasing the temperature (Pawlewicz 1974).

The effect of increasing the substrate temperature on the concentrations of neon and oxygen was determined by AES. The results obtained are plotted in figure (5.22).

5.3 SUBSTITUTIONAL DOPING BY GROUP V ELEMENTS

In the preceding sections results have been presented which indicate that the density of defect states can be reduced by optimising the sputtering conditions, rather than adding large quantities of dangling bond terminators such as hydrogen or fluorine to the silicon matrix. One of the tests to determine whether the density of states has been reduced is to study the doping effects of n- or p-type dopants. It has long been established that the properties of a-Si prepared by thermal evaporations or sputtering

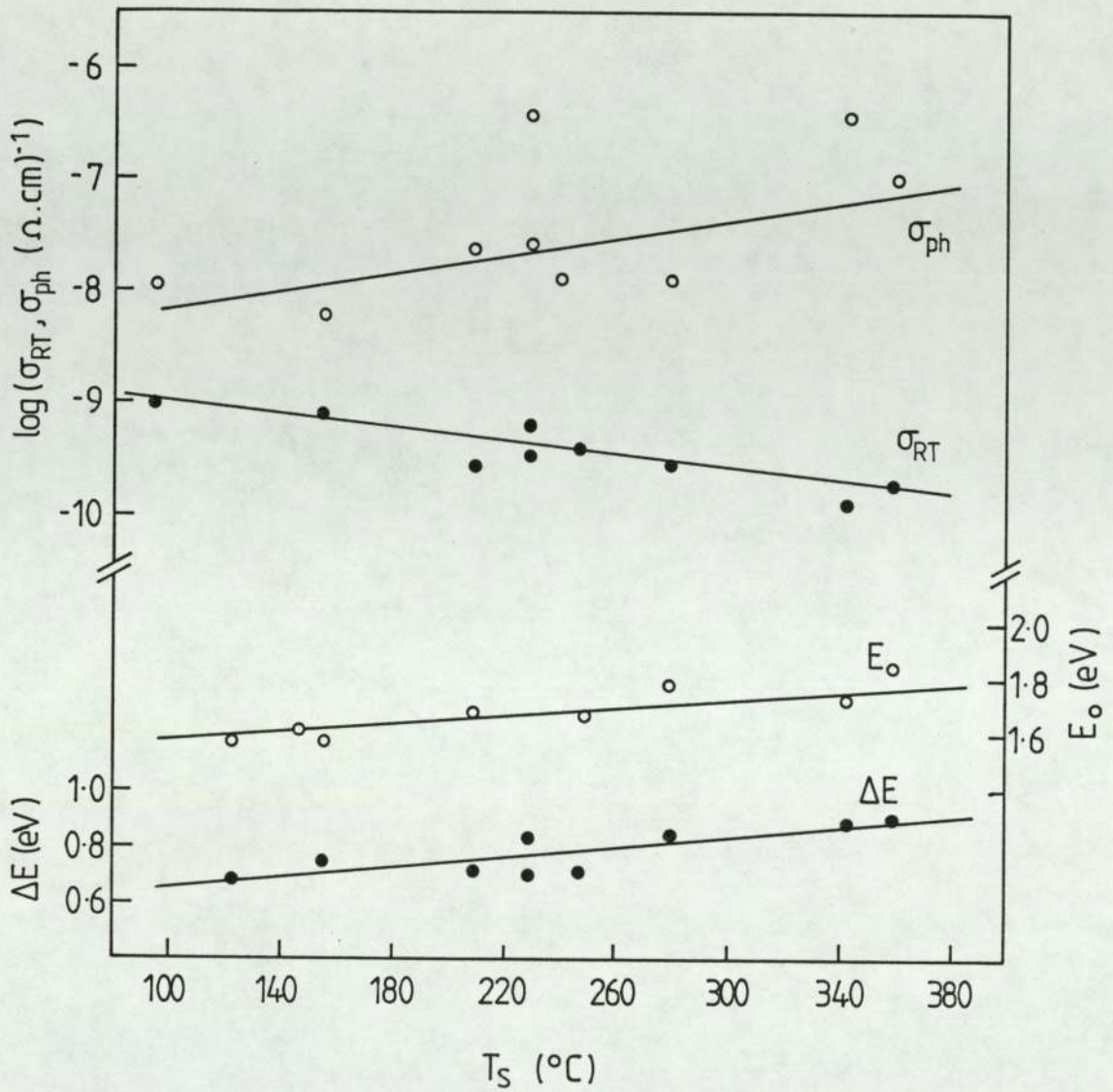


Figure 5.21 Variation of room-temperature electrical conductivity (σ_{RT}), photo conductivity (σ_{ph}), thermal activation energy (ΔE) and the optical gap (E_o) with the substrate temperature.

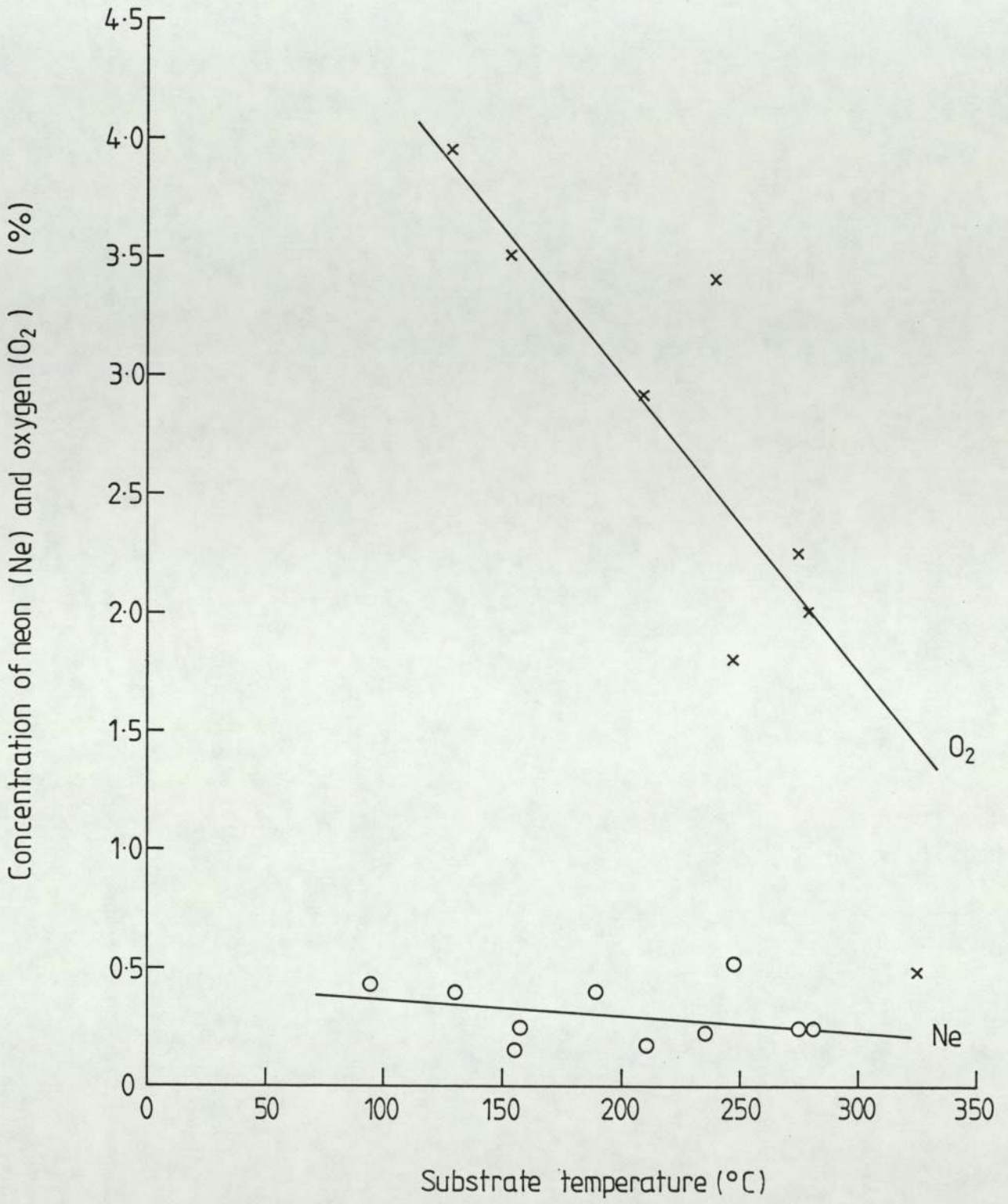


Figure 5-22 The effect of varying the substrate temperature on the concentrations of neon and oxygen in the films.

in pure argon are insensitive to the incorporation of impurities (Davis 1979). This behaviour has been attributed to the presence of large numbers of dangling bonds in these materials which satisfy the normal valency requirements of the impurity atoms (Mott 1967). Only when the density of defect states is reduced by hydrogenation (Spear et al 1975) or fluorination (Madan et al 1979) sensitive substitutional doping is observed.

Paul et al (1976) were the first to dope amorphous silicon produced by rf sputtering in an Ar/H₂ plasma. They produced n- and p- type a-Si by incorporating phosphorus and boron respectively into the silicon matrix by adding phosphine (PH₃) or diborane (B₂H₆) to the argon-hydrogen mixture. This method of incorporating the dopant from the gas phase has become quite common. Alternative methods of doping are; co-sputtering where the dopant is stuck onto the silicon target and sputtered (Thompson and Reinhardt 1980, Fane and Zaka 1983) and sputtering of doped silicon targets (Van Dong and Hai 1978, 1980, Thompson et al 1978).

In the present study n-type amorphous silicon was produced by co-sputtering with tantalum and sputtering targets predoped with arsenic and antimony. Although gas phase doping is the most efficient means of incorporating the impurities into the silicon films (Spear and Le Comber 1977) sputtering pre-doped targets and co-sputtering were chosen for their convenience. This is because for gas phase doping toxic and explosive gases are employed for which elaborate safety equipment and procedures are necessary.

5.3.1 Doping by co-sputtering with tantalum

Doping by tantalum was studied extensively because the concentration of tantalum could be varied easily by varying the size of the tantalum piece stuck onto the silicon target, whereas the variation of impurity concentration was limited with pre-doped targets.

Tantalum was chosen for n-type doping since it is readily available with the required purity (99.999%) and in a form suitable for incorporation into a sputtering target. Composite targets of tantalum and silicon were prepared by glueing pieces of various size tantalum on the silicon targets. The ratio of tantalum to silicon areas was varied from 0.03 - 1.80%. The films were characterised by measuring the electrical conductivity, (σ_{RT}), thermal activation energy (ΔE) and the optical gap (E_0) as a function of the tantalum concentration.

As before the electrical conductivity measurements were made in vacuum using the gap cell configuration with aluminium electrodes deposited immediately after the preparation of the film. The contacts were ohmic for the electrical field used - generally 10^2 V cm^{-1} . Figure (5.23) shows plots of $\log \sigma$ against T^{-1} for a number of intrinsic and n-type films. The concentration of tantalum was varied from 0.015 to 3.31% but all the films were deposited at the same sputtering conditions, namely, sputtering pressure 150 mtorr target substrate spacing 3.5 cm, dc self-bias voltage of 990 V and substrate temperature was maintained between 280-300°C. The conductivity was measured as a function of temperature from about -150°C to 200°C. As can be seen from figure (5.23) the conductivity

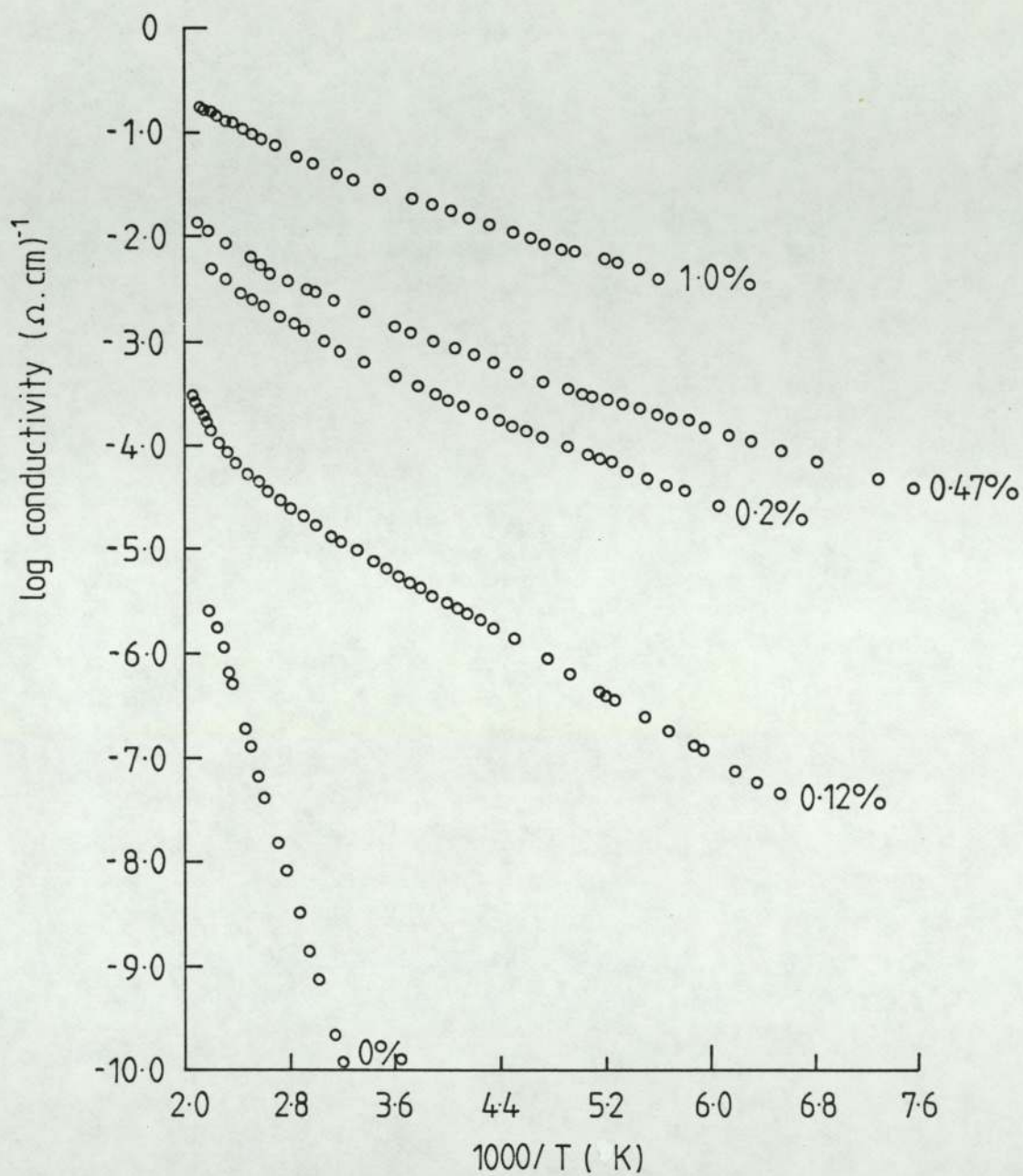


Figure 5.23 Dark conductivity vs $1000/T$ for various concentrations of tantalum.

was increased by more than nine orders of magnitude by tantalum doping. The increase in conductivity is due to the shift of the Fermi level towards the conduction band as is evident from the decrease in the thermal activation energy ($\Delta E = E_c - E_f$) with increasing tantalum concentration. The thermal activation energy (ΔE) and the room-temperature electrical conductivity were deduced from plots of conductivity versus temperature. Figure (5.24) and (5.25) show the variation of σ_{RT} and ΔE respectively with tantalum concentration. As shown in Figure (5.24) σ_{RT} was increased by about nine orders of magnitude by incorporating 3.31% of tantalum. Even very small amounts of tantalum, 0.2%, produced over five orders of magnitude change in σ_{RT} . The increase in conductivity is accompanied by a decrease in the thermal activation energy, indicating that the Fermi level has been moved towards the conduction band by tantalum doping. As shown in figure (5.25) thermal activation energy could be varied over a range of about 0.7 eV by doping with various concentrations of tantalum. The value of ΔE decreases sharply from 0.79 eV for intrinsic films to about 0.15 eV for lightly doped films ($\sim 0.2\%$ Ta), with further increase in the tantalum concentration ΔE decrease gradually to a value less than 0.1 eV.

Although there were large variations in the conductivity and thermal activation energy the variation in the optical gap with doping was much less. Figure (5.25) shows the variation of optical gap (E_o) with tantalum concentration, E_o decreases from about 1.6 eV for intrinsic films to about 1.33 eV for the highly doped film. Some of the representative plots of $(\alpha \hbar w)^{\frac{1}{2}}$ versus $\hbar w$ from which E_o was deduced are shown in figure (5.26).

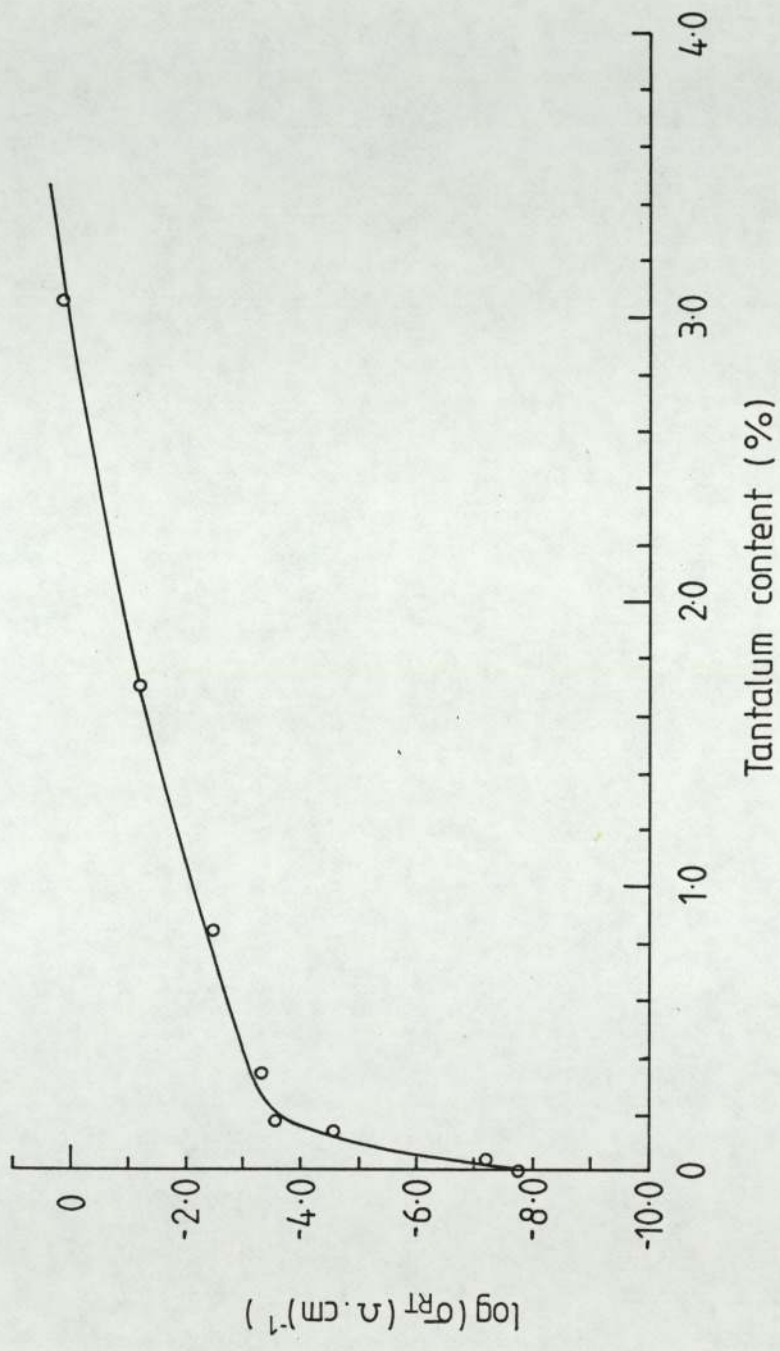


Figure 5.24 Room temperature electrical conductivity of tantalum doped films against the concentration of tantalum.

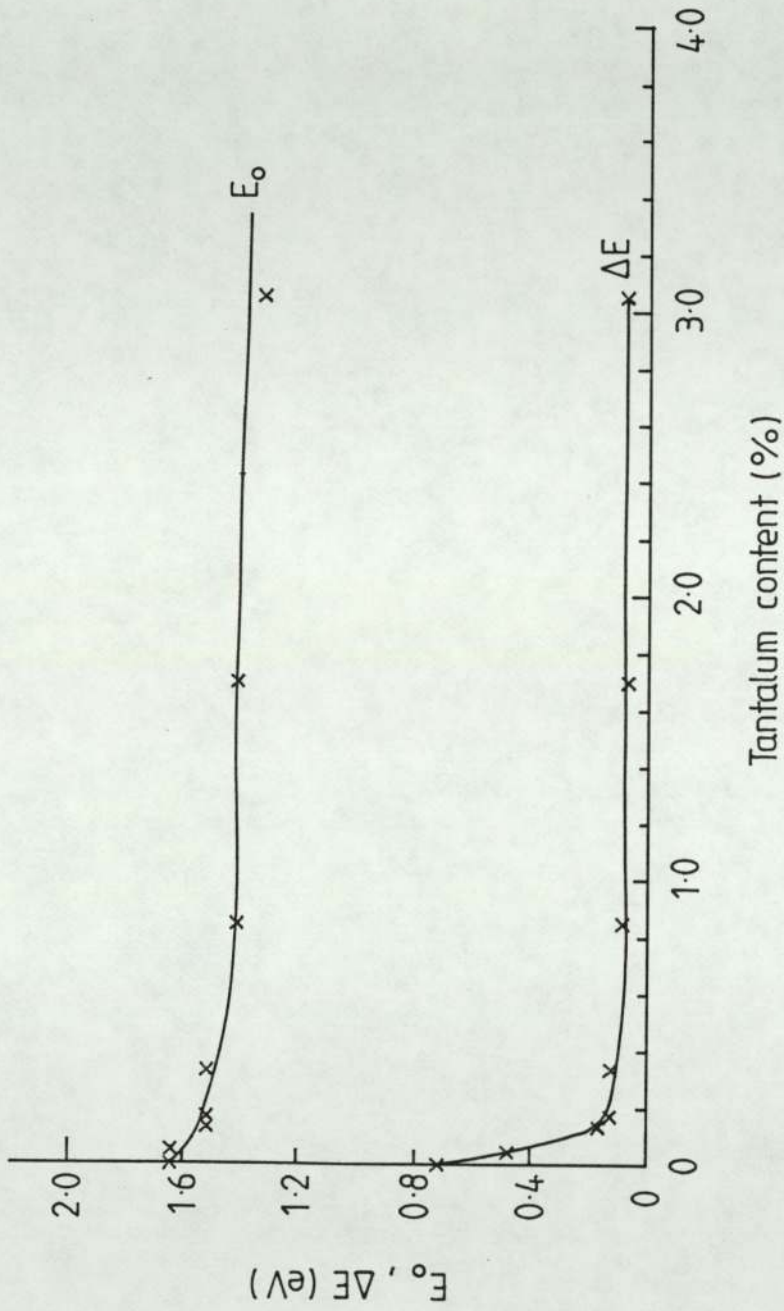


Figure 5.25 Thermal activation energy (ΔE) and the optical gap (E_o) versus the concentration of tantalum in the films.

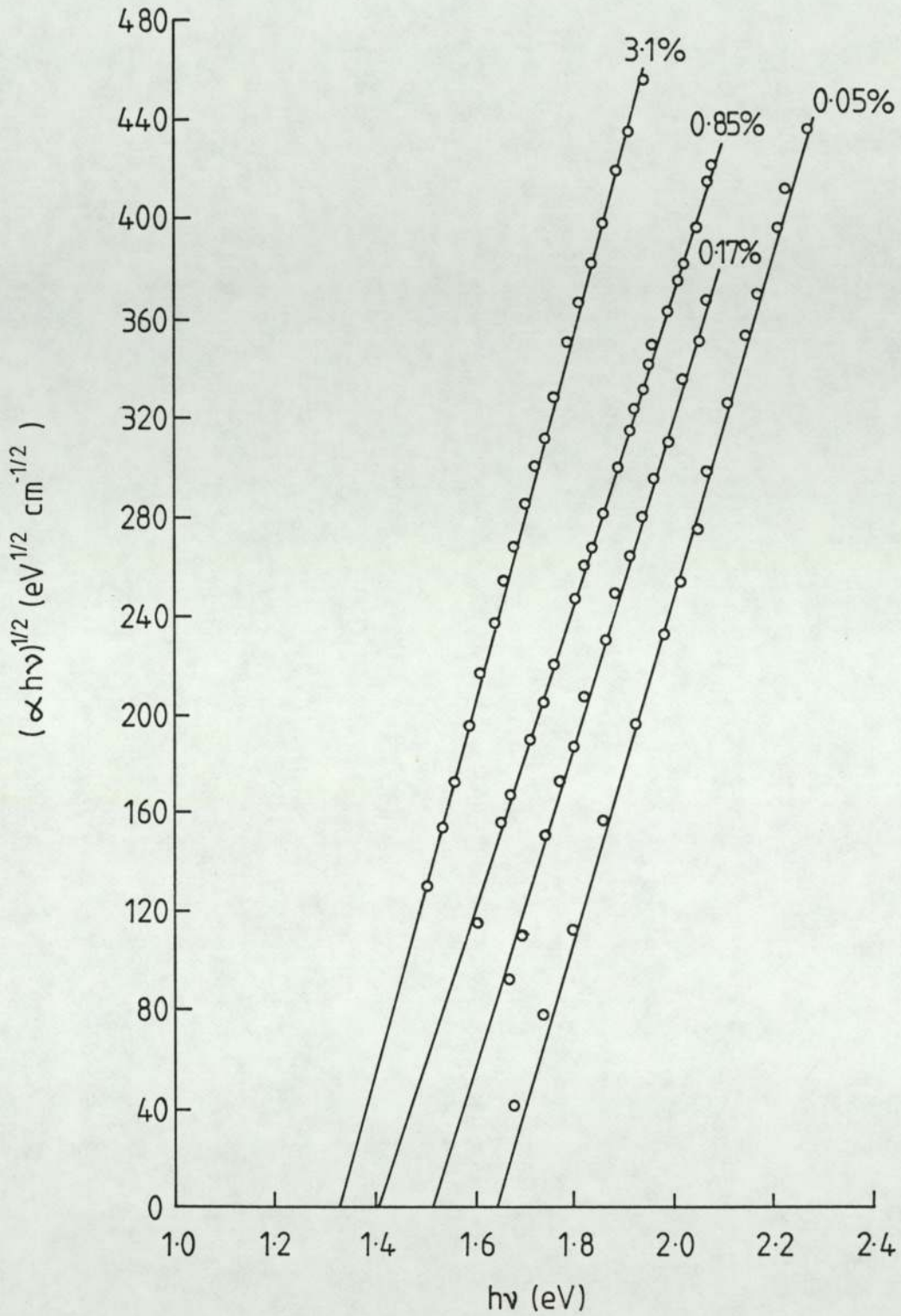


Figure 5-26 Plots of $(\alpha hv)^{1/2}$ vs $h\nu$ for various concentrations of tantalum.

To determine the effect on doping efficiency of sputtering conditions, a composite target containing 0.2% tantalum was sputtered at various neon pressures. Other sputtering parameters were set at the following values; target-substrate spacing 3.5 cm, dc self-bias voltage 990 V, magnetic field 0.01T and substrate temperature was between 280-300°C. Figure (5.27) shows the effect of varying the sputtering pressure increases the conductivity by nearly two orders of magnitude while the thermal activation energy is decreased by 0.4 eV from about 0.5 eV at 55 mtorr to 1.0 eV at 200 mtorr. These results are a further proof that increasing the pressure reduced the density of defect states and hence increased the doping efficiency.

The concentration of tantalum was determined by Rutherford backscattering spectroscopy (RBS) and X-ray photoelectron spectroscopy (XPS). RBS was particularly useful since the depth distribution of the elements could be easily determined. Figure (5.28) shows a typical RBS spectrum. The film was sputtered from a composite target containing 0.11% tantalum by area, on an alumina (Al_2O_3) substrate. We can see that the tantalum peak is well separated from the silicon peak and lies higher up the energy scale, making quantification much easier.

Both the silicon and the tantalum peaks were of the same thickness and no structure was observed in the peaks confirming the expectation that tantalum was distributed uniformly in the silicon matrix. The results from the RBS experiments indicated that there was a direct relationship between the area ratio of tantalum and its concentration in the film. Figure (5.29) is a plot of the ratio of tantalum and silicon areas against the concentration of tantalum

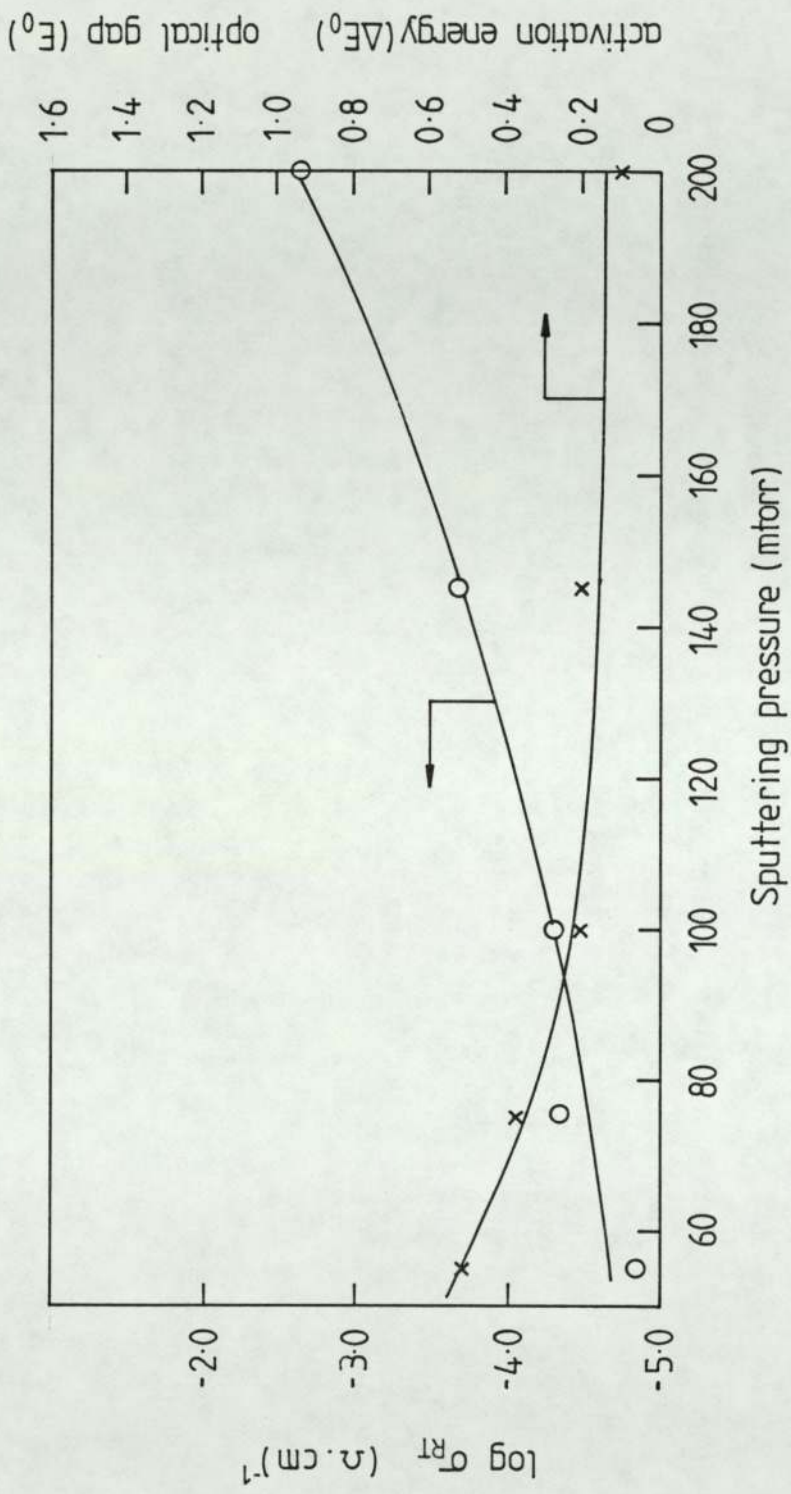


Figure 5.27 Variation of room-temperature electrical conductivity and thermal activation energy of films containing 0.2% tantalum with the sputtering pressure.

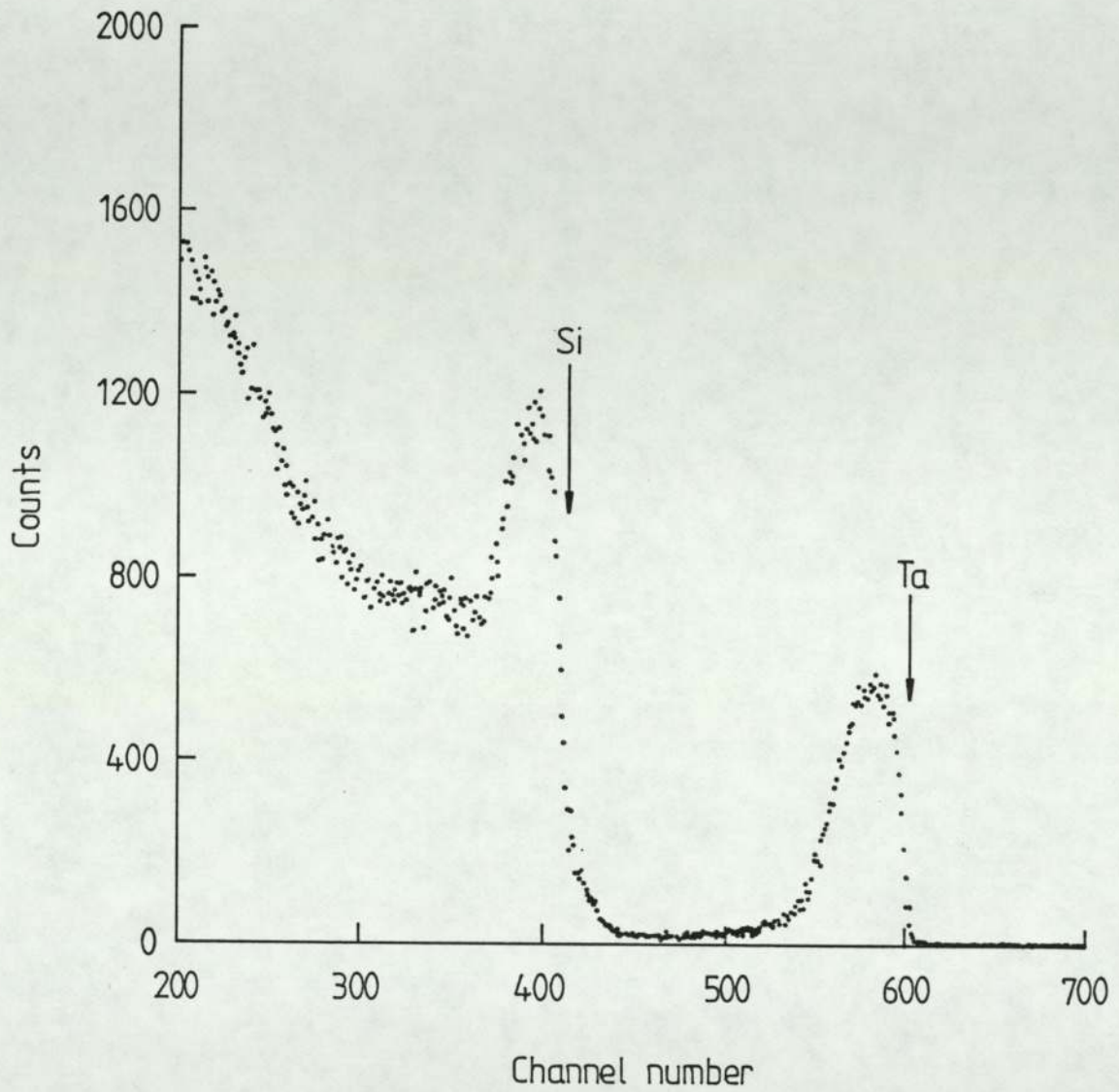


Figure 5-28 Typical RBS spectrum of a tantalum doped film deposited on an alumina (Al_2O_3) substrate

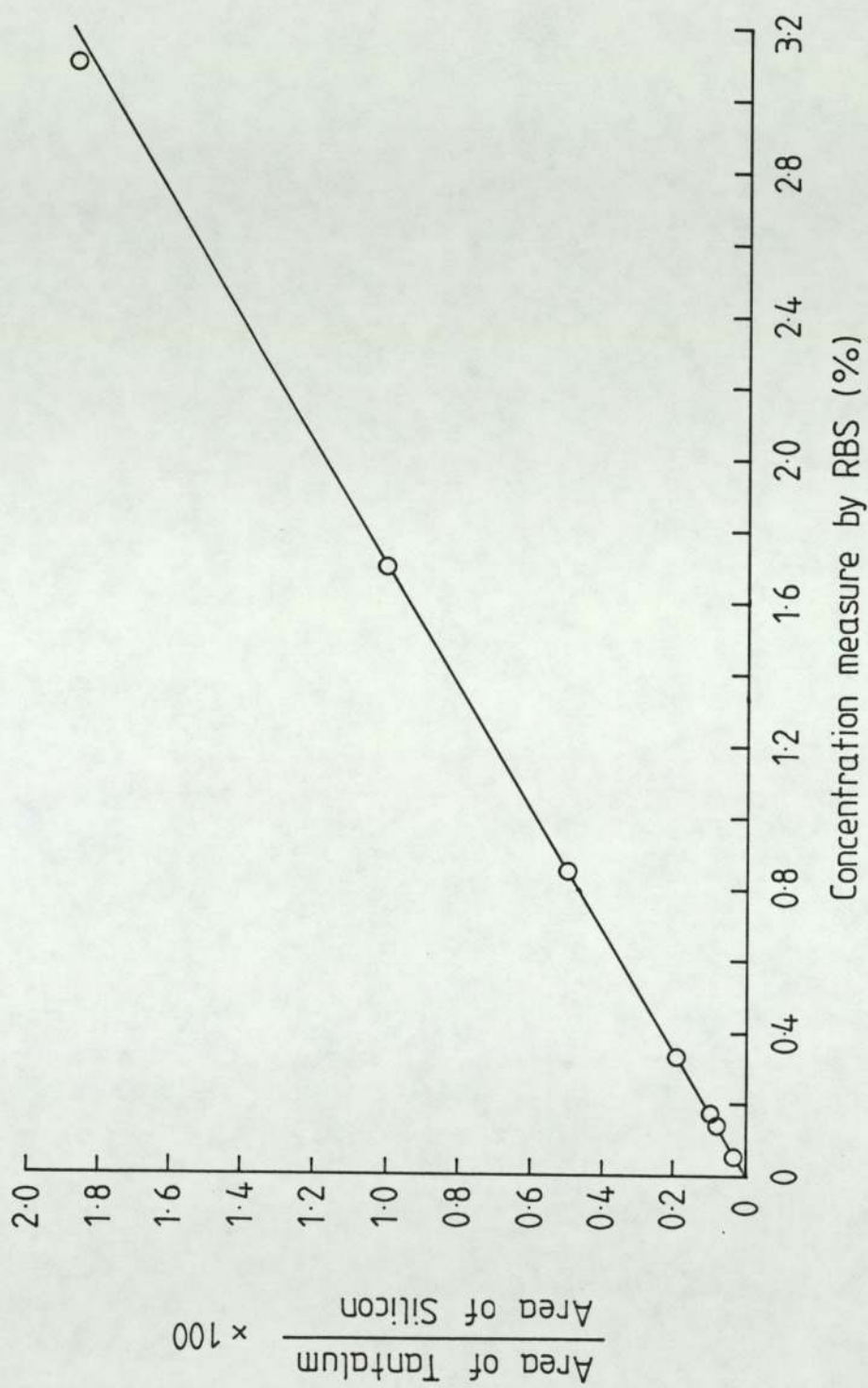


Figure 5.29 Area ratio of tantalum vs. concentration of tantalum determined by RBS

in the films. The concentration of tantalum can be related to the area of ratio of tantalum to silicon by measuring the slope of the plot in figure (5.29) and employing the equation:

$$\text{Conc. of Ta} = \frac{1}{\text{Slope}} \times \text{ratio of tantalum to silicon areas} \quad (5.2a)$$

$$\text{Conc. of Ta} = 1.79 \times \text{ratio of tantalum to silicon areas} \quad (5.2b)$$

Thus the concentration of any composite target could be determined by measuring the area ratio. The concentration of tantalum was found to be greater than that estimated from the area ratio and the relative sputtering rates (Carter and Colligon). This is probably due to the greater fraction of silicon atoms being backscattered to the target, or being scattered out of the target-substrate plane (Westwood, 1978). Some of the films were analysed by XPS. The results obtained agreed well with those obtained from the RBS experiments.

5.3.2 Doping from Pre-Doped Targets

A number of pre-doped silicon wafers were obtained from Mullard Limited. The wafers were either doped with antimony or arsenic and had room-temperature resistivities in the range 6-9 m Ω cm and 1-3 m Ω cm respectively. To study the effect of varying the sputtering conditions on the doping efficiency the pre-doped targets were sputtered at various pressures, while maintaining other sputtering conditions at the following values; target-substrate distance 3.5 cm, self-bias voltage 880 V magnetic field 0.01T and substrate temperature was between 280-300°C. The films were

characterized by measuring, the variation of dc dark conductivity with temperature, room-temperature photoconductivity, the optical gap and determining the composition of the films.

From the plots of conductivity versus inverse temperature the room-temperature dark conductivity (σ_{RT}) and thermal activation energy (ΔE) were deduced. Figure (5.30) shows the variations of room-temperature dark conductivity (σ_{RT}) and photoconductivity (σ_{ph}) with sputtering pressure for films sputtered from targets pre-doped with arsenic and antimony. For comparison the variation of σ_{RT} and σ_{ph} with pressure for undoped films is also shown. The concentration of arsenic and antimony in the films was 0.1% as determined by Rutherford backscattering spectroscopy. For films sputtered at low pressures there is very little difference in the values of σ_{RT} and σ_{ph} for the doped and intrinsic films. However for the films sputtered at high pressure σ_{RT} is over two orders of magnitude greater in doped films and σ_{ph} is nearly an order of magnitude greater. Again this indicates that increasing the sputtering pressure reduced the density of defect states. Figure (5.31) shows the variation of thermal activation energy (ΔE) and the optical gap (E_0) with sputtering pressure for films sputtered from a target predoped with arsenic. The dashed lines indicate the variation of ΔE and E_0 with pressure for undoped films. As before the difference between the thermal activation energy of intrinsic and doped targets is increased at higher pressures. However the optical gaps of intrinsic and doped films are similar over the entire range of pressures indicating that the basic band structure of the a-Si network has not been changed by the addition of the group V elements.

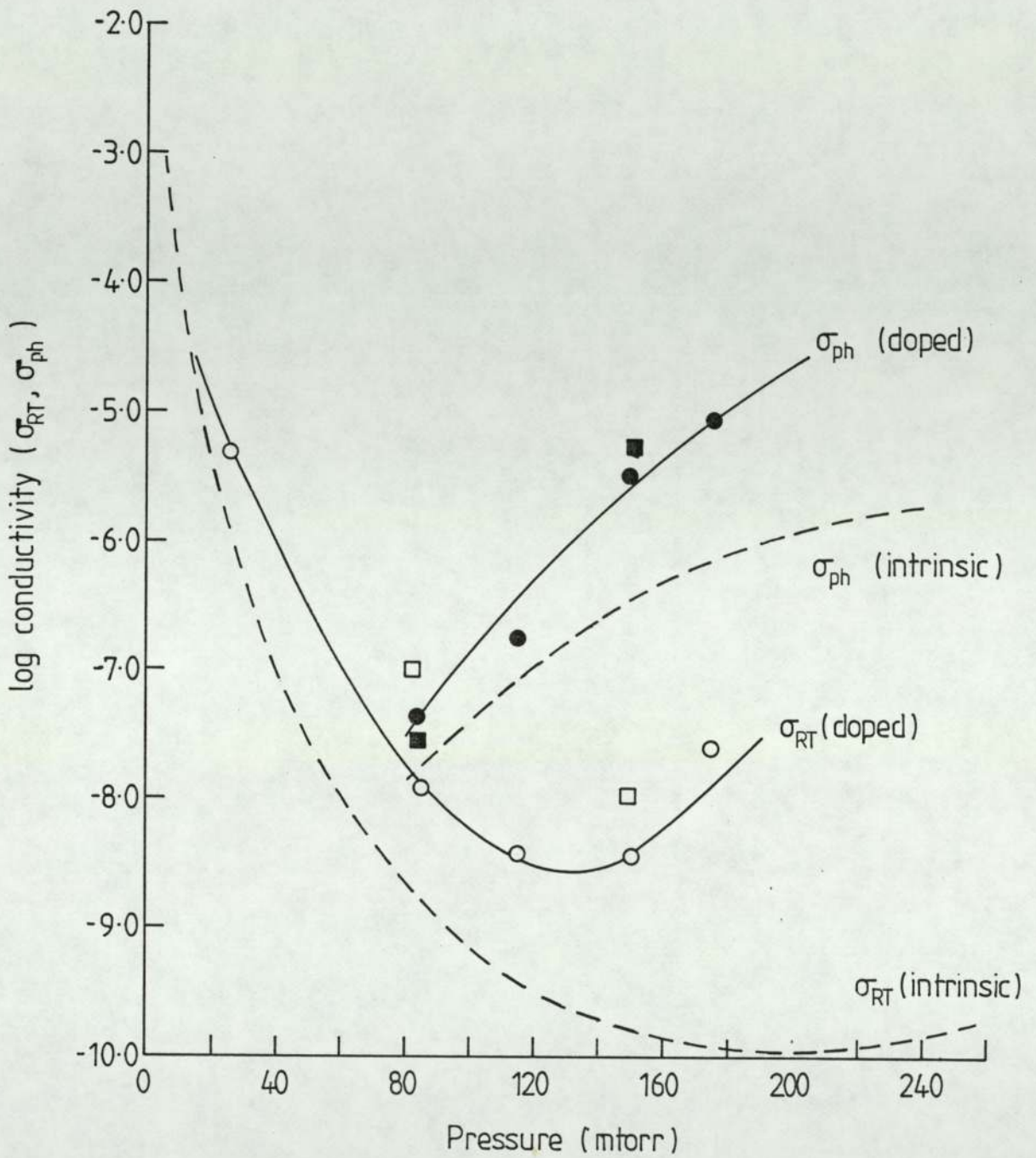


Figure 5.30 The variation of room temperature, dark conductivity (σ_{RT}) and photoconductivity (σ_{ph}) with sputtering pressure for film sputtered from targets pre-doped with arsenic (●, ○) and antimony (■, □). Dashed lines indicate the variation of σ_{RT} and σ_{ph} for intrinsic films.

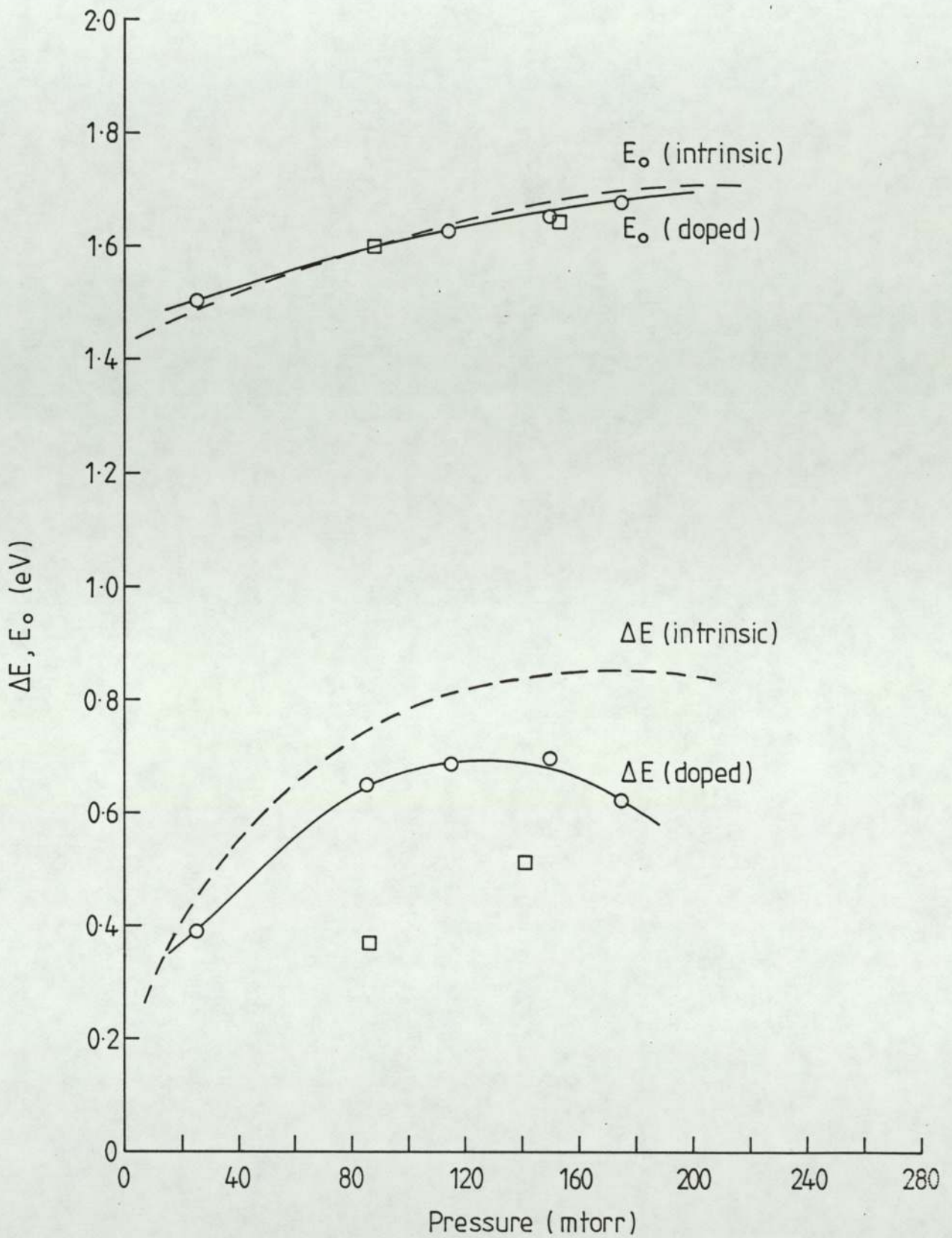


Figure 5.31 The variation of thermal activation energy (ΔE) and the optical gap (E_0) with sputtering pressure for films sputtered from a target predoped with arsenic (O, O) and antimony (\square , \square). Dashed lines indicate the variations of ΔE and E_0 for intrinsic films.

6. DISCUSSION OF EXPERIMENTAL RESULTS

6.1 THE EFFECT OF INCREASING THE ARGON PRESSURE ON THE PROPERTIES OF AMORPHOUS SILICON FILMS

As demonstrated by the results presented in section (5.1) the electrical and optical properties of amorphous silicon films deposited by r. f. sputtering are influenced significantly by varying the argon sputtering pressure. The results indicate that the density of defects (e.g. dangling bonds, microvoids) is reduced by sputtering at high pressures. This is evidenced by a decrease in room temperature electrical conductivity by more than five orders of magnitude from $\sim 10^{-3} (\Omega \text{ cm})^{-1}$ at 5 mtorr to less than $10^{-8} (\Omega \text{ cm})^{-1}$ at pressures greater than 40 mtorr with a corresponding increase in the thermal activation energy from 0.14 to 0.6 eV. The room-temperature photoconductivity increases monotonically with pressure to a value of about $10^{-7} (\Omega \text{ cm})^{-1}$, again suggesting that the density of defects is reduced by increasing the sputtering pressure.

The variation in the electrical and optical properties of a-Si as the pressure is increased is similar to the variation observed as hydrogen is added to the argon plasma in the case of argon sputtering. This is illustrated in table (6-1) where some of the electrical and optical properties of a-Si produced by conventional sputtering in pure argon are compared with those of material produced by reactive sputtering in an Ar/H₂ plasma.

Similar results on argon sputtering have been reported by others. Pawlewicz (1978) decreased σ_{RT} from about 10^{-3} to about

	Conventionally produced amorphous - silicon	Hydrogenated amorphous-silicon
Density of defect states	$\sim 10^{20} \text{ cm}^{-3} \text{ eV}^{-1}$	$\sim 10^{16} \text{ cm}^{-3} \text{ eV}^{-1}$
Room - temperature electrical conductivity (σ_{RT})	$\sim 10^{-3} (\Omega \text{ cm})^{-1}$	$\sim 10^{-9} (\Omega \text{ cm})^{-1}$
Thermal activation energy (ΔE)	$\sim 0.2 \text{ eV}$	$\sim 0.8 \text{ eV}$
Photoconductivity (σ_{ph})	$\sim 10^{-11} (\Omega \text{ cm})^{-1}$	$\sim 10^{-5} (\Omega \text{ cm})^{-1}$
Optical gap (E_0)	$\sim 1.2 \text{ eV}$	$\sim 1.7 \text{ eV}$
Doping	Cannot be doped Fermi level pinned near middle of gap.	Can be made n- or p-type by substitutional doping.

Table 6.1 Comparison of the properties of conventionally produced amorphous - silicon with those of reactively sputtered hydrogenated amorphous-silicon.

$10^{-7} (\Omega \text{ cm})^{-1}$ by increasing the argon gas pressure from 25 to 150 mtorr with a corresponding increase in the activation energy from 0.2 to 0.3 eV. Van Dong et al (1982) sputtered in a d.c. triode system and obtained, under a special condition of heating, not specified a-Si films with $\sigma_{\text{RT}} < 10^{-9} (\Omega \text{ cm})^{-1}$ and activation energy of about 0.8 eV. Shimizu et al (1979) decreased the electrical conductivity by more than five orders of magnitude by increasing the product (Pd) of argon pressure, P, and the target-substrate spacing, d, from 0.1 to 1.0 torr cm. The original suggestion by Pawlewicz, that increasing the sputtering pressure reduced the kinetic energy of the various species bombarding the film thus reducing the number of defects, seems to be consistent with the above results. However, recently it has been found that the low conductivity of the high pressure argon-sputtered films could be due in part to post-deposition oxidation because the films have a porous structure (Shimizu et al 1980, Anderson et al 1979). This is thought to be due to the fact that although bombardment by high energy species in the plasma is detrimental to the film properties, some bombardment is beneficial in that it helps to remove loosely bound atoms. Thus a film grown under the conditions of high pressure, where the plasma species have become completely thermalised before reaching the substrate tend to have a porous structure.

To investigate this hypothesis the oxygen content of the films was extracted from the relevant RBS spectra. The results are summarised in Fig (5.7). From these results it is evident that films produced in argon sputtering pressures up to 25-30 mtorr are essentially oxygen free (see section 6.6 for further discussion), while films produced at higher pressures contain about 20% oxygen.

The results presented in Section (5.1) appear to support the suggestion that as the gas pressure is increased to about 25-30 mtorr the electronic and optical properties of the films improve due to the reduction in the kinetic energy of the various species in the plasma which are continuously bombarding the growing film. This is evident from a decrease in σ_{RT} by four orders of magnitude as the pressure is increased from 5 to 25-30 mtorr, while maintaining essentially oxygen free films. Similar, sharp variations are observed in the thermal activation energy (ΔE), the optical gap (E_0) and the argon content as the pressure is varied over this range; ΔE and E_0 increase and the argon content decreases on increasing the pressure. However, increasing the pressure beyond 25-30 mtorr also removes low energy bombardment of the film, which is beneficial, in that, it removes loosely bound material from the surface of the film. Thus films produced at high argon pressures, where the plasma species have become thermalised tend to be porous and susceptible to post-deposition oxidation. This is evident by the large concentration of oxygen (~ 20%) in the films produced at pressures higher than 25-30 mtorr (Figure 5). The decrease in σ_{RT} as the pressure is increased beyond 25-30 mtorr is less sharp, levelling off at pressures of about 65 mtorr and is probably due to the oxidation of the films. Similarly ΔE and E_0 increase and the argon content decreases slightly as the pressure is increased beyond 25-30 mtorr and eventually levels off at about 65 mtorr.

Thus it would appear that the plasma species become thermalised at ^a pressure just in excess of 30 mtorr, and the optimum pressure of argon for the production of a low density of defect a-Si is about 25-30 mtorr. At this pressure range the bombardment of the film by high energy plasma species has essentially been removed, thus

reducing significantly the number of defects in the film, however low energy bombardment is still present, which ensures that loosely bound material on the surface is removed.

It should be remembered, however, that 25-30 mtorr is the optimum pressure for the present system at the sputtering conditions described earlier (section 5.1). This is because varying the target-substrate spacing or the d.c. self-bias voltage will also affect the energy of the plasma species. To determine the optimum pressure for any particular system and conditions a set of films over a wide range of pressures need to be deposited. The optimum pressure can then be deduced by observing the variation in the properties, discussed above, as the pressure is increased. As the energy of the plasma species is reduced on increasing the pressure a sharp variation in the properties is observed, however, once the plasma species have become thermalised, further increasing the pressure has little effect on the properties. Thus if the properties are plotted as a function of pressure, the optimum pressure is that pressure at which the properties cease to vary sharply with pressure. Figure (6.1) illustrates the concept for the results presented in section (5.1).

6.2 THE SIGNIFICANCE OF PREPARATION CONDITIONS OF NEON SPUTTERED FILMS

As discussed in the previous section the density of defects can be reduced and the properties of the films improved significantly by optimising the argon sputtering pressure. However, the electrical and optical properties of the pure a-Si thus produced are still inferior to those of the hydrogenated films. To improve the

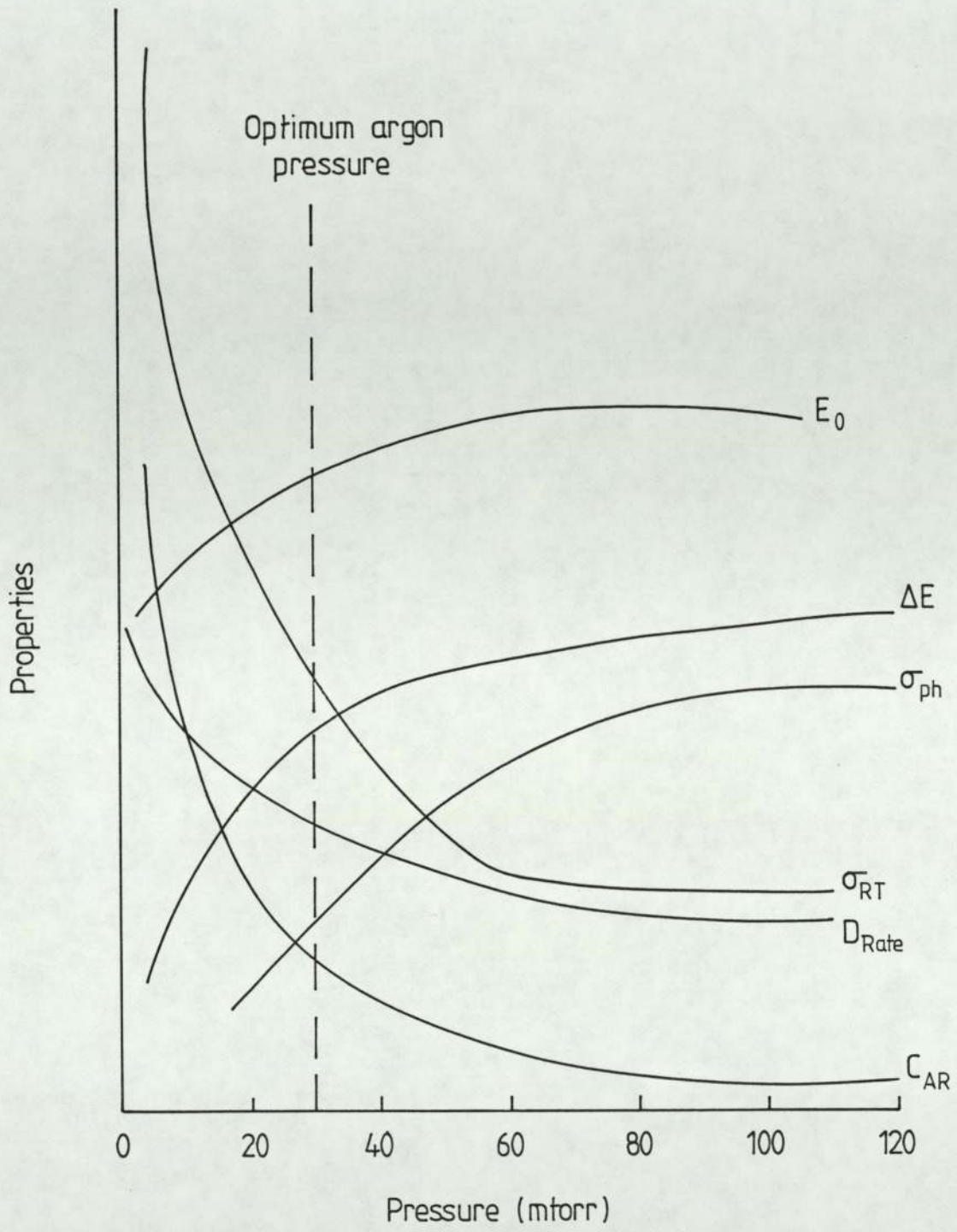


Figure 6.1 Variation of the various measured properties as a function of the argon sputtering pressure. The dashed line indicates the optimum argon pressure.

properties further sputtering in neon rather than the conventionally used argon was investigated. This is because neon having smaller atomic size should cause less damage to the film. The higher ionisation potential of neon as compared to argon (Gray 1970) should also be advantageous, since the likelihood of doubly charged ions is reduced. Also as a consequence of the smaller atomic size of neon the deformation in the silicon matrix atoms due to sputtering gas atoms embedded in the film is reduced.

Since no previous work on neon sputtering of a-Si films has been reported the effect of preparation conditions on the electrical and optical properties of a-Si was investigated in detail. The sputtering parameters; sputtering pressure, target-substrate distance, d.c. self-bias voltage magnetic field and the substrate temperature were varied over a wide range to determine the optimum conditions. The sputtering pressure, perhaps the most important parameter was varied from the conventionally used argon pressure of 5 mtorr to about 260 mtorr. As discussed earlier (section 4.1.1) the highest operating pressure is limited by the geometry of the apparatus. In this range nearly thirty films were produced during the course of the present work. The d.c. dark conductivity of the films was measured as a function of temperature, over a range of at least 150°C. For the films produced at high pressures ($P_s > 60$ mtorr) the conductivity was measured from room temperature to about 180°C. For low pressure films the conductivity measurements could be extended to a lower temperature since they generally exhibited higher conductivities. For all the films the conductivity was measured under vacuum, to temperatures in excess of 175°C. This is to eliminate any possible effects due to surface adsorbates such as

water vapour (Tanielian 1980, Paul and Anderson 1981) or exposure to high intensity light (Staebler and Wronski 1977, 1980).

The values of the room temperature conductivity (σ_{RT}) and the thermal activation energy (ΔE) were deduced from the plots of conductivity versus inverse temperature. The variation of σ_{RT} with inverse temperature is illustrated in figure (5.10). The scatter in the data, particularly at high pressures is probably due to genuine differences between films prepared under nominally identical conditions. The solid line is drawn only to indicate the apparent trend of the data, a sharp decrease in conductivity (over six orders of magnitude) as the pressure is increased from 5 to about 80-90 mtorr and a much gradual decrease, on further increasing the pressure, to less than $10^{-10} (\Omega \text{ cm})^{-1}$ at 150 mtorr. At still higher pressures the trend seems to reverse with σ_{RT} increasing slightly with pressure.

A similar trend was also observed in the variation of ΔE with pressure. A sharp increase in ΔE with pressure to about 0.8 eV at 80-90 mtorr, followed by a much more gradual increase to a maximum of about 0.9 eV at around 150 mtorr, but decreasing slightly on further increasing the pressure. For most of the high pressure films the plots of conductivity versus inverse temperature yielded a single straight line over a range in conductivity of over four orders of magnitude (Fig 4.8) enabling the thermal activation energy to be defined unambiguously. However for some of the films a 'kink' in the variation of conductivity with temperature was observed, for temperatures in excess of about 130°C. Similar 'kinks' have also been observed for hydrogenated films (Rehn et al 1977, Spear et al 1980, Anderson and Paul 1981, 1982). Anderson

and Paul (1982) suggest that extended state conductivity only dominates at these high temperatures and at lower temperatures charge carriers hopping around the tail states also contribute to conductivity. However, their suggestion is disputed and alternative explanations have been put forward (Le Comber and Spear 1970, Mott and Davis 1979, Dohler 1979, Overhof and Bayer 1980). In the present work for the samples showing the high temperature change of slope, the data above the kink have been ignored and ΔE has been defined over the broad intermediate temperature region. This is to facilitate comparison with other published work and is in accordance with the current practice in the field.

The magnitude of the room-temperature photoconductivity (σ_{ph}) as a function of pressure is illustrated in figure (5.10). The magnitude of the photoconductivity increases with sputtering pressure to a value of about $5.0 \times 10^{-5} (\Omega \text{ cm})^{-1}$ at the highest pressure. This behaviour is consistent with the explanation that the density of defects is reduced on increasing the sputtering pressure. However unlike the room temperature dark conductivity the photoconductivity does not saturate at higher pressures but increases monotonically with pressure. Although the dark conductivity and the thermal activation energy of the high pressure neon sputtered films are comparable with the values obtained for hydrogenated films, the photoconductivity of neon sputtered films is about an order of magnitude lower, than that exhibited by optimally prepared hydrogenated films.

The optical gap was deduced from the optical absorption studies in the near infrared and visible regions for films produced at various neon pressures. It was found that the optical absorption

edge sharpens and shifts to higher energies as the pressure was increased from 5 to about 90 mtorr. However, on further increasing the pressure a reversal in the trend was observed with the slope of the absorption edge decreasing slightly with increasing pressure. The optical gaps (E_0) were deduced from plots of $(\alpha \hbar \omega)^{\frac{1}{2}}$ vs $\hbar \omega$, and are plotted as a function of pressure in Figure (5.11). E_0 was found to increase with pressure from about 1.44 eV at 5 mtorr to about 1.7 eV at the highest pressures.

Again the increase in the slope of the absorption edge and the optical gap with increasing neon pressure indicate that the density of states in the mobility gap is reduced on increasing the pressure. A similar trend is observed for the optical absorption edge of sputtered hydrogenated a-Si. The optical absorption edge sharpens and shifts to higher energies upon increasing the partial pressure of hydrogen (Moustakas 1978). Optical gaps as high as 2.2 eV have been reported for hydrogenated films (Moustakas 1978). However in hydrogenated films the shift in the absorption edge is probably due to the combined effect of the removal of localised states by hydrogen saturation of dangling bonds and the enlargement of the gap as a result of alloying. Therefore the high optical gaps observed for films containing large concentrations of hydrogen ($C_H > 10\%$) could be due to alloying rather than efficient dangling bond removal. In fact, Brodsky et al (1972) have estimated that the optical gap for 'void free' a-Si film would be about 1.8 eV.

From the foregoing sections it is evident that the electrical and optical properties are improved if the energy of the particles bombarding the film is reduced by increasing the sputtering pressure. The reduction in the kinetic energy of the plasma species bombarding

the film can also be achieved by either increasing the target-substrate distance (d) or by decreasing the target self-bias voltage (V_{sb}). Figure (5.16) shows the variation of σ_{RT} , σ_{ph} , ΔE and E_o with the target-substrate spacing (d). By increasing d from 2 to 5 cm our σ_{RT} was decreased by more than two orders of magnitude, while σ_{ph} , ΔE and E_o increased, indicating the reduction in the density of defect states with increasing d . However, as in the present study, the variation d in most sputtering systems is limited, therefore the target-substrate spacing can not be normally employed for optimising the preparation conditions. The sputtering rate decreased monotonically from above 3.0 \AA S^{-1} to $\sim 1.0 \text{ \AA S}^{-1}$ as the distance was increased.

The d.c. self-bias voltage (V_{sb}) on the target was controlled by varying the input power to the discharge and measured by the circuit illustrated in figure (4.5). Figure (5.17) illustrates the relationship between the applied power density and the self-bias voltage. It should be noted however that for this set of experiments other sputtering parameters were kept constant, namely the pressure was fixed at 85 mtorr, and the target-substrate distance at 3.5 cm and figure (5.17) only applies for these conditions. Figure (5.18) shows the variation of σ_{RT} , σ_{ph} , ΔE and E_o as the target voltage is increased from 550 to approximately 1050 V. Again the variation of σ_{RT} , σ_{ph} , ΔE and E_o with V_{sb} indicate that the density of defects can be reduced significantly by reducing the energy of the bombarding species. The sputtering rate decreased monotonically with V_{sb} from 3.0 \AA S^{-1} to about 0.5 \AA S^{-1} .

Although the variation in the electrical and optical properties is similar on increasing the sputtering pressure or the target

substrate spacing or decreasing the self-bias voltage, other factors should be considered when optimising the preparation conditions. For instance varying the target-substrate spacing or the self-bias voltage has little effect on the contamination levels in the chamber but increasing the sputtering pressure will in general increase the background contamination of the chamber. The increased contamination arises from two main processes; (1) as the pressure is increased the glow-discharge spreads and its interaction with the chamber walls and the substrate holder is increased. This results in increased outgasing from the chamber walls and furniture. (2) Another source of contamination is the decomposition of oil vapours as a result of backstreaming from the diffusion pump when it is operated at high pressures. This problem can be partly overcome by throttling the diffusion pump and by the use of a liquid nitrogen trap and a thermoelectric baffle valve between the diffusion pump and the chamber. However throttling the diffusion pump will increase the contamination due to outgasing. Therefore the level of throttling is a compromise between the need to maximise the removal of gases but to minimise the backstreaming from the diffusion pump.

The uniformity of the films was found to be independent of the sputtering pressure or the d.c. bias voltage but was affected considerably by the target-substrate separation (d). The extremes in (d) resulted in a deterioration in uniformity and the optimum separation in this respect was found to be about 3.5 cm. Chopra (1969) has suggested that the best uniformity is achieved when the target substrate spacing is equal to about twice the thickness of the cathode dark space.

Although the decrease in the deposition rate is similar on increasing pressure or target-substrate spacing or decreasing the bias voltage the mechanisms causing the decrease in the deposition rate are different in each case. When the pressure is increased the current density increases and hence the sputtering yield increases. However as the pressure is increased an increasing fraction of the sputtered material is backscattered to the target, or scattered out of the target-substrate plane, resulting in a net decrease in the deposition rate (Maissel 1970). This is why the deposition rate increases slightly as the neon sputtering pressure is increased from 5 to about 10 mtorr but decreases monotonically with pressure on further increasing the pressure. The decrease in the deposition rate with increasing target-substrate spacing is due to the loss of the sputtered material by scattering. Decrease in the deposition rate with the self-bias voltage is due to the decrease in the sputtering yield (Chapman 1980).

Therefore as in the case of argon sputtering the optimum conditions for sputtering a low density of defect state film can be estimated by depositing films at various sputtering pressures but at fixed d and V_{sb} . The target-substrate distance (d) should be fixed at a value which gives maximum uniformity whereas V_{sb} should be as low as possible but greater than the sputtering threshold for the target. Then by inspecting the variation of the various properties with pressure, the pressure at which the high energy bombardment of the films has been removed, but the low energy bombardment is still present can be estimated. Figure 6.2 shows the variation of σ_{RT} , σ_{ph} , ΔE , E_o , neon concentration (C_{Ne}) and the deposition rate (D_r) versus the sputtering pressure. As we can see from the figure, for neon, the pressure range over which the properties

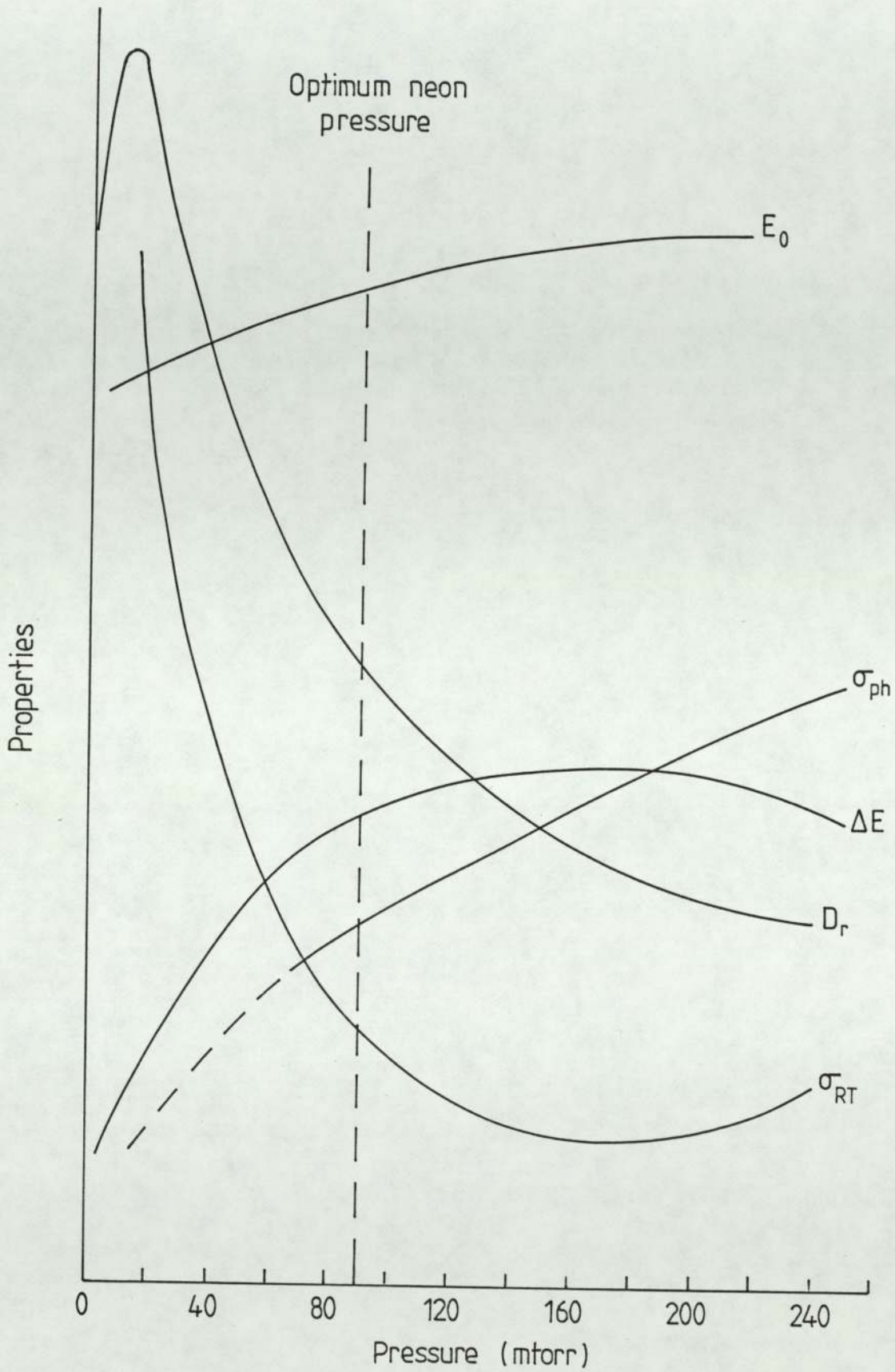


Figure 6-2 Variation of the various measured properties as a function of the neon sputtering pressure. The dashed line indicates the optimum neon pressure.

vary sharply extends up to about 80-90 mtorr. Above 80 mtorr the variation in the properties with pressure is more gradual. Thus the optimum sputtering pressure for $d = 3.5$ cm and $V_{sb} = 880$ V for the present system is about 80-90 mtorr.

6.3 THE EFFECT OF VARYING THE MAGNETIC FIELD

As discussed earlier (Section 5.2.4) axial magnetic fields are commonly employed to confine the plasma and hence increase the ionization efficiency and reduce the interaction of the plasma with the chamber walls and furniture. The reductions in the desorption of gases from the chamber walls, which represents the largest surface area, by confining the glow-discharge is particularly important. To determine the effect of the magnetic field on the properties of a-Si films, the magnetic field was varied from 0 to approximately 0.15 T by varying the current to the Helmholtz pair of coils from 0 to 5 A. The results of the investigation are presented in figures (5.19a, 5.19b, and 5.20). There is little variation in σ_{RT} or σ_{ph} with magnetic field (Figures 5.19a) however ΔE and E_0 decrease with increasing field. The explanation for this behaviour is not clear but the increase in ΔE and E_0 with decreasing magnetic field could be due to increased background contamination as the magnetic field is reduced. Since oxygen and hydrogen, the gases most likely to be outgassed, would probably effect the properties in a similar manner. Several authors have reported the apparent improvement in the properties (i.e. decrease in σ_{RT} and increase in σ_{ph} , ΔE and E_0) with the incorporation of oxygen, whether in situ or post deposition (Shimizu et al 1980, Paester et al 1978). Paesler et al (1978) suggest that oxygen acts in a similar manner to hydrogen in that it attaches itself to the

dangling bonds and hence reduces the density of states in the mobility gap. Unfortunately it was not possible to determine the oxygen concentration with the techniques employed for compositional analysis in the present study.

The increased efficiency of sputtering due to plasma confinement is evident from the increase in the deposition rate from 0.7 \AA s^{-1} at zero magnetic field to about 1.3 \AA s^{-1} at 0.015T (Figure 5.20). The variation of V_{sb} with the magnetic field is quite interesting. As shown in figure (5.20) that although the deposition rate increases V_{sb} decreases with increasing field for constant input power. The anomalous behaviour of V_{sb} with magnetic field can be explained by considering the mechanism for sheath formation on the target.

6.4 THE INFLUENCE OF SUBSTRATE TEMPERATURE

The variation of electrical and optical properties (σ_{RT} , σ_{ph} , ΔE , E_0) with the substrate temperature is illustrated in figure (5.21). Similar results for pure argon sputtered a-Si and a-Ge have been reported (Paul et al 1973, Pawlewicz 1978). The results presented here are consistent with the suggestion proposed by Paul et al (1973) to explain the increase in resistivity and the optical gap with increasing substrate temperature for a-Ge films. They suggested that increasing the temperature resulted in a slight but significant reorganisation of the bonding network resulting in a decrease in the void volume and hence the density of dangling bonds. The results obtained for a-Si have also been explained consistently on the basis of this explanation; although for a-Si

the reduction in defect density for substrate temperatures up to 500°C is small (Pawlewicz 1978).

However, the substrate temperature (T_s) influences the properties of hydrogenated films drastically. For a fixed hydrogen partial pressure increasing T_s to about 300°C results in the improvement of properties, as is evident from the displacement of the optical edge towards higher energies (Freeman and Paul 1979), the reduction in the hopping conductivity (Anderson and Paul 1981) and an increase in photoconductivity by three orders of magnitude (Moustakas et al 1979). Increasing the substrate temperature above 300°C however results in the deterioration of the properties: the optical absorption edge shifts towards lower energies (Freeman and Paul 1978) σ_{RT} increases with corresponding decrease in ΔE (Anderson and Paul 1981) and σ_{ph} decrease. This behaviour is explained by the fact that hydrogen begins to evolve at temperature in excess of 300°C. Thus the efficiency of hydrogen incorporation is reduced at temperature above 300°C which results in the deterioration of the properties (Paul and Anderson 1981).

Although all the films produced in the present study were sputtered in pure argon or neon gases it is possible that hydrogen present in the chamber due to the outgassing of the chamber walls and furniture could be influencing the results reported here. Since hydrogen could not be detected by the techniques employed in the present study for compositional analysis, the monotonic variation of the electrical and optical properties with temperature confirms the expectation that no hydrogen is present in the films.

The composition of the films was determined by XPS and AES. The main impurities detected were neon and oxygen. The concentration of neon and oxygen in the film as a function of substrate temperature is illustrated in Figures (5.22). The slight decrease in the neon content with substrate temperature is consistent with the ideas proposed by Winters and Kay (1967). They measured the argon content in sputtered nickel films and found it to decrease slightly with temperature. They suggested that since argon is probably physisorbed, it is less likely to be initially adsorbed and more likely to be subsequently desorbed, with increasing substrate temperature.

The oxygen concentration also decreases with increasing substrate temperature. However Figure 5.22 does not represent absolute values of the oxygen concentration. This is due to a design fault in the KRATOS spectrometer. Oxygen was introduced into the films when they were etched by argon bombardment. Further discussion on this point can be found in a later section (Section 6.6). Thus the results of Figure (5.22) for oxygen concentration are to be regarded as relative concentrations.

6.5 THE DOPING EFFECTS OF GROUP V ELEMENTS

Despite the voluminous work in the early years of research on the electronic properties of amorphous silicon, it appeared that the material was insensitive to substitutional doping. This was thought to be due to the inherent flexibility of the local bonding environment of the impurity atoms in an amorphous network thus without the rigid constraints present in crystals the extra valence (for n-type dopant) of the impurity atom could easily be accommodated (Mott 1967). It is now clear that the failure of substitutional

doping was due to the presence of a large number of electronic states in the 'forbidden gap'. Thus any addition of trace amounts of dopants had a negligible influence on the large background of states already present. Thus to achieve sensitive substitutional doping the material produced must have a low density of defect states. This has been achieved by a-Si produced by glow-discharge decomposition of silane where the density of defect states in the material is about five orders of magnitude lower than in evaporated or argon sputtered silicon (Spear and Le Comber 1975). RF sputtering in a plasma of argon and hydrogen also produces a material with a low density of defect states which can be doped n- or p- type with groups V and III elements respectively.

The success of these methods is due to the presence of large amounts of hydrogen in the plasma. The hydrogen attaches itself to the dangling bonds thus removing the defect states from the mobility gap. Other dangling bond terminators such as the halogens have been employed with equal success (Madan et al 1980).

However the alloy of silicon and hydrogen (a-Si:H) has the disadvantage of being thermally unstable; hydrogen effuses at 350°C and there is some evidence that it might even effuse at room-temperature (Tsai, 1977). Another disadvantage is that one is dealing with highly toxic and explosive gases in the glow-discharge process.

Therefore it is desirable to develop an alternative method of producing a-si with a low density of defect states. In the preceding chapter it has been demonstrated that the electrical and optical properties and hence the density of defect states in

a-Si films produced by r.f. sputtering in pure argon or neon can be influenced greatly by varying the deposition conditions. Increasing the argon or neon sputtering pressure reduces the density of defect states in the material, but the improvement of properties is greater for neon sputtered films than for argon sputtered films.

To determine the doping efficiency of the optimally prepared material in the present study (films produced at high neon sputtering pressure) n-type amorphous silicon was produced by co-sputtering with tantalum and by sputtering targets predoped with arsenic or antimony. Pre-doped targets of the required size were available with only one concentration of dopant. However the concentration of tantalum could be varied easily. As shown in figure (5.24) the room-temperature electrical conductivity (σ_{RT}) could be varied systematically over nine orders of magnitude by incorporating up to 3.31% tantalum in the films. The n-type behaviour of the tantalum doped films was confirmed by the 'hot probe' technique.

At low doping levels σ_{RT} and ΔE vary sharply on increasing the tantalum concentration. The room-temperature conductivity changes by nearly five orders of magnitude with a corresponding shift in the Fermi level of about 0.5 eV on the addition of approximately 0.2 at % of tantalum. On further increasing the tantalum concentration the variation in σ_{RT} and ΔE is gradual. This is probably due to the fact that as the material is doped the Fermi level moves towards the conduction band. At high doping levels it has moved into the high density of states near the tail states region (see figure 3.1c).

Although σ_{RT} was varied over many orders of magnitude with a corresponding variation in the thermal activation energy (0.79 eV

for intrinsic films, < 0.1 eV for highly doped films) the optical gap only changes from about 1.6 eV for intrinsic films to about 1.33 eV for highly doped films. It would appear, therefore, that the variation in the electrical properties is due to substitutional doping rather than alloying as been suggested for some a-Si films containing a high density of impurity (Thompson and Reinhard 1980).

As mentioned earlier, doping by co-sputtering with tantalum was chosen for its convenience although the doping efficiency is greater for gas-phase doping and for low atomic weight dopants (e.g. phosphorous). Even with these disadvantages the efficiency of tantalum doping in the present system is comparable with hydrogenated material. Figures (6.3) and (6.4) compare the variation of room-temperature electrical conductivity (σ_{RT}) and thermal activation energy (ΔE) as a function of the density of tantalum atoms, incorporated into neon sputtered silicon with gas phase doping of hydrogenated a-Si with phosphorous (Curve A) and ion implantation (Curve B). It is evident from figures (6.3) and (6.4) that the variation in σ_{RT} and ΔE of neon sputtered a-Si with tantalum is comparable with that achieved by phosphorous incorporation in a-Si:H. Although the doping efficiency of the present material is much better than ion-implanted a-Si:H it is not as good as gas phase doped a-Si:H. This could partly be due to the greater efficiency of doping from gas phase than by co-sputtering.

It is worth noting however that the tantalum doped films achieved much higher conductivities than the hydrogenated material. High conductivity n-type materials have, however, been produced in microcrystalline form (Spear et al 1981; Veprek et al 1981).

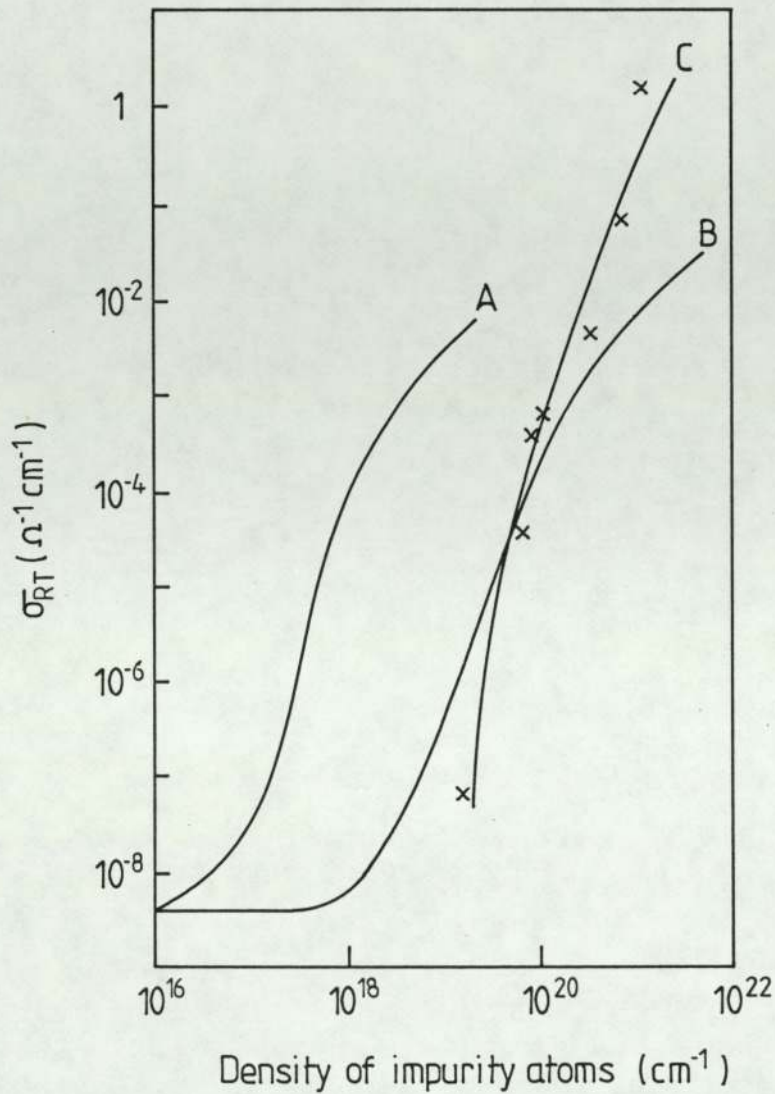


Figure 6.3 Room temperature conductivity (σ_{RT}) as a function of the density of impurity atoms. Curve A, gas phase doping of $\alpha\text{-Si:H}$ by phosphorous; curve B, ion implantation of phosphorous in $\alpha\text{-Si:H}$; curve C, tantalum doping by neon sputtering. A and B after Müller et al (1977).

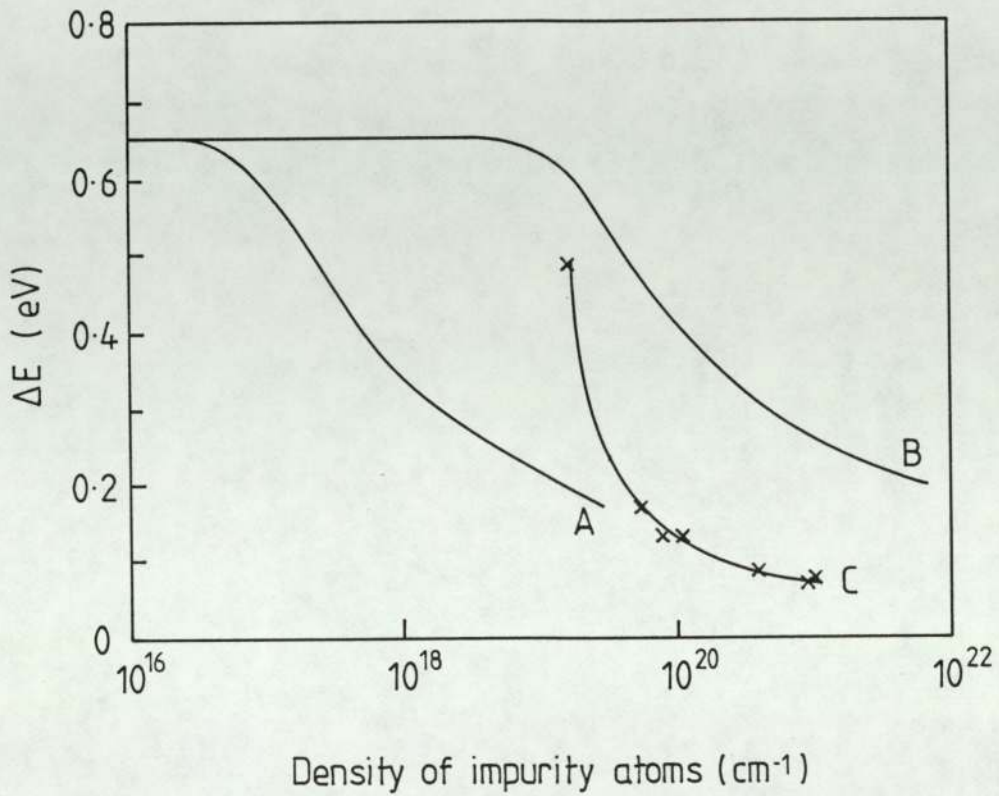


Figure 6.4 Conductivity activation energy as a function of the density of impurity atoms. Curve A, gas phase doping of α -Si:H by phosphorous; curve B, ion implantation of phosphorous in α -Si:H; curve C, tantalum doping by neon sputtering. A and B after Müller et al (1977)

Electron and x-ray diffraction studies of intrinsic and doped materials have failed to show crystallinity in the present material.

To confirm that the variation in the electrical properties with tantalum incorporated was due to substitutional doping and not due to some alloying effects a composite target resulting in 0.2% tantalum in the films was sputtered at various neon pressures. The results are illustrated in figure 5.27. The higher conductivity and lower thermal activation energy of the films prepared at high neon pressure are again evidence for the reduction of the density of defect states on increasing the sputtering pressure.

The results of the variation of σ_{RT} , σ_{ph} , ΔE and E_0 (figures 5.30 and 5.31) of the films sputtered from targets pre-doped with arsenic and antimony also suggest that the density of defect states in the intrinsic material is reduced on increasing the sputtering pressure.

It has been demonstrated that by optimising the sputtering conditions, pure a-Si can be produced with a density of states low enough to enable efficient substitutional doping. Although the results presented here are for n-type doping, p-type doping has also been achieved (Fane 1981, Fane and Abo-Namous 1983). Although doping efficiency is not as good as that achieved by gas phase doping of hydrogenated silicon (Spear and Le Comber 1976) it has been demonstrated that the electrical conductivity and thermal activation energy can be varied systematically over a wide range.

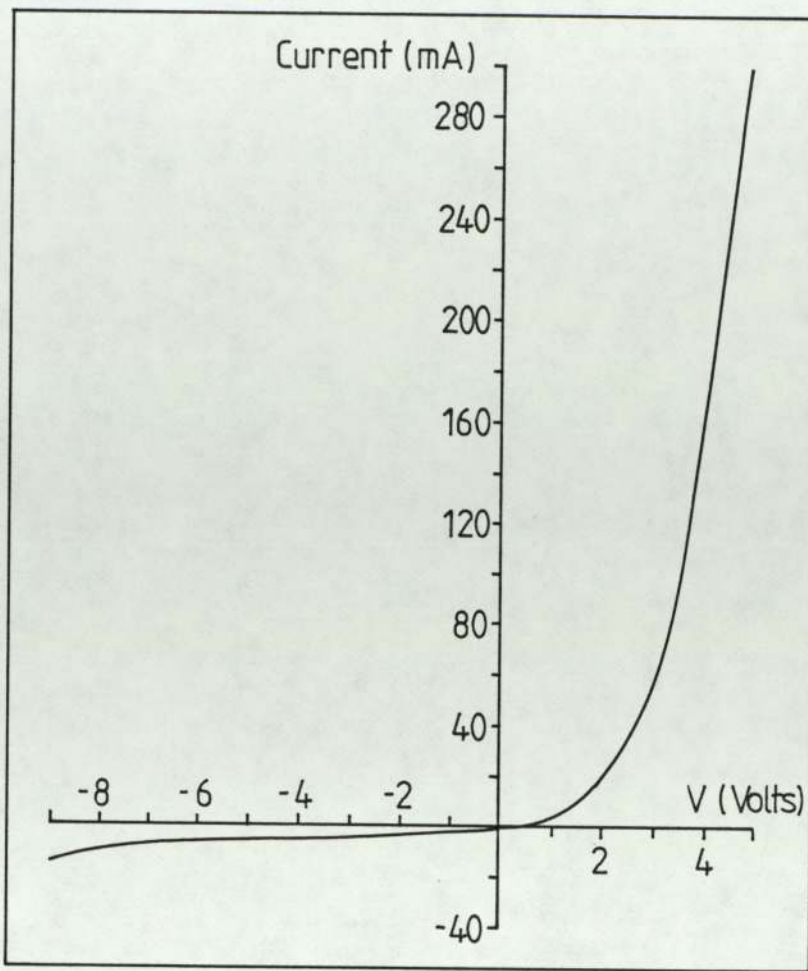


Figure 6.5a I.V. Characteristic for n-type α -Si / p-type crystalline junction.

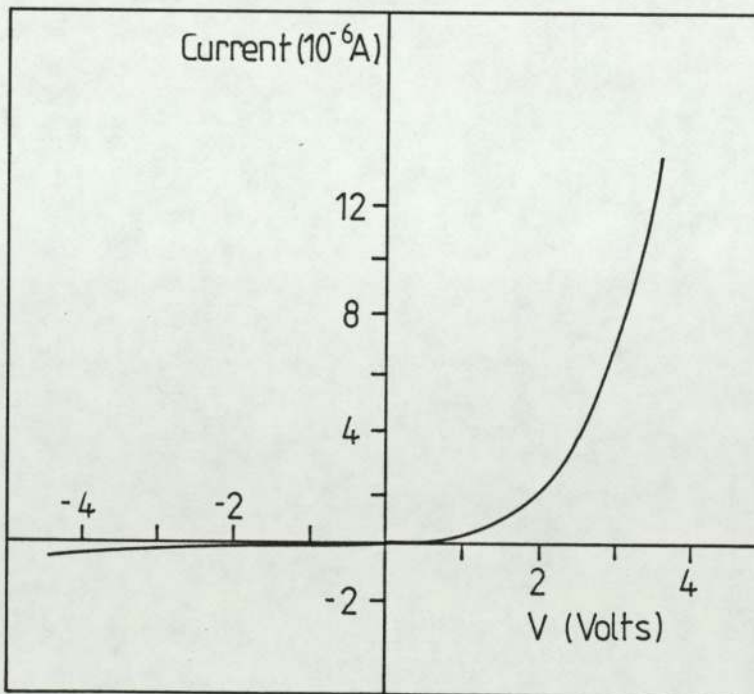


Figure 6.5b I.V. Characteristics for a typical p/n amorphous silicon junction. (p - layer aluminium doped, n - layer tantalum doped)

Preliminary p-n junctions of neon sputtered a-Si were constructed. Figure (6.5a) shows a heterojunction made from the deposition of a tantalum doped a-Si film onto a crystalline p-type silicon. Considering that no attempts have been made to optimise the process satisfactory rectification was observed. These results are comparable with those of Thompson et al (1978) on hydrogenated silicon doped by sputtering from pre-doped targets. A typical p-n junction made from tantalum and aluminium doped films is shown in figures (6.5b).

6.6 THE COMPOSITIONAL ANALYSIS OF THE FILMS

Three main techniques were employed for compositional analysis of the sputtered films as detailed in Section (4.3). They were Rutherford backscattering spectroscopy, X-ray photoelectron spectroscopy and Auger electron spectroscopy. The main impurities detected were the intentionally incorporated dopants (e.g. tantalum, arsenic and antimony) and the unintentionally incorporated oxygen and the noble gas (e.g. neon or argon) used for sputtering.

Rutherford backscattering spectroscopy proved to be a very useful technique for determining the concentration of argon in argon sputtered films and the concentration of all the dopants employed in the present study. This is because argon and the doping elements have atomic masses greater than silicon and consequently their peaks lie higher up the energy scale than the silicon peak (see figure 3.6). Therefore the concentration of the impurities can be simply obtained by measuring the peak heights and employing the equation (3.12b).

RBS has a high sensitivity for heavy atoms, since the Rutherford scattering cross-section is proportional to the square of the atomic number (Chu et al 1978). Another advantage of the technique is that the depth distribution of the elements can be readily determined by examining the spectra. Whereas for most other techniques (including XPS and AES) to obtain depth distribution of elements the surface needs to be etched and spectra obtained at various depths. As discussed later, etching, not only destroys the sample but can also alter the surface chemistry leading to incorrect conclusions.

The weakness of RBS lies in its insensitivity in detecting low atomic weight elements and impurity atoms which are lighter than the host material. Thus although the concentration of argon in argon sputtered films was readily determined, the concentration of neon in neon sputtered film could not be determined accurately using this technique.

As discussed earlier (section 6.1) sputtering at high pressures can lead to insitu and/or post deposition oxygenation of the films. Therefore it is important to determine the oxygen concentration of the films. The oxygen concentration of the argon sputtered films could be extracted from the relevant spectra. The results showed that films sputtered at pressure less than about 25 mtorr contained no oxygen while films sputtered at higher pressures contained approximately 20% oxygen (see figure 5.7). These results support the argument that although increasing the sputtering pressure is beneficial in that the high energy bombardment of the film by the various plasma species is removed increasing the pressure beyond a certain value also removes the low-energy bombardment of the

film. The low energy bombardment of the films is beneficial because it removes the loosely bound atoms from the surface, which would otherwise form weak bonds leading to a porous structure, susceptible to post-deposition oxygen.

A rough estimate of the minimum amount of oxygen, detectable by RBS can be obtained by considering equation (3.12a).

$$\text{i.e. } \frac{H_m}{H_i} = \frac{N_m \cdot \sigma_m \cdot [S]_i^m}{N_i \cdot \sigma_i \cdot [S_m]_m^m} \quad (6.1)$$

Then assuming that the detectable height of an impurity signal is about one-thousandth of the height of silicon signal (i.e. $H_i/H_m = 10^{-3}$), further assuming that the $[S]_i^m/[S_m]_m^m$ ratio is unity and that σ ratio is approximately equal to the Z^2 ratio, equation (6.1) gives a sensitivity limit of:

$$\frac{N_i}{N_m} = \frac{Z_m^2}{Z_i^2} \times 10^{-3} \quad (6.2)$$

Therefore the minimum amount of oxygen that can be detected in silicon is approximately 0.3%, where as for tantalum in silicon the minimum limit is approximately 0.004%.

The oxygen concentration of the neon sputtered films could not be determined because the oxygen and the neon peaks overlapped and were indistinguishable.

Another quantity which can be used to determine the porosity of a film is its density. In theory the density can be obtained by the RBS spectra, if the thickness of the film is measured independently, by employing the equation:

$$dE = [E] \frac{N_0 \rho}{A} \quad (6.3)$$

where dE is the energy difference between the energy of the ions scattered from the front surface of the target and the ions scattered from the back surface of the target, $[E]$ is the stopping cross-section, N_0 is the Avagadros number, A is the atomic weight of the element and ρ and t are the density and thickness of the film respectively. Since $[E]$ is tabulated (Chu et al 1978) the density can be obtained by measuring dE and the thickness of the film.

An attempt to measure the density of the films was made using films sputtered onto carbon substrates, since the carbon edge lies well below the silicon peak, but measurement of dE and the shape of the peak indicated that carbon and silicon had diffused into each other, resulting in the broadening of dE and hence an over-estimation of the density. To overcome this problem quartz and alumina substrates were employed and although no sign of diffusion seemed apparent, there was a large error in determining dE due to the overlap of the silicon and the substrate peaks. Thus, unfortunately in the present study the density of the films could not be determined accurately enough to examine the porosity of the films as a function of sputtering pressure. Another method which might yield more precise results would be to deposit the films onto a high atomic weight element, such as tantalum, tungsten

or gold. Then dE is given by the difference the energy of the front edge of the element with and without the film on it.

Although RBS is not very sensitive for light elements, XPS and AES both have relatively high sensitivities for low atomic weight elements. Initial experiments to determine the concentration of neon and oxygen in the films with XPS and AES were rather disappointing. This is because both of these techniques only examine the top few layers of a sample (Briggs and Seah 1983) and to determine the composition of the bulk, (since the surface is invariably oxidised) the surface needs to be etched away by argon ion bombardment. However the etching can itself cause various problems resulting in incorrect results. For example, in the spectrometer employed in the present study, when operating in the XPS mode the area etched by the ion gun is smaller than the area analysed, thus signal from the oxidised surface will always be picked up. It was also found that the etching process resulted in the incorporation of oxygen into the film.

Initial experiments to determine the neon concentration similarly, gave incorrect results. The problem again was due to the etching of the surface. The procedure adopted was to obtain a spectrum at the surface and then obtain spectra after etching for five minutes. The results showed that there was less than 0.5% neon incorporated in all the films, produced over a wide range of sputtering pressures. It was then realised that the etching could in fact be causing the evolution of neon from the surface of the sample. A model of the silicon surface to explain the results is shown in figure (6.6a). Since, both XPS and AES analyse only the top few monolayers of the sample, the spectrum obtained at

surface would only show the composition of the oxide layer, which has developed after the film has been deposited and hence contains no neon. A five minute etch would approximately erode 500 Å of the surface, therefore a spectrum obtained then should be characteristics of the bulk sample. However, etching by sputtering the atoms of the film by argon ion bombardment is a very inefficient method. Only about 1% of the argon ion energy is used to liberate the atoms from the surface, the rest is dissipated as heat (Chapman 1980). Thus the heat liberated at the surface by the impinging argon ions could result in the effusion of neon from the top few layers since neon is not chemically bonded to silicon but is only physisorbed (Winters and Kay). Thus when the spectrum is obtained it shows very little or no neon in the sample. To overcome these problems the procedure for obtaining the spectra was revised. Instead of obtaining the second spectrum after a five minute etch, spectra were obtained after etching intervals of a few seconds (typically 10 seconds). Therefore as the oxide layer is eroded the neon concentration should increase, maximising at the oxide/silicon interface, since etching into the silicon layer (as discussed above) will result in the effusion of neon. Figure (6.6b) shows the variation of neon as a function of the etching period. It is clearly evident that spectrum obtained at the surface and after five minute etch under estimate the quantity of neon in the films.

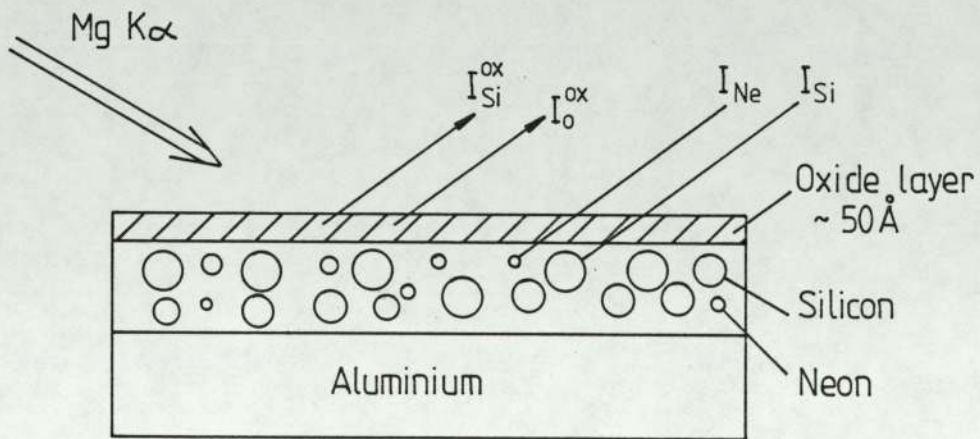


Figure 6.6a A model for the surface of the neon sputtered amorphous-silicon film.

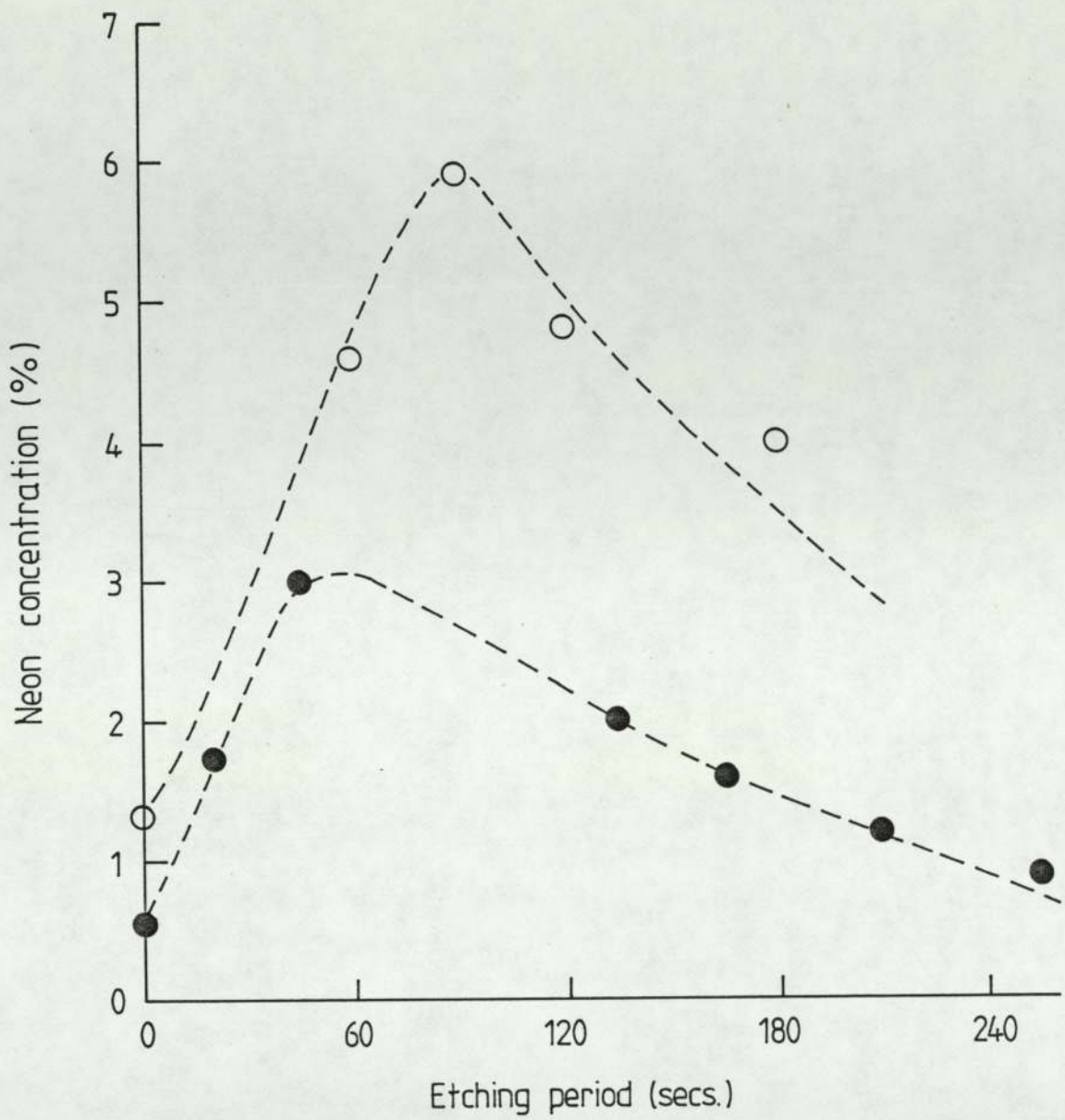


Figure 6.6b Concentration of neon as a function of the etching period.

7. CONCLUSION

The aim of the present study was to investigate the effect of varying the preparation conditions on the electrical and optical properties of pure amorphous silicon produced by r.f. sputtering. Conventionally amorphous silicon is produced by sputtering in a plasma of argon at a pressure of about 5 mtorr. However if pure argon is used the material is plagued with defects such as dangling bonds and microvoids which inhibit the control of the electrical properties by substitutional doping. The properties of the material can be improved substantially by incorporating large concentrations of dangling bond terminators such as hydrogen or the halogens.

The results presented in this dissertation suggest that the density of dangling bonds can be reduced by sputtering at higher pressures. This is due to the fact that at low pressures the film is bombarded by high energy particles in the plasma (i.e. ions and neutrals) which create defects in the film. By increasing the pressure the mean free path of the various species in the plasma is reduced and hence the energy with which they bombard the film is reduced. Although the high energy bombardment by the plasma species was found to be detrimental to the film properties, low energy bombardment is beneficial since it helps to remove loosely bound material from the surface of the film which would otherwise result in a porous structure. This was evident from the large concentration of oxygen in the films produced at the highest pressures. Therefore the optimum pressure for sputtering is that at which the high energy bombardment has been removed but the low energy bombardment is still retained. The optimum pressure for any system can be estimated by investigating the variation of the various properties of the film with sputtering pressure.

Although sputtering at the optimum argon pressure improved the properties substantially, the electrical and optical properties of the material thus produced were inferior to the properties of optimumly prepared hydrogenated silicon. To achieve further improvement sputtering in neon was investigated. Again by investigating the variation of the various properties (electrical conductivity, photoconductivity, thermal activation energy, optical gap, neon concentration, deposition rate) with pressure the optimum sputtering pressure were defined. The material produced at optimum neon pressure showed marked improvement in the electrical and optical properties, which were comparable to those of hydrogenated silicon. Increasing the target substrate distance or decreasing the d.c. self-bias voltage also results in the reduction in kinetic energy of the plasma species. By employing an axial magnetic field the efficiency of ionisation is enhanced and interaction of the plasma with the chamber walls is reduced. Increasing the substrate temperature also results in a slight reduction of the density of defects states.

It was shown that amorphous silicon produced by sputtering in neon at the optimum conditions can be doped efficiently, by co-sputtering with tantalum and targets pre-doped with arsenic or antimony. It is envisaged that the doping efficiency can be improved further if more efficient methods of doping are employed (e.g. gas phase doping).

The composition of the film was analysed by Rutherford backscattering spectroscopy, X-ray photoelectron spectroscopy and Auger electron spectroscopy. RBS proved to be a very useful technique for analysing argon sputtered and doped films, since the depth profile of the elements is readily available.

It has been shown by investigating the electrical and optical properties that the density of defect states can be reduced significantly by sputtering in neon rather than argon and by sputtering at high pressures. For future work it is suggested that the density of defect states is analysed quantitatively. It is envisaged that density of defects can be reduced further by negatively biasing the substrates. Other avenues of investigation which could yield interesting results are sputtering in a mixture of noble gases (i.e. helium and neon or neon and argon). Studying the effect of reactive sputtering with oxygen, hydrogen and the halogens.

REFERENCES

- ABBOT, A., Private Communication.
- ABELES, B., WRONSKI, C. R., TIEDIE, T. and CODY, G. O. Solid state Commun. 36, 537-540, 1980.
- ABO-NAMOUS, S. A., ZAKA, Y. and FANE, R. W. Phys. Stat. Sol. (a), 79, 477-482, 1983.
- ABO-NAMOUS, S. A. and FANE, R. W. J. Phys. C: Solid State Phys. 17, 1775, 1984.
- ABO-NAMOUS, S. A., ZAKA, Y. and FANE, R. W. Vacuum, 34, 1001-1004, 1984.
- ABO-NAMOUS, S. A., ZAKA, Y. and FANE, R. W. Presented at the Sixth Inter. Conf. Thin Films, Stockholm, Sweden, 1984.
- ADLER, D. 'Amorphous Semiconductors,' Butterworths, London. 1972.
- ANDERSON, D. A., MOUSTAKAS, T. D. and PAUL, W. Proc. 7th Inter. Conf. Amorphous and Liquid Semiconductors, Ed. Spear, W. E., Edinburgh, University of Edinburgh Press. pp 334-38, 1977.
- ANDERSON, D. A., MODDEL, G., PAESLER, M. A. and PAUL, W. J. Vac. Sci. Tech. 16, 906-911, 1979.
- ANDERSON, D. A. and PAUL, W. Phil. Mag. B. 44, 187-213, 1981.
- ANDERSON, D. A. and PAUL, W. Phil. Mag. B. 45, 1-23, 1982.
- ANDERSON, G. S., MAYER, W. N. and WEHNER, G. K. J. Appl. Phys. 33, 2991-2992, 1962.
- AST, D. G. BRODSKY, M. H., Phil. Mag. B. 41, 273, 1980
- BEYER, W. and STUKE, J. Proc. 5th Inter. Conf. Amorphous and Liquid Semiconductors, Eds. Stuke, J. and Brenig, W. Garmische, pp 251-240, 1973.
- BEYER, W., STUKE, J. and WAGNER, H. Phys. Stat. Sol. (a) 30, 231-240, 1974.
- BOOTH, D. C., ALLRED, D. D. and SERAPHIN, B. O. Solar Energy Materials, 2, 107-123, 1979.
- BRODSKY, M. H. J. Vac. Sci. Tech. 8, 125-133, 1971.
- BRODSKY, M. H. Ed. 'Topics in Applied Physics: Amorphous Semiconductors' 36, 1979.
- BRODSKY, M. H. and TITLE, R. S. Phys. Rev. Lett. 23, 581-585, 1969.
- BRODSKY, M. H., TITLE, R. S., WEISSER, K. and G. D. PETTIT. Phys. Rev. B. 1, 2632-2641, 1970.

- BRODSKY, M. H., CARDONA, M. and CUOMO, J. J., Phys. Rev. B. 16, 3556-3571, 1977 (a).
- BRODSKY, M. H., FRISCH, M. A., ZIEGLER, J. F. and LANFORD, W. A. Appl. Phys. Lett. 30, 561-563, 1977 (b).
- BRODSKY, M. H., EVANGELISTI, F., FISCHER, R., JOHNSON, R. W., REUTER, W. and SOLOMAN, I. Solar Cells. 2, 401-406, 1980.
- BRIGGS, D. and SEAH, M. P. 'Practical Surface Analysis by Auger and X-ray Photoelectron Spectroscopy' John Wiley & Sons, 1983.
- BUTLER, H. S. and KINO, G. S. Phys. Fluids, 6, 1346, 1963.
- CARLSON, D. E. and WRONSKI, C. R. 'Topics in Applied Physics', 36, 287-329, 1979.
- CARLSON, D. E. Solar Energy Materials, 3, 503-518, 1980.
- CARTER, G. and COLLIGON, J. S. 'Ion Bombardment of Solids', Heinemann Educational, London. pp 323.
- CHAPMAN, B. 'Glow-discharge Processes, Sputtering and Plasma Etching', John Wiley & Sons, N. Y., 1980.
- CHITTICK, R. C., ALEXANDER, J. H. and STERLING, H. F. J. Electrochem. Soc. 116, 77-80, 1969.
- CHU, W. K., MAYOR, J. W. and NICOLET, M. A. 'Backscattering Spectrometry', Academic Press, 1978.
- COHEN, M. H., FRITZSHE, H. and OVSHINSKY, S. R. Phys. Rev. Lett. 22, 1065-1068, 1969.
- CONNELL, G. A. N. and PAWLIK, J. R. Phys. Rev. B. 13, 787-804, 1976.
- CONNELL, G. A. N. in 'Topics in Applied Physics: Amorphous Semiconductors', Ed. Brodsky M. H. 36, 1979.
- DAVIS, E. A. and MOTT, N. E. Phil. Mag. 22, 903-922, 1970.
- DAVIS, E. A. in 'Topics in Applied Physics: Amorphous Semiconductors', 36, 41, 1979.
- DAVIS, L. E., MACDONALD, N. C., PALMBERG, P. W., RIACH, G. E. and WEBER, R. E. 'Handbook of Auger Electron Spectroscopy', Physical Electronics Industries Inc. 1978.
- DOHLER, G. H. Phys. Rev. B. 19, 2083-2091, 1979.
- FANE, R. W. J. Phys. D: Appl. Phys. 14, 2113, 1981.
- FANE, R. W. and ZAKA, Y. J. Phys. D: Appl. Phys. 16, 1993, 1983 (a).
- FANE, R. W. and ZAKA, Y. J. Non-Cryst. Solids, 57, 1, 1983 (b).

- FANE, R. W. and ABO-NAMOUS. J. Phys. C: Solid State Phys. 16, 6121, 1983.
- FOTI, G., MAYER, J. W. and RIMINI, E. 'Ion Beam Handbook of Material Analysis, Ed. Mayer, J. W. and Rimini, E. Academic, N. Y. pp 22, 1977.
- FREEMAN, E. C. and PAUL, W. Phys. Rev. B. 18, 4288-4300, 1978.
- FREEMAN, E. C. and PAUL, W. Phys. Rev. B. 20, 716-728, 1979.
- ^SFRITZCHE, H. Proc. 7th Inter. Conf. Amorphous and Liquid Semiconductors, Ed. Spear, W. E., University of Edinburgh Press, pp 3-15, 1977.
- ^SFRITZCHE, H., TANIÉLIEN, M., TSAI, C. C. and GACZI, P. J. J. Appl. Phys. 50, 3366-3369, 1979.
- ^SFRITZCHE, H. Solar Energy Materials, 3, 447-501, 1980 (a).
- ^SFRITZCHE, H. Solar Cells, 2, 289-300, 1980.
- GLANG, R., HOLMWOOD, R. A. and KURTZ, J. A. 'Handbook of Thin Film Technology', Ed. Maissel, L. I. and Glang, R. McGraw Hill Book Co. 1970.
- GROVE, W. R. Trans. Roy. Soc. 142, 87, 1852.
- HORWITZ, C. M. J. Vac. Sci. Technol. A, 1, 60-68, 1982.
- IMURA, T., USHITA, K. and HIRAKI, A. Jap. J. Appl. Phys. 19, 265-268, 1980.
- JACKSON, G. W. Thin Solid Films, 5, 209-246, 1970.
- JANAI, M., ALLRED, D. D., BOOTH, D. C. and SERAPHIN, B. O. Solar Energy Materials 1, 11, 1979.
- KAPLAN, D., SOL, N., VELASCO, G. and THOMAS, P. A. Appl. Phys. Lett. 33, 440-442, 1978.
- KNIGHTS, J. C. AIP Conf. Proc. 31, 296, 1976.
- KNIGHTS, J. C. and LUCOVSKY, C. R. C. Critical reviews in solid state and materials sciences. 9, 211-283, 1980.
- KOENING, H. R. and MAISSEL, L. I. IBM J. Res. Dev. 14, 168, 1970.
- LAMONT, L. T. and TURNER, F. T. J. Vac. Sci. Technol. 11, 47-51, 1973.
- LECOMBER, P. G. and SPEAR, W. E. Phys. Rev. Lett., 25, 509-511, 1970.

- LECOMBER, P. G., LOVELAND, R. J., SPEAR, W. E. and VAUGHAN, R. A. Proc. 5th Inter. Conf. Amorphous and Liquid Semiconductors. Eds. Stuke, J. and Brening, W. Taylor & Francis, London, pp 245-250, 1974.
- LECOMBER, P. G., JONES, D. I. and SPEAR, W. E. Phil. Mag. 35, 1173-1187, 1977.
- LECOMBER, P. G. and SPEAR, W. E. Topics in Applied Physics, 36, 251-285, 1979.
- LEWIS, A. J. Phys. Rev. B. 13, 2565-2575, 1976.
- LOVELAND, R. J., SPEAR, W. E. and AL-SHARBATY, A. J. Non-Crystalline Solids, 13, 55-68, 1973/1974.
- MADAN, A., LECOMBER, P. G. and SPEAR, W. E. J. Non-Cryst. Solids, 20, 239-257, 1976.
- MADAN, A., OVSHINSKY, S. R. and BENN, E. Phil. Mag. B. 40, 259-277 1979.
- MADAN, A., OVSHINSKY, S. R., CZUBATYJ, W. and SHUR, M. J. Electron. Mater. 9, 389, 1980.
- MAGEEM C. W. and CARLSON, D. E. Solar Cells 2, 365, 1980.
- MAISSEL, L. I. in 'Handbook of Thin Film Technology', Eds. Maissel, L. I. and Glang, R., McGraw Hill 1970.
- MALHOTRA, A. K. and NEUDECK, G. W. Appl. Phys. Lett., 28, 47-49, 1976.
- MEJIA, S. R., MCLEOD, R. D., KAO, K. C. and CARD, H. C. J. Non. Cryst. Solids., 59/60, 727-730, 1983.
- MEUNIER, M., FLINT, J. H., ADLER, D. and HAGGERTY, J. S. J. Non. Cryst. Solids., 59/60, 699-702, 1983.
- MOTT, N. F. Adv. Phys. 16, 49-144, 1967.
- MOTT, N. F. Phil. Mag. 22, 22-29, 1970.
- MOTT, N. F., DAVIS, E. A. and STREET, R. A. Phil. Mag. 32, 961-996 1975.
- MOTT, N. F. and DAVIS, E. A. 'Electronic Processes in Non-Crystalline Solids', Clarendon Press, Oxford, 1979.
- MOUSTAKAS, T. D. J. Electron. Mat. 8, 391-435, 1979.
- MOUSTAKAS, T. D. and PAUL, W. Phys. Rev. B. 16, 1564-1567, 1977.
- MOUSTAKAS, T. D., ANDERSON, D. A. and PAUL, W. Solid State Commun. 23, 155-158, 1977.

- NEWMAN, R. M. University of Aston in Birmingham, PhD Thesis, 1972.
- OGUZ, S. and PAESLER, M. A. Bull. Am. Phys. Soc. 23, 247, 1978.
- OVERHOF, H. and BEYER, W. J. Non. Cryst. Solids, 35/36, 375-380, 1980.
- PAESLER, M. A., ANDERSON, D. A., FREEMAN, E. C., MODDEL, G. and PAUL, W. Phys. Rev. Lett, 41, 1492-1495, 1978.
- PAUL, W., CONNELL, G. A. N. and TEMKIN, R. J. Adv. Phys. 23, 529-580, 1973.
- PAUL, W., LEWIS, A. J., CONNELL, G. A. N. and MOUSTAKAS, T. D. Solid State Commun. 20, 969-972, 1976.
- PAUL, W. and ANDERSON, D. A. Solar Energy Mat.
- PAWLEWICZ, W. T. J. Appl. Phys., 49, 5595-5601, 1978.
- PAWLIK, J. R. and PAUL, W. Proc. 7th Inter. Conf. Amorphous and Liquid Semiconductors. Ed., Spear, W. E., Edinburgh University Press, pp 437, 1977.
- PENN, O. R. J. Electron Spectroscopy, 9, 29, 1979.
- PENNING, F. M. and MOUBIS, J. H. A., Koninkl. Ned. Akad. Wetenschap. Proc. 43, 41, 1940.
- PROCEEDINGS of 7th Inter. Conf. on Amorphous and Liquid Semiconductors, Ed. Spear, W. E., Edinburgh, University of Edinburgh Press, 1977.
- PROCEEDINGS of 8th Inter. Conf. on Amorphous and Liquid Semiconductors, (Cambridge, Mass.) Published as J. Non. Cryst. Solids, 35/36, 1980.
- PROCEEDINGS of 9th Inter. Conf. on Amorphous and Liquid Semiconductors, (Grenoble, France) Published as J. De Physique, 42, (C4), 1981.
- PROCEEDINGS of 10th Inter. Conf. on Amorphous and Liquid Semiconductors, (Tokyo, Japan) Published as J. Non. Cryst. Solids, 59/60, 1983.
- RAY, S., CHAUBHURI, P., BATABYAL, A. K. and BARUA, A. K. Jap. J. Appl. Phys. 22, 23-28, 1983.
- REHM, W., FISCHER, R., STUKE, J. and WAGNER, H. Phys. Stat. Sol. (b) 94, 539, 1979.
- ROCK, F. C. and SMITH, C. W. J. Vac. Sci. Technol. 12, 943-945, 1975.
- ROSS, R. C. and MESSIER, R. J. Appl. Phys. 52, 5329-5339, 1981.
- SCOFIELD, J. H. J. Electron Spectroscopy, 8, 129, 1976.
- SEAH, M. P. in 'Practical Surface Analysis by Auger and X-ray Photoelectron Spectroscopy'. Eds. Briggs, D. and Sheah, M. P. John-Wiley & Sons, pp 181, 1983.

- SEAH, M. P. Vacuum, 34, 463-478, 1984.
- SHIMIZU, T., KUMEDA, M., WATANABE, I. and KAMONO, K. Jap. J. Appl. Phys. 18, 1923-1929, 1979.
- SHINDO, M., SATO, S., MYOKAN, I., MANO, S. and SHIBATA, T. J. Non. Cryst. Solids, 59/60, 747-750, 1983.
- SHIRLEY, D. A. Phys. Rev. B. 5, 4709-4714, 1972.
- SIGMUND, P. Phys. Rev. 184, 383-416, 1969.
- SOLOMON, I. in 'Fundamental Physics of Amorphous Semiconductors' Ed. Yonezawa, F., pp 33-39, 1981.
- SOLOMON, I., DIETT, T. and KAPLAN, D. J. De Physique 39, 1241-1246, 1978.
- SPEAR, W. E. and LECOMBER, P. G. J. Non. Cryst. Solids. 8-14, 727-738, 1972.
- SPEAR, W. E. Proc. 5th Inter. Conf. Amorphous and Liquid Semiconductors, Eds. Stuke, I. and Brening, W., Garmish, pp 1, 1974.
- SPEAR, W. E., LOVELAND, R. J. and AL-SHARBATY, A. J. Non. Cryst. Solids, 15, 410-422, 1974.
- SPEAR, W. E. and LECOMBER, P. G. Solid State Commun. 17, 1193-1195, 1975.
- SPEAR, W. E. and LECOMBER, P. G. Phil. Mag. 33, 935-949, 1976.
- SPEAR, W. E. and LECOMBER, P. G. in 'Photoconductivity and related phenomenon.' Eds. Mort, J. and Pai, D. M., Elsevier, N. Y., pp 213, 1976.
- SPEAR, W. E. and LECOMBER, P. G. Proc. 7th Inter. Conf. Amorphous and Liquid Semiconductors, Ed. Spear, W. E., Edinburgh 1977.
- SPEAR, W. E., ALLAN, D., LECOMBER, P. G. and GHAITH, A. J. Non-Cryst. Solids, 35/36, 357-362, 1980.
- STAEBLER, D. L. and WRONSKI, C. R. Appl. Phys. Lett. 31, 292-294, 1977.
- STAEBLER, D. L. and WRONSKI, C. R. J. Appl. Phys. 51, 3262-3268, 1980.
- STARK, F. Z. Electrochem., 15, 509, 1909.
- STERLING, H. F. and SWAN, R. C. G. Solid State Electron. 8, 653-654, 1965.
- SUZUKI, M., MAEKAWA, T., KUMEDA, M. and SHIMIZU, T. Jap. J. Appl. Phys. 19, (Supplement 19-2), 85-89, 1980.
- SUZUKI, M., MAEKAWA, T., OKANDO, S. and BANDON, T. Jap. J. Appl. Phys. 20, L485-L487, 1981.

- TANAKA, K., YAMASAKI, S., NAKAGAWA, K., MATSUDA, A., OKUSHI, H., MATSUMURA, M. and IIZIMA, S. *J. Non-Cryst. Solids*, 35/36, 475-480, 1980.
- TANIELIAN, M., CHATANI, M., FRITZCHE, H., SMID, V. and PERSANTS, P. D. *J. Non. Cryst. Solids* 35/36, 575-580, 1980.
- TAUC, J. in 'Amorphous and Liquid Semiconductors' Plenum Press, N. Y. 1974.
- TAUC, J. in 'The optical properties of solids', ed. Abeles, F. pp 277, North Holland, Amsterdam, 1970.
- TAUC, J. and MENTH, A. J. *Non-Cryst. Solids*, 8-10, 569, 1972.
- THOMPSON, M. J., ALLISON, J. and AIKAISI, M. M. *Solid state and Electronic devices*, 2, 511-514, 1978.
- THOMPSON, M. G. and REINHARD, D. K. *J. Non-Cryst. Solids*, 37, 325-333, 1980.
- TOLANSKY, S. 'Surface Microtopography', Interscience Publishers, London, 1960.
- TSAI, C. C., FRITZCHE, H., TANIELIAN, M. H., GACZI, P. J., PERSANS, P. D. and VESAGHI, K. A. *Proc. 7th Inter. Conf. Amorphous and Liquid Semiconductors*. Ed. Spear, W. E., Edinburgh, pp 339, 1977.
- TSAI, C. C., KNIGHTS, J. C., LUJAN, R. A., WACKER, B., STAFFORD, B. L. and THOMPSON, M. J. *J. Non-Cryst. Solids*, 59/60, 731-734, 1983.
- USAMI, K., KATAYAMA, Y. and SHIMADA, T. *Jap. J. Appl. Phys.* 19, 2065-2068, 1980.
- VAN DONG, N. and HAI, T. Q. *Phys. Stat. Solids (b)* 88, 555, 1978.
- VAN DONG, N. and HAI, T. Q. *J. Non-Cryst. Solids*, 35/36, 351-356, 1980.
- VANDON, N., FOURNIER, Y. and LENY, J. Y. *J. De Physique*, 42, 647-650, 1982.
- WEHNER, G. K. *Electronics and Electron Physics VII*, 239-298, 1955.
- WERNER, H. W. and GARTEN, R. P. H. *Rep. Prog. Phys.* 47, 221-344, 1984.
- WESTWOOD, W. D. *J. Vac. Sci. Technol.* 15, 1-9, 1978.
- YONEZAWA, F. Ed. 'Fundamental Physics of Amorphous Semiconductors'. Kyoto University, Japan, 1981.

ZAKA, Y., ABO-NAMOUS, S. A., CRUMPTON, D. and FANE, R. W. Vacuum
34, 975, 1984 (a).

ZAKA, Y., ABO-NAMOUS, S. A. and FANE, R. W. Presented at Sixth
Inter. Conf. on Thin Films, Stockholm, Sweden, 1984 (b).

ZAKA, Y. and FANE, R. W. Data Review, EMIS (INSPEC), RN = 11416,
Publ. Date: 21 March, 1984.

PUBLICATIONS

1. R W FANE and Y ZAKA
"Highly doped sputtered amorphous silicon without hydrogen."
J. Non-Cryst. Solids 57, 1, 1983.
2. R W FANE and Y ZAKA
"Highly doped amorphous silicon withough hydrogen."
J. Phys. D: Appl. Phys 16, 1993, 1983.
3. S A ABO-NAMOUS, Y ZAKA and R W FANE
"Dependence of the Electronic and Optical properties of
Unhydrogenated a-Si on preparation conditions."
Phys. Stat. Sol. (a). 79, 477, 1983.
4. S A ABO-NAMOUS, Y ZAKA and R W FANE
"Dependence of photoconductive properties of unhydrogenated
Ne-sputtered a-Si on preparation conditions."
Presented at "Vacuum '84", York University, 1984
Published in Vacuum, 34, 975, 1984.
5. Y ZAKA, S A ABO-NAMOUS, D CRUMPTON and R W FANE
"Composition and properties of unhydrogenated amorphous
silicon produced by sputtering in argon or neon gas."
Presented at "Vacuum '84", York University, 1984
Published in Vacuum, 34, 975, 1984.
6. S A ABO-NAMOUS, Y ZAKA and R W FANE
"Doping effects of groups III and elements in unhydrogenated
Ne-sputtered a-Si."
Presented at the 'Sixth Inter. Conf. on Thin Films', Stockholm,
Sweden, 1984.
7. Y ZAKA, S A ABO-NAMOUS and R W FANE
"Control of electrical and optical properties of unhydrogenated
Ne-sputtered a-Si by preparation conditions."
8. Y ZAKA and R W FANE
"Silicon, R.F. sputtered amorphous, unhydrogenated (1)
conductivity."
DATA REVIEW, EMIS (INSPEC), RN = 11416,
Publ. Date: 21 March 1984.

HIGHLY DOPED SPUTTERED AMORPHOUS SILICON WITHOUT HYDROGEN

R.W. FANE and Y. ZAKA

Physics Department, University of Aston in Birmingham, UK

Received 21 September 1982

Revised manuscript received 28 January 1983

A method of producing high resistivity amorphous silicon ($\sim 10^8 \Omega \text{ cm}$) by sputtering without any addition of hydrogen or halogen is described. Such material has been doped n-type using tantalum, to give conductivity values in excess of $1 (\Omega \text{ cm})^{-1}$.

1. Introduction

In a previous communication the production of amorphous silicon without the addition of hydrogen was described [1] using a diode sputtering system employing neon in place of the more usual argon as sputtering gas. The effect of the addition of aluminium was also considered. Recently some other attempts to produce α -Si without hydrogen or a halogen have been reported notably by Vandong et al. [2]. A special dc sputtering technique was used and results showed that high resistivity intrinsic material could be produced and conductivities up to about $5 \times 10^{-4} (\Omega \text{ cm})^{-1}$ were obtained by suitable doping. High pressure argon sputtering has also been reported [3,4]. Although high intrinsic resistivity was obtained in these films there was some evidence of porosity. The incorporation of aluminium changed the conductivity but the activation energy was always $> 0.5\text{eV}$ and was accompanied by a change in the optical gap. This change in band gap was thought to be mainly responsible for the conductivity changes observed.

Theoretically a material with a low density of gap states should be possible. Polk [6] suggested a random network with all bonds satisfied provided small deviations in bond length and angle are allowed. Our early trials coupled with esr measurements indicated that better films could be produced by a method similar to that described here when compared with argon sputtering. Gas content of the film is difficult to determine but preliminary electron-probe results indicate much less neon inclusion in neon sputtered films than argon in the case of argon sputtering. We have no evidence so far that films prepared as described below satisfy such models as that proposed but they have interesting properties, namely a high intrinsic resistivity ($\sim 10^8 \Omega \text{ cm}$), a thermal

activation energy of about 0.7 eV and can be made n or p-type. Previously [1] results of the inclusion of aluminium were given and the work has now been extended using tantalum doping to give films with n-type characteristics, some of which have very high conductivity.

2. Experimental details

The apparatus consists of a diffusion pumped rf diode sputtering arrangement with a liquid nitrogen trap. A Helmholtz pair of coils gave a field of about 0.01 T at the centre of the discharge. The target potential is usually measured using a circuit similar to that described by Rock and Smith [6] and Lamont and Turner [7]. The silicon target has a diameter of 7.5 cm and is water cooled. In all cases prior to operation the system was baked and the substrate thoroughly outgassed so that the base pressure was about 5×10^{-7} Torr. The pumping speed is reduced by means of a baffle valve. Neon gas (99.999%) is admitted by a needle valve, the flow rate can thus be adjusted to give the required pressure, generally 200 mTorr. The clean Corning 7059 substrates were protected by a shutter so that clean and stable sputtering conditions could be established before film deposition commenced.

For doping experiments composite targets were used, a piece of tantalum, 0.03–1.80% of the total area being placed on the silicon. So far analysis of the impurity content of the films has not been completed and the figures quoted are for the expected percentage of doping species in the plasma relative to silicon allowing for the sputtering rate [8]. Tantalum was chosen for n-type doping as it is readily available with the required purity and in a form suitable for incorporation into a sputtering target. The temperature of the substrate holder is monitored by a thermocouple during the deposition, and can be maintained at the required temperature by reducing the current to the substrate heater during deposition to offset the heat generated by the plasma. This technique allows the temperature to be varied between 150–400°C. Most of the films were deposited at 300°C. Film thickness, generally 0.5 to 1 μm , was determined by multiple beam interferometry on an edge produced by masking and overlaid with aluminium.

3. Experimental results

3.1. Electrical characteristics

Electrical conductivity measurements were made in vacuum using the gap-cell configuration with nichrome or aluminium deposited immediately after preparation of the film. These contacts were ohmic for the electric field used, generally 10^2 V cm^{-1} . Fig. 1 shows plots of $\log \sigma$ against T^{-1} for a

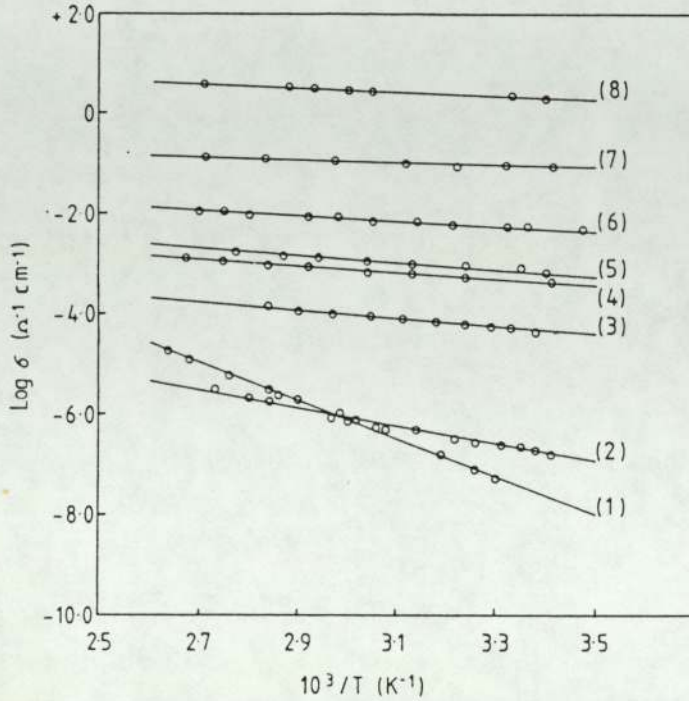


Fig. 1. Log σ against $1/T$ for varying percentages of tantalum in the composite target.

number of intrinsic and n-type films. Table 1 summarises the results including room temperature conductivities (σ_{RT}) and activation energies (ΔE), satisfying the equation

$$\sigma = \sigma_0 \exp(-\Delta E/kT). \quad (1)$$

Films 7 and 8 should be particularly noted as having very high room temperature conductivities and low thermal activation energies.

Table 1

The variation of electrical conductivity at room temperature σ_{RT} , activation energy ΔE and the optical gap E_0 with tantalum concentration

Sample	Impurity conc. Ta (at. %)	Room temperature conductivity ($\Omega^{-1} \text{cm}^{-1}$)	ΔE (eV)	Optical gap (eV)
(1)	intrinsic	2.5×10^{-8}	0.73	1.64
(2)	0.015	8.0×10^{-8}	0.48	1.64
(3)	0.04	4.5×10^{-5}	0.17	1.52
(4)	0.05	4.3×10^{-4}	0.13	1.52
(5)	0.1	6.6×10^{-4}	0.13	1.52
(6)	0.25	5.0×10^{-3}	0.09	1.41
(7)	0.50	8.0×10^{-2}	0.07	1.41
(8)	0.90	2.0	0.08	1.33

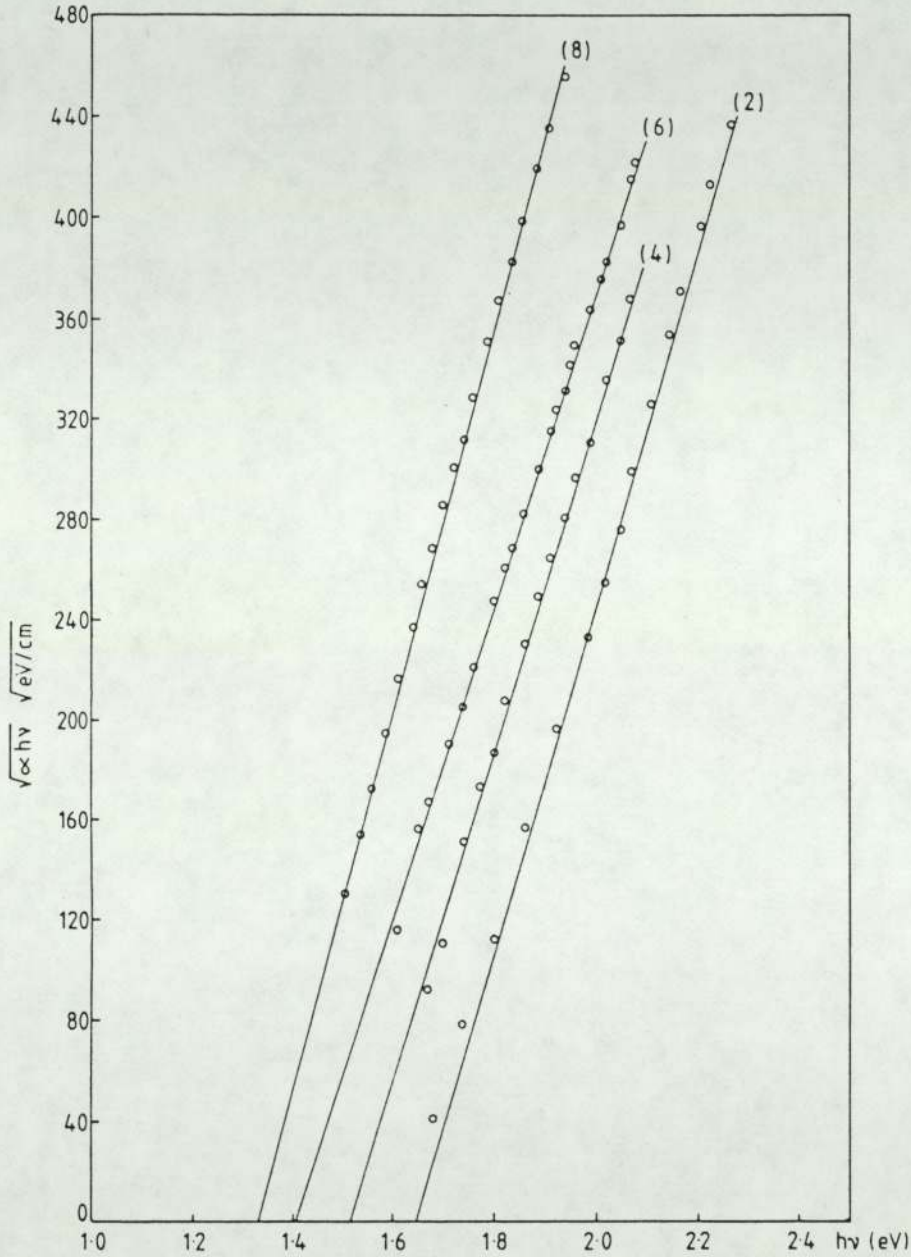


Fig. 2. $(\alpha h\nu)^{1/2}$ versus $h\nu$ for samples deposited from composite targets with 0.015–0.90 at % tantalum. For clarity only samples 2(0.015 at. % Ta), 4(0.05 at. % Ta), 6(0.25 at. % Ta) and 8(0.90 at. % Ta) are included.

3.2. Optical gap measurements

Fig. 2 shows the absorption data for some of the samples determined by means of an optical spectrophotometer. The data has been plotted in the usual way as $(\alpha h\nu)^{1/2}$ against photon energy, $h\nu$, where α is the absorption coefficient, on the assumption of constant matrix elements for electron transitions and a parabolic density of states. Good straight lines were obtained resulting in the optical gaps as summarised in table 1.

4. Discussion

It has been demonstrated that the material, produced as described above, can be doped n or p-type [1]. Confirmation of the type of doping has been by thermoelectric measurements. In addition heterojunctions have been made from the deposition of tantalum-doped α -Si on to crystalline p-type silicon. Satisfactory rectification was observed (fig. 3). The results are comparable with those of Thompson et al. [9]. The same construction but based on n-type crystalline silicon showed no rectifying characteristic.

It will be seen that while the conductivity can be changed over many orders of magnitude and the Fermi level moved by more than 0.6 eV the optical gap only changes from 1.66 eV to 1.33 eV in the extreme cases. Consequently we believe the material has been doped in the accepted manner rather than being modified to a different material as has been suggested for some α -Si containing high density of impurities [10,11].

The highly doped specimens numbered 7 and 8 are of particular interest. We are not aware of any other cases where the conductivity of α -Si has been increased to such high values except for flourinated α -Si [12] and some cases where the film was thought to have changed to a microcrystalline structure [13,14]. Electron and X-ray diffraction studies of intrinsic and doped samples have failed to show any crystallinity in our material.

In the intrinsic case conduction is in the extended states characterised by a unique activation energy while some form of hopping in the delocalised states takes place in heavily doped specimens as is observed generally [15-17].

The films are stable and do not show porosity effects as observed in high pressure argon sputtered films [3,4]. No Si-O bonds have been detected by infra-red absorption or ESCA. Neon, having a smaller atomic weight than argon, and in a relatively high pressure plasma, will result in less kinetic energy of the various species bombarding the film during formation and results in a film having a lower concentration of defects. Sputtering gas is continually trapped and expelled from the silicon film during formation. The small atomic size of the neon is most likely an additional aid to the growth of films with less microvoids and included gas than is the case for argon sputtered films.

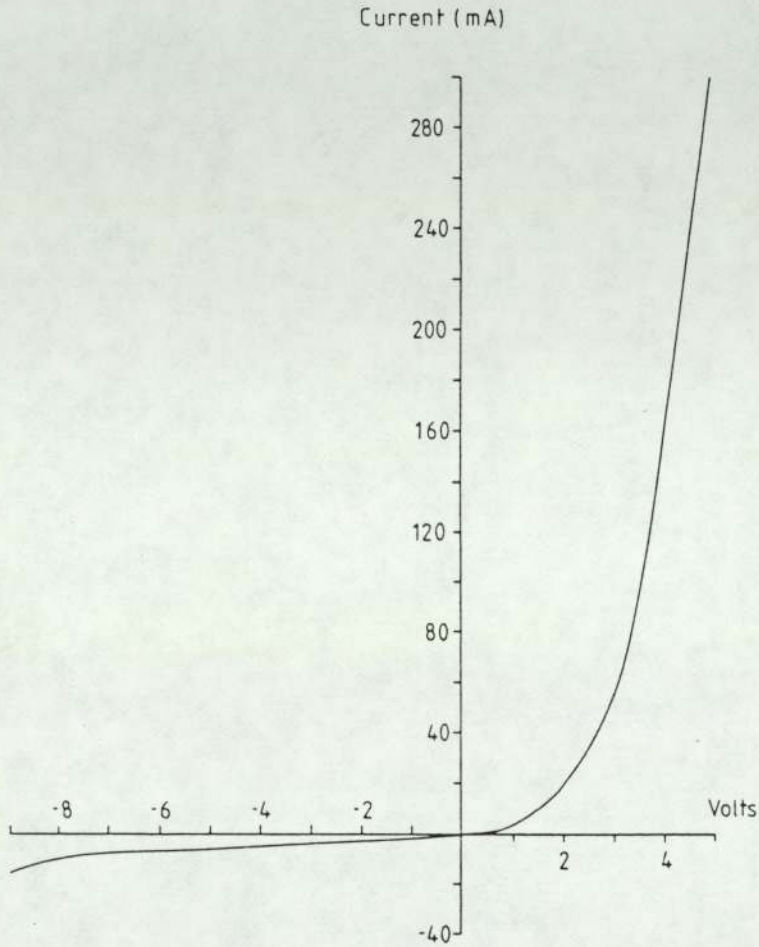


Fig. 3. Characteristic for n-type α -Si/p-type crystalline junction.

References

- [1] R.W. Fane, *J. Phys. D.: Appl. Phys.* 14 (1981) L113.
- [2] N. Vandong, *J. de Phys.* 42 (C4) (1981) 647.
- [3] T. Shimizu, M. Kumeda, I. Watanabe and Y. Kiriya, *Jap. J. Appl. Phys.* 19 (1980) L235.
- [4] M. Suzuki, A. Nakao, T. Mackawa, M. Kumeda and T. Shimizu, *Jap. J. Appl. Phys.* (1980) Suppl. 19.2, p. 85.
- [5] D.E. Polk, *J. Non-Crystalline Solids* 5 (1971) 365
- [6] F.C. Rock and C.W. Smith, *J. Vac. Sci. Technol.* 12 (1975) 943.
- [7] L.T. Lamont and F.T. Turner, *J. Vac. Sci. Technol.* 11 (1974) 47.
- [8] G. Carter and J.S. Colligon, *Ion Bombardment of Solids* (Heinemann Educational, London) p. 323.

- [9] M.J. Thompson, J. Allison and M.M. Alkaisy, *Solid State and Electron Devices* 2 (1978) S11.
- [10] M.G. Thompson and D.K. Reinhard, *J. Non-Crystalline Solids* 37 (1980) 325.
- [11] S.R. Ovshinsky, *Amorphous and Liquid Semiconductors*, ed. W.E. Spear (Dundee, 1977) p. 519.
- [12] A. Madan, S.R. Ovshinsky and E. Benn, *Phil. Mag.* 40 (1979) 259.
- [13] W.E. Spear, G. Willeke, P.G. LeComber and A.G. Fitzgerald, *J. de Phys.* 42 (C4) (1981) 257.
- [14] S. Veprek, Z. Iqbal, H.R. Oswald and A.P. Webb, *J. Phys. C: Solid State Phys.* 14 (1981) 295.
- [15] D.A. Anderson and W. Paul, *Phil. Mag.* 44 (1981) 187; *Phil. Mag. B* 46 (1982) 177.
- [16] H. Fritzsche, *Solar Energy Materials* 3 (1980) 447.
- [17] G.M. Döhler, *Phys. Rev. B* 19 (1979) 2083.

Highly doped amorphous silicon without hydrogen

R W Fane and Y Zaka

Department of Physics, The University of Aston in Birmingham, Birmingham, B4 7ET, UK

Received 11 February 1983

Abstract. Amorphous silicon films with high intrinsic resistivity have been produced by RF sputtering without the addition of hydrogen or halogen. Co-sputtering with tantalum resulted in n-type material with resistivity $<1 \Omega \text{ cm}$ and a shift in the Fermi level of 0.6 eV.

1. Introduction

Amorphous silicon (a-Si) is commonly produced by the breakdown of silane gas in a glow discharge or by RF sputtering in a plasma of argon and hydrogen (Spear and LeComber 1975, Paul *et al* 1976). The material produced in this way contains a low density of states (Madan *et al* 1976) and can be doped n- or p-type (Spear and LeComber 1976, Müller *et al* 1977).

The detail of the function of hydrogen is, however, not yet clear. In some respects the inclusion of hydrogen is thought to have disadvantages, for example, the anti-bonding states are located near the conduction band and modify the transport properties in the way discussed by Moustakas *et al* (1977). The production of a-Si without hydrogen or halogen is consequently of interest. In a previous communication (Fane 1981) a method of preparing high resistivity a-Si was described and some results on doping with aluminium given. We have extended this work to investigate conductivity mechanisms over a wide range of temperatures and the doping effect of the aluminium for various preparation conditions. The photoelectric and optical properties are being studied and a full report of this work will be given later.

In this communication we are reporting results of n-type doping by the incorporation of tantalum. High conductivities ($\sim 2 \Omega^{-1} \text{ cm}^{-1}$) and low activation energies ($<0.1 \text{ eV}$) with reasonable doping efficiency have been obtained. The composition of the films has been analysed by x-ray photoemission spectroscopy (XPS) and Rutherford back-scattering of α particles (RBS).

2. Experimental details and results

The apparatus consisted of a diffusion pumped RF diode sputtering arrangement with a liquid nitrogen trap. A Helmholtz pair of coils gave a field of about 0.01 T at the centre of the discharge. The power input to the target was varied to give a DC bias potential on the target of about 1.1 kV. The target potential was usually measured using a circuit

similar to that described by Rock and Smith (1975) and Lamont and Turner (1974). The silicon target had a diameter of 7.5 cm and was water cooled. In all cases prior to operation the system was baked and the substrate thoroughly outgassed so that the base pressure was about 5×10^{-7} Torr. The pumping speed was reduced by means of a baffle valve. Neon gas (99.999%) was admitted by a needle valve; the flow rate could thus be adjusted to give the required pressure, generally 200 mTorr. The clean Corning 7059 substrates were protected by a shutter so that clean and stable sputtering conditions could be established before film deposition commenced. All the films reported here were produced at a target-substrate spacing of 3.5 cm, giving deposition rates of about 2 \AA s^{-1} .

For doping experiments composite targets were used, a piece of tantalum 0.03–1.80% of the total area being placed on the silicon. The composition of the films was analysed by x-ray photoemission spectroscopy (XPS) and Rutherford back-scattering experiments. X-ray photoemission studies were carried out using a Kratos XSAM 800 XPS-Auger spectrometer. Magnesium $K\alpha$ x-rays were used as the incident radiation. Composition was estimated from relative peak areas and cross-sections (Scofield 1976). Rutherford back-scattering experiments were performed using 2 MeV α particles; the energy of the back-scattered particles was measured using a silicon surface barrier detector. By analysing the silicon and tantalum peaks the thickness of the specimen as well as the composition was determined (Ziegler 1975). Tantalum was chosen for n-type doping as it is readily available with the required purity and in a form suitable for incorporation into a sputtering target. The temperature of the substrate holder is monitored by a thermocouple during the deposition, and can be maintained at the required temperature by reducing the current to the substrate heater during deposition to offset the heat generated by the plasma. The technique allows the temperature to be varied between 150 and 400 °C. Most of the films were deposited at 300 °C. Film thickness, generally 0.5 to 1 μm , was determined by multiple beam interferometry on an edge produced by masking and overlaid with aluminium.

Electrical conductivity measurements were made in vacuum using the gap-cell configuration with nichrome or aluminium deposited immediately after preparation of the film. These contacts were ohmic for the electric field used, generally 10^2 V cm^{-1} . Figure 1 shows plots of $\lg \sigma$ against T^{-1} for a number of intrinsic and n-type films. Films 7 and

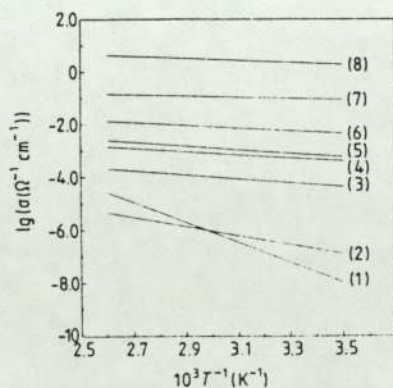


Figure 1. Logarithm of conductivity against T^{-1} for films containing various amounts of tantalum. (1) Intrinsic; (2) 0.05%; (3) 0.14%; (4) 0.17%; (5) 0.34%; (6) 0.85%; (7) 1.7%; (8) 3.1%.

8 should be particularly noted as having very high room temperature conductivity and low thermal activation energy.

Figure 2 shows the absorption data for some of the samples determined by means of an optical spectrophotometer. The data have been plotted in the usual way as $(\alpha h\nu)^{1/2}$

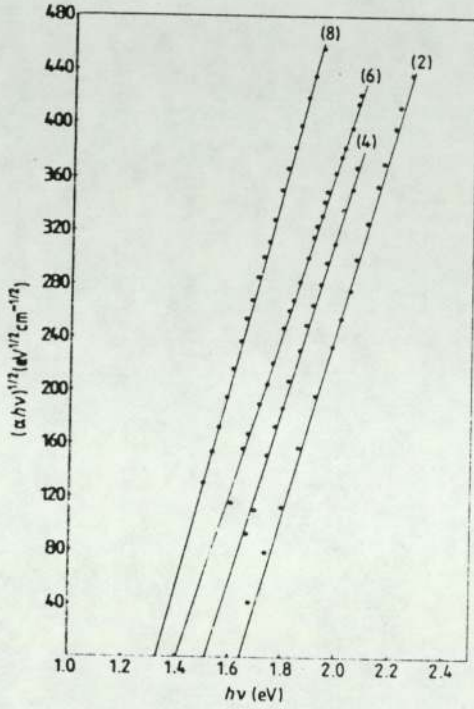


Figure 2. $(\alpha h\nu)^{1/2}$ versus $h\nu$ for some of the films shown in figure 1.

against photon energy, $h\nu$, where α is the absorption coefficient, on the assumption of constant matrix elements for electron transitions and a parabolic density of states.

The variation in room temperature conductivity, the optical gap and the thermal activation energy with tantalum content are shown in figure 3.

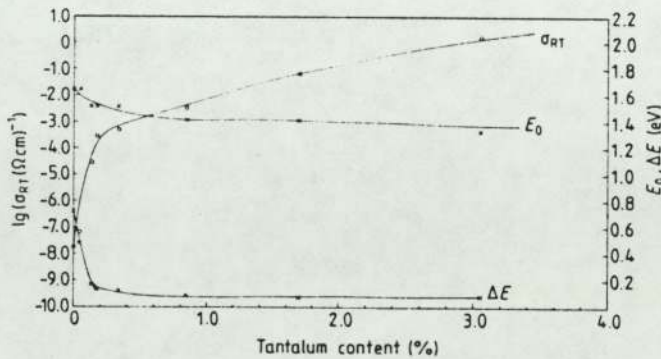


Figure 3. Room temperature conductivity, optical gap and thermal activation energy as a function of tantalum content.

3. Discussion

It has been adequately demonstrated that the material, produced as described above, can be doped satisfactorily n- or p-type (Fane 1981). Thermoelectric measurements have confirmed the type of conductivity. It will be seen that while the conductivity can be changed over many orders of magnitude the optical gap only changes from 1.64 to 1.33 eV in the extreme cases. It would appear, therefore, that doping has taken place in the accepted manner rather than a change to a very different form of material, as has been suggested for some a-Si containing a high density of impurity (Thompson and Reinhard 1980). The highly doped specimens numbered 7 and 8 are of particular interest. We are not aware of any other cases where the conductivity of a-Si, with or without hydrogen, has been increased to such a high value. High conductivity n-type materials have, however, been produced in microcrystalline form (Spear *et al* 1981, Veprek *et al* 1981). Electron and x-ray diffraction studies of intrinsic and doped materials have failed to show crystallinity in the present material.

Compositional analysis of the films has revealed that the amount of tantalum incorporated into the film is higher than that estimated earlier from relative areas and deposition rates of silicon and tantalum (Fane and Zaka 1983). This discrepancy is probably due to the back-scattering of silicon in the plasma. However, the efficiency of doping is still comparable with other techniques. Figures 4 and 5 compare the variation

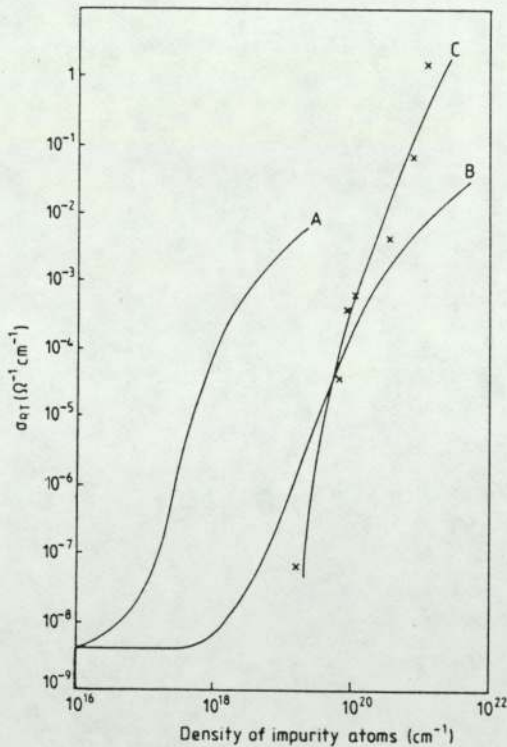


Figure 4. Room temperature conductivity as a function of the density of impurity atoms. Curve A, gas phase doping by phosphorus; curve B, ion implantation of phosphorus; curve C, tantalum doping by neon sputtering. A and B after Müller *et al* (1977).

of room temperature, electrical conductivity and thermal activation energy as a function of the density of impurity atoms, incorporated into silicon by (curve A) gas phase doping using phosphorus, (curve B) ion implantation and (curve C) neon sputtering. It should be noted that the efficiency for n-type doping by neon sputtering could be improved if dopants with atomic mass comparable with that of silicon were used, e.g. phosphorus or arsenic. Tantalum was chosen for the reasons given above.

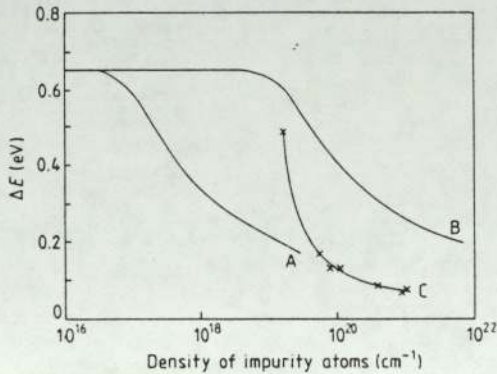


Figure 5. Conductivity activation energy as a function of the density of impurity atoms. Curve A, gas phase doping by phosphorus; curve B, ion implantation of phosphorus; curve C, tantalum doping by neon sputtering. A and B after Müller *et al* (1977).

It is highly likely that some form of hopping conduction takes place in such heavily doped material and further experiments are being carried out to clarify the conduction mechanism.

Theoretically a material with a low density of gap states should be possible. Polk (1971) suggested a random network with all bonds satisfied provided small deviations in bond length and angle are allowed. The present material may have a structure which approaches this and, although not perfect, has a sufficiently low density of defect states, as evidenced by high resistivity ($\sim 10^8 \Omega \text{ cm}$) and high activation energy ($>0.7 \text{ eV}$) in the intrinsic case, to enable the Fermi level to be moved by the addition of impurities.

The films are stable and do not show apparent porosity effects. No Si-O bands have been observed in infrared absorption measurements. Neon, having a smaller atomic weight than argon, and in a relatively high pressure plasma, would result in less kinetic energy of the various species bombarding the film during formation. Sputtering gas is continually trapped and expelled from the silicon film during formation. The small atomic size of the neon is most likely an additional aid to the formation of films with fewer microvoids and included gas.

Acknowledgments

The authors are grateful to Dr D Crumpton for assistance with RBS analysis and Mr A Abbott and Mr A E Marriott-Reynolds for technical assistance with XPS experiments and preparation of the paper respectively. One author (YZ) wishes to acknowledge support by SERC.

References

- Fane R W 1981 *J. Phys. D: Appl. Phys.* **14** L113-16
Fane R W and Zaka Y 1983 *J. Non-Cryst. Solids* at press
Lamont L T and Turner F T 1974 *J. Vac. Sci. Tech.* **11** 47-51
Madan A, LeComber P G and Spear W E 1976 *J. Non-Cryst. Solids* **20** 239-57
Moustakas T D, Anderson D A and Paul W 1977 *Solid State Commun.* **23** 155-8
Müller G, Kalbitzer S, Spear W E and LeComber P G 1977 *7th Int. Conf. on Amorphous and Liquid Semiconductors, Edinburgh* (Edinburgh: University of Edinburgh CIGL) pp 442-6
Paul W, Lewis A J, Connell G A N and Moustakas T D 1976 *Solid State Commun.* **20** 969
Polk D E 1971 *J. Non-Cryst. Solids* **5** 365-76
Rock F C and Smith C W 1975 *J. Vac. Sci. Tech.* **12** 943-5
Schofield J H 1976 *J. Electron Spectrosc. Relat. Phenom.* **8** 129-32
Spear W E and LeComber P G 1975 *Solid State Commun.* **17** 1193
— 1976 *Phil. Mag.* **33** 935-49
Spear W E, Willeke G, LeComber P G and Fitzgerald A G 1981 *J. de Physique* **42** 257-60
Thompson M G and Reinhard D K 1980 *J. Non-Cryst. Solids* **37** 325-33
Veprek S, Igbal Z, Oswald H R and Webb A P 1981 *J. Phys. C: Solid State Phys.* **14** 295-307
Ziegler J F 1975 *New Uses of Ion Accelerators* (New York: Plenum Press)

phys. stat. sol. (a) 79, 477 (1983)

Subject classification: 14.3 and 20.1; 16; 22.1.2

Physics Department, University of Aston, Birmingham¹⁾

Dependence of the Electronic and Optical Properties of Unhydrogenated a-Si on Preparation Conditions

By

S. A. ABO-NAMOUS²⁾, Y. ZAKA, and R. W. FANE

The optical and electronic properties of undoped a-Si are studied over a wide range of preparation conditions. The results indicate that the conductivity, photoconductivity, optical gap, and the position of the Fermi level in the gap can be controlled by varying the product (Pd/U_{sb}); P , d , and V_{sb} are the gas pressure, the target-substrate distance, and the self-bias voltage on the target, respectively. This is attributed to controlling the density-of-states distribution in the gap.

Die optischen und elektronischen Eigenschaften von undotiertem a-Si werden für einen großen Bereich der Präparationsbedingungen untersucht. Die Ergebnisse zeigen, daß die Leitfähigkeit, Photoleitfähigkeit, optische Bandlücke und die Lage des Fermi-niveaus in der Bandlücke durch Variation des Produkts (Pd/V_{sb}) gesteuert werden können; P , d und V_{sb} bedeuten dabei den Gasdruck, den Abstand Target-Substrat bzw. die Eigenvorspannung des Targets. Das wird der Steuerung der Zustandsdichteverteilung im Gap zugeordnet.

1. Introduction

Over the last decade the techniques for producing hydrogenated amorphous silicon (a-Si:H) have become well established [1, 2]. Although a-Si:H has some useful and interesting properties, there seems to be uncertainty about its thermal stability [3] and the role of hydrogen [4]. In recent years attempts have been made to produce a-Si, without hydrogen, which has properties comparable with those of a-Si:H. The resistivity of a-Si produced by rf sputtering in pure argon has been increased from 10^3 to 10^8 Ωcm by increasing the argon gas pressure or the target-substrate distance [5], but the films were found to be porous and susceptible to oxygen contamination. Attempts to change the electrical properties by substitutional doping were only moderately successful. Amorphous silicon produced by magnetron sputtering in argon has also shown promising results.

In this laboratory we have produced a-Si with room temperature resistivity of the order of 10^8 Ωcm by rf sputtering in high pressure neon [6], and recently n- and p-type doping by co-sputtering from composite targets [7, 8] has shown doping efficiencies comparable with other techniques.

In an attempt to understand how the preparation conditions affect the quality of the films produced, we have studied the optical and electronic properties of a-Si films over a wide range of preparation conditions. In this communication we report the effect of varying the neon gas pressure between 40 and 220 mTorr, the substrate-target distance between 2 and 5.3 cm, and the rf self-bias on the target from 650 to 1000 V.

¹⁾ Gosta Green, Birmingham B4 7ET, Great Britain.

²⁾ Permanent address: Material Science Department, Kuwait Institute for Scientific Research, Kuwait.

2. Sample Preparation

The amorphous silicon was deposited in a radio-frequency diode sputtering system, with a water cooled target holder and substrate holder in a plane-parallel arrangement with a rotatable shutter between them. The target was a single crystal wafer of electronic grade silicon. The substrate can be electrically heated up to 500 °C, but for the present experiments all the films were deposited at around 300 °C. A Helmholtz pair of coils gives a field of about 0.01 T at the centre of the discharge. The base pressure in the sputtering chamber was of the order of 10^{-7} Torr achieved by an oil diffusion pump with a baffle and a liquid nitrogen cooled trap. Corning 7059 glass substrates were ultrasonically cleaned in a detergent, rinsed in distilled water, and then boiled in isopropyl alcohol before placing in the chamber.

Neon gas (99.999%) was admitted into the chamber via a needle valve, thus by controlling the flow rate the desired pressure can be attained. The target-substrate separation was varied from 2 to 5.3 cm.

The composition of the films was analysed by X-ray photoemission. The neon incorporated into the film was below the detection limit of this technique. Also the presence of surface plasmons and the absence of chemical shifts in the photoemission spectra are indicative of oxide free films.

3. Measurements and Results

The film thickness was measured using a multiple-beam interferometer with an estimated uncertainty of $\pm 10\%$. The film thickness ranged from 0.3 to 1.5 μm . The deposition rate D_R of the films was measured as a function of the ratio (Pd/U_{sb}) of the sputtering gas pressure (P), the target-substrate separation (d), and the rf self-bias voltage (U_{sb}). This is shown in Fig. 1. It can be seen from this figure that D_R varies exponentially from about 4 $\text{\AA}/\text{s}$ for low Pd/U_{sb} to ≈ 1 $\text{\AA}/\text{s}$ for high Pd/U_{sb} . This type of variation seems to be consistent with the fact that the number of silicon atoms which reach the substrate without suffering collisions would be expected to be proportional to the exponent of $-Pd$. The very slow variation in D_R at higher Pd/U_{sb} products would also logically follow from this.

The dc dark conductivity was measured using gap-cell configurations with Al electrodes separated by 1 mm. A Keithley 610C electrometer was used for the measurements with an applied field of about 10^2 Vcm^{-1} . Al electrodes proved to make good ohmic contacts with a-Si within the range of applied field used. The room temperature conductivity, σ_{RT} , can be varied systematically over more than four orders of magnitude from $\approx 10^{-5}$ to less than 10^{-9} $\Omega^{-1}\text{cm}^{-1}$ by varying the product Pd/U_{sb} (Fig. 2).

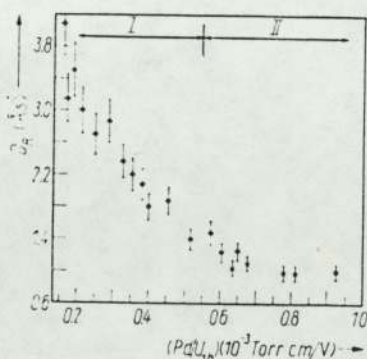


Fig. 1. The deposition rate D_R as a function of Pd/U_{sb} . P , d , and U_{sb} are gas pressure, target-substrate separation, and self-bias voltage, respectively

Although this effect has been observed in Ar sputtering [9] the final conductivity attained by Ne sputtering is two to three orders of magnitude lower than that produced by Ar sputtering.

The dark conductivity of the films was measured as a function of temperature, and the thermal activation energy ΔE_a was deduced from the $\lg \sigma$ versus $1/T$ plots. Fig. 2 also shows the change in ΔE_a with Pd/U_{sb} ; which is seen to change in a manner consistent with the variation in σ_{RT} , and approaches a steady value of nearly 0.85 eV. This value is comparable with those values using glow-discharge and Ar/H₂ sputtering techniques.

The conduction type of these intrinsic films was readily determined from the polarity of the room temperature thermopower sign observed by the hot-probe technique. All the amorphous samples reported here were n-type.

The optical gap E_0 was determined from the plots of $(ah\omega)^{1/2}$ versus $h\omega$ according to the relation [10, 11]

$$(\alpha h\omega)^{1/2} = B(h\omega - E_0) \tag{1}$$

B is a constant, $h\omega$ the photon energy, and α the absorption coefficient calculated from the transmission data, assuming a reflection coefficient independent of wavelength at long wavelengths. The dependence of E_0 on Pd/U_{sb} is shown in Fig. 2. The optical gap increases from about 1.4 eV at low values of Pd/U_{sb} to about 1.85 eV at higher Pd/U_{sb} .

The absorption coefficient α is plotted against $h\omega$ for a few samples with different Pd/U_{sb} products (Fig. 3). The lower values of α were determined by normalizing the photoconductivity data at low energies using the method of Moddel et al. [12]. It is apparent from Fig. 3 that upon increasing the value of Pd/U_{sb} the density of gap states due to bonding defects is reduced. The data presented in this figure are compar-

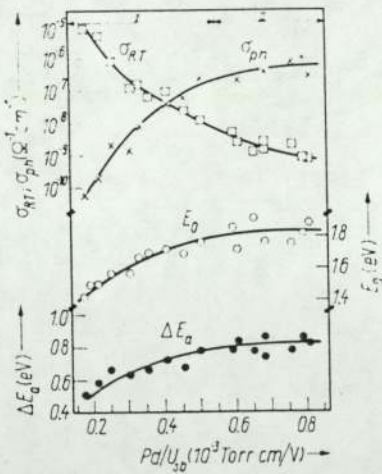


Fig. 2

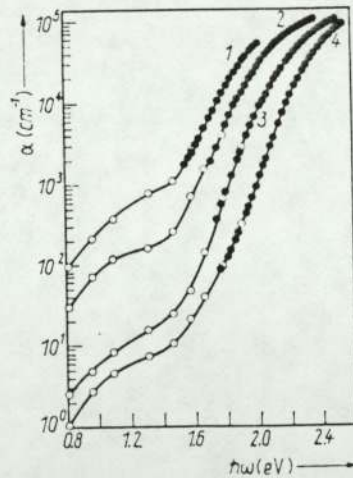


Fig. 3

Fig. 2. The room temperature conductivity σ_{RT} , the photoconductivity σ_{ph} , the thermal activation energy ΔE_a , and the optical gap E_0 as functions of Pd/U_{sb}

Fig. 3. The absorption coefficient α vs. photon energy $h\omega$ for different values of Pd/U_{sb} . (1) 0.31, (2) 0.46, (3) 0.61, and (4) 0.79 mTorr cm/V. The open circles are the normalized photoconductivity using Harvard group's method [12]

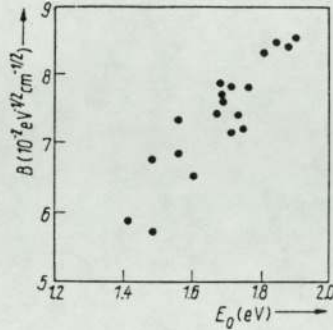


Fig. 4. The slope B of the plot $(\alpha h\nu)^{1/2}$ vs. $h\nu$ against the optical gap E_0 .

able to the results for a-Si:H obtained elsewhere [13]. Also the variation in the constant B in the above equation with the optical gap E_0 (Fig. 4) is further support for the above conclusion.

The shift of the absorption curve of Fig. 3 to higher energies with increased Pd/U_{sb} product is similar to the shift found for a-Si:H films upon increasing H_2 content [14].

The variation in the optical properties with Pd/U_{sb} is consistent with the variation of both the electrical conductivity and thermal activation energy mentioned earlier.

It is interesting to note that the absorption at lower energies (< 1.5 eV) is reduced upon increasing Pd/U_{sb} . This implies a reduction in the localized-defect-states density comparable to results found for glow-discharge and Ar/ H_2 sputtered material.

The photoconductive experiments were carried out using the same gap-cell configuration as for the dark conductivity measurements. The steady photocurrent was measured for an applied field of about 10^2 Vcm $^{-1}$. The films were illuminated by a monochromatic light with energy 1.89 eV and $\leq 10^{15}$ photon/cm 2 s flux intensity. The room temperature photoconductivity σ_{ph} is shown as a function of Pd/U_{sb} product in Fig. 2. It can be seen from this figure that σ_{ph} increases rapidly as Pd/U_{sb} is increased. A steady value of $\approx 10^{-6}$ Ω^{-1} cm $^{-1}$ compares well with the photoconductivity of a-Si:H [15, 16]. It can be concluded from Fig. 2 that σ_{ph} increases with ΔE_n in an analogous way to that observed for a-Si:H with low H_2 content (Paul and Anderson [17]). Evidently, increasing Pd/U_{sb} leads to a reduction of the overall density of states in the mobility gap.

4. Discussion and Conclusion

The similarities between the changes in optical and electrical properties and the deposition rate shown in Fig. 1 and 2 imply that the deposition rate (D_R) plays an important role in controlling the properties of the films. Upon increasing Pd/U_{sb} , at a fixed substrate temperature, the decrease in dark conductivity σ_{RT} and the increase in photoconductivity σ_{ph} are consistent with the increase in both the thermal activation energy of the dark conductivity ΔE_n and the optical gap E_0 (Fig. 2). It is interesting to point out that the increase in σ_{ph} with Pd/U_{sb} of our films is qualitatively similar to the increase of σ_{ph} with hydrogen content in a-Si:H produced at low hydrogen partial pressure by Ar/ H_2 sputtering [17]. This has been attributed to reducing the density of states in the mobility gap.

The slow change both in the deposition rate (Fig. 1, range II) and in the optical and electronic properties (Fig. 2, range II) indicates the optimum range of the parameters U_{sb} , P , and d for Ne sputtering. It may be possible, however, to improve further the films by changing some other parameters not examined here. For example negative substrate bias has recently been shown to improve the electronic and optical properties of a-Si [18].

From the plots of α versus $h\omega$ for various films prepared under different conditions (Fig. 3), it can be seen that upon increasing the product Pd/U_{sb} , the absorption edge between $\alpha = 10^4$ and 10^5 cm^{-1} is displaced to higher energies. Similar changes have been reported for a-Si:H [13], and were attributed to hydrogen satisfying the dangling bonds and relaxing the a-Si network. The slope B in (1), plotted against the optical gap E_0 in Fig. 4, shows a linear relationship. This is similar to the case for glow-discharge [14] and sputtered [17] a-Si:H. This relation may suggest that the increase in the optical gap is due to reduction of the band tail-states density or gap defect states or both [17], which in turn might lower the overall density of states in the mobility gap. Lowering the shoulder around 1.2 eV in the optical absorption data of Fig. 3 upon increasing the Pd/U_{sb} product is in support of this argument.

The above results demonstrate the control of electronic and optical properties of intrinsic a-Si by the preparation conditions, when sputtering in Ne plasma. Relatively high gas pressure and moderate target-substrate spacings and self-bias voltage can produce films with low density of states in the mobility gap. It can be argued that the deposition rate is controlled both by the kinetic energy of the sputtering gas species, ions and neutral particles, bombarding the target and the subsequent collisions within the gas, which include the Ne-Ne and Si-Ne collisions (both ions and neutrals). In addition the plasma contains energetic electrons that are accelerated across the target plasma sheath [19]: these electrons hit the substrate. Increasing Pd product enhances the collisions within the plasma and hence reduces the kinetic energy of the particles arriving at the substrate surface. Priestland and Jackson [20] estimated that with $P = 10^{-3}$ Torr and $d = 6$ cm, about 60% of the sputtered material will experience collision with the sputtering gas species during transit from the target to the substrate. U_{sb} is also expected to play a role in controlling the kinetic energy of the particles arriving at the substrate surface. Therefore, moderating the kinetic energy of the Ne species and the sputtered Si particles, by the above quantities, will result in less damage in the deposited film in addition to the possibility of re-constructing some weak bonds in the Si network.

Comparison of the influence of the preparation conditions of sputtering in Ne on the film properties with that of sputtering in Ar [9] indicates that Ne produces a material with less defect states. This is consistent with the bigger energy exchange to be expected in the case of Si-Ne collisions compared with Si-Ar collisions.

Acknowledgements

The help of Mr. A. E. Marriott-Reynolds with preparation of diagrams is gratefully acknowledged. The authors S.A.A.-N. and Y. Z. wish to acknowledge the receipt of grants from Kuwait Institute for Scientific Research and S.E.R.C., respectively.

References

- [1] W. E. SPEAR and P. G. LECOMBER, *Solid State Commun.* **17**, 1193 (1975).
- [2] W. PAUL, A. J. LEWIS, G. A. N. CONNELL, and T. D. MOUSTAKAS, *Solid State Commun.* **20**, 969 (1976).
- [3] C. C. TSAI, H. FRITZSCHE, M. H. TANIELIAN, P. J. GACZI, P. D. PERSANS, and M. A. VESAGHI, 7th Internat. Conf. Amorphous and Liquid Semiconductors, Ed. W. E. SPEAR, C.I.C.L., University of Edinburgh 1977 (p. 339).
- [4] G. D. CODY, T. TIEDJE, B. ABELES, B. BROOKS, and Y. GOLDSTEIN, *Phys. Rev. Letters* **47**, 1480 (1981).
- [5] T. SHIMIZU, M. KUMEDA, I. WATANABE, and K. KAMONO, *Japan. J. appl. Phys.* **18**, 1923 (1979).
- [6] R. W. FANE, *J. Phys. D* **14**, L113 (1981).

- [7] R. W. FANE and Y. ZAKA, *J. non-crystall. Solids* **57**, 1, 1983.
- [8] R. W. FANE and S. A. ABO-NAMOUS, *J. Phys. C*, to be published.
- [9] W. T. PAWLEWICZ, *J. appl. Phys.* **49**, 5595 (1978).
- [10] N. F. MOTT and E. A. DAVIS, *Electronic Processes in Non-Crystalline Materials*, Clarendon Press, Oxford 1979.
- [11] J. TAUC, *Optical Properties of Solids*, Ed. F. ABELES, North-Holland Publ. Co., Amsterdam 1970.
- [12] G. MODDEL, D. A. ANDERSON, and W. PAUL, *Phys. Rev. B* **22**, 1918 (1980).
- [13] For example E. C. FREEMAN and W. PAUL, *Phys. Rev. B* **20**, 716 (1979).
- [14] For example G. D. CODY, C. R. WRONSKI, B. ABELES, R. B. STEPHENS, and B. BROOKS, *Solar Cells* **2**, 227 (1980).
- [15] T. D. MOUSTAKAS, D. A. ANDERSON, and W. PAUL, *Solid State Commun.* **23**, 155 (1977).
- [16] W. E. SPEAR, R. J. LOVELAND, and A. AL-SHARBATY, *J. non-crystall. Solids* **15**, 410 (1974).
- [17] W. PAUL and D. A. ANDERSON, *Solar Energy Mater.* **5**, 229 (1981).
- [18] MASAKUNI SUZUKI, MAKOTO SUZUKI, M. KANADA, and Y. NAKIMOTO, *Japan. J. appl. Phys.* **21**, L89 (1982).
- [19] For example I. BRODIE, L. T. LAMONT, and D. O. MYERS, *J. Vacuum Sci. Technol.* **6**, 124 (1969).
- [20] C. PRIESTLAND and G. N. JACKSON, *1st Internat. Conf. Application of Vacuum Science and Technology to Coating and Surface Structures*, Dijon, October 15 to 19, 1968.

(Received July 4, 1983)

Dependence of photoconductive properties of hydrogenated Ne-sputtered a-Si on preparation conditions

A Abo-Namous*, Y Zaka and R W Fane, *Physics Department, University of Aston in Birmingham, Birmingham B4 7ET, UK*

The photoresponse of undoped a-Si films, prepared by rf sputtering in Ne without the addition of hydrogen or oxygen, has been investigated as a function of the preparation conditions; gas pressure (P), target-substrate distance (d), self-bias voltage on the target (V_{sb}) and substrate temperature (T_s). Also, the temperature dependence of photoconductivity of these films has been measured as a function of the preparation conditions. The photoresponse of films produced at relatively high values of (Pd/V_{sb}) ratio and moderate T_s suggests a low density-of-states in the mobility gap.

Introduction

It has been believed, for a long time, that sputtered or evaporated amorphous silicon (a-Si) possesses a high density-of-states in the gap and consequently could not be doped. On the other hand, hydrogenated amorphous silicon (a-Si:H), prepared by glow-discharge decomposition of silane¹, or rf sputtering in Ar/H₂², was found to have a low density-of-states in the gap.

In recent years, attempts have been made to produce a-Si with a low density-of-states, without the addition of hydrogen or oxygen, by sputtering at high Ar pressure³, or at high Ne pressure⁴. Ar-sputtered a-Si was found to exhibit low doping efficiency and a poor photoresponse. On the other hand, Ne-sputtered a-Si exhibited a higher doping efficiency^{5,6} and high photoresponse⁷, which were comparable with the properties of a-Si:H.

However, the electronic and optical properties of a-Si seem to depend strongly on the preparation conditions. In this paper, the photoresponse of Ne-sputtered a-Si, without hydrogen or oxygen, is studied as a function of various preparation conditions, such as the gas pressure, the target-substrate distance, the self-bias voltage on the target and the substrate temperature. In addition, the temperature dependence of photoconductivity as a function of these conditions is reported.

Preparation and characterization

A radio-frequency diode-type sputtering system, was used to deposit amorphous silicon films. A single crystal wafer of

electronic grade silicon was used as a target which was water-cooled. The substrate holder could be electrically heated to vary the substrate temperature, T_s , between 150 and 500°C. The substrate temperature was measured with a chromel alumel thermocouple, placed on top of the substrate. A field of about 0.01 T at the centre of the discharge was produced by a Helmholtz pair of coils. The base pressure was of the order of 10^{-7} torr, obtained by a conventional vacuum system of oil diffusion pump with a baffle and liquid nitrogen cooled trap. Corning 7059 glass substrates were ultrasonically cleaned in a detergent, rinsed in distilled water and then boiled in isopropyl alcohol prior to placing in the chamber.

Neon gas (99.999%) was admitted into the chamber via a needle valve, and the pressure, P , in the chamber was varied between 40 and 200 mtorr. The distance, d , between the target and the substrate was varied between 2 and 5.3 cm. The self-bias voltage, V_{sb} , on the target was varied between 650 and 1100 V, measured using a circuit similar to that described by Rock and Smith⁸. It has been found that, at constant T_s , different combinations of P , d and V_{sb} , within the ranges indicated above, giving a fixed Pd/V_{sb} ratio result in films with the same electrical and optical properties. Therefore the preparation conditions are represented here by two parameters, Pd/V_{sb} and T_s . To study the dependence of the properties of a-Si on substrate temperature, Pd/V_{sb} was fixed at about $0.68 \text{ mtorr-cm V}^{-1}$, and T_s was varied between 150 and 460°C.

The film thickness was measured using a multiple-beam interferometer with an estimated uncertainty of $\pm 10\%$. The deposition rate ranged from about 4 to 1 \AA s^{-1} as Pd/V_{sb} was varied from 0.2 to $1 \text{ mtorr-cm V}^{-1}$. In addition, increasing T_s from 150 to 460°C reduced the deposition rate from 1.3 to 0.8 \AA s^{-1} . The results of compositional analysis by X-ray photoemission spectroscopy will be reported elsewhere⁹.

*Permanent address: Materials Application Department, Kuwait Institute for Scientific Research, Kuwait.

Measurements and results

The results reported here were for films of approximately the same thickness (about 0.5 μm), therefore no correction for the light penetration was needed for comparison. The dark conductivity and photoconductivity were measured under vacuum using gap-cell configurations with Al electrodes 1 mm apart. Al electrodes proved to make good ohmic contacts with a-Si for electric fields up to about 10⁴ V cm⁻¹. However, a field of 10² V cm⁻¹ was used for all the measurements reported here. The films were illuminated by a tungsten lamp and selective filters were used to give photon energies from 0.8 to 3.5 eV. For the photoresponse spectral distribution, the photocurrent, *i_{ph}*, defined as the difference between the current under illumination and the dark current, was measured at room temperature, and normalized to 10¹⁴ photons cm⁻² s⁻¹, where at this range of illumination intensity, it was found that the photocurrent was proportional to the light intensity.

The steady-state photocurrent was measured as a function of photon energy, *hν*, for a number of undoped a-Si films deposited at about 300 C with a range of *Pd/V_{sb}* values between 0.21 and 0.95 mtorr-cm V⁻¹. Figure 1 shows the steady-state photoresponse, represented as [*i_{ph}*/e*F*(1 - *R*)], as a function of *hν* in the

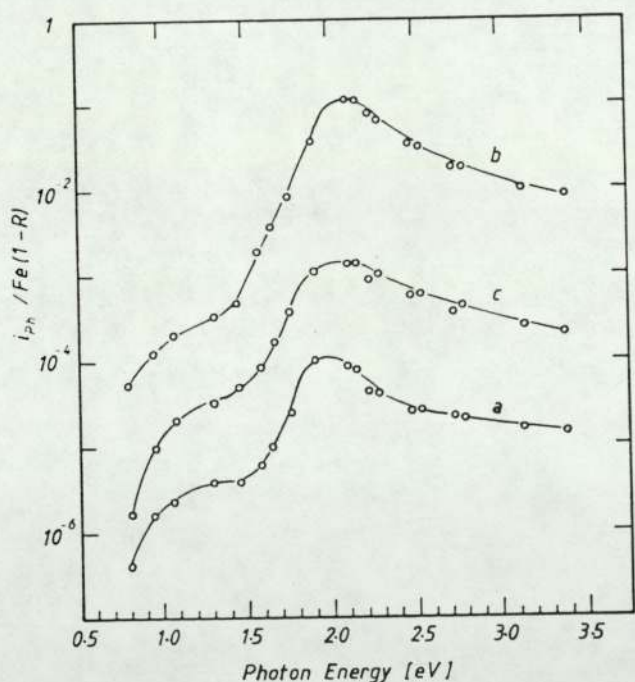


Figure 1. The photoresponse spectral distribution for films prepared at *T_s* = 300 C and different *Pd/V_{sb}* values; (a) 0.31, (b) 0.76 and (c) 0.95 mtorr-cm V⁻¹.

range of 0.8 ≤ *hν* ≤ 3.5 eV, for three films prepared at various *Pd/V_{sb}* values and *T_s* = 300 C. *F*(1 - *R*) is the number of photons incident on 1 cm² of the specimen per second, corrected for surface reflection. It has been shown⁷, that the photoresponse increased as the *Pd/V_{sb}* value increased up to about 0.80 mtorr-cm V⁻¹. The effects of *Pd/V_{sb}* values higher than 0.80 mtorr-cm V⁻¹ on the photoresponse are shown in Fig. 1 (curve c). It can be seen from the figure that for *Pd/V_{sb}* = 0.95 mtorr-cm V⁻¹, the photoresponse is reduced.

The photoresponse spectral distribution was also measured as a function of *T_s*, for *Pd/V_{sb}* = 0.68 mtorr-cm V⁻¹ and is shown in

Figure 2 for three films with *T_s* = 150, 300 and 390 C. It can be seen from this figure that the highest photoresponse is for films prepared at *T_s* = 300 C, while for temperatures higher or lower than this temperature, the photoresponse is reduced.

In general, the photoresponse curves of Figures 1 and 2 have common features. They show peaks between 1.8 and 2.15 eV, which may approach, or even exceed, unity if higher fields were applied. The photoresponse drops rapidly at energies lower than 0.8 eV and shows a shoulder around 1.2 eV followed by a rapid rise in the photoresponse above about 1.6 eV. These features are very similar to those reported for a-Si:H prepared by glow-discharge decomposition of silane^{10,11} or rf sputtering in Ar/H₂ mixture¹².

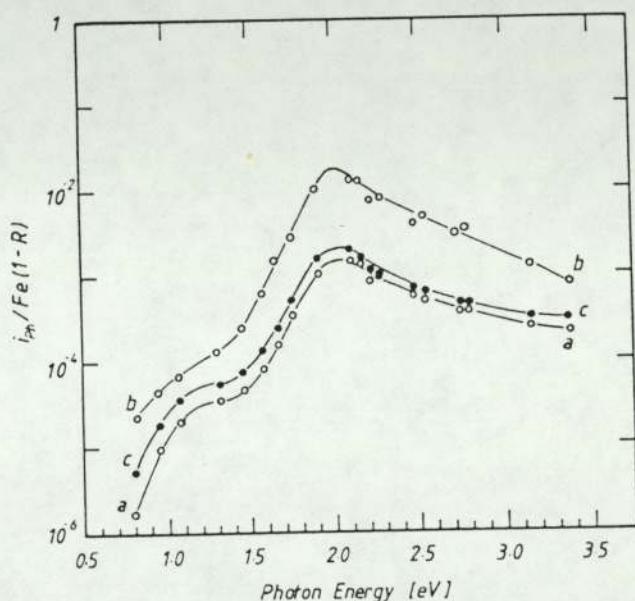


Figure 2. The photoresponse spectral distribution for films prepared at *Pd/V_{sb}* = 0.68 mtorr-cm V⁻¹ and different substrate temperatures, *T_s*: (a) 150, (b) 300 and (c) 390 C.

For the temperature dependence of photoconductivity, the films were illuminated by a monochromatic light with energy 1.89 eV at a flux intensity of about 8 × 10¹⁴ photons cm⁻² s⁻¹ (Figures 3 and 4). The photoconductivity, *σ_{ph}*, was measured as a function of temperature in the range from about -30 C to about 115 C, for several films prepared under various conditions of *Pd/V_{sb}*, with *T_s* = 300 C. The plots of log *σ_{ph}* vs 1/*T* are shown in Figure 3. Curves a, b and c are for films prepared at 0.31, 0.76 and 0.95 mtorr-cm V⁻¹ respectively. The films were excited by 8 × 10¹⁴ photons cm⁻² s⁻¹. Also, shown in Figure 3 is the dark conductivity, *σ*, for the film prepared at *Pd/V_{sb}* = 0.76 mtorr-cm V⁻¹.

All the photoconductivity curves of Figure 3 show maxima in *σ_{ph}* at relatively high temperatures, beyond which the photocurrent was difficult to measure with a reasonable accuracy because *σ_{ph}* < *σ*.

The log *σ_{ph}* vs 1/*T* data suggest a thermally activated photocurrent with an activation energy between 0.15 and 0.2 eV. There was no systematic dependence of the thermal activation energy of *σ_{ph}* on *Pd/V_{sb}*, or light intensity⁷.

The log *σ_{ph}* vs 1/*T* plots for films prepared at *Pd/V_{sb}* = 0.68 mtorr-cm V⁻¹ and different substrate temperatures, *T_s*, are shown in Figure 4. In this figure, curves a, b and c represent

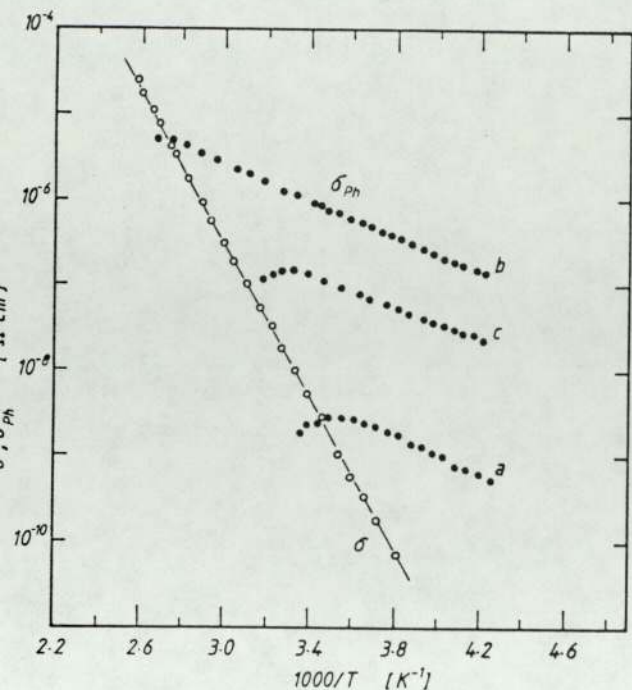


Figure 3. The plots of $\log \sigma_{ph}$ vs $1/T$ for films prepared at $T_s = 300$ C and different Pd/V_{sb} values: (a) 0.31, (b) 0.76 and (c) 0.95 mtorr-cm V^{-1} . The excitation energy was 1.89 eV and the flux intensity was 8×10^{14} photons $cm^{-2} s^{-1}$. $\log \sigma$ vs $1/T$ represents film (b).

films prepared at $T_s = 150, 300$ and 390 C respectively. The films were illuminated by monochromatic light of energy 1.89 eV at a flux intensity of 8×10^{14} photons $cm^{-2} s^{-1}$. The dark conductivity plot represents a film prepared at 300 C. It can be seen from Figure 4 that the dependence of σ_{ph} on $1/T$ is similar to the dependence on Pd/V_{sb} shown in Figure 3. Also, the figure shows that the photoconductivity is improved for $T_s = 300$ C, while for T_s other than 300 C (curve c, Figure 4), it is reduced. An interesting observation is that the thermal activation energy of σ_{ph} always lies in the range between 0.15 and 0.20 eV, and does not vary systematically with T_s . This may suggest that, within the experimental errors expected from this type of measurement, the possibility of a significant change in the degree of order of the films with T_s may be remote in this range of substrate temperatures.

Discussion and conclusions

The high photoresponse of films prepared at Pd/V_{sb} in the range from about 0.6 mtorr-cm V^{-1} to about 0.8 mtorr-cm V^{-1} suggests a low density-of-states. The shoulder around 1.2 eV has been attributed to an optical transition from occupied localized states ϵ_c above the valence-band edge to the conduction band^{12,13}. It has been suggested that these localized states could be defect states. However, the occurrence of this shoulder at approximately the same energy in all the films, suggests that there is a rapid rise in the gap density-of-states at about 1 eV below the conduction-band edge as demonstrated by the field-effect measurements of low-discharge a-Si:H¹⁴. The change in the height of the shoulder with preparation conditions (Figure 1 and 2) indicates that the localized states in the mobility gap can be controlled by these conditions. The high photosensitivity of the films prepared at $V_{sb} = 0.80$ mtorr-cm V^{-1} and $T_s = 300$ C (curve b, Figure 1) could be a result of increasing recombination lifetime. It has been

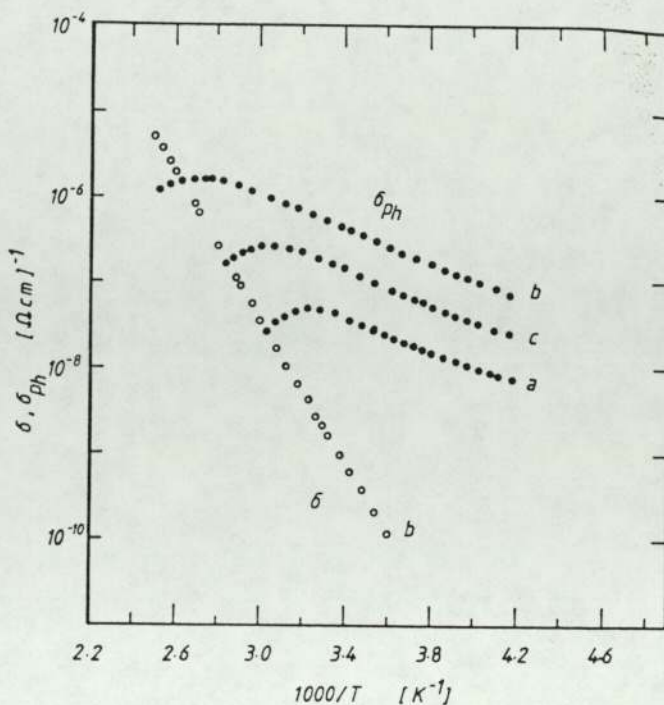


Figure 4. The plots of $\log \sigma_{ph}$ vs $1/T$ for films prepared at $Pd/V_{sb} = 0.68$ mtorr-cm V^{-1} and different T_s : (a) 150, (b) 300 and (c) 390 C. The excitation energy was 1.89 eV and the flux intensity was 8×10^{14} photons $cm^{-2} s^{-1}$. $\log \sigma$ vs $1/T$ represents film (b).

thought that for these preparation conditions, the plasma species are thermalized enough³ to result in films with less microvoids and defect states as indicated by the corresponding optical and electronic properties^{7,15}, as well as from the doping efficiency⁵. On the other hand, when Pd/V_{sb} exceeds 0.80 mtorr-cm V^{-1} and/or T_s exceeds 300 C, the photosensitivity is reduced, suggesting a decreasing recombination lifetime. This is consistent with the dependence of the electrical and optical properties on $Pd/V_{sb} (> 0.80$ mtorr-cm $V^{-1})$ and $T_s (> 300$ C)¹⁶.

Taking into consideration that the transport of photocarriers takes place, predominantly, in the extended electron states¹⁷, according to the relation

$$\sigma_{ph} = e\mu_c(G/K)^{1/2} [N(\epsilon_c)/N(\epsilon_A)] \exp[-(\epsilon_c - \epsilon_A)/kT]$$

the position of the band-tail edge, ϵ_A , with respect to ϵ_c , $(\epsilon_c - \epsilon_A)$ can be determined from the slopes of $\log \sigma_{ph}$ vs $1/T$ curves on the low temperature side. The detailed meaning of different symbols in this equation can be found elsewhere¹⁸. From Figures 3 and 4 and other similar plots (not shown here), the band-tail width $(\epsilon_c - \epsilon_A)$ seems not to change significantly with the parameters Pd/V_{sb} and T_s . This could mean that no significant change in the degree of disorder has occurred upon varying the quantities P , d , V_{sb} and T_s within the ranges indicated earlier. Instead, these quantities are more likely to affect the defect-states-centres through the deposition mechanism, as suggested by the change in the height of the localized-states peak at 1.2 eV (Figures 1 and 2). The consistency between the dependence of the electronic and optical properties of a-Si on the deposition rate and on Pd/V_{sb} has been reported elsewhere¹⁵. Furthermore it has been found that at substrate temperatures higher than 300 C the electrical and optical properties deteriorate, increased conductivity is accompanied by a reduction in the photoconductivity, optical gap and

thermal activation energy of the dark conductivity. Also, the deposition rate was found to decrease with increasing substrate temperature. More detailed work is required to explain the observed effects of substrate temperature.

The increase in the peak intensity at 1.2 eV in the photoresponse spectral distribution (Figure 2) with increasing T_s may be interpreted, according to the Dundee group model¹⁴ as an indication of increasing localized defect-states.

From the present results and the electrical and optical results reported elsewhere^{7,15}, it can be concluded that films with a low defect-state-density are produced by sputtering in Ne gas at moderate combination of P , d , V_{sb} and T_s . Furthermore, the photoresponse of these films may suggest potential photovoltaic and semiconductor applications. However, investigation of other parameters, such as negative bias of the substrate and, possibly, the use of magnetron sputtering, is worthwhile, to improve further the properties of a-Si films.

Acknowledgement

The authors would like to thank Mr R S Bassi for technical assistance.

References

- ¹ W E Spear and P G LeComber, *J Non-Cryst Solids*, **8** 10, 727 (1972)
- ² W Paul, A J Lewis, G A N Connell and T D Moustakas, *Solid State Commun.*, **20**, 969 (1976).
- ³ M Suzuki, A Makae, T Mackawa, M Kumeda and T Shimizu, *Jpn J Appl Phys.*, **19** 20, 85 (1980).
- ⁴ R W Fane, *J Phys D: Appl Phys.*, **14**, L113 (1981).
- ⁵ R W Fane and S A Abo-Namous, *J Phys C: Solid State Phys.*, **16**, 612 (1983).
- ⁶ R W Fane and Y Zaka, *J Non-Cryst Solids*, **57**, 1 (1983).
- ⁷ S A Abo-Namous and R W Fane, *J Phys C: Solid state Phys.*, **17**, 177 (1984).
- ⁸ F C Rock and C W Smith, *J Vac Sci Technol.*, **12**, 943 (1975).
- ⁹ Y Zaka, S A Abo-Namous, D Crumpton and R W Fane, *Vacuum*, **34**, 975 (1984).
- ¹⁰ R J Loveland, W E Spear and A Al-Sharbaty, *J Non-Cryst Solids*, **13**, 55 (1973/1974).
- ¹¹ S Ray, P Chaudhuri, A K Batabyal and A K Barua, *Jpn J Appl Phys* **22**, 23 (1983).
- ¹² D A Anderson, G Moddel and W Paul, *J Non-Cryst Solids*, **35** 36, 345 (1980).
- ¹³ G Moddel, D A Anderson and W Paul, *Phys Rev B*, **22**, 1918 (1980).
- ¹⁴ A Madan, P G LeComber and W E Spear, *J Non-Cryst Solids*, **20**, 239 (1976).
- ¹⁵ S A Abo-Namous, Y Zaka and R W Fane, *Physica Status Solidi (a)*, **79**, 477 (1983).
- ¹⁶ S A Abo-Namous, unpublished data.
- ¹⁷ P G LeComber and W E Spear, *Phys Rev Lett*, **25**, 509 (1970).
- ¹⁸ W E Spear, R J Loveland and A Al-Sharbaty, *J Non-Cryst Solids*, **15**, 410 (1974).

Composition and properties of unhydrogenated amorphous silicon produced by sputtering in argon or neon gas

M. A. H. Al-Jarrah, S. A. Abo-Namous*, D. Crumpton and R. W. Fane, *Physics Department, University of Aston in Birmingham, Birmingham B4 7ET, UK*

Abstract: The electrical and optical properties of amorphous silicon produced by rf sputtering in pure argon or neon gas are compared. The effect of varying the inert gas pressure has been investigated. It is shown that the density of defect states can be reduced by sputtering in high pressure neon instead of the conventionally used argon. The composition of the films has been studied by Rutherford backscattering spectroscopy (RBS) and X-ray photoemission spectroscopy (XPS).

Introduction

Present in all methods of producing amorphous silicon (a-Si) is the presence of large numbers of dangling bonds and voids. These defects introduce localized states in the mobility gap between the conduction and valence bands, thus interfering with the control of electrical properties by substitutional doping¹. Hence a large fraction of research has been directed towards reducing the density of defects to a sufficiently low level to allow efficient doping.

In 1975 Spear *et al*² were the first to dope a-Si produced by the glow-discharge decomposition of SiH₄ with phosphorous and boron. Their method succeeded because the hydrogen present in the plasma attached itself to the dangling bonds thus reducing the density of states in the gap. Soon after, a-Si produced by rf sputtering in Ar/H₂ plasma was also doped successfully³. The success with doping a-Si:H alloy and the realization of its potential device capabilities have diverted a lot of attention away from the need to investigate the basic parameters affecting film properties and to optimize them to achieve 'pure' a-Si films with a low density-of-defect-states. Instead experimentalists have saturated the silicon with dangling-bond terminators such as hydrogen or the halogens to achieve the desired properties. The concentration of these intentionally incorporated impurities can be as large as 26%⁴. Compensation by hydrogen may remove the defect states, but the interaction of nearby Si-H units may reproduce gap states near the conduction band⁵. The long term stability of these films is questionable since hydrogen effuses at room temperature and there is some evidence that hydrogen effuses even at low temperature⁶.

It is therefore important to optimize the preparation conditions to give pure a-Si films with a low density-of-defect-states. In this paper we report the effects of varying the sputtering gas and pressure on the composition and electrical and optical properties of a-Si films produced by rf sputtering in (99.999%) pure argon and neon gases. The films produced have been characterized by measuring the electrical conductivity over a temperature range of 200 C. The optical gap has been determined by transmission measurements in an UV-Vis spectrophotometer. Compositional analysis has been carried out by Rutherford backscattering spectroscopy (RBS) and X-ray photoelectron spectroscopy (XPS). In particular, the amount of rare gas incorporated into the silicon matrix as a function of gas pressure was investigated. Problems related to the determination of the density of the films from the RBS spectra are also discussed.

Experimental details

Experimental details have been described elsewhere⁷. Briefly, the apparatus consists of a diffusion pumped, rf diode sputtering arrangement with a baffle and liquid nitrogen cooled trap. A Helmholtz pair of coils gives a field of about 0.01 T at the centre of the discharge. The power input is adjusted to give an rf self bias on the target of about 900 V. The target-substrate distance is set at 3.5 cm and the substrate temperature maintained at approximately 200 C, measured with a chromel alumel thermocouple. Films were deposited simultaneously on several substrates. Corning 7059 glass was used for electrical and optical measurements; for RBS measurements, carbon, crystalline silicon, alumina and quartz substrates were used while aluminium substrates were used for XPS measurements. The rare gases entered the chamber via a needle valve which controlled the flow rate to achieve the desired pressure.

*Permanent address: Material Application Department, Kuwait Institute for Scientific Research, Kuwait.

m thickness, measured by a multiple-beam interferometer, varied from about 200 to 1000 nm. Deposition rate varied from about 0.2 nm s⁻¹ for high pressure argon films to about 0.1 nm s⁻¹ for low pressure films, for neon-sputtered films the deposition rate decreased from about 0.3 to 0.1 nm s⁻¹ on increasing the sputtering pressure.

Electrical and optical properties

The room-temperature electrical conductivity of the films was measured in the manner described elsewhere⁷. Figure 1 shows the variation of room-temperature electrical conductivity, σ_{RT} , with sputtering pressure for argon and neon gases. It is seen that by increasing the sputtering pressure from 0.67 Pa to about 5.3 Pa, σ_{RT} decreases by more than five orders of magnitude, any further increase in pressure has little effect on σ_{RT} other than increasing it slightly at higher pressures. The highest pressure at which we can operate with argon is limited by the geometry of the system and is about 32 Pa beyond which the mean free path of the argon ions becomes comparable to the spacing between the target and the grounded shield surrounding it. For neon this limitation is not so severe and sputtering pressures up to 40 Pa can be tolerated. For argon, an increase in the pressure from 0.67 to 5.3 Pa had a similar

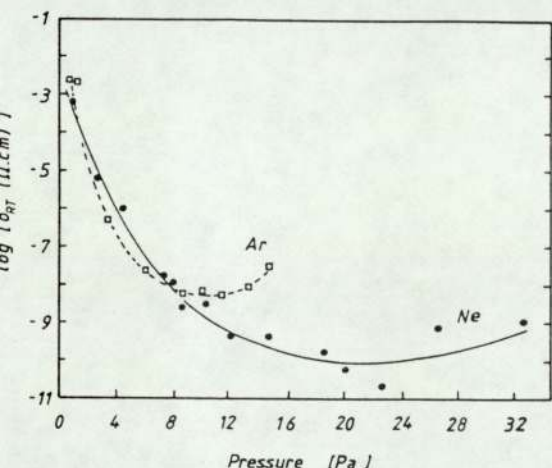


Figure 1. The room-temperature conductivity, σ_{RT} , as a function of sputtering pressure.

but an increase in the pressure to about 20 Pa further increased the conductivity by more than three orders of magnitude. Any further increase in pressure again, as in the case of argon, produced a reversal in the trend with the conductivity increasing with pressure.

A similar behaviour is observed in the variation of thermal activation energy, ΔE , and the optical gap, E_g , with pressure as illustrated in Figure 2. For argon ΔE increases from 0.14 eV to about 0.6 eV as the pressure is increased from 0.67 to 8.6 Pa and any further increase in pressure has little effect. For neon, ΔE increases with pressure to a value of about 0.9 eV at 14.6 Pa, higher pressures result in a slight decrease in ΔE . The optical gap was determined from the plots of $(\alpha h\nu)^{1/2}$ vs $h\nu$ according to the equation:

$$(\alpha h\nu)^{1/2} = \beta(h\nu - E_g)$$

where β is a constant, $h\nu$ the photon energy and α the absorption

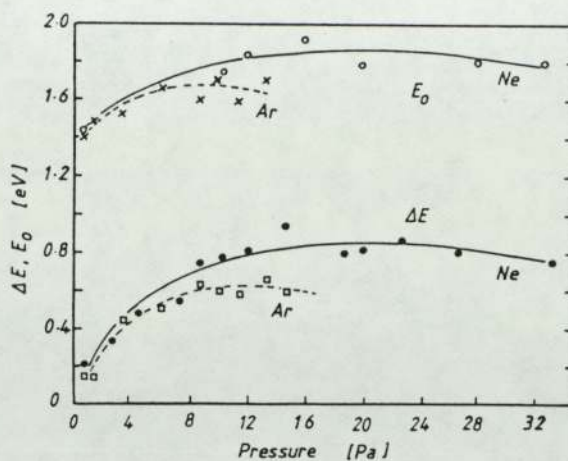


Figure 2. The variation of thermal activation energy, ΔE , and the optical gap, E_g , with sputtering pressure.

coefficient. The optical gap, E_g , increases from about 1.4 eV at low pressure to about 1.7 eV for high-pressure sputtering in argon and 1.8 eV for the neon case.

Compositional analysis

Figure 3 shows the ratio of argon and neon atoms to silicon atoms in the films as a function of sputtering pressure. Rutherford backscattering spectroscopy using 2.8 MeV He ions and XPS using Mg K α radiation were used to determine the argon and neon contents of the films respectively. The ratio of argon to silicon atoms of the films was found to decrease from about 6.0% at low pressure to less than 0.5% for high pressure. The variation of neon in the films with pressure exhibits a similar trend to that of argon; however, at any given sputtering pressure the neon incorporated in the films is approximately twice as much as argon. Inspection of RBS spectra readily confirmed that the argon was distributed uniformly throughout the films; however, to verify the uniformity of neon in the silicon matrix, films had to be etched by argon bombardment and spectra taken at various depths.

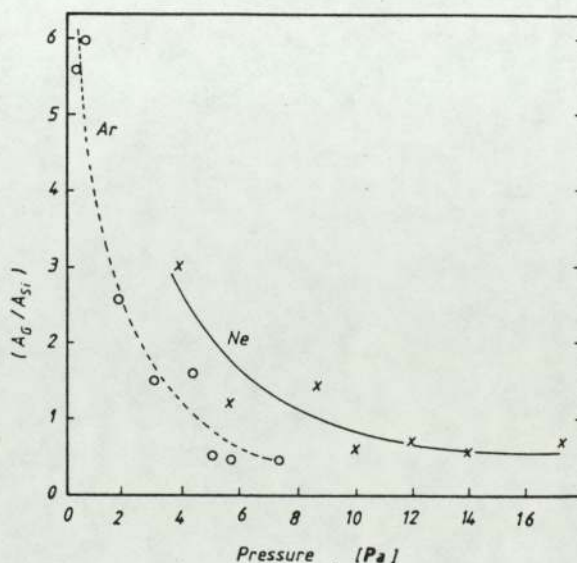


Figure 3. The ratio of argon and neon atoms to silicon atoms in the film as a function of sputtering pressure.

Discussion and conclusions

Our results indicate that the density of defect states in a-Si can be reduced by sputtering at high pressures. For sputtering in pure argon this is evidenced by a decrease in room-temperature electrical conductivity by more than five orders of magnitude and an increase in the thermal activation energy from 0.14 to 0.6 eV as argon pressure is increased from the conventionally used value of 0.67 Pa to 8.7 Pa.

Similar results on argon sputtering have been reported by Pawlewicz⁹ who decreased σ_{RT} from about 10^{-3} to about 10^{-7} ($\Omega\text{ cm}^{-1}$) by increasing the argon gas pressure from 3.3 to 20 Pa. There was a corresponding increase in the activation energy from 0.2 to 0.3 eV. Van Dong *et al.*¹⁰ sputtered in a dc triode system and obtained, under a special condition of heating, a-Si films with $\sigma_{RT} < 10^{-9}$ ($\Omega\text{ cm}^{-1}$) and activation energy of about 0.6 eV. Shimizu *et al.*¹¹ decreased the electrical conductivity by more than five orders of magnitude by increasing the product of argon pressure, P , and target-substrate spacing, d , from 13 to 130 cm. The original suggestion by Pawlewicz⁹, that increasing the sputtering pressure reduced the kinetic energy of the various species bombarding the film thus reducing the number of defects, seems to be consistent with the above results. However, recently it has been found that the low conductivity of the high pressure neon-sputtered films could be due in part to post-deposition oxidation because the films have a porous structure¹². This is thought to be due to the fact that although bombardment by high energy species (ions, neutrals, electrons) in the plasma is detrimental to the film properties, some bombardment is beneficial in that it helps to remove loosely bound atoms. Thus a film grown under the condition of high pressure, where the plasma species have become thermalized before reaching the substrate; tends to have a porous structure.

To investigate this hypothesis, the oxygen content of the films was extracted from the relevant RBS spectra. The results are summarized in Figure 4. From these results it is evident that films produced in argon sputtering pressures up to 3.5 Pa are essentially

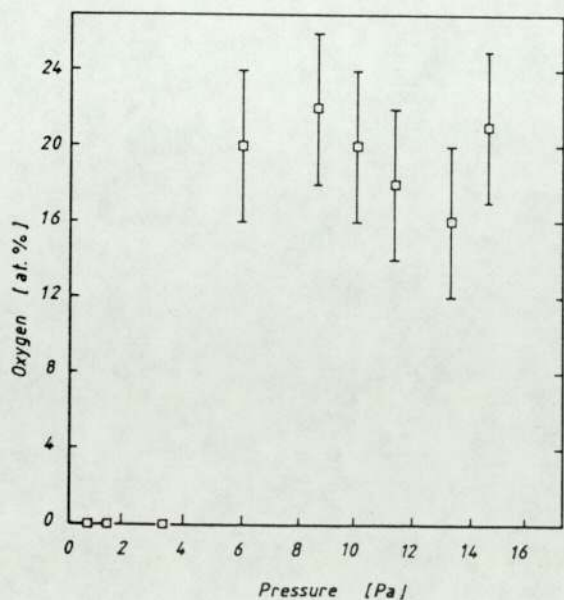


Figure 4. Concentration of oxygen in argon-sputtered films as a function of sputtering pressure.

oxygen free, while films produced at higher pressures contain about 20% oxygen.

Our results appear to support the suggestion that as the gas pressure is increased the electronic and optical properties of the films improve due to the reduction in the kinetic energy of the various species in the plasma which are continuously bombarding the growing film. This is evident from a decrease in σ_{RT} by four orders of magnitude as the pressure is increased from 0.67 to 3.5 Pa, while maintaining essentially oxygen free films. The variations of thermal activation energy, optical gap and the argon content with argon pressure have a similar relationship: ΔE and E_0 increase and the argon content decreases sharply as the pressure is increased from 0.67 to 3.5 Pa. Increasing the pressure beyond 3.5 Pa also removes low energy bombardment of the film which is beneficial in that it removes loosely bound material from the surface of the films, thus films produced at high argon pressure tend to be porous and susceptible to post-deposition oxidation as is evident by a sharp increase in the oxygen content of the films produced at pressure higher than 3.5 Pa. The decrease in σ_{RT} as the pressure is increased beyond 3.5 Pa is less sharp, levelling off at pressures of about 8.6 Pa and is probably due to the oxygenation of the films. Similarly ΔE and E_0 increase and the argon content decreases slightly as pressure is increased beyond 3.5 Pa and eventually levels off at about 8.6 Pa.

Another quantity which can be used to support the above argument is the measurement of the density of the films. This could in theory be readily obtained from the RBS spectra and the thickness of the film, measured independently by other means, employing the relation¹³

$$\Delta\epsilon = [\theta] \frac{N_0 \rho}{A} t$$

where $\Delta\epsilon$ is the energy difference between the energy of the ions scattered from the front surface of the target and the ions scattered from the back surface of the target, $[\theta]$ is the stopping cross-section, N_0 is Avogadro's number, A is the atomic weight of element and ρ and t are the density and thickness of the film respectively. Since $[\theta]$ is tabulated¹⁴ the density can be obtained by measuring $\Delta\epsilon$ and the thickness of the film. We attempted to measure the density by depositing the films on carbon substrates since the carbon edge lies well below the silicon peak, but measurement of $\Delta\epsilon$ and the shape of the peak indicated that carbon and silicon had diffused into each other, resulting in the broadening of $\Delta\epsilon$, and hence an over-estimation of the density. To overcome this problem, quartz and alumina substrates were employed and although no sign of diffusion seemed apparent, there was a large error in determining $\Delta\epsilon$ due to the overlap of the silicon and the substrate peaks. Thus, so far we have been unable to measure the density of the films but further work to overcome the problems indicated above and to investigate alternative methods is in progress.

It can be seen by inspection of Figures 1-3 that the variations in properties of neon-sputtered films follow the same general trend as for argon. However, in this case the region of rapid changes in properties with increase in pressure extends up to 12 Pa. An increase in pressure from 0.67 to 12 Pa results in a decrease in σ_{RT} by more than six orders of magnitude to less than 10^{-9} ($\Omega\text{ cm}^{-1}$), accompanied by an increase in ΔE and E_0 by 0.6 eV and 0.4 eV respectively. The neon concentration in these films decreases to about 1.0 at.% at 12 Pa and levels off at about 0.5 at.% at higher pressures.

the pressure region 0.67–12 Pa for neon corresponds to the region 0.67–3.5 Pa for argon, in that the improvement in film properties is believed to result from the thermalization of plasma species. However it is apparent from the results that improvement in film quality is greater for neon-sputtered films. Further increase in pressure leads to contamination by oxygen, although figures for oxygen content have only been obtained for argon-sputtered films.

Detailed examination of the sputtering plasma is required to determine the factors which result in an improvement in film quality when using neon as opposed to argon sputtering. Thermalization as mentioned above, is important but this may be achieved in either case by using the appropriate pressure. Other factors may be important. The higher ionization potential for neon means that there is less likelihood of doubly charged ions which would result in greater damage to the film. For a given energy the smaller stopping distance for argon ions results in a higher energy dissipation per unit path length and consequently more damage to the growing film. Small atomic size could also be important in causing less structural deformation. There is a higher probability for clusters of atoms to be sputtered with argon¹⁵ which could result in film inhomogeneity and also lead to lower sputtering efficiency¹⁶.

Finally, the effect of the magnetic field needs to be assessed and, although this feature is again common to both gases used in our experiment, the effectiveness of this constraint will be different in the two cases.

In summary, the present results indicate that sputtering in high pressure neon can produce a-Si with low density-of-defect-states. Further support for this observation is given by photoconductivity measurements¹⁷ and efficient n- and p-type doping^{18,19}.

References

- ¹ E A Davis, in *Topics in Applied Physics* (Edited by M H Brodsky), Springer, Vol 36, 41 (1979).
- ² W E Spear and P G LeComber, *Solid State Commun.*, **17**, 1193 (1975).
- ³ W Paul, A J Lewis, G A N Connell and T D Moustakas, *Solid State Commun.*, **20**, 969 (1976).
- ⁴ H Fritzsche, M Tanielian, C C Tsai and P J Gaczi, *J Appl Phys.*, **50**, 3366 (1976).
- ⁵ T D Moustakas, D A Anderson and W Paul, *Solid State Commun.*, **23**, 155 (1977).
- ⁶ C C Tsai, H Fritzsche, M H Tanielian, P J Gaczi, P D Persans and M A Vesaghi, *Proc 7th Int Conf. on Amorphous and Liquid Semiconductors* (Edited by W E Spear), p 339, University of Edinburgh Press, Edinburgh (1977).
- ⁷ R W Fane, *J Phys D: Appl Phys.*, **14**, L113 (1981).
- ⁸ N F Mott and E A Davis, *Electronic Processes in Non-Crystalline Materials*, Clarendon Press, Oxford (1979).
- ⁹ W T Pawlewicz, *J Appl Phys.*, **49**, 5595 (1978).
- ¹⁰ N Van Dong, *J Physique*, **42**, 647 (1982).
- ¹¹ T Shimizu, M Kumeda, I Watanabe and K Kamono, *Jpn J Appl Phys.*, **18**, 1923 (1979).
- ¹² T Shimizu, M Kumeda, I Watanabe and Y Kiriyama, *Jpn J Appl Phys.*, **19**, L235 (1980).
- ¹³ D G Simons, C R Growe and M D Brown, *J Appl Phys.*, **53**, 3900 (1982).
- ¹⁴ W K Chu, J W Mayer and M A Nicolet, *Backscattering Spectroscopy*, Academic Press, New York (1978).
- ¹⁵ G K Wehner and G S Anderson, in *Handbook of Thin Film Technology* (Edited by L I Maissel and R Glang), Chapter 3, McGraw-Hill Book Company, New York (1970).
- ¹⁶ M G Thompson and D K Reinhard, *J Non-Cryst Solids*, **37**, 325 (1980).
- ¹⁷ S A Abo-Namous, Y Zaka and R W Fane, *Physica Status Solidi (a)*, **79**, 477 (1983).
- ¹⁸ R W Fane and Y Zaka, *J Non-Cryst Solids*, **57**, 1 (1983).
- ¹⁹ R W Fane and S A Abo-Namous, *J Phys C: Solid State Phys.*, **16**, 6121 (1983).

DOPING EFFECTS OF GROUP-III AND V ELEMENTS IN

UNHYDROGENATED Ne-SPUTTERED a-SI

S A Abo-Namous*, Y Zaka and R W Fane
Physics Department
University of Aston in Birmingham
Birmingham, B4 7ET, UK

ABSTRACT

Amorphous silicon has been doped p- and n-type by co-sputtering with Group III and V elements. Pure neon, instead of the conventionally used Ar/H₂ mixture, has been used as the sputtering gas. The room-temperature conductivity has been varied over 9 orders of magnitude, with a corresponding shift in the Fermi level of about 1.2 eV in the mobility gap, without significant change in the optical gap. Comparison of the results with those of other techniques suggests that the material has a relatively low density-of-defect-states and a reasonable doping efficiency can be achieved. Furthermore, p-n junctions made of this material imply potential semiconductor applications.

* Permanent address: Materials Application Department, Kuwait
Institute for Scientific Research, KUWAIT.

INTRODUCTION

In recent years, amorphous silicon (a-Si) has received increasing attention because it is a promising material for low-cost solar cells [1]. Amorphous silicon prepared by thermal evaporation or r.f. sputtering in Ar has been known to have a high density of defect states in the mobility gap; these states hinder the doping of this material. The introduction of hydrogen, either by glow-discharge decomposition of silane [2] or by sputtering in Ar/H₂ atmosphere [3] satisfies dangling bonds and relaxes the structure of a-Si [4] resulting in a low density-of-states in the mobility gap. High doping efficiencies have been reported for hydrogenated amorphous silicon (a-Si:H) doped from the gas phase by the introduction of phosphine or diborane into the discharge [5]. However, the above techniques have some disadvantages. It has been reported that hydrogen concentration [6]. Also, the location of antibonding states of Si-H bond near the conduction band, may lower the photoresponse [7]. However, recently, the incorporation of halogens, such as fluorine, which make stronger bonds with silicon than in the case of hydrogen, has resulted in a more stable a-Si:F:H alloy [8, 9]. Above all, handling of the dangerous gases involved in the production of a-Si:H or a-Si:F:H makes it desirable to find a more safe method of preparation Pawlewicz [10], reported that the properties of Ar-sputtered a-Si depend strongly on the preparation conditions, such as the sputtering-gas pressure, target-substrate distance and substrate temperature. A relatively low density of gap-states have been reported for a Si prepared by high pressure Ar-sputtering without the intentional incorporation of hydrogen or halogen [11].

Doping efficiency of unhydrogenated Ar-sputtered a-Si has been reported to depend on the preparation conditions [12]. Recently, p-type and n-type doping with Al and Ta, respectively have been reported for a-Si prepared by r.f. sputtering in Ne [13, 14], where the conductivity was varied over 9 orders of magnitude, accompanied with a shift in the Fermi level by about 1.2 eV within the mobility gap. This is an indication that material with low density-of-states in the gap has been produced, in support of other results on undoped a-Si [15].

In this paper, doping effects in a-Si, of Group III and V elements, by Ne-sputtering from a composite target or sputtering a predoped target, are presented and compared with doping by other techniques.

EXPERIMENTAL DETAILS

The details of the preparation method can be found elsewhere [13]. In brief, a-Si films were deposited in a conventional r.f. diode sputtering system using Ne gas (99.999%). The target was a single crystal wafer of electronic grade silicon. The substrate temperature, T_s was about 300°C. The gas pressure, P , the target-substrate distance, d , and the r.f. self-bias voltage, V_{sb} , on the target were adjusted to give (Pd/V_{sb}) value of about 0.76 mtorr.cm. v^{-1} . It has been reported [16] that various combinations of P , d and V_{sb} , giving the same value of (Pd/V_{sb}) result in films with similar properties, provided that P , d and V_{sb} are kept within a certain range [16]. A magnetic field of about 0.01 T, induced by a Helmholtz pair of coils, was used to collimate the discharge.

For doping, a composite target was used, where the dopant material (Al, B, Ga or Ta) was fixed on the centre of the Si target. In the case of boron doping, pellets were made of boron powder. A B-predoped target was also used to deposit B-doped a-Si. Films thickness was measured using multiple-beam interferometry with an estimated error of $\pm 10\%$. Typically, the thickness of the films reported here, was about 0.5 μm .

The d.c. dark conductivity was measured under vacuum using gap-cell configurations with thermally evaporated Al-electrodes separated by 1 mm. The applied electric field was $10^2 \text{ V}\cdot\text{cm}^{-1}$. Al proved to make good ohmic contacts with a-Si films for fields up to about $10^4 \text{ V}\cdot\text{cm}^{-1}$.

The atomic percentage of the dopant in the Si films was calculated from the x-ray photoemission measurements (Al, Ga and Ta), Rutherford backscattering spectroscopy (Ta) and the etching profile of the target using the available sputtering yields (Al) [17]. In the case of boron, the superposition of the photoemission lines of Si and B made it very difficult to calculate the B/Si atomic ratio. However, it could be estimated that the B/Si atomic ratio did not exceed the B/Si area ratio. Therefore the B/Si area ratio was considered as the upper limit of the atomic ratio. The above measurements showed that that the Al/Si atomic ratio is 1.15 times the Al/Si target area ratio and the Ta/Si atomic ratio is 1.8 Ta/Si area ratio.

The type of doping was readily checked by the sign of the polarity of thermoelectric power. P-type doping was found for Al-, Ga- and B-doped films while n-type doping was found for Ta-doped films.

RESULTS

The d.c. dark conductivity, σ , for doped a-Si films, was measured as a function of temperature, T, in the range from -120°C to 150°C . It has been reported [13] that the plots of σ vs. $1/T$ for lightly (≤ 2.5 at %) Al-doped films, a singularly activated conductivity even at temperatures far below room temperature, indicating that conduction in the extended states is the dominant conduction mechanism. On the other hand, for high concentrations (≥ 2.5 at %) of Al in a-Si, the plots of σ vs $1/T$ curve up at temperatures below room temperature, indicating the hopping conduction is markedly contributing to conduction.

The composition dependence of the room temperature conductivity, σ_{RT} , and the thermal activation energy ΔE_a , is shown in Fig. 1. It is seen from this figure that, initially, σ_{RT} decreases with increased Al concentration which corresponds to a slight increase in ΔE_a as compensation takes place and the Fermi level moves towards the bottom of the density of states near the centre of the mobility gap, according to the Dundee group model [18]. Thereafter, σ_{RT} increases monotonically up to about $0.4 \Omega^{-1}\text{cm}^{-1}$, with the increased Al concentration up to 12.4 at %.

Fig. 1 also shows the plots of σ_{RT} and ΔE_a , as functions of B content in a-Si, for B-doped films prepared by co-sputtering with B. As in the case of Al doping, Fig. 1 shows that initially, with the addition of a very small amount of B to Si ($\sim 0.02\%$), σ_{RT} is reduced by at least an order of magnitude while the thermal activation energy increased to about 0.8 eV. Upon increasing the B content up to 2.2% (area ratio), the room-temperature conductivity

increased rapidly by over 7 orders of magnitude accompanied by a shift in the Fermi-level position to less than 0.2 eV from the valence band. The total shift of the Fermi level within the mobility gap was about 0.7 eV.

Furthermore, sputtering from a B-predoped Si target, with an estimated 1 at. ($\pm 10\%$) B, under the same conditions as for sputtering from a composite target, gave a large change in the conductivity (up to about 10^{-3} cm^{-1}), and the thermal activation energy down to about 0.2 eV from the valence band edge.

Since Ga has a low melting point, it was very difficult to control the required Ga/Si area ratio during sputtering. Accordingly, it was difficult to achieve a pre-determined Ga/Si atomic ratio in the film and reproducibility was almost impossible. Therefore, only two specimens of Ga-doped Si are presented here, to show the possibility of p-type doping with Ga using co-sputtering technique. It can be seen from Fig. 1 that the room-temperature conductivity, Ga-doped films, increases by 6-7 orders of magnitude upon increasing the Ga content up to 2.2 at %. This is accompanied by a change in E_a of about 0.7 eV.

The 'dip' in σ_{RT} and the peak in ΔE_a in Fig. 1 are indicative of p-type doping in a-Si, since undoped films showed in n-type conductivity [15].

The electrical conductivity, for Ta-doped films prepared by co-sputtering in Ne, was measured as a function of temperature. The Ta concentration was varied up to 3 at.%. The variations in σ_{RT} and ΔE_a with Ta content are shown in fig 2. Also, shown in Fig. 2,

are the variations in σ_{RT} and ΔE_a with B content in a-Si, these values are recalled from Fig. 1, to compare two different doping types. It can be seen from Fig. 2 that a change in the room-temperature conductivity of the films over 8 orders of magnitude is achieved by doping with 3 at.% Ta. Also, it can be concluded from the figure that the Fermi level moved about 1.2 eV within the mobility gap.

DISCUSSION AND CONCLUSIONS

The results demonstrated a variation in the room-temperature conductivity, over many orders of magnitude accompanied with an overall shift of 1.2 eV in the Fermi-level position within the mobility gap. These variations are comparable with the best results reported for doping a-Si:H from the gas phase [5]. It should be emphasised that the optical absorption measurements showed only a slight change in the optical gap with the addition of an impurity to a-Si [13, 14]. This change, however, is expected since high doping levels may introduce defect states in the a-Si network [19]. In Fig. 3, a comparison is made between the doping efficiency of different impurities using different techniques, as indicated. The atomic concentration of dopant elements in the present films was determined using XPS and/or RBS techniques as mentioned earlier. From Fig. 3 we see that, in the region of low dopant concentrations, σ_{RT} for films doped by co-sputtering is generally lower than for the gas phase doping. On the other hand, the maximum σ_{RT} of our doped samples is about two orders of magnitude higher than the maximum conductivity obtained by boron doping from the gas phase.

However, comparison of the doping efficiency of the same impurity, for different techniques shows the following:

- (i) The efficiency of B-doping by co-sputtering in Ne is slightly higher than that of B-doping by ion implantation, although the former is lower than for the gas phase doping with B at low doping levels.
- (ii) ρ_T in the case of Al-doping by co-sputtering in Ne is a few orders of magnitude higher than for Al-doping by co-sputtering in Ar/H₂ mixture [20].

The doping efficiency was calculated following a method explained elsewhere [13]. It has been estimated that about 1 in 800 Al atoms acts as acceptor centre, which is slightly less than that for Al doping by ion implantation [21]. The doping efficiencies for B-doping by co-sputtering and sputtering from a B-pre-doped target, in Ne, are (1/150) and (1/75) respectively. These efficiencies are higher than those reported for B implantation [21]. Bearing in mind that the undoped a-Si has a low room-temperature conductivity ($\sim 10^{-8} \Omega^{-1}\text{cm}^{-1}$) and a high thermal activation energy (~ 0.8 eV), as well as high photoresponse [16], the conclusion can be made that the material produced by sputtering in Ne under the conditions mentioned earlier, possesses a low density-of-states in the mobility gap. In addition, the relatively doping efficiency in the case of co-sputtering in Ne, compared to that in the case of doping from the gas phase, is believed to be due to the doping method rather than to the nature of the basic material. Results in support of this conclusion are shown in Fig. 4 where the Al-doping efficiency has increased, accompanied by a reduction in ΔE_a , upon annealing

Al-doped samples at 470°C for 90 minutes. Annealing undoped a-Si films resulted only in a 4-fold increase in conductivity. It is highly unlikely that this is responsible for the increase of 4 orders of magnitude in conductivity of the doped samples. Rather, the activation of the dopants by annealing is responsible for enhancing the doping efficiency.

It should be emphasised that p- or n-type doping, in the conventional sense has taken place rather than an alloying effect as reported by others [20,22, 23]. The control of conductivity over many orders of magnitude and the shift in the Fermi level position by about 1.2 eV which are accompanied by a slight change in the optical gap, are in support of the above statement.

A p-n junction made of amorphous Al-doped Si/amorphous Ta-doped Si demonstrate reasonable rectification characteristics as can be seen in Fig. 5. This, in conjunction with the photoconductive properties of a-Si [16] indicate potential semiconductor and possibly photovoltaic applications, which need to be investigated in more detail.

REFERENCES

1. H Fritzche, C C Tsai and P Persans, *Solid State Technol.*, 21 (1978) 55.
2. W E Spear and P G LeComber, *J. Non-Cryst. Solids*, 8-10 (1972) 727.
3. W Paul, A J Lewis, G A N Connell and T D Moustakas, *Solid State Commun.*, 20, (1976) 969.
4. H Fritzche, *Solar Energy Materials*, 3 (1980) 447.
5. W E Spear and P G LeComber, *Solid State Commun.*, 17 (1975) 1193.
6. C C Tsai and H Fritzche, *Solar Energy Materials*, 1 (1979) 29.
7. T D Moustakas, D A Anderson and W Paul, *Solid State Commun.*, 23 (1977) 155.
8. A Madan, S R Ovshinsky, W Czubytyj and M Shur, *J. Electr. Mater.*, 9 (1980) 385.
9. P Nielsen and V L Dalal, *Appl. Phys. Lett.*, 37 (1980) 1090.
10. W T Pawlewicz, *J. Appl. Phys.*, 49 (1978) 5595.
11. M Suzuki, Makoto Suzuki, M Kanda and Y Kakimoto, *Jap. J. Appl. Phys.*, 21 (1982) L89.
12. M Suzuki, A Nakao, T Maekawa, M Kumeda and T Shimizu, *Jap. J. Appl. Phys.*, 19 (suppl. 19-2) (1980) 85.
13. R W Fane and S A Abo-Namous, *J. Phys. Stat. Sol. (a)*, 79 (1983) 447.
14. R W Fane and Y Zaka, *J. Non-Cryst. Solids*, 57 (1983) 1.
15. S A Abo-Namous, Y Zaka and R W Fane, *Phys. Stat. Sol. (a)*, 79 (1983) 447.
16. S A Abo-Namous and R W Fane, *J. Phys. C: Solid State Phys.*, 17 (1984) 1775.
17. G Cartet and J S Colligon, *Ion Bombardment of Solids*, Heinemann Educational Book, (1968) p 323.
18. A Madan, P G LeComber and W E Spear, *J. Non-Cryst. Solids*, 20 (1976) 239.
19. D A Anderson, G Moddel and W Paul, *J. Non-Cryst. Solids*, 35/36 (1980) 345.
20. M G Thompson and D K Reinhard, *J. Non-Cryst. Solids*, 37 (1980) 325.

21. G Muller, S Kalbitzer, W E Spear and P G LeComber, Proc. 7th Inter. Conf. Amorphous and Liquid Semiconductors, ed. W E Spear, University of Edinburgh Press, Edinburgh, (1977) p 442.
22. S R Ovshinsky, Proc. 7th Int. Conf. Amorphous and Liquid Semiconductors, ed. W E Spear, University of Edinburgh Press, Edinburgh, (1977) p 519.
23. L Xu, C L Foiles and D K Reinhard, Phil. Mag. B, 49 (1984) 249.

FIGURE CAPTIONS

Figure 1: $\log \sigma_{RT}$ and ΔE_a as functions of dopant content in a-Si, prepared by co-sputtering with Al (o), B (●) or Ga (x) or by sputtering a B-predoped target (□).

Figure 2: $\log \sigma_{RT}$ and ΔE_a as functions of dopant content in B-doped and Ta-doped a-Si as indicated. (B% represents target area ratio).

Figure 3: $\log \sigma_{RT}$ as a function of dopant concentration for different n- or p-type doping using various techniques. B_G and P_G are for B- and P- doping from gas phase, B_I and P_I are for B- and P-doping by ion implantation [21], Al_{CS} is for doping with Al by co-sputtering in Ar/H₂ [20], Al, B and Ta represent co-sputtering in Ne [present work].

Figure 4: $\log \sigma_{RT}$ and ΔE_a as functions of Al at.% for as-deposited films (o) and annealed films (o) at 470°C for 90 minutes.

Figure 5: I-V characteristic curve of a typical p-amorphous/n-amorphous Si-junction. The p-type layer is Al-doped while the n-type layer is Ta-doped a-Si, both prepared by co-sputtering in Ne.

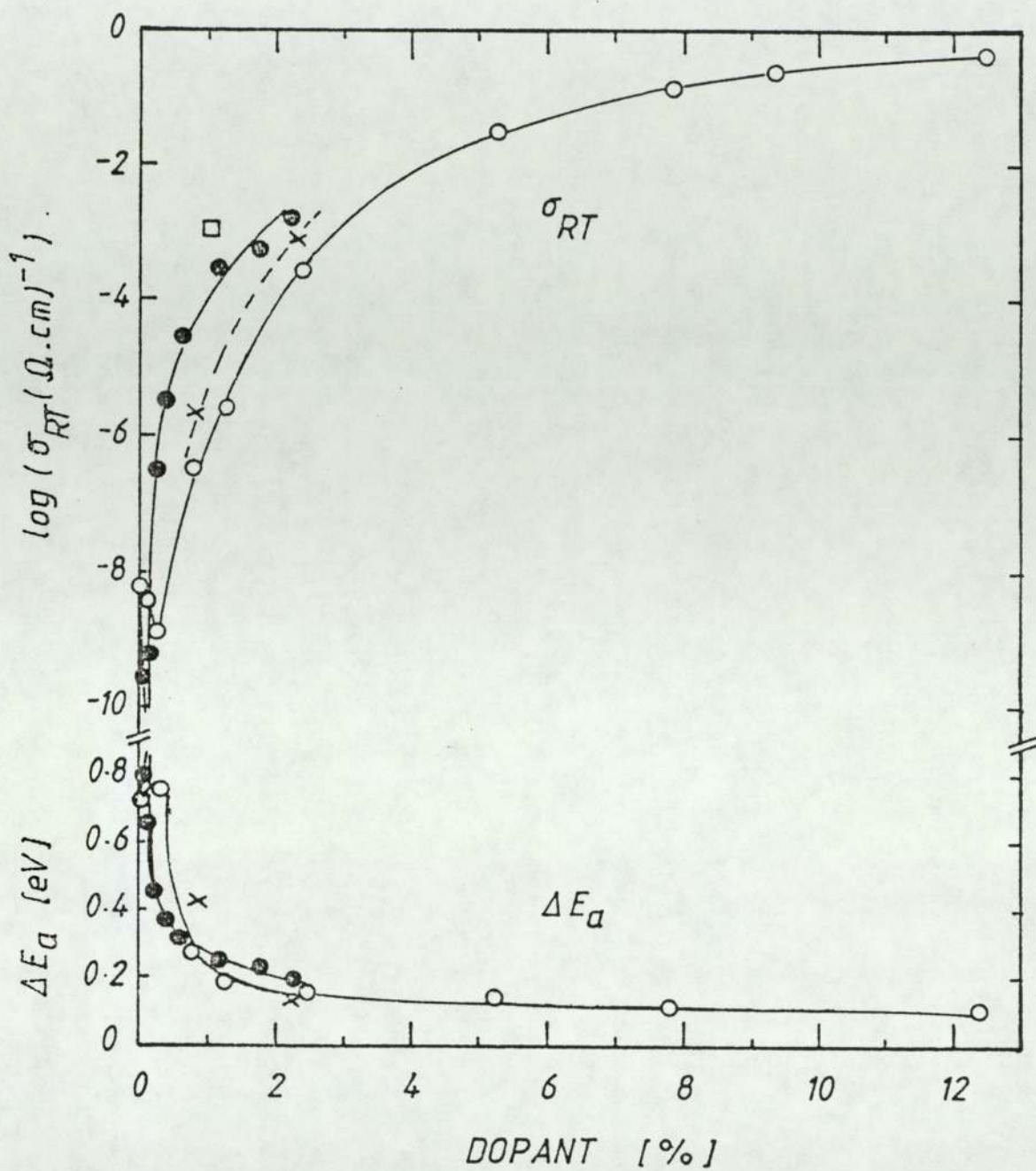


Fig. 1: $\log \sigma_{RT}$ and ΔE_a as functions of dopant content in a-Si, prepared by co-sputtering with Al (o), B (●) or Ga (x) or by sputtering a B-predoped target (□).

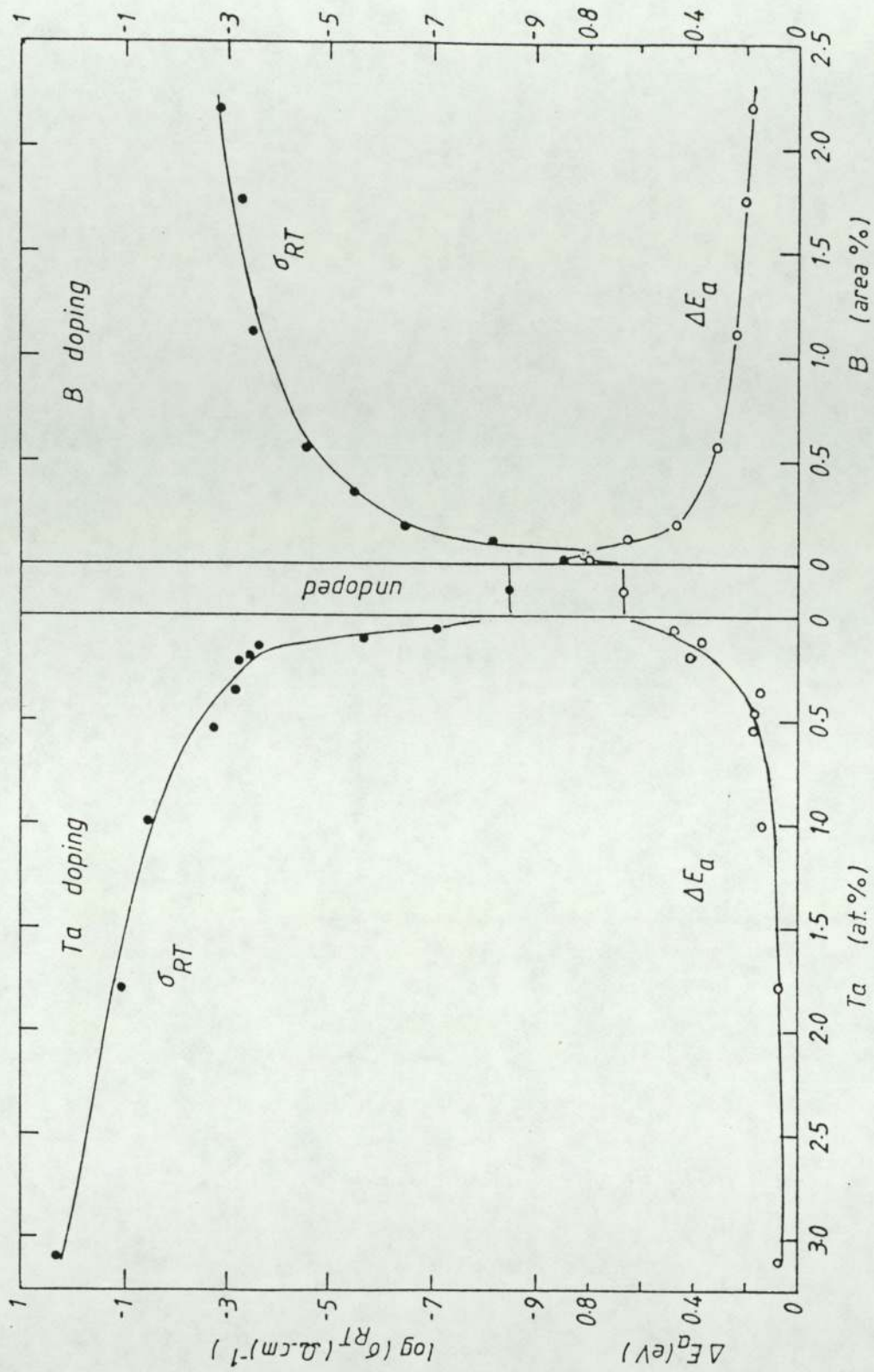


Fig. 2: $\log \sigma_{RT}$ and ΔE_a as functions of dopant content in B-doped and Ta-doped n-Si as indicated. (50 represents target area ratio)

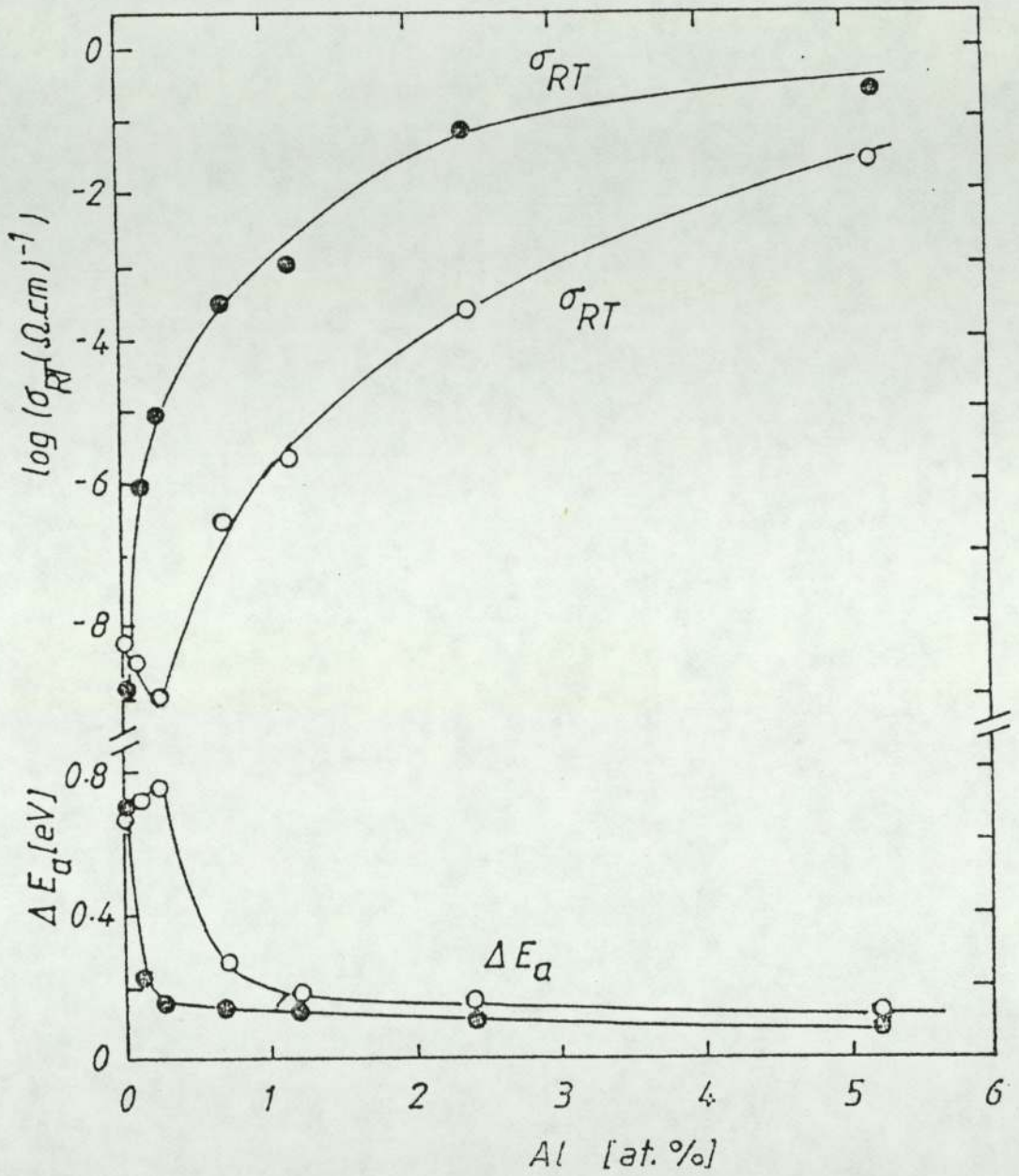


Fig. 4: $\log \sigma_{RT}$ and ΔE_a as functions of Al at.% for as-deposited film and annealed films (●) at 470 °C for 90 minutes.

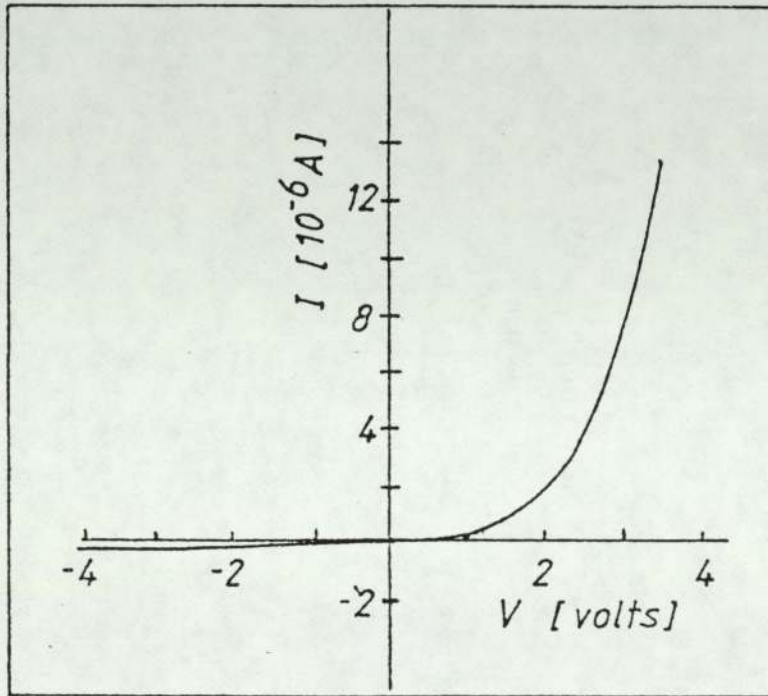


Fig. 5: I-V characteristic curve of a typical p-amorphous/n-amorphous Si junction: The p-type layer is Al-doped while the n-type layer is Ta-doped a-Si, both prepared by co-sputtering in Ne.

CONTROL OF ELECTRICAL AND OPTICAL PROPERTIES OF UNHYDROGENATED

Ne-SPUTTERED a-Si BY PREPARATION CONDITIONS

Y Zaka, S A Abo-Namous* and R W Fane
Physics Department
University of Aston in Birmingham
Birmingham, B4 7ET, UK

ABSTRACT

Amorphous silicon films have been prepared by r.f. sputtering in a Ne plasma without hydrogen. The preparation conditions have been varied through the gas pressure (P), the target-substrate distance (d), the self-bias voltage on the target (V_{sb}) and the substrate temperature (T_s). The dark d.c. conductivity, photoconductivity, optical gap and the position of the Fermi level in the mobility gap were investigated as functions of P , d , V_{sb} and T_s . The results indicate that the electronic and optical properties can be controlled over a wide range by varying the P , d , V_{sb} and T_s . This has been attributed to controlling the density-of-states distribution in the gap by the above quantities, where a high P and/or d and a moderate V_{sb} and T_s , can produce a material with low density-of-states in the gap.

* Permanent address: Materials Application Department, Kuwait
Institute for Scientific Research, KUWAIT.

INTRODUCTION

During the last decade interest in the production and control of electrical and optical properties of a-Si has grown rapidly. This is because a-Si is potentially a low cost Solar-Cell material. Amorphous silicon also has the advantage of having relatively high absorption coefficient and photoconductivity in the visible spectrum. In fact a-Si has an absorption coefficient more than one order of magnitude larger than single crystal silicon (1).

However, a-Si produced by thermal evaporation (2) or r.f. sputtering in an argon plasma (3) contains a large number of dangling bonds and microvoids. These defects introduce localised states in the mobility gap between the conduction and valance bonds. The density of defect states can be as large as $10^{20} \text{ cm}^{-3} \text{ eV}^{-1}$, thus pinning the Fermi level near the centre of the gap and hindering the control of electrical properties by substitutional doping. Such films are further characterised by a relatively high electrical conductivity (room temperature electrical conductivity, $10^{-3} (\text{ cm})^{-1}$ which is only weakly temperature dependent (thermal activation energy, 0.2 eV). This is because at moderate temperatures the electrical conductivity is dominated by hopping between states around the Fermi level.

Therefore if a-Si is to be of any use as a potential low cost material for electronic devices the density of defects must be reduced to a sufficiently low level to allow efficient substitutional doping and hence systematic control of electrical and optical properties. This has been achieved by a-Si produced by glow-discharge decomposition of silane where the density of defect states

has been reduced by more than 5 orders of magnitude (4). R.F. sputtering in a plasma of argon and hydrogen also produces a material with similar properties; namely, room temperature electrical conductivity less than $10^{-9} (\Omega \text{ cm})^{-1}$ which is thermally activated above room-temperature ($\Delta E \sim 0.8 \text{ eV}$) (5). These films have been doped n- or p-type with group V and group III elements respectively.

However, the alloy of silicon and hydrogen (a-Si:H) has the disadvantage of being thermally unstable, hydrogen effuses at 350°C and there is some evidence that it might even effuse at room-temperature (6). Another disadvantage is that one is dealing with highly toxic and explosive gases in the glow-discharge process. In previous communications we have reported on the effect of varying the sputtering gas and pressure on the electrical and optical properties of r.f. sputtered amorphous silicon (7). It was shown that better quality films could be produced by sputtering in high pressure neon rather than conventionally used argon. We have also successfully doped films n- and p-type by co-sputtering with groups V and (III respectively (8, 9)).

In this paper we present results of detailed investigation of the effect of varying the sputtering conditions on the electrical and optical properties of a-Si, and hence the density of defects. The neon sputtering pressure (P), target-substrate spacing (d) and the d.c. self-bias voltage on the target (V_{sb}) have been varied over a wide range, also the substrate temperature has been varied from 100° to 360°C .

SAMPLE PREPARATION AND MEASUREMENTS

The films were deposited in an r.f. powered diode sputtering system, evacuated to base pressures of less than 5×10^{-7} torr. The experimental procedure and the description of the apparatus have been described elsewhere (8, 9).

Films were deposited on Corning 7059 glass slides. The thickness, generally in the range 0.5 - 1 μ m was measured by a Tolansky multiple beam interferometer to an accuracy of better $\pm 10\%$.

For conductivity measurements aluminium electrodes were evaporated over the films in a gap cell configuration. A Keithley 610C electrometer was used for the measurements with an applied field of about 10^2 Vcm⁻¹. The substrate temperature could be varied from -150°C to 200°C and from plots of conductivity against inverse temperature the thermal activation energy was deduced. The optical gap was determined from plots of $(\alpha \hbar \omega)^{\frac{1}{2}}$ vs $\hbar \omega$ according to the relation (13).

$$(\alpha \omega)^{\frac{1}{2}} = \beta (\hbar \omega - E_0)$$

where β is a constant, $\hbar \omega$ the photon energy and α the absorption coefficient determined from transmission measurements in a Vis - U.V. spectrophotometer.

The photoconductivity experiments were carried out using the same gap-cell configuration as for the dark conductivity measurements. The steady photocurrent was measured for an applied electric field

of 10^2 Vcm^{-1} by a laser of wavelength 6328 and intensity of approximately $5 \times 10^{16} \text{ photons cm}^{-2}\text{s}^{-1}$.

RESULTS AND DISCUSSIONS

There are several parameters which affect the electrical and optical properties of a-Si. In this paper we present the results of varying the sputtering gas pressure (P), the target-substrate distance (d), the d.c. self-bias voltage (V_{sb}) and the substrate temperature (T_s) on the properties of a-Si sputtered in pure neon plasma.

The neon pressure was varied from 5 to 245 mtorr, keeping all other parameters fixed; $d = 3.5 \text{ cm}$, $V_{sb} = 880 \text{ V}$ and $T_s = 300^\circ\text{C}$. As shown in Figure (1) this results in a decrease in room-temperature conductivity (σ_{RT}) by more than seven orders of magnitude from $\sim 10^{-3} (\Omega\text{cm})^{-1}$ at 5 mtorr to $\sim 10^{-10} (\Omega\text{cm})^{-1}$ at the highest pressures. This is accompanied by an increase in the thermal activation energy (ΔE) from $\sim 0.2 \text{ eV}$ to 0.8 eV . Where as films produced at low pressures were thermally unactivated even up to the highest temperatures, films produced at pressures higher than about 60 mtorr showed singly activated thermal activation energy above about 80°C . The photoconductivity (σ_{ph}) negligible for films prepared at low pressures, increases to approximately $10^{-6} (\Omega\text{cm})^{-1}$ at high pressures. The optical gap (E_o) also increases from about 1.4 eV to 1.7 eV . The sputtering rate decreases from about 4.0 \AA/S at 5 mtorr to about 0.5 \AA/S at the highest pressures.

The decrease in σ_{RT} and an increase in σ_{ph} , ΔE and E_o with increasing pressure suggest that the density of defects decreases

as the pressure is increased. This is due to the fact that the kinetic energy of various species bombarding the film is reduced as the pressure is increased.

Other workers investigating the effect of varying the pressure on the properties of a-Si produced r.f. sputtering in pure argon plasma have come to similar conclusions (14, 15).

Thus it would appear that by eliminating the high energy bombardment of the films the number of dangling bonds can be reduced. However, recently it has been found that the low conductivity of the high pressure argon sputtered films could be due in part to post-deposition oxidation because the films have a porous structure (16). This is thought to be due to the fact that although bombardment by high energy species (ions, neutrals and electrons) in the plasma is detrimental to the film properties, some bombardment is beneficial in that it helps to remove loosely bound atoms. Thus a film grown under the conditions of high pressure, where the plasma species have become completely thermalised before reaching the substrate tend to have a porous structure. Preliminary analysis by x-ray photoemission spectroscopy (XPS), Auger electron spectroscopy (AES) and Rutherford backscattering spectroscopy (RBS) has shown some oxygen in the films sputtered at pressures greater than 200 mtorr, a more detailed analysis to investigate the compositional variation with sputtering conditions is in progress.

The reduction in the kinetic energy of the plasma species bombarding the film can also be achieved by either increasing the target substrate distance (d) or by decreasing the target self-bias voltage (V_{sb}). Figure (2) shows the variation of room temperature

dark and photo-conductivities, thermal activation energy (ΔE) and the optical gap (E_0) with target substrate distance. For this set of experiments the pressure was 85 mtorr and the d.c. self-bias voltage set at 880 volts. By increasing the target-substrate spacing from 2 cm to 5 cm σ_{RT} decreased by more than two orders of magnitude with a corresponding increase in σ_{ph} , ΔE and E_0 also increase. The sputtering rate decrease monotonically from above 3.0 Å/S to ~ 1.0 Å/S as the distance is increased. By varying the input power the d.c. self-bias voltage on the target can be changed. To investigate the variation of the electrical and optical properties with the target voltage the pressure was fixed at 85 mtorr and the target substrate distance at 3.5 cm. Figure (3) shows the variation of σ_{RT} , σ_{ph} , E and E_0 as the target voltage is increased from 550 to 1050 volts. Again the variation of σ_{RT} , σ_{ph} , ΔE and E_0 with V_{sb} indicate that the density of defects can be reduced significantly by reducing the energy of the bombarding species. The sputtering rate reduced monotonically with the d.c. self-bias voltage from 3.0 Å/S to 0.5 Å/S.

Figure (4) shows the variation of the properties with substrate temperature. For this set of experiments the pressure was fixed at 150 mtorr, the target-substrate spacing was set at 3.5 cm and target voltage was 880 volts.

The results indicate that there is a slight decrease in the density of defects as the temperature is increased.

We have shown that the properties of a-Si prepared by r.f. sputtering are influenced significantly by the preparation conditions, and that the density of defects is reduced by decreasing the kinetic

energy of the various species bombarding the film by either increasing the sputtering pressure and the target-substrate distance or decreasing the d.c. self-bias voltage on the target. Increasing the substrate temperature also slightly reduces the number of defects, but the effect of substrate temperature on the properties is much less significant, since σ_{RT} and σ_{ph} change by less than one order of magnitude over a temperature range of 250°C.

Although the properties of a-Si films produced in pure argon plasma are effected in a similar way, the improvement of film quality is greater for neon-sputtered films. This could be due to the fact that neon having a smaller atomic size than argon will cause less damage to the film. The possibility of clusters of atoms being sputtered from the target is also reduced and since neon has a higher ionization potential the possibility of bombardment by doubly ionized ions is also reduces.

CONCLUSION

We have demonstrated that a very significant change in the room-temperature dark, and photo-conductivities, thermal activation energy and the optical gap of r.f. sputtered a-Si can be achieved by increasing the neon sputtering pressure from 5 to 245 mtorr. Conventionally a-Si is sputtered at 5 mtorr, we believe that at such low pressure the growing film is bombarded by energetic species in the plasma which create defects in the structure of the films. By increasing the sputtering pressure the kinetic energy of the various ions and neutrals in the plasma is reduced till they are completely thermalised before reaching the substrate, thus eliminating the high energy bombardment of the film. The decrease in the

density of defect states is evident from the electrical and optical properties which are comparable to that of glow-discharge, or hydrogenated sputtered silicon. The energy of the bombarding species can also be reduced by increasing the target-substrate distance or reducing the target voltage, but variation in these parameters is limited. However, the decrease in the density of defect states could partly be due to contamination of the films. Oxygen whether incorporated in-situ or by post deposition oxidation can also act as a dangling bond terminator (14). Finally the substrate temperature has very little effect on the properties of a-Si, there being only a slight decrease in the density of defects as the temperature is increased.

REFERENCES

1. For example, R A Gibson, P G LeComber and W E Spear, Solid State and Electronic Devices (Special Issue), 2 (1978) S3.
2. For example, A Madan, P G LeComber and W E Spear, J. Non-Cryst. Solids, 20 (1976) 239.
3. For example, T D Moustakas, J. Electron. Mater., 8 (1979) 391.
4. W E Spear and P G LeComber, Solid State Commun., 17 (1975) 1193.
5. W Paul, A J Lewis, G A N Connell and T D Moustakas, Solid State Commun. 20 (1976) 969.

6. C C Tsai, H Fritzsche, M H Tanielian, P J Gaczi, P D Persans and K A Vesaghi, Proc. 7th Inter. Conf. Amorphous and Liquid Semiconductors, ed. W E Spear, University of Edinburgh Press, Edinburgh (1977) p 339.
7. Y Zaka, S A Abo-Namous, D Crumpton and R W Fane, Vacuum "84" Conference, York, UK., (1-4 April 1984). To be published in Vacuum.
8. R W Fane and Y Zaka, J. Phys. D: Appl. Phys., 16 (1983) 1993.
9. R W Fane and S A Abo-Namous, J. Phys. C: Solid State Phys., 16 (1983) 6121.
10. N F Mott and E A Davis, Electronic Processes in Non-Crystalline Materials, Clarendon Press, Oxford, (1979)
11. W T Pawlewicz, J. Appl. Phys., 49 (1978) 5595.
12. T Shimizu, M Kumeda, I Watanabe and K Kamono, Jap. J. Appl. Phys., 18 (1979) 1923.
13. For example, T Shimizu, M Kumeda, I Watanabe and Y Kiryama, Jap. J. Appl. Phys., 19 (1980) L235.
14. M A Paesler, D A Anderson, E C Freeman, G Moddel and W Paul, Phys. Rev. Lett., 41, 1492, 1978.

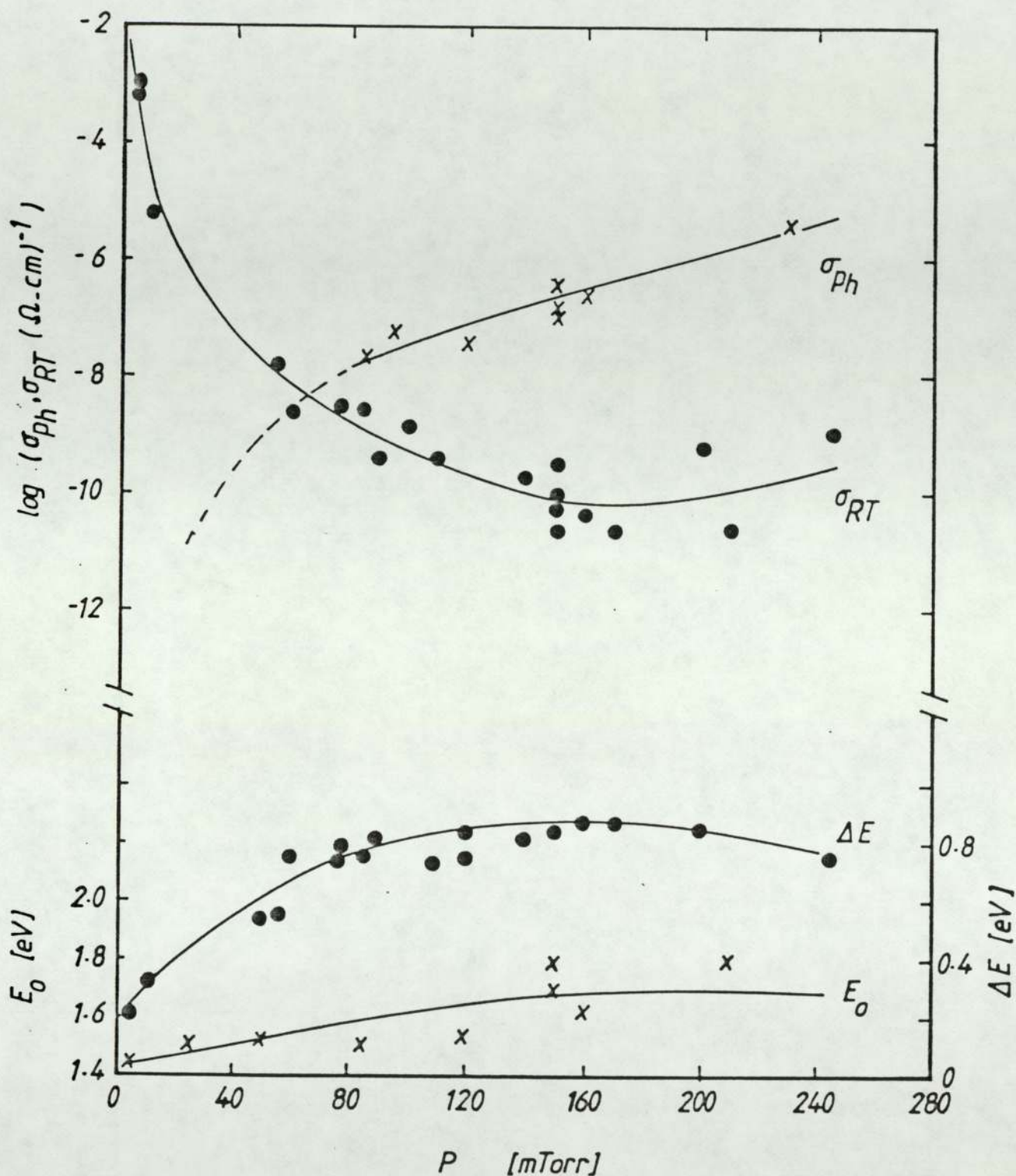


Fig. (1) Variation of room temperature electrical conductivity (σ_{RT}), photoconductivity (σ_{ph}), thermal activation energy (ΔE) and the optical gap (E_0) with sputtering pressure (P).

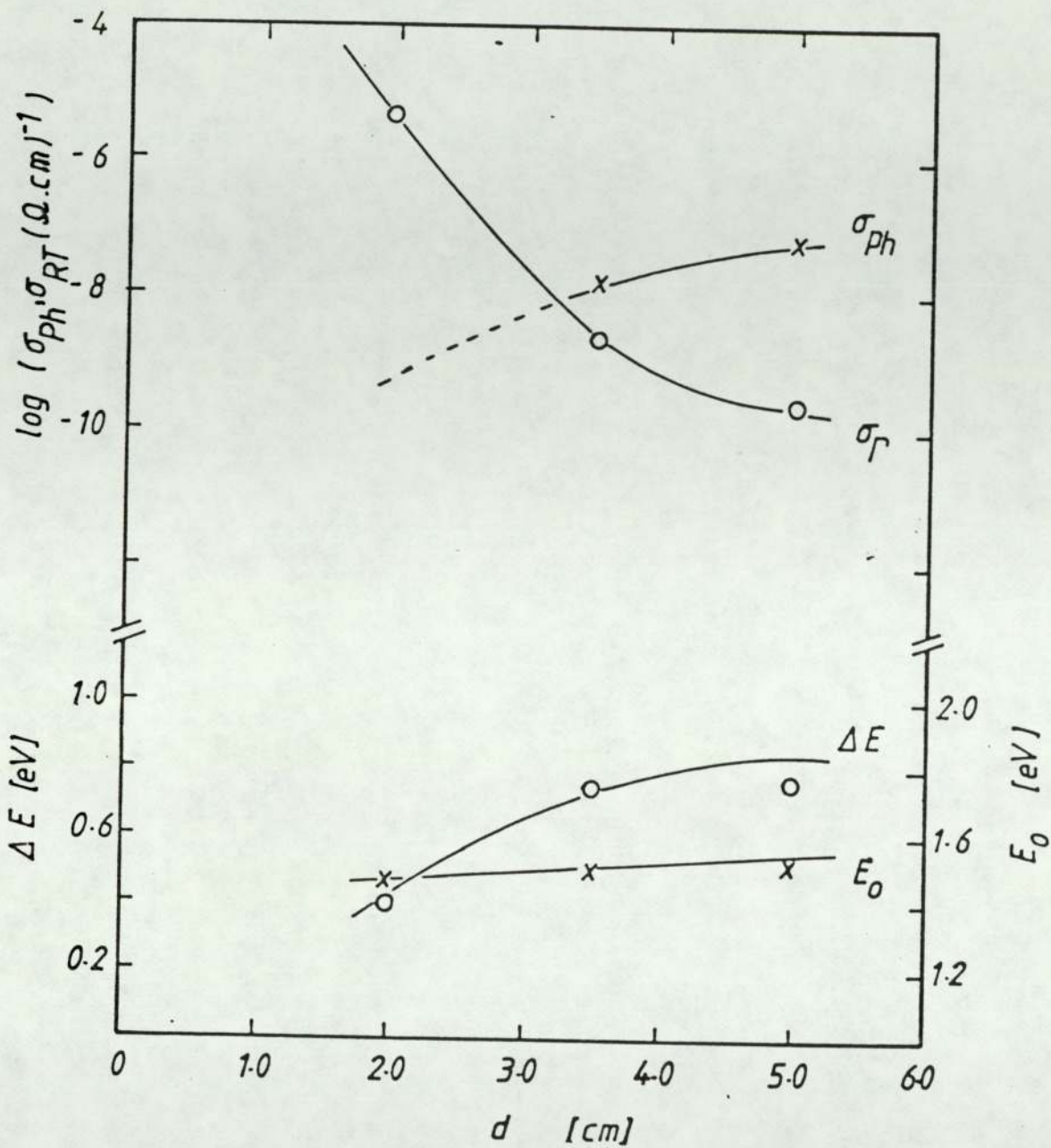


Fig. (2) Variation of room-temperature electrical conductivity (σ_{RT}), photoconductivity (σ_{ph}), thermal activation energy (ΔE) and the optical gap E_0 with the target-substrate distance (d).

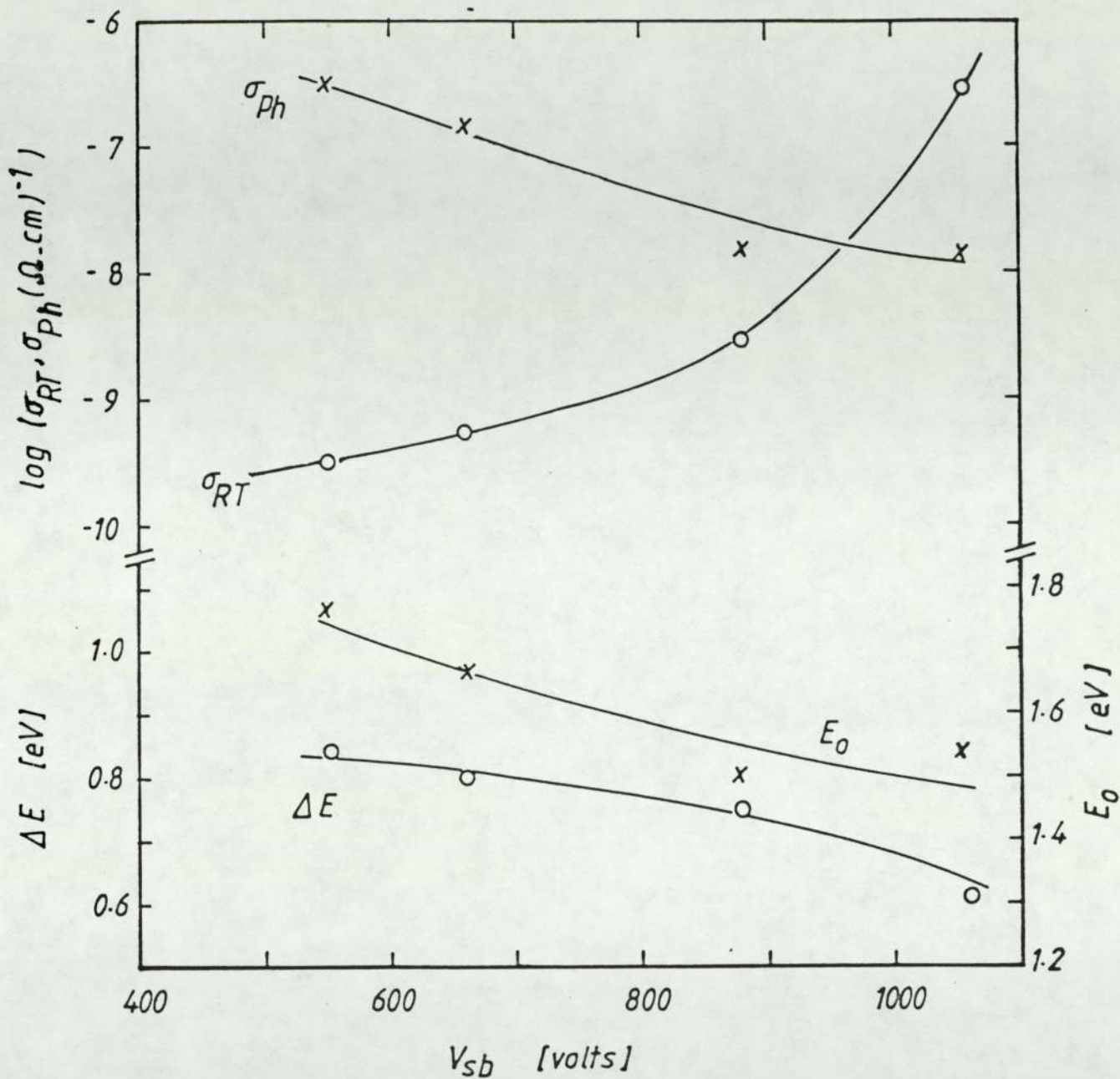


Fig.(3) Variations of room-temperature electrical conductivity (σ_{RT}), photoconductivity (σ_{ph}), thermal activation energy (ΔE) and the optical gap E_0 with the d.c. self bias voltage on the target (V_{sb}).

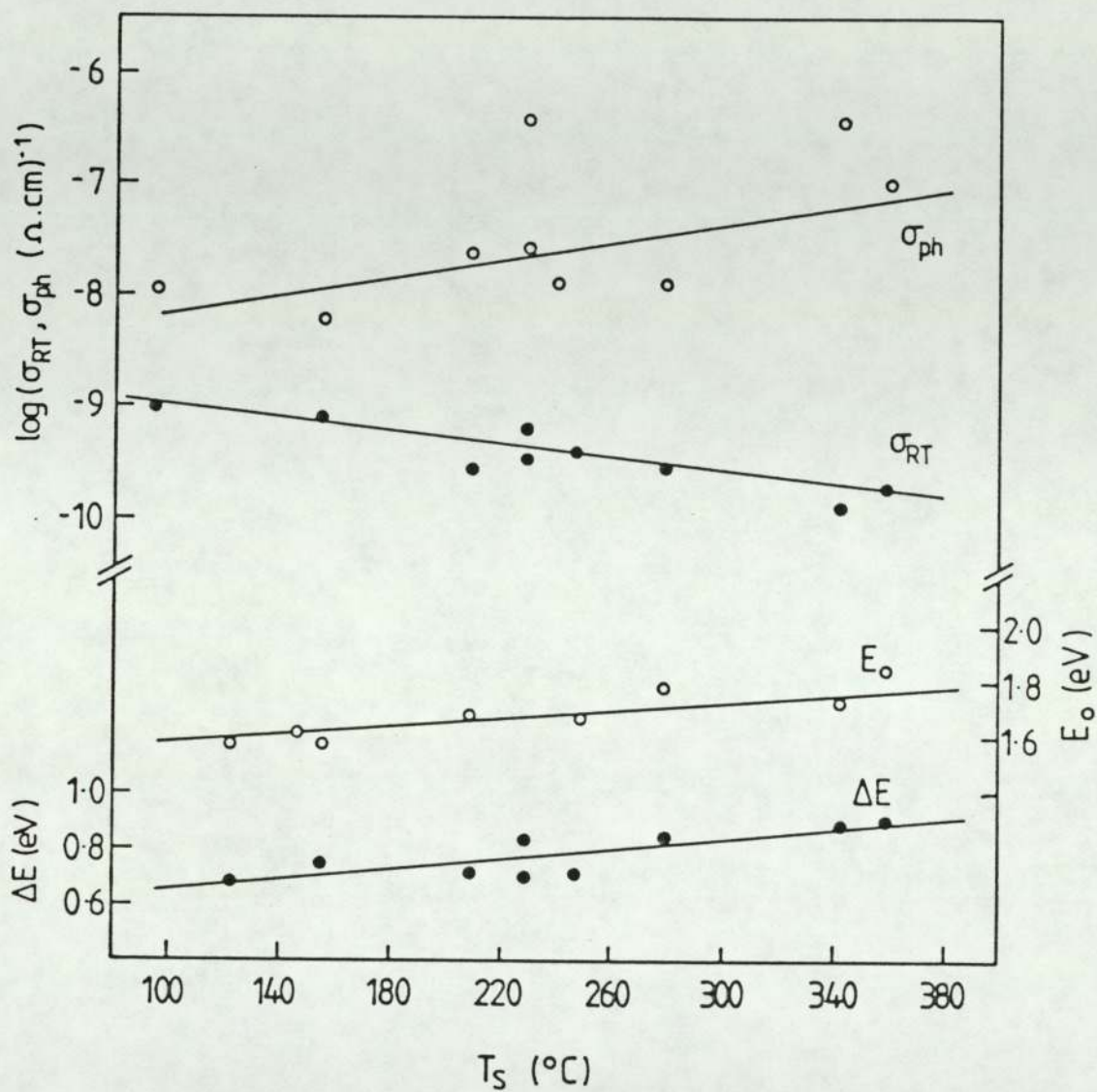


Fig. (4) Variation of room-temperature electrical conductivity (σ_{RT}), photoconductivity (σ_{ph}), thermal activation energy (ΔE) and the optical gap E_0 with the substrate temperature (T_S).

SILICON, RF SPUTTERED AMORPH., UNHYDROGENATED (2)
CONDUCTIVITY, ELEC.

DATA REVIEW by Y Zaka and R W Fane

Date Received: 840227

Anderson et al [1]: sputtered at an argon pressure of 5×10^{-3} torr and found a decrease in room temperature conductivity from 10^{-3} to 10^{-4} mho/cm with increased substrate temperature from 250 to 540°C . Conductivity temperature dependence was weak and non-activated.

Pawlewicz [2]: reported similar results but also found a stronger dependence of conductivity on pressure, 10^{-2} mho/cm at 25 mtorr and 3×10^{-7} mho/cm at 150 mtorr.

Shimizu et al [3]: varied argon pressure (P) and substrate-target spacing (d). Conductivity varied from 3×10^{-3} to 2×10^{-8} mho/cm with a change in Pd, from 0.1 to 1.0 torr-cm. A further decrease of two orders was achieved by annealing at 300°C for 2 hours. Later [4]: they showed that, for films sputtered at 300 mtorr, the room temperature conductivity decreased from about 10^{-7} mho/cm to 10^{-9} mho/cm on exposure to air, but little effect was found with films deposited at low pressure (50 mtorr) having conductivities of 3×10^{-3} mho/cm for pressures 2 to 20 mtorr respectively and activation energies of approximately 0.4 to 1 eV.

Fane [5]: used a pure neon plasma at 150 mtorr. The room-temperature conductivity was decreased from 5×10^{-8} to 4×10^{-9} mho/cm by increasing substrate temperature from 140 to 300°C ; activation energy 0.39-0.54 eV.

Abo-Namous et al [6]: varied neon pressure (P), target-substrate distance (d), and RF self-bias U, room-temperature conductivity was about 10^{-5} mho/cm for $(\text{Pd}/\text{U}) = 0.15$ to less than 10^{-9} mho/cm for $(\text{Pd}/\text{U}) = 0.8$ with corresponding activation energy 0.5 to 0.8 eV.

REFERENCES

- [1] D A Anderson, T D Moustakas, W Paul [Prod. Int. Conf. Amorph. and Liq. Semicond., Edinburgh, Ed. W E Spear, Edinburgh Univ. Press (1977) p 334]
- [2] W T Pawlewicz [J. Appl. Phys. (USA) vol. 49 (1978) p 5595]
- [3] T Shimizu, M Kumeda, I Watanabe, K Kamono [Jap. J. Appl. Phys. (Japan) vol. 18 (1979) p 1923]
- [4] T Shimizu, M Kumeda, I Watanabe, Y Kiriyama [Japn. J. Appl. Phys. (Japan) vol. 19 (1980) p L235]
- [5] R W Fane [J. Phys. D (GB) vol. 14 (1981) p L113]
- [6] S A Abo-Namous, Y Zaka, R W Fane [Phys. Status Solidi a (Germany) vol. 79 (Oct 1983) p 477]

SOURCE

Y Zaka, R W Fane
Phys. Dept., Univ. Aston, Birmingham B4 7ET, England

RETRIEVAL CODES: MC=SI%

PC=CE